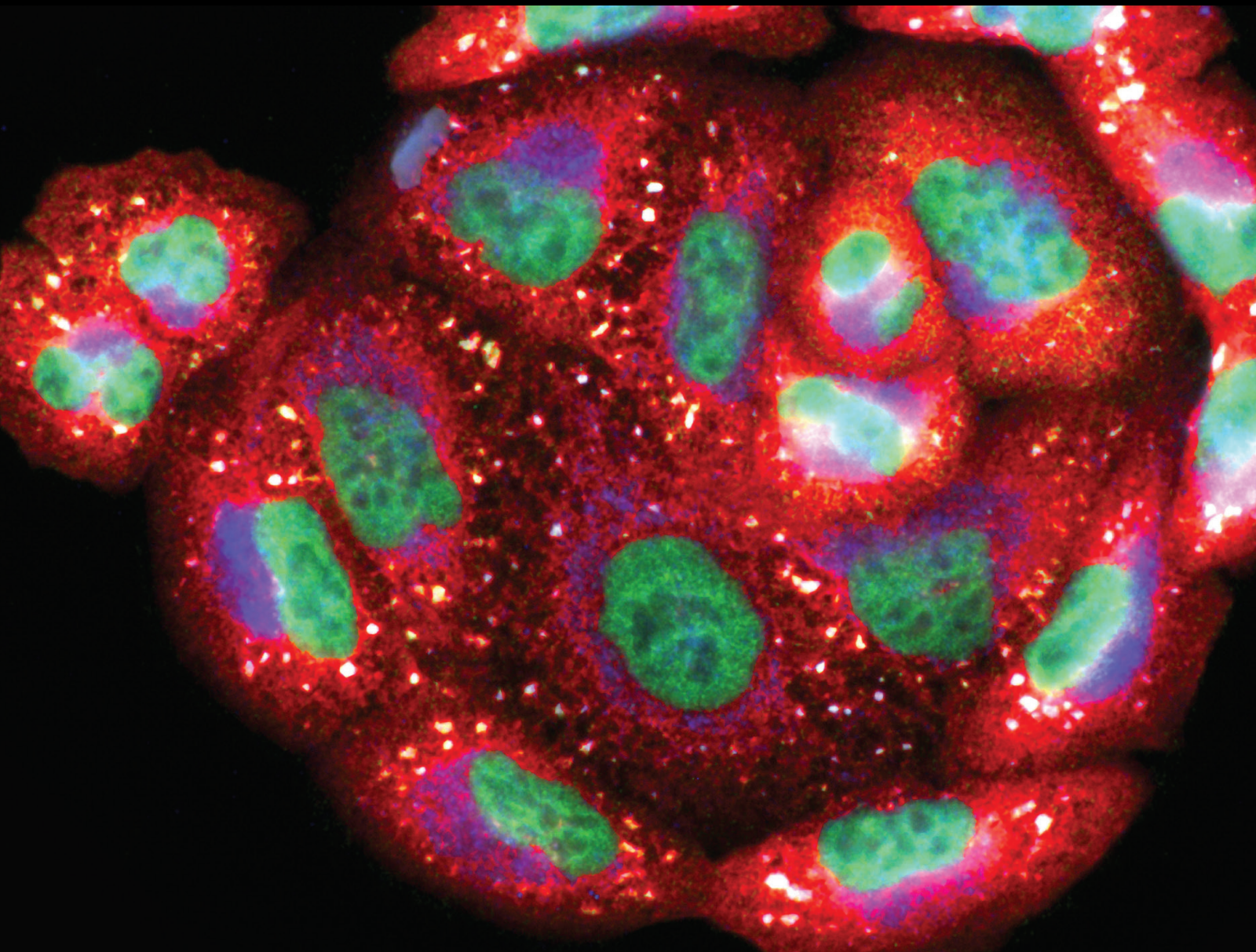


Modulation of Redox Signaling in Chronic Diseases and Regenerative Medicine 2020

Lead Guest Editor: Carlo Gabriele Tocchetti

Guest Editors: Gilda Varricchi, Claudia Penna, Giulio Agnetti, and Laura Sartiani





**Modulation of Redox Signaling in Chronic
Diseases and Regenerative Medicine 2020**

Oxidative Medicine and Cellular Longevity

**Modulation of Redox Signaling in
Chronic Diseases and Regenerative
Medicine 2020**

Lead Guest Editor: Carlo Gabriele Tocchetti

Guest Editors: Gilda Varricchi, Claudia Penna,
Giulio Agnetti, and Laura Sartiani



Copyright © 2021 Hindawi Limited. All rights reserved.

This is a special issue published in "Oxidative Medicine and Cellular Longevity" All articles are open access articles distributed under the Creative Commons Attribution License, which permits unrestricted use, distribution, and reproduction in any medium, provided the original work is properly cited.

Chief Editor

Jeannette Vasquez-Vivar, USA

Associate Editors

Amjad Islam Aqib, Pakistan
Angel Catalá , Argentina
Cinzia Domenicotti , Italy
Janusz Gebicki , Australia
Aldrin V. Gomes , USA
Vladimir Jakovljevic , Serbia
Thomas Kietzmann , Finland
Juan C. Mayo , Spain
Ryuichi Morishita , Japan
Claudia Penna , Italy
Sachchida Nand Rai , India
Paola Rizzo , Italy
Mithun Sinha , USA
Daniele Vergara , Italy
Victor M. Victor , Spain

Academic Editors

Ammar AL-Farga , Saudi Arabia
Mohd Adnan , Saudi Arabia
Ivanov Alexander , Russia
Fabio Altieri , Italy
Daniel Dias Rufino Arcanjo , Brazil
Peter Backx, Canada
Amira Badr , Egypt
Damian Bailey, United Kingdom
Rengasamy Balakrishnan , Republic of Korea
Jiaolin Bao, China
Ji C. Bihl , USA
Hareram Birla, India
Abdelhakim Bouyahya, Morocco
Ralf Braun , Austria
Laura Bravo , Spain
Matt Brody , USA
Amadou Camara , USA
Marcio Carcho , Portugal
Peter Celec , Slovakia
Giselle Cerchiaro , Brazil
Arpita Chatterjee , USA
Shao-Yu Chen , USA
Yujie Chen, China
Deepak Chhangani , USA
Ferdinando Chiaradonna , Italy

Zhao Zhong Chong, USA
Fabio Ciccarone, Italy
Alin Ciobica , Romania
Ana Cipak Gasparovic , Croatia
Giuseppe Cirillo , Italy
Maria R. Ciriolo , Italy
Massimo Collino , Italy
Manuela Corte-Real , Portugal
Manuela Curcio, Italy
Domenico D'Arca , Italy
Francesca Danesi , Italy
Claudio De Lucia , USA
Damião De Sousa , Brazil
Enrico Desideri, Italy
Francesca Diomede , Italy
Raul Dominguez-Perles, Spain
Joël R. Drevet , France
Grégory Durand , France
Alessandra Durazzo , Italy
Javier Egea , Spain
Pablo A. Evelson , Argentina
Mohd Farhan, USA
Ioannis G. Fatouros , Greece
Gianna Ferretti , Italy
Swaran J. S. Flora , India
Maurizio Forte , Italy
Teresa I. Fortoul, Mexico
Anna Fracassi , USA
Rodrigo Franco , USA
Juan Gambini , Spain
Gerardo García-Rivas , Mexico
Husam Ghanim, USA
Jayeeta Ghose , USA
Rajeshwary Ghosh , USA
Lucia Gimeno-Mallench, Spain
Anna M. Giudetti , Italy
Daniela Giustarini , Italy
José Rodrigo Godoy, USA
Saeid Golbidi , Canada
Guohua Gong , China
Tilman Grune, Germany
Solomon Habtemariam , United Kingdom
Eva-Maria Hanschmann , Germany
Md Saquib Hasnain , India
Md Hassan , India

Tim Hofer , Norway
John D. Horowitz, Australia
Silvana Hrelia , Italy
Dragan Hrnčić, Serbia
Zebo Huang , China
Zhao Huang , China
Tarique Hussain , Pakistan
Stephan Immenschuh , Germany
Norsharina Ismail, Malaysia
Franco J. L. , Brazil
Sedat Kacar , USA
Andleeb Khan , Saudi Arabia
Kum Kum Khanna, Australia
Neelam Khaper , Canada
Ramoji Kosuru , USA
Demetrios Kouretas , Greece
Andrey V. Kozlov , Austria
Chan-Yen Kuo, Taiwan
Gaocai Li , China
Guoping Li , USA
Jin-Long Li , China
Qiangqiang Li , China
Xin-Feng Li , China
Jialiang Liang , China
Adam Lightfoot, United Kingdom
Christopher Horst Lillig , Germany
Paloma B. Liton , USA
Ana Lloret , Spain
Lorenzo Loffredo , Italy
Camilo López-Alarcón , Chile
Daniel Lopez-Malo , Spain
Massimo Lucarini , Italy
Hai-Chun Ma, China
Nageswara Madamanchi , USA
Kenneth Maiese , USA
Marco Malaguti , Italy
Steven McAnulty, USA
Antonio Desmond McCarthy , Argentina
Sonia Medina-Escudero , Spain
Pedro Mena , Italy
V́ctor M. Mendoza-Núñez , Mexico
Lidija Milkovic , Croatia
Alexandra Miller, USA
Sara Missaglia , Italy

Premysl Mladenka , Czech Republic
Sandra Moreno , Italy
Trevor A. Mori , Australia
Fabiana Morroni , Italy
Ange Mouithys-Mickalad, Belgium
Iordanis Mourouzis , Greece
Ryoji Nagai , Japan
Amit Kumar Nayak , India
Abderrahim Nemmar , United Arab Emirates
Xing Niu , China
Cristina Nocella, Italy
Susana Novella , Spain
Hassan Obied , Australia
Pál Pacher, USA
Pasquale Pagliaro , Italy
Dilipkumar Pal , India
Valentina Pallottini , Italy
Swapnil Pandey , USA
Mayur Parmar , USA
Vassilis Paschalis , Greece
Keshav Raj Paudel, Australia
Ilaria Peluso , Italy
Tiziana Persichini , Italy
Shazib Pervaiz , Singapore
Abdul Rehman Phull, Republic of Korea
Vincent Pialoux , France
Alessandro Poggi , Italy
Zsolt Radak , Hungary
Dario C. Ramirez , Argentina
Erika Ramos-Tovar , Mexico
Sid D. Ray , USA
Muneeb Rehman , Saudi Arabia
Hamid Reza Rezvani , France
Alessandra Ricelli, Italy
Francisco J. Romero , Spain
Joan Roselló-Catafau, Spain
Subhadeep Roy , India
Josep V. Rubert , The Netherlands
Sumbal Saba , Brazil
Kunihiro Sakuma, Japan
Gabriele Saretzki , United Kingdom
Luciano Saso , Italy
Nadja Schroder , Brazil

Anwen Shao , China
Iman Sherif, Egypt
Salah A Sheweita, Saudi Arabia
Xiaolei Shi, China
Manjari Singh, India
Giulia Sita , Italy
Ramachandran Srinivasan , India
Adrian Sturza , Romania
Kuo-hui Su , United Kingdom
Eisa Tahmasbpour Marzouni , Iran
Hailiang Tang, China
Carla Tatone , Italy
Shane Thomas , Australia
Carlo Gabriele Tocchetti , Italy
Angela Trovato Salinaro, Italy
Rosa Tundis , Italy
Kai Wang , China
Min-qi Wang , China
Natalie Ward , Australia
Grzegorz Wegrzyn, Poland
Philip Wenzel , Germany
Guangzhen Wu , China
Jianbo Xiao , Spain
Qiongming Xu , China
Liang-Jun Yan , USA
Guillermo Zalba , Spain
Jia Zhang , China
Junmin Zhang , China
Junli Zhao , USA
Chen-he Zhou , China
Yong Zhou , China
Mario Zoratti , Italy

Contents

H₂S Pretreatment Is Promigratory and Decreases Ischemia/Reperfusion Injury in Human Microvascular Endothelial Cells

Elisa Zicola , Elisa Arrigo , and Daniele Mancardi 

Research Article (13 pages), Article ID 8886666, Volume 2021 (2021)

Atrial Dyssynchrony Measured by Strain Echocardiography as a Marker of Proarrhythmic Remodeling and Oxidative Stress in Cardiac Surgery Patients

Francisco J. Sánchez , Valeria A. Gonzalez, Martin Farrando, Ariel O. Baigorria Jayat, Margarita Segovia-Roldan , Laura García-Mendivil , Laura Ordovás , Natalia J. Prado , Esther Pueyo , and Emiliano R. Diez 

Research Article (14 pages), Article ID 8895078, Volume 2020 (2020)

Cardioprotective Effects of Taurisolo® in Cardiomyoblast H9c2 Cells under High-Glucose and Trimethylamine N-Oxide Treatment via De Novo Sphingolipid Synthesis

Stefania Lama, Vincenzo Monda, Maria Rosaria Rizzo, Marco Dacrema, Maria Maisto, Giuseppe Annunziata, Gian Carlo Tenore , Ettore Novellino, and Paola Stiuso 

Research Article (11 pages), Article ID 2961406, Volume 2020 (2020)

Chicoric Acid Ameliorates Nonalcoholic Fatty Liver Disease via the AMPK/Nrf2/NFκB Signaling Pathway and Restores Gut Microbiota in High-Fat-Diet-Fed Mice

Xiaoqin Ding , Tunyu Jian , Jiawei Li , Han Lv , Bei Tong , Jing Li , Xiuhua Meng , Bingru Ren , and Jian Chen 

Research Article (20 pages), Article ID 9734560, Volume 2020 (2020)

Saikosaponin A-Induced Gut Microbiota Changes Attenuate Severe Acute Pancreatitis through the Activation of Keap1/Nrf2-ARE Antioxidant Signaling

Jing Li, Jinfeng Han, Juan Lv, Shiji Wang, Lai Qu, and Yanfang Jiang 

Research Article (19 pages), Article ID 9217219, Volume 2020 (2020)

ROS-Mediated Necroptosis Is Involved in Iron Overload-Induced Osteoblastic Cell Death

Qing Tian, Bo Qin, Yufan Gu, Lijun Zhou, Songfeng Chen, Song Zhang, Shuhao Zhang, Qicai Han , Yong Liu, and Xuejian Wu

Research Article (22 pages), Article ID 1295382, Volume 2020 (2020)

African Vegetables (*Clerodendrum volubile* Leaf and *Irvingia gabonensis* Seed Extracts) Effectively Mitigate Trastuzumab-Induced Cardiotoxicity in Wistar Rats

Olufunke Olorundare, Adejuwon Adeneye , Akinyele Akinsola, Sunday Soyemi, Alban Mgbehoma, Ikechukwu Okoye, James M. Ntambi, and Hasan Mukhtar 

Research Article (15 pages), Article ID 9535426, Volume 2020 (2020)

Roles of Reactive Oxygen Species in Cardiac Differentiation, Reprogramming, and Regenerative Therapies

Jialiang Liang , Min Wu, Chen Chen, Mingjie Mai, Jinsong Huang , and Ping Zhu 

Review Article (14 pages), Article ID 2102841, Volume 2020 (2020)

The Impact of Lipoprotein Apheresis on Oxidative Stress Biomarkers and High-Density Lipoprotein Subfractions

Agnieszka Mickiewicz , Ewelina Kreft, Agnieszka Kuchta , Ewa Wieczorek, Joanna Marłęga, Agnieszka Ćwiklińska, Milena Paprzycka, Marcin Gruchała, Marcin Fijałkowski, and Maciej Jankowski
Research Article (6 pages), Article ID 9709542, Volume 2020 (2020)

Ticagrelor Conditioning Effects Are Not Additive to Cardioprotection Induced by Direct NLRP3 Inflammasome Inhibition: Role of RISK, NLRP3, and Redox Cascades

Claudia Penna , Manuela Aragno , Alessia Sofia Cento , Saveria Femminò , Isabella Russo , Federica Dal Bello , Fausto Chiazza , Debora Collotta , Gustavo Ferreira Alves , Massimo Bertinaria , Elisa Zicola , Valentina Mercurio , Claudio Medana , Massimo Collino , and Pasquale Pagliaro 
Research Article (12 pages), Article ID 9219825, Volume 2020 (2020)

Research Article

H₂S Pretreatment Is Promigratory and Decreases Ischemia/Reperfusion Injury in Human Microvascular Endothelial Cells

Elisa Zicola , Elisa Arrigo , and Daniele Mancardi 

Department of Clinical and Biological Sciences, University of Turin, Italy

Correspondence should be addressed to Daniele Mancardi; daniele.mancardi@unito.it

Received 11 August 2020; Revised 23 September 2020; Accepted 1 April 2021; Published 17 April 2021

Academic Editor: Jan Gebicki

Copyright © 2021 Elisa Zicola et al. This is an open access article distributed under the Creative Commons Attribution License, which permits unrestricted use, distribution, and reproduction in any medium, provided the original work is properly cited.

Endothelial cell injury and vascular function strongly correlate with cardiac function following ischemia/reperfusion injury. Several studies indicate that endothelial cells are more sensitive to ischemia/reperfusion compared to cardiomyocytes and are critical mediators of cardiac ischemia/reperfusion injury. H₂S is involved in the regulation of cardiovascular system homeostasis and can act as a cytoprotectant during ischemia/reperfusion. Activation of ERK1/2 in endothelial cells after H₂S stimulation exerts an enhancement of angiogenesis while its inhibition significantly decreases H₂S cardioprotective effects. In this work, we investigated how H₂S pretreatment for 24 hours prevents the ischemia/reperfusion injury and promotes angiogenesis on microvascular endothelial cells following an ischemia/reperfusion protocol in vitro, using a hypoxic chamber and ischemic buffer to simulate the ischemic event. H₂S preconditioning positively affected cell viability and significantly increased endothelial cell migration when treated with 1 μM H₂S. Furthermore, mitochondrial function was preserved when cells were preconditioned. Since ERK1/2 phosphorylation was extremely enhanced in ischemia/reperfusion condition, we inhibited ERK both directly and indirectly to verify how H₂S triggers this pathway in endothelial cells. Taken together, our data suggest that H₂S treatment 24 hours before the ischemic insult protects endothelial cells from ischemia/reperfusion injury and eventually decreases myocardial injury.

1. Introduction

Cardiovascular diseases represent the leading cause of death and disabilities in the industrialized countries, and ischemic heart disease (IHD) majorly represents them. IHD causes 46% of cardiovascular deaths in men and 38% in women worldwide [1]. One of the major challenges in treating the ischemic heart is to avoid ischemia reperfusion injury (IRI); the limitation of which can result of pivotal importance in case of programmed ischemia/hypoxia such as open-heart surgery, transplantation, or primary percutaneous coronary intervention [2–4].

IRI is the trigger leading to cell death by apoptosis and necrosis, and the causes of the activation of these phenomena are mainly oxidative stress, inflammation, and intracellular Ca²⁺ overload [5, 6]. In addition, reperfusion can also lead to severe ventricular arrhythmia and, as a consequence, death

[7]. Low cardiac output, perioperative myocardial infarction, and arrhythmias can, in turn, be the causes of I/R injury following cardiac surgery [8].

Paradoxically, the restoration of blood flow in the ischemic tissue can exacerbate the damage more than the ischemic event itself, causing a phenomenon known as reperfusion injury [2, 9]. Indeed, the restoration of coronary blood flow, although necessary after the ischemic episode, leads to the death of cardiac myocytes that were potentially viable at the onset of reperfusion [10].

Since 1980, many important contributions shed light on the importance of the endothelium in the cardiovascular system, redirecting the investigating approach to the cardiovascular system [5, 6, 11–16]. In the last 40 years, many advances have been made toward a deeper comprehension of the role of different cell types participating in the ischemic scenario and the attention on ECs proportionally increased.

In support to these findings, several studies indicate that endothelial cells are as sensitive to ischemia/reperfusion as cardiomyocytes and therefore are critical mediators of cardiac IRI [17–22].

Furthermore, reoxygenation of the ischemic tissue causes oxidative stress: during reperfusion, xanthine oxidase, NADPH oxidase, and the mitochondrial electron transport chain (mETC) generate reactive oxygen species (ROS), mediating an increased myocardial injury [23, 24]. The above-mentioned enzymes also provide the greatest amount of superoxide anion in ECs [6].

During IRI, there is a deficiency of vasodilator molecules such as endothelin [25], angiotensin, prostacyclin, and nitric oxide, which directly influence metabolic and contractile function in the adult heart [22, 26]. After the IR insult, ECs undergo changes in cytoskeletal architecture and expression of adhesion molecules (e.g., CAMs and E- and P-selectins). The activation of quiescent ECs induces the recruitment of neutrophils which initiate the inflammatory response. In parallel, ECs permeability increase resulting in the loss of barrier function and capillary leakage [3, 5, 27].

The process of angiogenesis, which is *de novo* formation of micro vessels, in pathological conditions is not only essential to prevent heart failure in the long term but also has the potential to support the recovery of the ischemic myocardium in the days following myocardial infarction. Impairment of myocardial angiogenesis causes a reduction in myocardial perfusion and fatal ischemic cardiomyopathy [28–30]. Moreover, EC injury and vascular function strongly correlate with the cardiac performance following IRI [31].

To prevent pathological remodeling in the structure of blood vessels, ECs produce and release two endogenous gasotransmitters, hydrogen sulfide (H_2S) and nitric oxide (NO). In particular, H_2S has been known for many years for being a toxic agent. Nowadays, it is recognized as being a key factor in the regulation of inflammatory and immune response, cardiovascular and nervous systems, and gastrointestinal tract function [32–35]. The cardiac tissue is capable of producing H_2S endogenously, due to the presence of a discreet quantity of cystathionine- γ -lyase (CSE), one of the enzymes responsible for the production of this gasotransmitter [36]. H_2S can act as a cytoprotectant against oxidative stress and as an antiapoptotic agent by preserving mitochondrial function during ischemia/reperfusion [37, 38].

The identification of the reperfusion injury salvage kinase (RISK) pathway led the way to understand how to improve the clinical outcomes of acute myocardial infarction by mediating a programmed cell survival [9, 39, 40] when activated specifically at the time of reperfusion [41]. The RISK pathway is linked to two signaling cascades: PI3K-Akt and MEK1-ERK1/2. Hu et al. observed not only that preconditioning rat myocytes with NaHS (1–100 μM) increased cell viability but also that if ERK1/2 or Akt were blocked during preconditioning or ischemia there was a significant decrease of the H_2S cardioprotective effect [42].

Studies on isolated rat liver mitochondria showed a biphasic effect of H_2S on mETC. Concentrations ranging from 100 nM to 1 μM stimulated electron transport, whereas 10 μM or higher provoked its inhibition [43]. The same

bimodal effect has been shown by Pupo et al., where H_2S induced no effect at the lowest and highest concentrations (0.5 and 100 μM) and a significant cellular response at 1 μM in terms of cell migration and proliferation [44].

Both PI3K-Akt and MEK-ERK1/2 pathways have been demonstrated to be downstream effectors of H_2S signaling cascade also in ECs, thus promoting migration, proliferation, and angiogenesis [35, 45–48].

Despite the growing literature in the field, it is still not clear whether H_2S could be more effective as a preconditioning or postconditioning agent [7, 19, 40, 42, 49, 50].

In our study, we decided to investigate the role of H_2S as a preconditioning trigger molecule, by using different micromolar concentrations of an inorganic H_2S donor, namely, sodium hydrosulfide (NaHS). Specifically, we investigated whether a 24-hour treatment could trigger a cascade that would enhance the endothelial response after an ischemic insult in an *in vitro* model of human microvascular endothelial cells (HMEC-1). The *in vitro* model is particularly feasible to address functional recovery of ECs since it allows exposure to hypoxia and drugs while maintaining the ability to proliferate and migrate and, therefore, performing experimental assays.

2. Materials and Methods

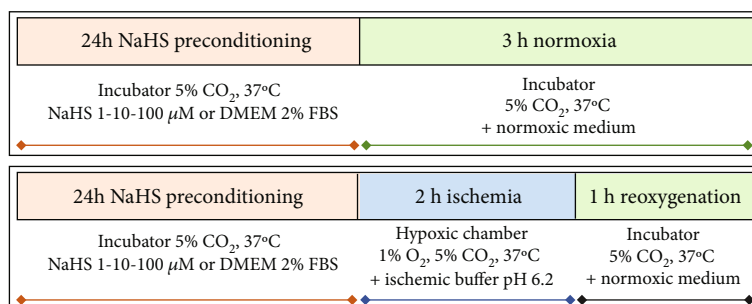
2.1. Cell Culture. Human microvascular endothelial cells 1 (HMEC-1) (ATCC® CRL3243™) were cultured in EndoGRO™-MV Complete Culture Media Kit (Millipore) and 1% penicillin/streptomycin (Pan Biotech) and passed 80–90% confluence.

Dulbecco's Modified Eagle's Medium (DMEM) with phenol red (Sigma-Aldrich) 2% FBS (Microgem), 1% penicillin/streptomycin, and 1% L-glutamine (Microgem) was used for preconditioning and reoxygenation processes.

2.2. Hydrogen Sulfide Preconditioning and Ischemia/Reperfusion Protocol. Sodium hydrosulfide hydrate (NaHS) (Sigma-Aldrich) was used as a saline hydrogen sulfide donor. NaHS was freshly prepared in phenol red DMEM 2% FBS on the day of the experiment at a concentration of 5 mM; the stock solution was used for dilutions to reach our working conditions (1–10–100 μM).

In vitro simulation of ischemia/reperfusion injury was induced using an ischemic buffer (pH 6.2) as described in literature [25], and severe hypoxic conditions were reached through incubation in a sealed chamber (see Scheme 1) endowed with a regulator of gas mixture (InvivO₂ 200, Ruskinn, United Kingdom).

A minimum level of 1% O₂ can be achieved by this system, and no complete anoxia is guaranteed from the manufacturer. Moreover, to the best of our knowledge, 1% O₂ at atmospheric pressure matches the oxygen partial pressure of ischemic tissues, including the myocardium [51]. The buffer was equilibrated overnight in a hypoxic chamber (1% O₂, 5% CO₂, 37°C). CO₂ levels were set to 5% to buffer pH in medium, matching normoxic incubation. Cells were put in the hypoxic chamber, and the medium was changed with the equilibrated ischemic buffer. Ischemic protocol lasted



SCHEME 1: Schematic representation of the experimental design used. On the upper side is represented the “normoxia” setting, whereas on the lower panel is the setting used to simulate the *in vitro* “ischemia-reperfusion” condition.

for 2 hours in every experiment; cells were then reoxygenated with fresh medium for 1 hour in a normoxic incubator (37°C, 5% CO₂).

2.3. Solutions and Reagents

2.3.1. Ischemic Buffer. The buffer was freshly prepared before each experiment. The following formulation was used: NaCl 137 mM, KCl 12 mM, MgCl₂ 0.49 mM, CaCl₂ 0.9 mM, HEPES 4 mM, and Na L-lactate 20 mM (all purchased from Sigma-Aldrich). The ingredients were dissolved into double-distilled water, and pH was adjusted to reach 6.2 before bringing the solution to the required volume (100 mL).

2.3.2. AZD6244. Also called Selumetinib, it is a selective MEK1/2 inhibitor. The inhibitor was solubilized in DMSO, as 10 mM stock solutions at -20°C. The stock was diluted to obtain a final concentration of 1 μM.

2.3.3. SCH772984 (Aurogene). Selective ERK1/2 inhibitor was dissolved in DMSO, as 5 mM stock solutions at -80°C. The stock was diluted to reach a working concentration of 1 μM.

2.3.4. Antibodies. Primary antibodies anti-Heat-shock protein 90 (HSP90), p44/42 MAPK (ERK1/2), and phospho-p44/42 MAPK (p-ERK1/2) were all purchased from Cell Signaling Technology (The Netherlands). Secondary anti-rabbit antibody was purchased from ImmunoReagents, Inc. (North Carolina, USA). All antibodies were used according to the manufacturer’s instructions.

2.4. Viability Assay. In order to address how cell viability could be influenced by preconditioning, an MTT assay was performed at 24 hours from the end of reoxygenation. Cells were plated in a 96-well plate at a density of 0.5×10^4 cells/well in growth medium. On the next day, cells were preconditioned as previously described. After 24 hours of preconditioning, cells would undergo normoxic or IR condition following the ischemia/reperfusion protocol mentioned earlier. At the end of reperfusion, media was changed for all cells to DMEM 2% FBS, in order to keep cells alive for the next 24 hours but avoiding cell proliferation. After one day, MTT solution was added to each well (10 μL/well), and plates were kept in the dark in an incubator for 3 hours. Then, media was removed and 100 μL DMSO was added to each well, and absorbance was detected at 570 nm using a micro-

plate reader. At least eight wells for each condition were analyzed.

2.5. Cell Migration Assay. To assess cell migration, cells were plated into three-chamber silicone-culture inserts (Ibidi) in a 12-well plate at a density of 4×10^5 cells/mL in growth medium. This density was chosen as the most appropriate to have cells at 90-100% confluence overnight. On the next day, cells were treated with NaHS as described before, by removing the medium from each chamber and adding the desired treatment or just control medium, being careful not to scratch cells away. After 24 hours, all culture inserts were removed, and cells were gently washed with warm PBS with Ca/Mg. At this point, cells underwent IR protocol for 2 hours. At the end of the ischemia, cells were gently washed with warm PBS and growth medium was added to each well. After 6 hours of migration, cells were fixed in 4% PAF. Images were then acquired using a Nikon Eclipse Ti-E microscope with a $\times 10$ lens. The MetaMorph software was used to both acquire and analyze all images. Cell motility was expressed as percentage of wound closure. At least three fields for each condition were analyzed.

2.6. In Vitro Angiogenesis Assay. The formation of capillary-like structures *in vitro* was studied on growth factor-reduced Matrigel (Corning, USA). Matrigel was used according to the manufacturer’s instructions. ECs were plated into Petri dishes and treated according to our protocols on the following day. After *in vitro*-simulated IR injury, cells were seeded at 2.5×10^4 cells per well onto Matrigel-precoated 24-well plate in growth medium. After 16 hours, cell organization was observed using a 5x lens. Images were acquired using the Infinity Analyze software (Lumenera Corporation). A minimum of three fields was analyzed for each condition.

Image analysis was performed using ImageJ’s plugin Angiogenesis Analyzer, which works on phase contrast (RGB colors, 24 bit) or fluorescence images (8 or 16 bit). In order to avoid artifacts, some background noise had to be removed from the images using the “blurred mask tool.” Once the image has been modified, the program can be run and the images are automatically analyzed. The images are returned with different paths traced in a color-code mode and a table with different automatically measured parameters. We choose to include in our analysis three parameters:

(I) number of master segments, (II) total master segment length, and (III) number of isolated segments.

2.7. Quantification of Mitochondrial Mass and Membrane Depolarization. To measure the depolarization of mitochondrial membrane in relationship with mitochondrial mass, endothelial cells were plated at a density of 2×10^4 cells/well on 1.5 mm ϕ cover slips in growth medium. Cells were treated as previously described (see Hydrogen Sulfide Preconditioning and Ischemia/Reperfusion Protocol) with $1 \mu\text{M}$ NaHS. After reperfusion, all specimens were incubated in DMEM 2% FBS with both MitoTracker™ Green FM (Thermo Fisher) 200 nM and MitoTracker™ Red CMXRos (Thermo Fisher) 50 nM in the dark for 30 minutes at 37°C . After staining, cells were washed with PBS and fixed with 4% PAF. After fixation, coverslips were mounted on microscope slides and observed at a confocal microscope (Zeiss LSM800) with a 63x oil-immersion objective. GMT has an absorption/emission spectrum of 490 nm/516 nm, while the RMT one is 579 nm/599 nm. Images were acquired with ZEN System software with a resolution of 512×512 pixels.

2.8. Western Blot. Cells were seeded into Petri dishes and were allowed to reach confluence before being treated with NaHS ($1\text{--}10\text{--}100 \mu\text{M}$) and/or AZD6244 $1 \mu\text{M}$ and then underwent IR simulation protocol. At the end of the protocol, cells were scraped and lysed with RIPA buffer (Sigma-Aldrich), containing protease and phosphatase inhibitors (Complete protease inhibitor tablets and PhosStop, Roche). Whole cell lysates were separated by SDS-PAGE and wet-transferred on PVDF membranes, according to the manufacturer's protocol (Bio-Rad). After transfer, membranes were blocked in 4% nonfat dried milk or 4% BSA (depending on the primary antibody), for 1 hour at room temperature. Membranes were washed once in TBST and incubated with antibodies against HSP90 (1:1,000), ERK1/2 (1:1,000), and phospho-p44/42 MAPK (Erk1/2) (Thr202/Tyr204) (1:1,000) overnight at 4°C . Membranes were washed with TBST three times for 10 min. Anti-rabbit secondary antibody incubation (1:5,000) lasted for 1 hour. After another 30' of washing with TBST 1x, chemiluminescence was detected using the ECL system (Bio-Rad) using a ChemiDoc Touch instrument (Bio-Rad).

2.9. Image Analysis

2.9.1. Tubulogenesis Assay. During the analysis, we kept into consideration the following parameters: number of master segments, number of master junctions, total master segment length, and number of isolated segments. A well-constructed network should have more master elements (segments and junctions), thus creating a more physiological and functional structure. The images were analyzed with ImageJ's Angiogenesis Analyzer plugin, and only the aforementioned parameters were kept into consideration. All images were converted to RGB format if needed.

2.9.2. Mitochondrial Staining. Multichannel images were split to separate the two channels. Then, the corrected total cell fluorescence (CTCF) was calculated for each cell in both

channels as described in literature [52]. For each cell, the ratio between mitochondrial depolarization and mass was calculated and normalized on the control condition.

2.9.3. Image Lab Quantification. Using Image Lab software, bands were detected automatically and then subtracting the background to obtain a better quantification. Density of bands was computed keeping into consideration the value of the integrated density adjusted by subtracting the background. All proteins were quantified by normalizing the density over the loading control (HSP90).

2.10. Statistical and Computer Analysis. Results are expressed as mean \pm SEM. Differences between groups were analyzed by one-way ANOVA or Kruskal-Wallis or Mann-Whitney *t*-test. Significance was established at *p* value < 0.05 . All raw data were analyzed using Microsoft Excel and Prism 6. All experiments were repeated at least three times.

3. Results

3.1. Biological Effects of NaHS Preconditioning. During acute myocardial infarction, endothelial cells can go towards death through apoptosis, necrosis, or autophagy [53–55]. To assess endothelial cell response after IR injury in terms of viability, an MTT assay was performed after 24 hours from the injury.

As shown in Figure 1, there was a decrease in the IR condition compared to normoxia, but H_2S did not significantly increase cell viability in the post-IR condition.

The highest viability was observed at $10 \mu\text{M}$, but only in normoxic conditions.

Cell migration is one of the essential processes during angiogenesis. In fact, cells have to migrate to create new vessels. The creation of new vessels is important after IR injury in order to allow an adequate blood supply to the myocardium and, eventually, to replace arteries that have been disrupted by the ischemic event and subsequent reperfusion. To study this process, we observed cell migration following IR simulation. After 6 hours, the percentage of wound closure was calculated and compared to the normoxic control condition (Figure 2(b)).

We observed a significant improvement of cell migration in cells treated with NaHS, with the strongest effect at $1 \mu\text{M}$ NaHS, both in normoxia and post-IR.

To study whether NaHS treatment had a proangiogenic effect on cells that underwent IR injury simulation, we studied their ability to form capillary-like structures *in vitro* focusing on the most promising concentration of $1 \mu\text{M}$ NaHS.

After IR, cells were detached and plated in Matrigel-precoated 24-well multiwell in EndoGRO 10% FBS for 16 hours. As shown in Figure 3, there is a positive trend in terms of capillary formation in both normoxia and IR, upon treatment of cells with $1 \mu\text{M}$ NaHS, but no statistical significance was observed.

We decided to perform a double MitoTracker™ staining on all samples to investigate whether mitochondria were affected by NaHS preconditioning. MitoTracker™ Green FM stains all mitochondria, whereas MitoTracker™

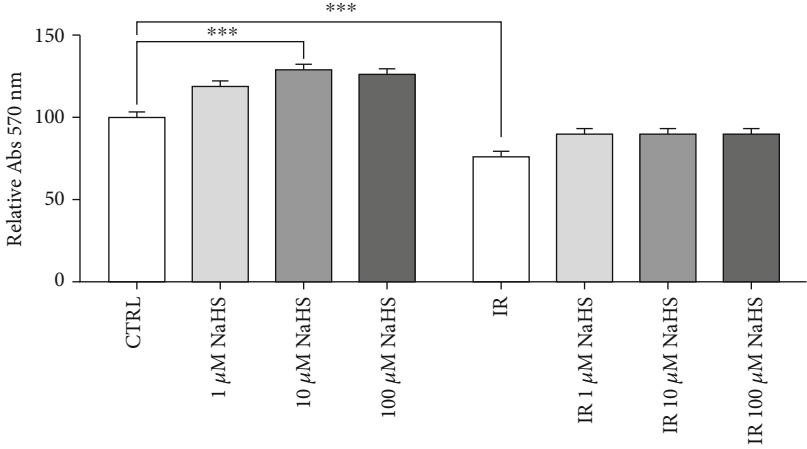
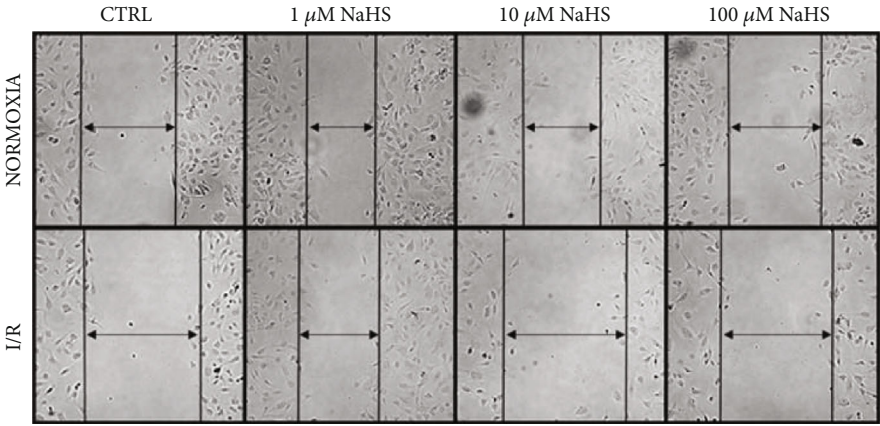
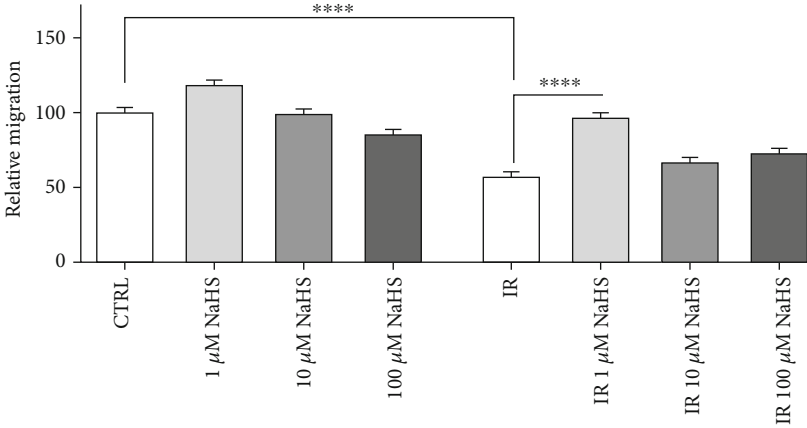


FIGURE 1: Normalized viability on the normoxic control condition. Statistical significance was set at p value < 0.05 (***) $p \leq 0.001$.



(a)



(b)

FIGURE 2: (a) Representative images of cells after 6 hours in the different experimental conditions. (b) Relative migration, all data sets were normalized on the normoxic control condition (CTRL). Statistical significance: **** $p < 0.0001$.

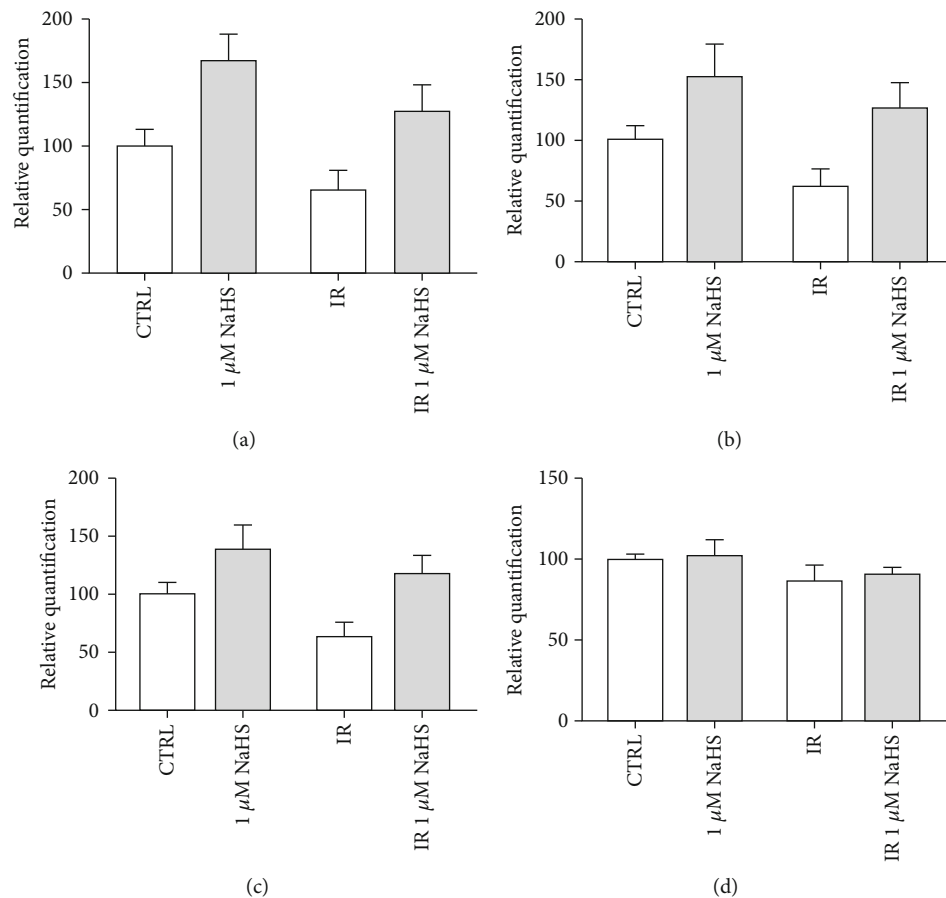


FIGURE 3: Quantification of main elements of the *in vitro* capillary network: (a) total master segment length; (b) number of master segments; (c) number of junctions; (d) number of isolated elements.

Red CMXRos stains only viable mitochondria. Red fluorescence is directly proportional to membrane depolarization.

By calculating the ratio between red and green fluorescence, we determined the influence of NaHS and IR on mitochondria in endothelial cells.

NaHS treatment decreased the mitochondrial mass with a similar fashion in normoxia and IR (Figure 4(b)). However, the mitochondrial function did not change much between the two IR experimental conditions. On the other hand, NaHS treatment caused an improvement in mitochondria viability, observed as an increased ratio between vital (red) and total (green) mitochondria, both in IR and normoxic conditions (Figures 4(a)–4(d)).

3.2. NaHS Preconditioning and IR Injury Influence ERK1/2 Phosphorylation. Since ERK1/2 is deeply implicated in both cell migration and angiogenesis, but also in inducing apoptosis, we evaluated whether IR and/or NaHS treatment could influence its level of phosphorylation. Protein expression and phosphorylation levels were assessed through western blot.

ERK appeared to be strongly phosphorylated in IR condition, whereas NaHS treatment attenuated the p-ERK/ERK ratio, bringing it towards a more physiological condition (Figure 5).

3.3. Effects of MEK-ERK Pathway Inhibition. After assessing the levels of ERK phosphorylation, we decided to investigate if NaHS directly modulated the ERK pathway.

At first, we targeted its upstream modulator, MEK, using its specific inhibitor AZD6244 before preconditioning. Both viability and cell migration were tested.

Considering cell viability, there was no relevant difference with or without inhibitor and/or $1 \mu\text{M}$ NaHS, confirming what we had already observed (see Figure 1).

When we tested the effects on cell migration, we confirmed the effect of preconditioning with $1 \mu\text{M}$ NaHS in both normoxia and IR. Moreover, we observed that the treatment with MEK inhibitor only slightly decreased the rate of cell migration compared to the control condition, especially in normoxia. An even slighter effect was observed when we used both the inhibitor and NaHS (Figure 6(b)).

After evaluating the effects on upstream inhibition, we decided to investigate whether NaHS preconditioning could rescue the biological effects after direct ERK1/2 inhibition.

Again, we assessed the inhibition on both cell viability and cell migration, which are two key pathways in which ERK1/2 is strongly involved.

No relevant changes were observed in IR condition, but a significant decrease in cell viability was observed in normoxia when cells were treated with both ERK inhibitor and NaHS (Figure 7(a)).

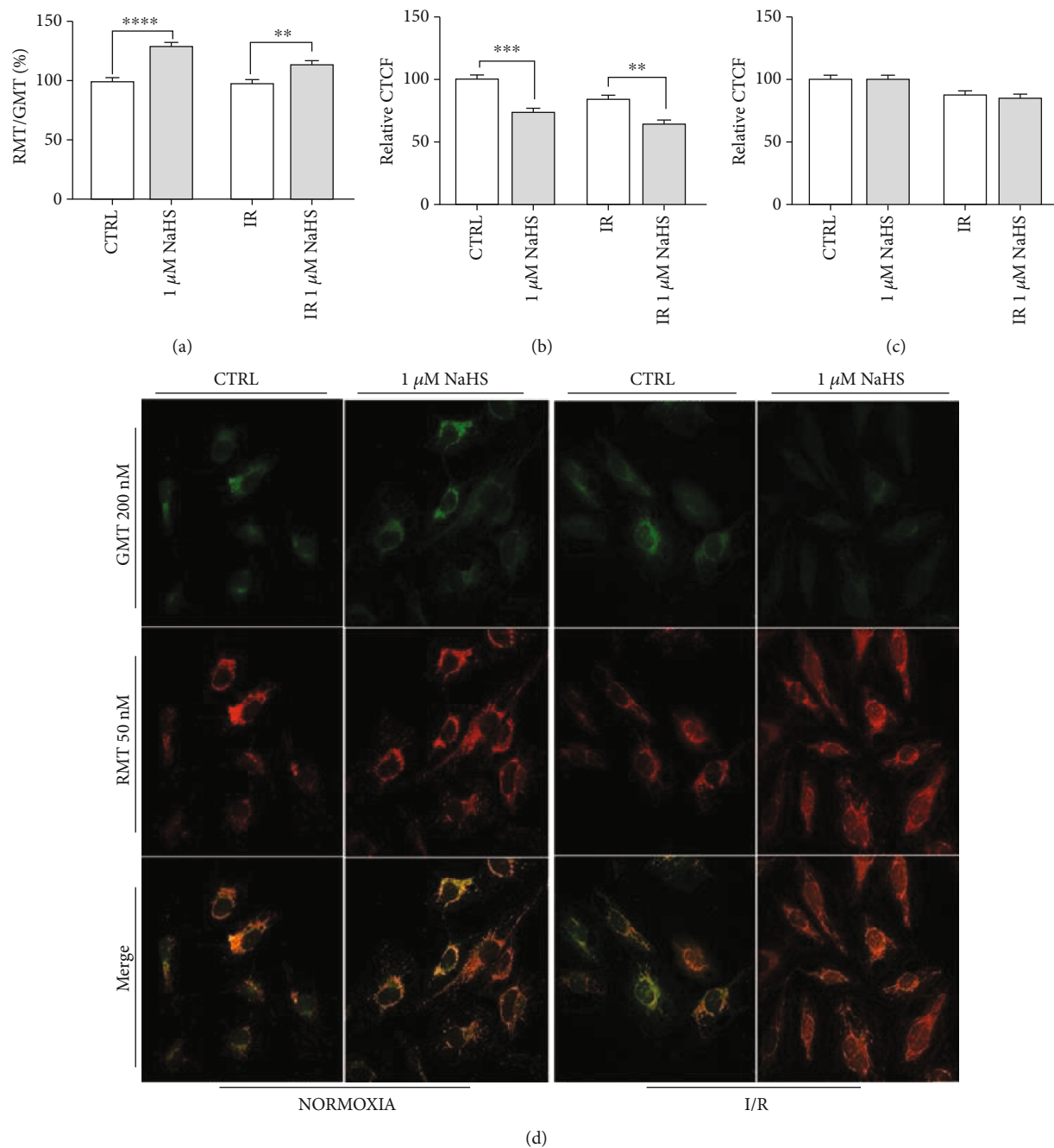


FIGURE 4: (a) Ratio between red (RMT) and green (GMT) MitoTracker™; (b, c) GMT and RMT fluorescence, respectively, calculated for each experimental condition as a percentage of CTRL; (d) representative fields of stained cells. All data sets were normalized on the normoxic control condition (CTRL). Statistical significance: ** $p < 0.01$, *** $p < 0.001$, and **** $p < 0.0001$.

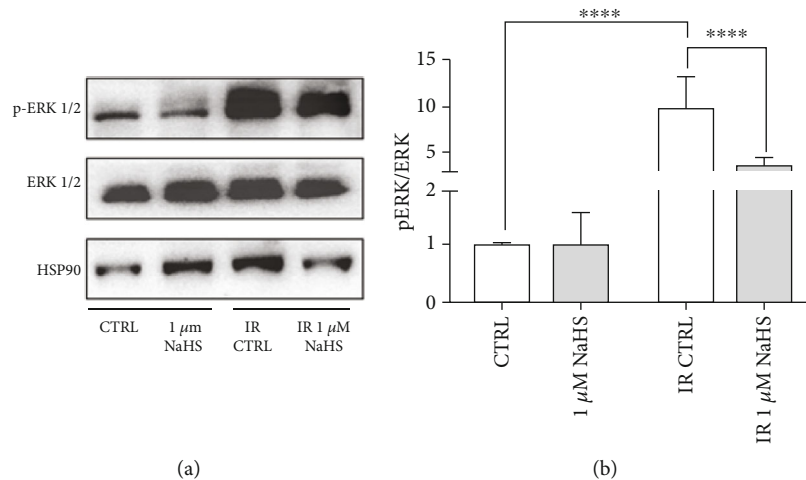


FIGURE 5: (a) Representative experiment of ERK1/2 and p-ERK1/2; (b) ratio of p-ERK on total ERK ($n = 4$). Both total and phosphorylated proteins were first normalized on the loading control (HSP90), and then, the ratio was calculated. All data sets were normalized on the normoxic control condition (CTRL). Statistical significance: **** $p < 0.0001$.

Focusing on cell migration, in normoxia, ERK inhibition caused a significant decrease in cell migration, but NaHS treatment was able to rescue this inhibition, restoring the migration (Figure 7(b)). However, in IR, the direct inhibition of ERK actually caused a very strong decrease in cell migration when compared to the IR untreated cells, which could not be rescued by NaHS treatment (Figure 7(b)).

4. Discussion

Cardiovascular diseases are the leading cause of death worldwide. In 2016, they represented up to 30% of all global deaths [56, 57]. CVDs include different clinical conditions, most of which are associated to a pathological condition known as ischemia/reperfusion injury, such as myocardial infarction and stroke [58–61]. Whether this phenomenon affects the clinical outcome, it depends on the site, the duration, and the severity of the ischemic event itself. Nevertheless, post-ischemic reperfusion could exacerbate the damage both locally and systemically. This paradox relies on an increase in inflammatory response and, later on, to a profound tissue injury [2]. During an ischemic insult, moreover, there are several biochemical and cellular changes caused by the rapid depletion of oxygen and nutrients that cells cannot bear altogether with exacerbated effects during the reperfusion phase [62–64].

Endothelial integrity is pivotal for a proper vascularization which is, in turn, a key step for restoration of the physiological state as demonstrated by the several complications for patients undergoing incomplete cardiac revascularization [65, 66]. In this regard, it is reported that endothelial cells are very sensitive to IRI, even more than other cell types [20, 22, 27]. In addition, they are critical mediators for the onset of the inflammatory response, the generation of ROS, and the rapid restoration of the physiological pH.

In the ischemic myocardium, these events negatively affect the surrounding tissue, exacerbating the reperfusion injury and worsening the outcomes [2, 67].

A considerable part of literature about IRI has its focus on cardiac cells, while a small amount of data is available about endothelial cells, despite their importance in this context. Considering the role of ECs in both injury and recovery after the ischemic insult, the role of endothelial function in the hypoxic/ischemic scenario is of scientific relevance to ameliorate tissue recovery.

To this end, the action of hydrogen sulfide as a protective agent on endothelial cells against hypoxic/ischemic stress is promising because of the recent description of its beneficial effects in similar settings [68, 69]. H_2S is known to act as a secondary messenger [70, 71], and there is evidence that it can be beneficial in IRI in several experimental models [72, 73]; hence, its potential as endogenous and exogenous therapeutic agent is gaining scientific attention. In order to study the effects solely on the endothelium, we decided to use an *in vitro* model of human microvascular endothelial cells to test the direct effects of hydrogen sulfide as a preconditioning agent, by using the inorganic donor NaHS. The aim was to recover the physiological state after the ischemic event. In particular, we expected to trigger a response in endothelial cells that would last until the end of the ischemic event, although NaHS is known to be rapidly hydrolyzed in water, establishing equilibrium between H_2S and $S^{2-} + HS^-$ species [74].

The preconditioning phenomenon can play an important role in the attenuation of ischemic consequences as demonstrated by the modulation of angiogenic activity of ECs. We verified this hypothesis by addressing the effects of H_2S on cell migration and the ability to create capillary-like structures *in vitro*. Data showed that $1 \mu M$ NaHS pretreatment in cells that underwent IR protocol was able to rescue the defect in the migration rate, restoring the properties observed in the control-normoxic condition. This finding suggests a potential role of the gasotransmitter in promoting tissue repair following IRI.

There is still open debate about the actual *in vivo* levels of endogenous hydrogen sulfide. In order to test different

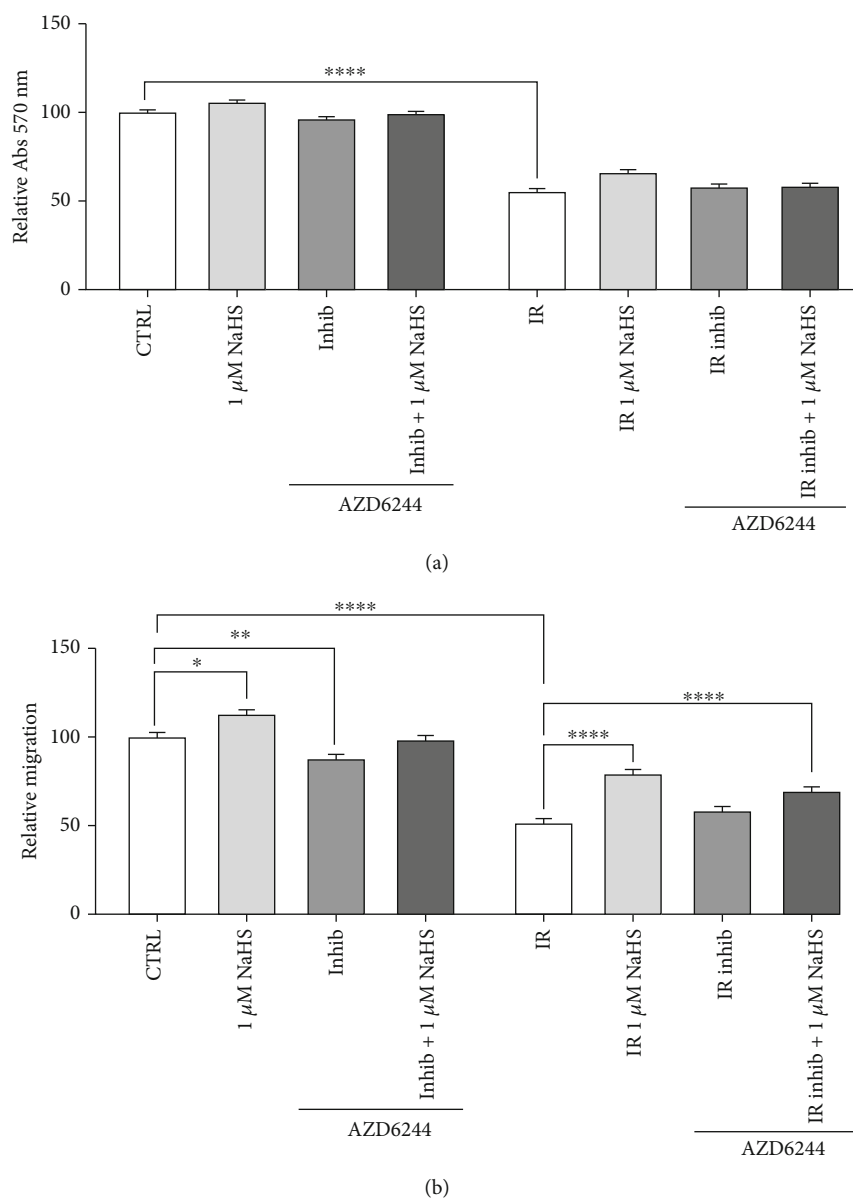


FIGURE 6: (a) Cell viability after MEK inhibition (1 μ M AZD6244) and 1 μ M NaHS preconditioning. (b) Cell migration after MEK inhibition (1 μ M AZD6244) and 1 μ M NaHS preconditioning. Statistical significance: * $p < 0.05$, ** $p < 0.01$, and **** $p < 0.0001$.

conditions, the comparison of 2 putative concentrations (1 and 10 μ M) can help decipher the biological effects of constitutive deficiency. Low levels, 1 μ M NaHS, restored the physiological condition in cell migration, whereas 10 μ M gave a less intense increase in consistency with previously described bimodal activities shown in other cell types [44]. These data contribute to the hypothesis that endogenous and exogenous H_2S , and their respective levels, might have opposite effects on some important cellular functions.

Gouvern et al. suggest that exogenous H_2S could function as an electron donor and as a potential inorganic energy source in mammalian cells at low micromolar concentrations [75]. The described mitoprotectant behavior could involve mitochondrial biogenesis and dynamics, as demonstrated in an endothelial model of rat aortic endothelial cells (RAEC) in which exogenous H_2S exerts antifission and promitophagy

effects when compared to the control in which endogenous H_2S is modulated [76]. An enhanced mitophagy could explain diminished mitochondrial content in preconditioned I/R cells compared to the untreated control (Figure 4).

Despite the decrease in the mitochondrial mass, the ratio of functional mitochondria was enhanced in cells pretreated with NaHS. These data could be explained by an H_2S -mediated enhancement of mitochondrial function and its suggested role of ROS scavenger.

The next step was to understand whether a 24-hour preconditioning could trigger a modulation of ERK phosphorylation, because of the role that the MEK/ERK pathway has in endothelial cell migration, other than apoptosis. Most interestingly, IR alone significantly enhanced ERK1/2 phosphorylation, while 1 μ M NaHS treatment managed to drastically reduce this effect, going towards a more physiological

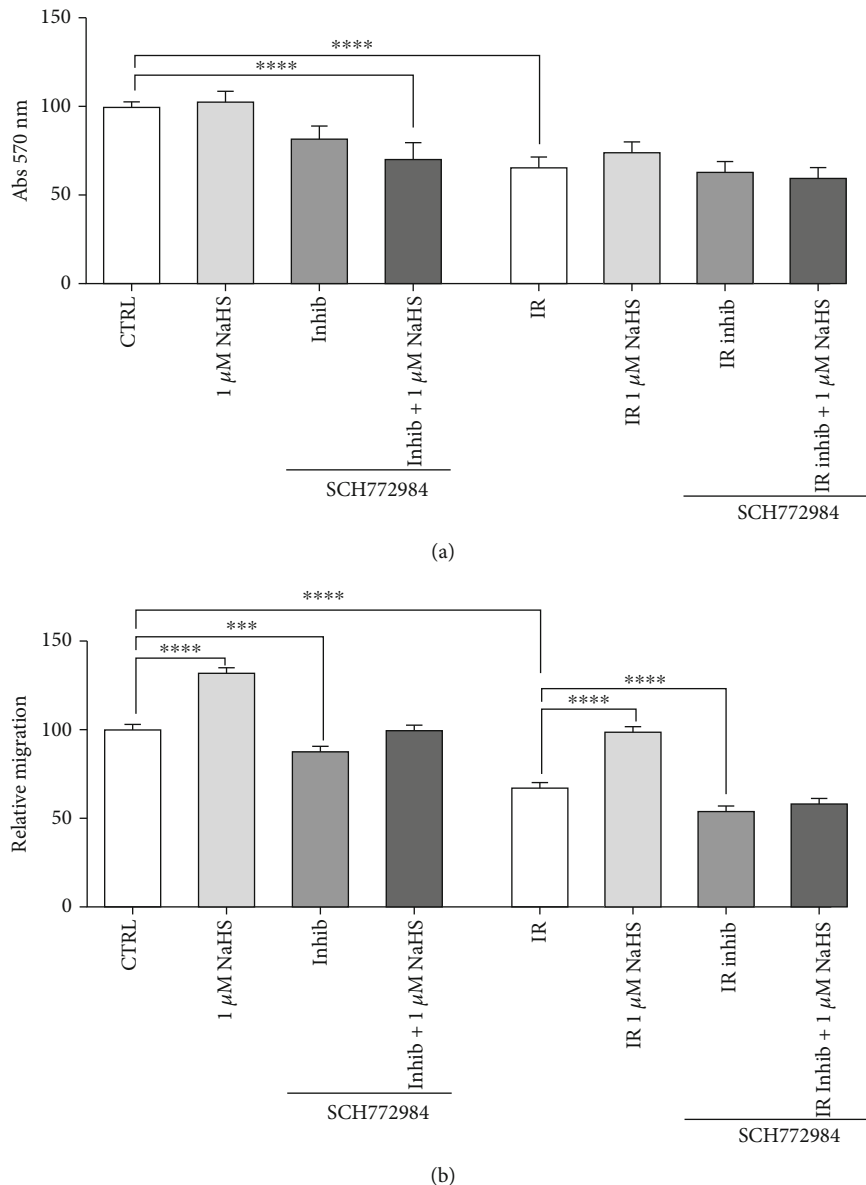


FIGURE 7: (a) Normalized viability after direct ERK1/2 inhibition (1 μ M SCH772984) and 1 μ M NaHS preconditioning. (b) Cell migration on 1 μ M NaHS preconditioned cells after ERK1/2 inhibition (1 μ M SCH772984). Statistical significance: ** $p < 0.01$, *** $p < 0.001$, and **** $p < 0.0001$.

(CTRL) phosphorylation state. On the other hand, the treatment did not affect ERK1/2 phosphorylation in normoxic cells.

Last, since it appeared that ERK was modulated by the NaHS treatment, we inhibited both ERK1/2 and its upstream activator, MEK, with the selective inhibitors AZD6244 and SCH772984. After testing the effects on cell viability and cell migration, we observed that the direct inhibition of ERK, but not MEK, decreased cell migration and could not be rescued by H₂S treatment, thus indicating that H₂S modulates the ERK pathway acting at the level of ERK phosphorylation.

Further experiments are needed to better describe the involvement of this pathway activated 24 hours ahead of the ischemic insult and how it is sustained over time. Moreover, it might be interesting to see whether the same concen-

trations could trigger similar effects in the postconditioning window and what similarities the pre- and postconditioning scenarios might have in common.

5. Conclusion

In our study, we showed that, despite its rapid metabolization, H₂S could be used as a long-term preconditioning agent to ameliorate the effects of IRI. Moreover, this work is aimed at investigating the role of H₂S as a modulator of an ERK1/2-dependent pathway, thus suggesting an important role for microvascular endothelial cells to participate in the response to ischemia/reperfusion injury. A deeper comprehension of endothelial cells in this context can contribute to design

better strategies to preserve and repair tissues after a hypoxic/ischemic insult.

Data Availability

All the data used to support the findings of this study are included within the article.

Conflicts of Interest

The authors declare no conflict of interest.

Authors' Contributions

E.Z. was responsible for conceptualization; E.Z. was responsible for methodology; E.Z. and E.A. were responsible for software; E.Z. and E.A. were responsible for validation; E.Z. and E.A. were responsible for formal analysis; E.Z. and D.M. were responsible for investigation; E.Z. and E.A. were responsible for data curation; E.Z. and E.A. were responsible for writing—original draft preparation; E.Z., E.A., and D.M. were responsible for writing—review and editing; D.M. was responsible for supervision; D.M. was responsible for funding acquisition. All authors have read and agreed to the published version of the manuscript.

Acknowledgments

The authors would like to thank the constant support given by Dr. Tullio Genova and the Laboratory of Cellular and Molecular Angiogenesis, led by Prof. Luca Munaron (University of Turin). We would also like to thank Prof. Luca Primo and his group (IRCCS Institute, Candiolo—University of Turin) for their support. This research was funded by “Fondo Finanziamento delle Attività Base di Ricerca” and “Fondo Ricerca Locale” 2018, 2019, and 2020.

References

- [1] S. S. Virani, A. Alonso, E. J. Benjamin et al., “Heart disease and stroke statistics-2020 update: a report from the American Heart Association,” *Circulation*, vol. 141, no. 9, pp. e139–e596, 2020.
- [2] D. M. Yellon and D. J. Hausenloy, “Myocardial reperfusion injury,” *The New England Journal of Medicine*, vol. 357, no. 11, pp. 1121–1135, 2007.
- [3] Q. Yang, G. W. He, M. J. Underwood, and C. M. Yu, “Cellular and molecular mechanisms of endothelial ischemia/reperfusion injury: perspectives and implications for postischemic myocardial protection,” *American Journal of Translational Research*, vol. 8, no. 2, pp. 765–777, 2016.
- [4] A. Kiss, S. Heber, A.-M. Kramer et al., “MicroRNA expression profile changes after cardiopulmonary bypass and ischemia/reperfusion-injury in a porcine model of cardioplegic arrest,” *Diagnostics*, vol. 10, no. 4, p. 240, 2020.
- [5] E. Bassenge, “Endothelial function in different organs,” *Progress in Cardiovascular Diseases*, vol. 39, no. 3, pp. 209–228, 1996.
- [6] P. F. Davies, “Flow-mediated endothelial mechanotransduction,” *Physiological Reviews*, vol. 75, no. 3, pp. 519–560, 1995.
- [7] Y. Nakamura, S. Saito, S. Miyagawa et al., “Perioperative ischaemic reperfusion injury and allograft function in the early post-transplantation period,” *Interactive Cardiovascular and Thoracic Surgery*, vol. 29, no. 2, pp. 230–236, 2019.
- [8] A. T. Turer and J. A. Hill, “Pathogenesis of myocardial ischemia-reperfusion injury and rationale for therapy,” *The American Journal of Cardiology*, vol. 106, no. 3, pp. 360–368, 2010.
- [9] R. O. S. Soares, D. M. Losada, M. C. Jordani, P. Évora, and O. Castro-E-Silva, “Ischemia/reperfusion injury revisited: an overview of the latest pharmacological strategies,” *International Journal of Molecular Sciences*, vol. 20, no. 20, p. 5034, 2019.
- [10] H. M. Piper, D. García-Dorado, and M. Ovize, “A fresh look at reperfusion injury,” *Cardiovascular Research*, vol. 38, no. 2, pp. 291–300, 1998.
- [11] T. M. Griffith, D. H. Edwards, M. J. Lewis, A. C. Newby, and A. H. Henderson, “The nature of endothelium-derived vascular relaxant factor,” *Nature*, vol. 308, no. 5960, pp. 645–647, 1984.
- [12] L. J. Ignarro, “Biological actions and properties of endothelium-derived nitric oxide formed and released from artery and vein,” *Circulation Research*, vol. 65, no. 1, pp. 1–21, 1989.
- [13] S. Moncada, R. M. Palmer, and E. A. Higgs, “Nitric oxide: physiology, pathophysiology, and pharmacology,” *Pharmacological Reviews*, vol. 43, no. 2, pp. 109–142, 1991.
- [14] J. S. Pober and R. S. Cotran, “Cytokines and endothelial cell biology,” *Physiological Reviews*, vol. 70, no. 2, pp. 427–451, 1990.
- [15] J. R. Vane, “The Croonian Lecture, 1993. The endothelium: maestro of the blood circulation,” *Philosophical Transactions of the Royal Society of London. Series B: Biological Sciences*, vol. 343, no. 1304, pp. 225–246, 1994.
- [16] M. Yanagisawa, H. Kurihara, S. Kimura et al., “A novel potent vasoconstrictor peptide produced by vascular endothelial cells,” *Nature*, vol. 332, no. 6163, pp. 411–415, 1988.
- [17] P. S. Tsao, N. Aoki, D. J. Lefer, G. Johnson, and A. M. Lefer, “Time course of endothelial dysfunction and myocardial injury during myocardial ischemia and reperfusion in the cat,” *Circulation*, vol. 82, no. 4, pp. 1402–1412, 1990.
- [18] A. M. Lefer, P. S. Tsao, D. J. Lefer, and X. L. Ma, “Role of endothelial dysfunction in the pathogenesis of reperfusion injury after myocardial ischemia,” *The FASEB Journal*, vol. 5, no. 7, pp. 2029–2034, 1991.
- [19] V. Richard, N. Kaeffer, C. Tron, and C. Thuillez, “Ischemic preconditioning protects against coronary endothelial dysfunction induced by ischemia and reperfusion,” *Circulation*, vol. 89, no. 3, pp. 1254–1261, 1994.
- [20] A. K. Singhal, J. D. Symons, S. Boudina, B. Jaishy, and Y.-T. Shiu, “Role of endothelial cells in myocardial ischemia-reperfusion injury,” *Vascular Disease Prevention*, vol. 7, no. 1, pp. 1–14, 2010.
- [21] D. J. Hausenloy and D. M. Yellon, “Ischaemic conditioning and reperfusion injury,” *Nature Reviews. Cardiology*, vol. 13, no. 4, pp. 193–209, 2016.
- [22] S. Hernández-reséndiz, M. Muñoz-vega, W. E. Contreras, and G. E. Crespo, “Responses of endothelial cells towards ischemic conditioning following acute myocardial infarction,” *Conditioning Medicine*, vol. 1, pp. 247–258, 2018.
- [23] J. Hofmann, G. Otashvili, A. Meszaros et al., “Restoring mitochondrial function while avoiding redox stress: the key

- to preventing ischemia/reperfusion injury in machine perfused liver grafts?" *International Journal of Molecular Sciences*, vol. 21, no. 9, p. 3132, 2020.
- [24] M. Yadav, P. Kumari, V. Yadav, and S. Kumar, "Pharmacological preconditioning with phosphodiesterase inhibitor: an answer to stem cell survival against ischemic injury through JAK/STAT signaling," *Heart Failure Reviews*, vol. 25, no. 2, pp. 355–366, 2020.
- [25] C. Rocca, S. Femminò, G. Aquila et al., "Notch1 mediates preconditioning protection induced by GPER in normotensive and hypertensive female rat hearts," *Frontiers in Physiology*, vol. 9, p. 521, 2018.
- [26] D. L. Brutsaert, "Cardiac endothelial-myocardial signaling: its role in cardiac growth, contractile performance, and rhythmicity," *Physiological Reviews*, vol. 83, no. 1, pp. 59–115, 2003.
- [27] H. Yu, T. Kalogeris, and R. J. Korthuis, "Reactive species-induced microvascular dysfunction in ischemia/reperfusion," *Free Radical Biology & Medicine*, vol. 135, pp. 182–197, 2019.
- [28] A. M. van der Laan, J. J. Piek, and N. van Royen, "Targeting angiogenesis to restore the microcirculation after reperfused MI," *Nature Reviews. Cardiology*, vol. 6, no. 8, pp. 515–523, 2009.
- [29] A. M. Shah and D. L. Mann, "In search of new therapeutic targets and strategies for heart failure: recent advances in basic science," *The Lancet*, vol. 378, no. 9792, pp. 704–712, 2011.
- [30] P. Carmeliet, Y.-S. Ng, D. Nuyens et al., "Impaired myocardial angiogenesis and ischemic cardiomyopathy in mice lacking the vascular endothelial growth factor isoforms VEGF164 and VEGF188," *Nature Medicine*, vol. 5, no. 5, pp. 495–502, 1999.
- [31] P. Di Napoli, A. Di Crecchio, G. Contegiacomo et al., "Endothelial protective effect of verapamil against acute myocardial contractile dysfunction in isolated working rat hearts subjected to global ischemia," *Annals of the New York Academy of Sciences*, vol. 853, no. 1 CARDIAC SARCO, pp. 311–315, 1998.
- [32] X. Zhang and J.-S. Bian, "Hydrogen sulfide: a neuromodulator and neuroprotectant in the central nervous system," *ACS Chemical Neuroscience*, vol. 5, no. 10, pp. 876–883, 2014.
- [33] H. Kimura, *Hydrogen sulfide: its production, release and functions*, vol. 41, Springer Vienna, 2011.
- [34] G. I. Lobov, I. B. Sokolova, O. P. Gorshkova, M. E. Shvetsova, and D. P. Dvoretiskii, "Contribution of hydrogen sulfide to dilation of rat cerebral arteries after ischemia/reperfusion injury," *Bulletin of Experimental Biology and Medicine*, vol. 168, no. 5, pp. 597–601, 2020.
- [35] L. Zhang, Y. Wang, Y. Li et al., "Hydrogen sulfide (H₂S)-releasing compounds: therapeutic potential in cardiovascular diseases," *Frontiers in Pharmacology*, vol. 9, 2018.
- [36] B. Geng, J. Yang, Y. Qi et al., "H₂S generated by heart in rat and its effects on cardiac function," *Biochemical and Biophysical Research Communications*, vol. 313, no. 2, pp. 362–368, 2004.
- [37] J. W. Elrod, J. W. Calvert, J. Morrison et al., "Hydrogen sulfide attenuates myocardial ischemia-reperfusion injury by preservation of mitochondrial function," *Proceedings of the National Academy of Sciences*, vol. 104, no. 39, pp. 15560–15565, 2007.
- [38] L.-L. Yao, X.-W. Huang, Y.-G. Wang, Y.-X. Cao, C.-C. Zhang, and Y.-C. Zhu, "Hydrogen sulfide protects cardiomyocytes from hypoxia/reoxygenation-induced apoptosis by preventing GSK-3 β -dependent opening of mPTP," *American Journal of Physiology-Heart and Circulatory Physiology*, vol. 298, no. 5, pp. H1310–H1319, 2010.
- [39] D. Hausenloy and D. M. Yellon, "New directions for protecting the heart against ischaemia-reperfusion injury: targeting the reperfusion injury salvage kinase (RISK)-pathway," *Cardiovascular Research*, vol. 61, no. 3, pp. 448–460, 2004.
- [40] D. M. Yellon and D. J. Hausenloy, "Realizing the clinical potential of ischemic preconditioning and postconditioning," *Nature Clinical Practice. Cardiovascular Medicine*, vol. 2, no. 11, pp. 568–575, 2005.
- [41] X. Rossello and D. M. Yellon, "The RISK pathway and beyond," *Basic Research in Cardiology*, vol. 113, no. 1, p. 2, 2018.
- [42] Y. Hu, X. Chen, T. T. Pan et al., "Cardioprotection induced by hydrogen sulfide preconditioning involves activation of ERK and PI3K/Akt pathways," *Pflügers Archiv - European Journal of Physiology*, vol. 455, no. 4, pp. 607–616, 2007.
- [43] K. Módis, C. Coletta, K. Erdélyi, A. Papapetropoulos, and C. Szabo, "Intramitochondrial hydrogen sulfide production by 3-mercaptopyruvate sulfurtransferase maintains mitochondrial electron flow and supports cellular bioenergetics," *The FASEB Journal*, vol. 27, no. 2, pp. 601–611, 2013.
- [44] E. Pupo, A. Fiorio Pla, D. Avanzato et al., "Hydrogen sulfide promotes calcium signals and migration in tumor-derived endothelial cells," *Free Radical Biology & Medicine*, vol. 51, no. 9, pp. 1765–1773, 2011.
- [45] G. K. Kolluru, X. Shen, and C. G. Kevil, "A tale of two gases: NO and H₂S, foes or friends for life?," *Redox Biology*, vol. 1, no. 1, pp. 313–318, 2013.
- [46] H. J. Sun, Z. Y. Wu, X. W. Nie, and J. S. Bian, "Role of endothelial dysfunction in cardiovascular diseases: the link between inflammation and hydrogen sulfide," *Frontiers in Pharmacology*, vol. 10, 2020.
- [47] A. Katsouda, S. I. Bibli, A. Pyriochou, C. Szabo, and A. Papapetropoulos, "Regulation and role of endogenously produced hydrogen sulfide in angiogenesis," *Pharmacological Research*, vol. 113, Part A, pp. 175–185, 2016.
- [48] F. Lin, Y. Yang, S. Wei et al., "Hydrogen sulfide protects against high glucose-induced human umbilical vein endothelial cell injury through activating PI3K/Akt/eNOS pathway," *Drug Design, Development and Therapy*, vol. 14, pp. 621–633, 2020.
- [49] S. A. Banu, S. Ravindran, and G. A. Kurian, "Hydrogen sulfide post-conditioning preserves inter-fibrillar mitochondria of rat heart during ischemia reperfusion injury," *Cell Stress & Chaperones*, vol. 21, no. 4, pp. 571–582, 2016.
- [50] N. A. Garcia, J. Moncayo-Arlandi, A. Vazquez et al., "Hydrogen sulfide improves cardiomyocyte function in a cardiac arrest model," *Annals of Transplantation*, vol. 22, pp. 285–295, 2017.
- [51] L. Boyman, G. S. B. Williams, A. P. Wescott, J. B. Leach, J. P. Y. Kao, and W. J. Lederer, "Real-time local oxygen measurements for high resolution cellular imaging," *Journal of Molecular and Cellular Cardiology*, vol. 127, pp. 97–104, 2019.
- [52] A. Burgess, S. Vigneron, E. Brioudes, J. C. Labbé, T. Lorca, and A. Castro, "Loss of human Greatwall results in G2 arrest and multiple mitotic defects due to deregulation of the cyclin B-Cdc2/PP2A balance," *Proceedings of the National Academy of Sciences of the United States of America*, vol. 107, no. 28, pp. 12564–12569, 2010.
- [53] C. Penna, D. Mancardi, S. Raimondo, S. Geuna, and P. Pagliaro, "The paradigm of postconditioning to protect the heart," *Journal of Cellular and Molecular Medicine*, vol. 12, no. 2, pp. 435–458, 2008.

- [54] H. Takagi, Y. Matsui, and J. Sadoshima, "The role of autophagy in mediating cell survival and death during ischemia and reperfusion in the heart," *Antioxidants & Redox Signaling*, vol. 9, no. 9, pp. 1373–1382, 2007.
- [55] J. Vinten-Johansen, A. Granfeldt, J. Mykytenko, V. V. Undyala, Y. Dong, and K. Przyklenk, "The multidimensional physiological responses to postconditioning," *Antioxidants & Redox Signaling*, vol. 14, no. 5, pp. 791–810, 2011.
- [56] D. J. Hausenloy, E. Boston-Griffiths, and D. M. Yellon, "Cardioprotection during cardiac surgery," *Cardiovascular Research*, vol. 94, no. 2, pp. 253–265, 2012.
- [57] A. N. Nowbar, M. Gitto, J. P. Howard, D. P. Francis, and R. Al-Lamee, "Mortality from ischemic heart disease," *Circulation. Cardiovascular Quality and Outcomes*, vol. 12, no. 6, p. e005375, 2019.
- [58] D. L. Carden and D. N. Granger, "Pathophysiology of ischaemia-reperfusion injury," *The Journal of Pathology*, vol. 190, no. 3, pp. 255–266, 2000.
- [59] M.-G. Perrelli, "Ischemia/reperfusion injury and cardioprotective mechanisms: role of mitochondria and reactive oxygen species," *World Journal of Cardiology*, vol. 3, no. 6, pp. 186–200, 2011.
- [60] D. Yang, P. Xie, and Z. Liu, "Ischemia/reperfusion-induced MKP-3 impairs endothelial NO formation via inactivation of ERK1/2 pathway," *PLoS One*, vol. 7, no. 7, p. e42076, 2012.
- [61] M.-Y. Wu, G.-T. Yiang, W.-T. Liao et al., "Current mechanistic concepts in ischemia and reperfusion injury," *Cellular Physiology and Biochemistry*, vol. 46, no. 4, pp. 1650–1667, 2018.
- [62] K. Szocs, "Endothelial dysfunction and reactive oxygen species production in ischemia/reperfusion and nitrate tolerance," *General Physiology and Biophysics*, vol. 23, no. 3, pp. 265–295, 2004.
- [63] D. Dymkowska, B. Drabarek, P. Podrzywałow-Bartnicka, J. Szczepanowska, and K. Zabłocki, "Hyperglycaemia modifies energy metabolism and reactive oxygen species formation in endothelial cells in vitro," *Archives of Biochemistry and Biophysics*, vol. 542, pp. 7–13, 2014.
- [64] E. E. Essick and F. Sam, "Oxidative stress and autophagy in cardiac disease, neurological disorders, aging and cancer," *Oxidative Medicine and Cellular Longevity*, vol. 3, no. 3, p. 177, 2010.
- [65] S. Yamazaki, Y. Fujibayashi, R. E. Rajagopalan, S. Meerbaum, and E. Corday, "Effects of staged versus sudden reperfusion after acute coronary occlusion in the dog," *Journal of the American College of Cardiology*, vol. 7, no. 3, pp. 564–572, 1986.
- [66] G. Tong, B. Zhang, X. Zhou et al., "Kappa-opioid agonist U50,488H-mediated protection against heart failure following myocardial ischemia/reperfusion: dual roles of heme oxygenase-1," *Cellular Physiology and Biochemistry*, vol. 39, no. 6, pp. 2158–2172, 2016.
- [67] D. J. Hausenloy and D. M. Yellon, "Myocardial ischemia-reperfusion injury: a neglected therapeutic target," *Journal of Clinical Investigation*, vol. 123, no. 1, pp. 92–100, 2013.
- [68] A. Papapetropoulos, A. Pyriochou, Z. Altaany et al., "Hydrogen sulfide is an endogenous stimulator of angiogenesis," *Proceedings of the National Academy of Sciences of the United States of America*, vol. 106, no. 51, pp. 21972–21977, 2009.
- [69] M.-J. Wang, W.-J. Cai, N. Li, Y.-J. Ding, Y. Chen, and Y.-C. Zhu, "The hydrogen sulfide donor NaHS promotes angiogenesis in a rat model of hind limb ischemia," *Antioxidants & Redox Signaling*, vol. 12, no. 9, pp. 1065–1077, 2010.
- [70] R. Wang, "Two's company, three's a crowd: can H₂S be the third endogenous gaseous transmitter?," *The FASEB Journal*, vol. 16, no. 13, pp. 1792–1798, 2002.
- [71] I. Andreadou, E. K. Iliodromitis, T. Rassaf, R. Schulz, A. Papapetropoulos, and P. Ferdinandy, "The role of gasotransmitters NO, H₂S and CO in myocardial ischaemia/reperfusion injury and cardioprotection by preconditioning, postconditioning and remote conditioning," *British Journal of Pharmacology*, vol. 172, no. 6, pp. 1587–1606, 2015.
- [72] D. Mancardi, A. Florio Pla, F. Moccia, F. Tanzi, and L. Munaron, "Old and new gasotransmitters in the cardiovascular system: focus on the role of nitric oxide and hydrogen sulfide in endothelial cells and cardiomyocytes," *Current Pharmaceutical Biotechnology*, vol. 12, no. 9, pp. 1406–1415, 2011.
- [73] D. Mancardi, C. Penna, A. Merlino, P. Del Soldato, D. A. Wink, and P. Pagliaro, "Physiological and pharmacological features of the novel gasotransmitter: hydrogen sulfide," *Biochimica et Biophysica Acta*, vol. 1787, no. 7, pp. 864–872, 2009.
- [74] M. N. Hughes, M. N. Centelles, and K. P. Moore, "Making and working with hydrogen sulfide," *Free Radical Biology and Medicine*, vol. 47, no. 10, pp. 1346–1353, 2009.
- [75] M. Gubern, M. Andriamihaja, T. Nübel, F. Blachier, and F. Bouillaud, "Sulfide, the first inorganic substrate for human cells," *The FASEB Journal*, vol. 21, no. 8, pp. 1699–1706, 2007.
- [76] N. Liu, J. Wu, L. Zhang et al., "Hydrogen sulphide modulating mitochondrial morphology to promote mitophagy in endothelial cells under high-glucose and high-palmitate," *Journal of Cellular and Molecular Medicine*, vol. 21, no. 12, pp. 3190–3203, 2017.

Research Article

Atrial Dyssynchrony Measured by Strain Echocardiography as a Marker of Proarrhythmic Remodeling and Oxidative Stress in Cardiac Surgery Patients

Francisco J. Sánchez ^{1,2}, Valeria A. Gonzalez,³ Martin Farrando,² Ariel O. Baigorria Jayat,² Margarita Segovia-Roldan ⁴, Laura García-Mendivil ⁴, Laura Ordovás ^{4,5}, Natalia J. Prado ⁶, Esther Pueyo ^{4,7} and Emiliano R. Diez ^{1,6}

¹Department of Morphophysiology, School of Medicine, National University of Cuyo, Centro Universitario, Mendoza 5500, Argentina

²Department of Cardiovascular Surgery, Clinic of Cuyo, Mendoza 5500, Argentina

³Department of Cardiology, Lagomaggiore Hospital, Mendoza 5500, Argentina

⁴Biomedical Signal Interpretation and Computational Simulation (BSICoS), Aragon Institute of Engineering Research (I3A), University of Zaragoza Instituto de Investigación Sanitaria (IIS), Zaragoza 50018, Spain

⁵Aragon Agency for Research and Development (ARAID), Zaragoza 50018, Spain

⁶Institute of Experimental Medicine and Biology of Cuyo (IMBECU)-CONICET, Mendoza 5500, Argentina

⁷Biomedical Research Networking Center in Bioengineering, Biomaterials and Nanomedicine (CIBER-BBN), Zaragoza 50018, Spain

Correspondence should be addressed to Emiliano R. Diez; diez.emiliano@fcm.uncu.edu.ar

Received 22 September 2020; Revised 12 November 2020; Accepted 20 November 2020; Published 30 December 2020

Academic Editor: Laura Sartiani

Copyright © 2020 Francisco J. Sánchez et al. This is an open access article distributed under the Creative Commons Attribution License, which permits unrestricted use, distribution, and reproduction in any medium, provided the original work is properly cited.

Aging leads to structural and electrophysiological changes that increase the risk of postoperative atrial arrhythmias; however, noninvasive preoperative markers of atrial proarrhythmic conditions are still needed. This study is aimed at assessing whether interatrial dyssynchrony determined using two-dimensional speckle tracking echocardiography relates to proarrhythmic structural and functional remodeling. A cohort of 45 patients in sinus rhythm referred for cardiac surgery was evaluated by echocardiography and surface electrocardiogram the day before the intervention. Transmembrane potential, connexin, and potassium channel distribution, inflammatory, and nitrooxidative markers were measured from right atrial tissue obtained from patients. A difference greater than 40 milliseconds between right and left atrial free wall contraction confirmed the presence of interatrial dyssynchrony in 21 patients. No difference in relation with age, previous diseases, and 2-dimensional echocardiographic findings as well as average values of global longitudinal right and left atrial strain were found between synchronic and dyssynchronic patients. Postoperative atrial fibrillation incidence increased from 8.3% in the synchronic group to 33.3% in the dyssynchronic ones. P wave duration showed no difference between groups. Action potentials from dyssynchronous patients decreased in amplitude, maximal rate of depolarization, and hyperpolarized. Duration at 30% of repolarization increased, being markedly shorter at 90% of repolarization. Only the dyssynchronous group showed early and delayed afterdepolarizations. Atrial tissue of dyssynchronous patients displayed lateralization of connexin 40 and increased connexin 43 expression and accumulation of tumor necrosis factor- α in the intercalated disc. Tumor necrosis factor- α did not colocalize, however, with lateralized connexin 40. Nitrooxidative marks and K_{ATP} channels increased perivascularly and in myocytes. Our results demonstrate that, as compared to a traditional surface electrocardiogram, the novel noninvasive echocardiographic evaluation of interatrial dyssynchrony provides a better identification of nonaged-related proarrhythmic atrial remodeling with increased susceptibility to postoperative atrial fibrillation.

1. Introduction

Arrhythmias usually complicate cardiovascular surgery, and aging is the main risk factor. Atrial fibrillation is the most frequent sustained arrhythmia with a peak of appearance between the second and fifth days of the postoperative stay [1]. Its incidence progressively increases from 18% in sexagenarians to 50% in octogenarians [2]. Arrhythmic events are usually self-limited, and treatment frequently restores sinus rhythm. However, postoperative atrial fibrillation (POAF) prolongs hospital stay and increases the risk of stroke and mortality [1].

Atrial aging is an elusive prooxidative and proarrhythmic condition. Oxidative stress, hyperadrenergic states, and inflammation contribute to age-related atrial remodeling, but these tissue alterations are challenging to identify noninvasively [3, 4]. In this context, atrial enlargement, stiffness, and conduction blockade are known risk factors, but they are present in only a few patients. Therefore, the mechanisms involved in the onset and perpetuation of POAF are difficult to foresee [5]. Additionally, surgery *per se* facilitates arrhythmias due to ischemia-reperfusion injury, which increases the preexisting oxidative stress state. The lack of tools to estimate the proarrhythmic substrate evidences the absence of preventive interventions.

Structure and function of the beating heart can reveal atrial hidden oxidation and inflammation. Signs of tissue remodeling, before dilatation, arise from atrial dynamic cyclic changes. New echocardiographic techniques like strain and strain rate represent the magnitude and rate of myocardial deformation. Strain can reflect distensibility and atrial contractility [6]. Nonmyocytic cells and extracellular matrix mainly affect distensibility [7]. Cardiomyocyte structure and intercellular communication determine contractile function. Each atrial segment follows a trajectory during the cardiac cycle representative of the tissue physiology [8]. Electrical remodeling involves alterations in both myocytes and nonmyocytic cells, which manifest as contractile dyssynchrony in the echocardiogram, in a similar way as reported for the ventricles [9].

Gap junctions in the heart provide low resistance pathways for propagating the action potential across the myocardium, contributing to electrical coupling and signal propagation [10]. Alteration of cardiomyocyte gap junctions and their main components, connexins (Cx), has been suggested to contribute to the formation of arrhythmias, including atrial fibrillation [11–13]. Accumulating evidence also suggests that inflammation and oxidative stress are involved in atrial remodeling. Detection of protein 3-nitrotyrosine is regarded as a marker of nitrooxidative stress and is observed especially in inflammatory processes. The reaction of peroxynitrite with tyrosine leads to the formation of 3-nitrotyrosine and promotes protein, lipid, and DNA damage [14, 15]. ATP-regulated potassium channels (K_{ATP}) are well-characterized metabolic and oxidative sensors in ischemia/reperfusion arrhythmias and here postulated as an interesting substrate of POAF [16].

This study is aimed at assessing whether interatrial dyssynchrony, determined by using two-dimensional speckle

tracking echocardiography, relates to proarrhythmic structural and functional remodeling of the atria and whether this increases the susceptibility for POAF.

2. Materials and Methods

2.1. Subjects and Ethical Considerations. Patients with coronary artery disease, aortic stenosis, or the combination of both pathologies, scheduled for surgery at the Department of Cardiac Surgery (Clinic of Cuyo, Mendoza, Argentina), were prospectively enrolled between January 2018 and March 2020. Coronary disease and aortic valve stenosis severity were defined according to current ESC Guidelines to determine surgery indication [17, 18]. All subjects provided written informed consent under the research protocol approved by the Ethics Committee of the National University of Cuyo (Exp-Cuy: 22959/2017).

Clinical data including age, gender, and history of previous myocardial infarction and heart failure was collected. The presence of preoperative atrial fibrillation was determined according to previous electrocardiographic reports or diagnosis in medical history. Information regarding the following cardiovascular risk factors was collected: hypertension, dyslipidemia (low-density lipoprotein cholesterol above 100 mg/dL or the use of lipid-lowering drugs), smoking (current or any smoking habit in the past ten years), and diabetes mellitus (previous diagnosis of diabetes mellitus or glycated hemoglobin greater than 6.5%). The preoperative use of medications was also documented.

2.2. Inclusion and Exclusion Criteria. Patients over 18 years of age in sinus rhythm with an indication of cardiovascular surgery that gave written informed consent were included in the study. Exclusion criteria were as follows: indication of mitral or tricuspid valve repair or replacement, being older than 80 years, history of previous atrial fibrillation, presence of moderate valvular disease or valvular prosthesis, history of congenital cardiac abnormalities or cardiac tumors, emergency surgery, inability to provide informed consent, and a not entirely detectable left and right atrial profile from the apical four-chamber view during preoperative echocardiography.

2.3. Preoperative Electrocardiogram. Before surgery, patients underwent a 12-lead electrocardiogram (ECG) using the Synchronous ECG software V1.3.5. Measurement in milliseconds of the P wave and the PR segment was performed with the software caliper. According to the current classification, these patients were evaluated for the presence of an interatrial conduction disturbance called Bayes syndrome [19]. There are two major categories for this syndrome: complete and incomplete, both based on P wave duration and morphology in the 12-lead ECG.

2.4. Echocardiography and Atrial Strain. All patients were imaged in a left lateral decubitus position using ESAOTE ultrasound system equipment (MyLab30Gold Cardiovascular) with a 2–4 MHz/PA240 probe. Two-dimensional speckle tracking strain imaging was performed from the apical position by an experienced technician. The average frame rate for analysis was 60–80 frames/s. During a single breath-hold,

three consecutive cardiac cycles were stored digitally for off-line analysis in the four-, two-, and three-chamber view. The entire right and left atriums were carefully visualized to prevent walls' dropout.

Measurements focused on evaluating the indexed volume of the left atrium and the area of the right atrium. In the parasternal long-axis or short-axis view, M-mode of the left ventricle chamber was measured for diameter and wall thickness. In the apical 4-chamber view, the left ventricle ejection fraction was determined using the Simpson measurement. Mitral and tricuspid inflows were recorded at the tip of the valve leaflets. The peak velocities of early and late diastolic filling waves (E wave and A wave) and the E/A velocity ratio were measured. The e velocity was obtained by tissue Doppler averaging the lateral and septal mitral annulus values and the e wave of the tricuspid lateral wall. E/e' values were obtained from both ventricles.

Strain and strain rate datasets were analyzed using a wall motion tracking software (ESAOTE MyLab). In apical views (4-chamber, 3-chamber, and 2-chamber), left atrial endocardial boundaries were manually measured at the end-diastolic phase. Right atria were only registered in the 4-chamber view. The values of the reservoir, conduit, and atrial contraction strain were recorded according to the EACVI/ASE/Industry Task Force to standardize deformation imaging [20]. The values of strain rate for the reservoir phase, the conduit, and contraction phases were also recorded (Figure 1). The same was also done in 4 chambers for the right atrium. The left atrium was subsequently divided into basal, medial, and roof atrial segments. This determined a total of 15 segments for the left atria when the 3 apical views were added. The right atrium was evaluated similarly, but only the lateral segments were taken into account, adding 3 more segments, thus making a total of 18 segments. Septal segments were considered as left atria.

Deformation rate time (DRT) was recorded from the beginning of the P wave in the ECG to the maximum deflection of the atrial contraction in the strain rate for each of the segments, as indicated in Figures 1(a) and 1(e).

To determine interatrial synchrony, an adaptation of atrial strain was performed to evaluate the right and left atrial walls at the same time. This new evaluation was called "Omega" (ω) because of the form the strain takes in the images. Here, the maximal time difference between the strain rate contraction peaks of both right and left atrial lateral walls was recorded (Figure 2). Blinded analysis of the echocardiograms was performed by two independent researchers (FJS and VAG).

2.5. Atrial Transmembrane Potential. Right atrium samples taken in the operating room were transferred within 15 to 20 minutes to the laboratory using a cold oxygenated Ringer-type solution with albumin. Upon arrival, all samples were dissected into smaller pieces, pinned at the bottom of a perfusion chamber with the endocardial surface facing up, and continuously superfused with a modified Krebs-Henseleit solution containing (in mM): 121 NaCl, 25 NaHCO₃, 1.2 Na₂HPO₄, 5 KCl, 2 CaCl₂, 1.2 MgSO₄, and 11 glucose. Once equilibrated with 5% CO₂ in O₂ at 36.5 ± 0.5°C, the pH of the solution was 7.4 ± 0.02.

The membrane potential was recorded with flexibly mounted glass microelectrodes from subendocardial trabecular atrial cells. Microelectrodes were filled with 3 mM KCl and had resistances of 10–15 MΩ. After 20 to 30 minutes of stabilization, we continuously obtained epicardial transmembrane potential using a custom-made microelectrode amplifier. The signals were digitized with an analog-to-digital converter (NI PCI-6221; National Instruments, Austin, Texas) and recorded using LabView SignalExpress 2.5 (National Instruments, Austin, Texas).

The following properties of the transmembrane potentials were quantified: action potential amplitude, resting potential, maximum upstroke velocity ($\Delta V/\Delta t_{\max}$), and action potential duration at 30 and 90% of repolarization. Arrhythmic events and arrhythmogenic triggers were evaluated by visual supervision of the traces blindly regarding the patient's characteristics.

2.6. Structural, Inflammatory, and Nitrooxidative Evaluation by Fluorescent Immunohistochemistry. Part of each atrial sample was fixed in a 4% paraformaldehyde solution for 1 h at 4°C before embedding in paraffin blocks. Five-micrometer-thick tissue sections were stained using the following primary antibodies or label: rabbit polyclonal anti-Cx40 (Cx40 H-116, Santa Cruz, sc-28658, dilution 1:300), rabbit polyclonal anti-Cx43 (Cx43, Abcam, ab11370, dilution 1:1000), rabbit polyclonal anti-Kir6.1 (Kir6.1, Thermo Fisher, PA5-48354, dilution 1:500), mouse monoclonal anti-TNF α (TNF α 52B83, Santa Cruz, sc-52746, dilution 1:300), mouse monoclonal antinitrotyrosine (3-nitrotyrosine, Santa Cruz, sc-32757, dilution 1:200), and mouse monoclonal anti-SERCA2a (ab2817 Abcam, dilution 1:1000). Wheat germ agglutinin (WGA) conjugated to Alexa Fluor 555 against the extracellular matrix (W32464 Thermo Fisher, dilution 1:500) and fluorescently conjugated F-actin against the intracellular content (ab112124 Abcam, dilution 1:300). The secondary antibodies were anti-rabbit conjugated with Alexa Fluor 633 and anti-mouse labeled with the Alexa Fluor 488 (Jackson ImmunoResearch Laboratories Inc., West Grove, PA, USA, dilution 1:500). Images were acquired with a confocal microscope Zeiss LSM 880 and processed with the Zen Blue 2.5 software (Carl Zeiss Microscopy GmbH, 2018).

The maximum intensity projection of 20 to 40 z stacks was used to analyze the lateralization of connexins and the integrated optical density (IOD). Lateralization was measured with an open access automated program designed by our group called MARTA [21]. This software generates cell masks, contours individual cells, and splits the cells into 4 rectangles to estimate the lateral-to-total ratio of connexins. The IOD quantified the area (>3 pixels connected) multiplied by the average intensity using the software ImageProPlus 4.5, 2001 (Media Cybernetics, Inc., Rockville, MD, USA). Values of IOD measured for 18 pictures per immunofluorescence channel were grouped after the blinded analysis was completed by two independent researchers (NJP and ERD), and the results were assigned to the corresponding groups. The values of IOD are relatively expressed to the level measured in the synchronic group.

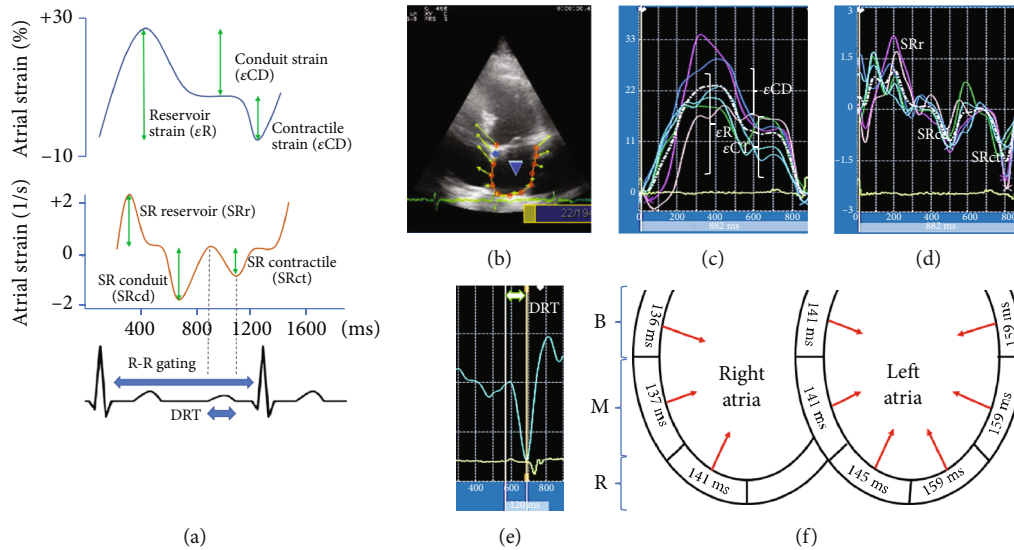


FIGURE 1: Two-dimensional atrial strain curves. (a) Atrial strain and strain rate curves and determination of atrial mechanics according to an R-R wave-timed analysis. Deformation rate time (DRT) is determined from the beginning of the P wave in the electrocardiogram to the maximum deflection of the strain rate contractile phase (STct). (b) Four-chamber view of speckle tracking left atrial strain. (c) Atrial strain curves. The white, dashed, and dotted line shows the average strain curve for the six segments of the atria in that view. (d) Atrial strain rate curves. (e) Determination of DRT in a segment of left atria. The measurement agreed with the scheme in (a). (f) Schematic four-chamber view of how DRT can show the activation in time of different segments from both atria. B: base segment; M: medium segment; R: roof segment.

2.7. Postoperative Atrial Fibrillation Detection. Continuous ECG monitoring after surgery was performed in the cardiovascular intensive care unit for 48–96 hours to detect any new onset of atrial fibrillation. Arrhythmic events of at least 1 min length were considered POAF when assessed by a monitoring system or using a 12-lead ECG in case of a symptomatic episode that required intervention.

2.8. Statistical Analysis. Qualitative variables are expressed as number and percentage. Quantitative variables are expressed as mean \pm standard deviation (SD) if they are normally distributed and median with a range if they are not normally distributed. For qualitative data, the chi-square test is used. For nonnormally distributed data, the Mann–Whitney tests are used; for normally distributed data, the Student *t*-test is used. The receiver-operating characteristic (ROC) curve analysis is performed to determine the cutoff value of atrial variables as predictors of POAF. The area under the curve and 95% confidence interval (CI) are used to determine the parameters' incremental diagnostic value. Log-rank (Mantel Cox) test is used to assess the incidence of POAF. A *p* value below 0.05 was chosen as an indicative of statistical significance. The GraphPad Prism version 9.0.0, 2020 (GraphPad Software, San Diego, CA, USA, <http://www.graphpad.com>) was used for statistical analysis.

3. Results

3.1. Postoperative Atrial Fibrillation, Patient Characteristics, and Classification regarding Interatrial Synchrony. A total of 45 patients were included in the study. Forty-one underwent coronary artery bypass surgery, three aortic valve

replacement, and one combined surgery. The mean age was 67.4 ± 7.7 years, and 69% were male. No patient was under treatment with digitalis or antiarrhythmics.

This population was divided into synchronic and dyssynchronic patients based on the difference between the activation of the lateral right and left atrial walls determined from the echocardiogram (Omega). This was used as a factor related to the incidence of POAF. A time difference greater than 40 milliseconds had a sensitivity of 88.9% and a specificity of 55.6% for identifying the atrial fibrillation events, with an area under the curve of 0.728 (95% CI 0.575–0.850) (Figure 3(a)).

Dyssynchronic patients suffered from a higher incidence of POAF. The median time of atrial fibrillation onset after surgery was 2.5 days (Figure 3(b)). All patients recovered sinus rhythm prior to discharge from hospital with the use of intravenous amiodarone. No electrical cardioversion was required.

The receiver-operating characteristic curve (ROC) of atrial echocardiographic measurements had the following areas under the curve and cutoff values: right atrial area 0.796 (95% CI 0.650–0.902), cutoff 17.6 cm^2 ; left atrial volume index 0.742 (95% CI 0.590–0.861), cutoff 29.86 mL/m^2 ; left atria contraction strain 0.645 (95% CI 0.488–0.782), cutoff 15.4%; left atrial reservoir strain 0.636 (95% CI 0.479–0.774), cutoff 30.7%. After adjusting the right atrial area, left atrial volume index, left atrial reservoir strain, and left atria contraction strain for the cutoff values, according to current guidelines, only left atrial volume index remained as predictors of postoperative atrial fibrillation (area under the curve: 0.681 95% CI 0.525–0.812), but the area under the curve was lower than the one obtained with the interatrial

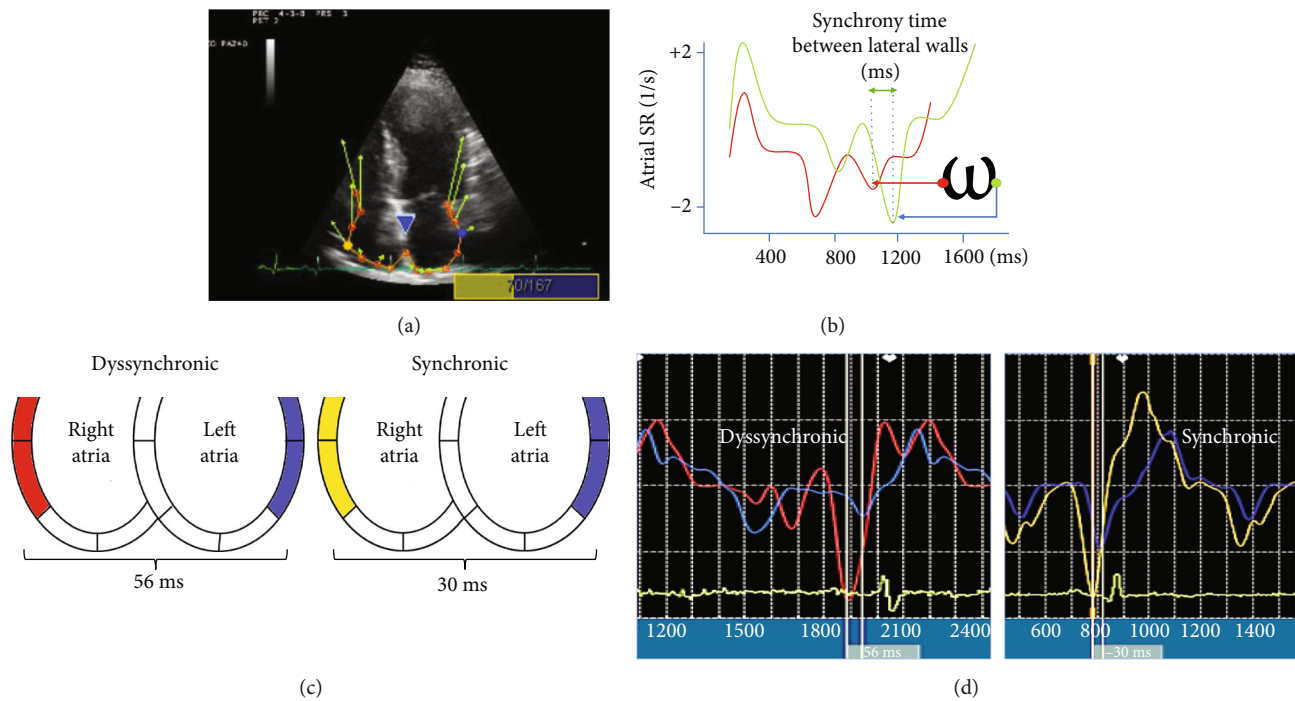


FIGURE 2: (a) Longitudinal strain echocardiography in a four-chamber view with the Omega (ω) adaptation for the analysis technique of time activation between lateral walls. Yellow and blue dots show the measured segment of the lateral wall. (b) Measurement technique to determine differences between the activation time of two segments at the lateral atrial walls, from one maximal deflection strain rate contraction of a curve to the same point in the other curve. (c) Schematic visualization in a four-chamber view with an example of the determination of time difference in activation between the lateral wall of the right and left atria. (d) Example of strain rate from right and left atrial walls in synchronic and dyssynchronic patients.

dyssynchrony [22–24]. These results supported dyssynchrony as the grouping variable for the comparisons throughout the study.

Patients in the synchronic and dyssynchronic groups did not show differences in age, type of surgery, comorbidity, risk factors, or treatment received before surgery (Table 1). The average pump time of the patients was 118 ± 39 minutes, and the clamping time was 75 ± 24 minutes, with no significant differences between groups. During the study, there was only one death from a patient in the synchronic group.

3.2. Atrial-Related ECG. P wave duration in the ECG was 125 ± 15 ms and 118 ± 12 ms in the synchronic and dyssynchronic groups, respectively ($p = 0.128$ by *t*-test). PR interval was longer in the synchronic group than in the dyssynchronic group (179 ± 32 ms vs. 160 ± 25 ms, respectively; $p = 0.044$ by Mann–Whitney test). No significant differences in Bayes syndrome incidence were found between groups ($p = 0.985$).

3.3. Echocardiography and Atrial Strain. Regarding general data from the echocardiograms, the mean ejection fraction of the left ventricle was $56.83 \pm 15.36\%$. The mean indexed volume of the left atrium was 30.78 ± 9.04 mL/m², and the area of the right atrium was 16.20 ± 3.36 cm². The E/e' ratio of the left ventricle showed a value of 8.6 ± 3.5 , which indicated end-diastole pressures at the normal upper limit in most patients (Table 2). There was no other significant difference between the groups in echocardiographic findings,

except for the left ventricular index mass. The analysis of the atrial speckle tracking strain showed no significant differences between groups in the deformation rate times corresponding to the activation of any of the 18 atrial segments (Table 3).

The rest of the usual strain analysis also showed no differences between groups (Table 4).

3.4. Action Potentials and Proarrhythmic Triggers. Action potentials from dyssynchronous patients decreased by 3.9 ± 1.9 mV in amplitude and by 66 ± 13 V/s in the maximal upstroke velocity (Figures 4(b) and 4(c)).

During the beginning of the upstroke of the action potential, we observed that a segment of the ascendent activation had a little nudge, like a foot that delayed the maximal upstroke occurrence. The resting membrane potential was hyperpolarized by 3.3 ± 1.3 mV in the atrial tissue samples from dyssynchronic patients. The action potential duration at 30% of repolarization increased by 4.0 ± 0.7 ms but markedly shortened when measured at 90% of repolarization by 107 ± 12 ms. Only action potentials from synchronic patients displayed a plateau and slow repolarization typical of a standard atrial action potential. Early and delayed afterdepolarizations were only observed in the dyssynchronic group.

3.5. Atrial Remodeling, Inflammation, and Nitrooxidative Stress. Cx40 lateralization increased by 9.81% (95% CI of difference 7.71–10.93) in samples from dyssynchronic patients with respect to synchronic ones (Figure 5).

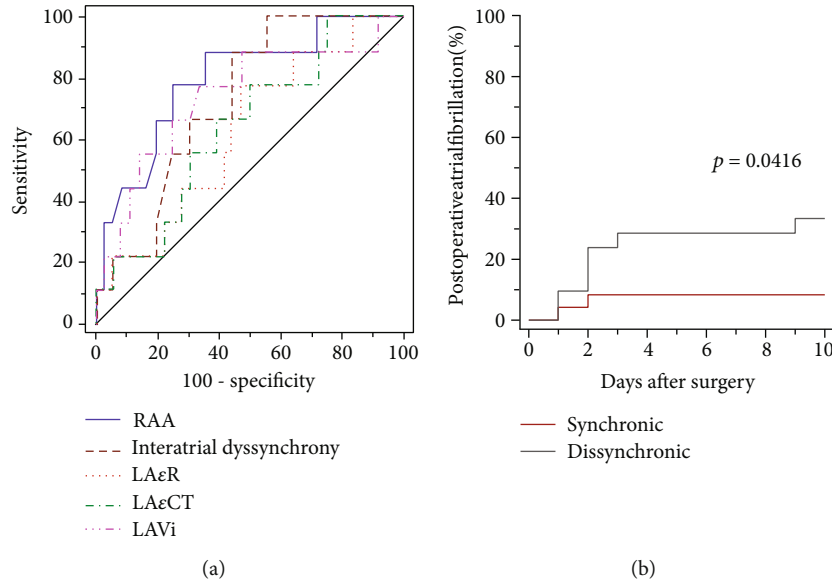


FIGURE 3: Receiver-operating characteristic curves (ROC) for atrial fibrillation incidence after cardiac surgery. (a) ROC curves for right atrial area (RAA), interatrial dyssynchrony, left atrial reservoir strain (LAεR), left atria contraction strain (LAεCT), and left atrial volume index (LAVi). (b) Postoperative atrial fibrillation incidence in patients with synchronous and dyssynchronous activation of the right and left atrial lateral walls.

TABLE 1: Demographics and medication of patients before surgery.

Variables	Dyssynchronous ($n = 21$)	Synchronous ($n = 24$)	p value
Demographics			
Age in years (n)	68 ± 9	67 ± 7	0.262
Patient sex (male)	15 (71.4)	16 (66.6)	0.731
Type of surgery: coronary	20 (95.2)	21 (87.5)	0.559
Coronary disease	20 (95.2)	23 (95.8)	0.923
Diabetes mellitus	13 (61.9)	10 (41.6)	0.175
Hypertension	20 (95.2)	22 (91.6)	0.632
Dyslipidemia	19 (90.5)	20 (83.3)	0.482
Dilated cardiomyopathy	4 (19.0)	1 (4.2)	0.113
Chronic pulmonary obstructive disease	1 (4.8)	3 (12.5)	0.363
Chronic renal failure	3 (14.3)	1 (4.2)	0.234
Obesity	10 (47.6)	8 (33.3)	0.329
Stroke	0	1 (4.2)	0.344
Heart failure in last month	3 (14.3)	5 (20.8)	0.567
Smoker	2 (9.5)	4 (16.6)	0.482
Presurgical medications			
Aspirin use	21 (100)	24 (100)	1
β Blocker use	15 (71.4)	17 (70.8)	0.965
Statins	20 (95.2)	24 (100)	0.280
ACEI or ARA	15 (71.5)	14 (58.3)	0.360
Spiroinolactone or eplerenone	5 (23.8)	2 (8.3)	0.153
Furosemide	3 (14.3)	2 (8.3)	0.526

Data are expressed as number and (%), unless otherwise indicated. p values are calculated by Kruskal-Wallis test or chi-square test. ACEI: angiotensin-converting enzyme inhibitors; ARA: angiotensin II, type 1 receptor antagonists.

TABLE 2: Comparative echocardiographic measurements in both groups.

Echocardiographic variables	Dyssynchronous	Synchronous	<i>p</i> value
Atrial index volume (mL/m ²)	32.51 ± 8.27	29.45 ± 9.76	0.534
Right atrial area (cm ²)	17.07 ± 3.54	15.57 ± 3.13	0.694
Fey Simpson (%)	54.71 ± 15.36	59.21 ± 15.47	0.887
Mitral E wave velocity (cm/sec)	68.14 ± 20.32	71.83 ± 16.82	0.216
Mitral A wave velocity (cm/sec)	85.33 ± 21.44	76.96 ± 18.4	0.568
E/e ratio LV	8.83 ± 3.83	8.53 ± 3.44	0.542
E/e ratio RV	4.42 ± 1.37	4.38 ± 1.08	0.404
LV index mass (g/m ²)	138.29 ± 52.97	108.33 ± 33.61	0.021

Data are expressed as mean and SD. *p* values are analyzed by *t*-test. LA: left atria; RA: right atria; LVEF: left ventricular ejection fraction; LV: left ventricle; RV: right ventricle.

TABLE 3: Deformation rate time per segment in both groups.

Deformation rate time	Dyssynchronous	Synchronous	<i>p</i> value
Left atria			
Base septum segment	138.95 ± 44.43	142.46 ± 39.48	0.780
Medium septum segment	146.57 ± 40.89	136.54 ± 30.11	0.350
Roof septum segment	157.76 ± 47.46	134.46 ± 30.11	0.078
Base lateral segment	168.38 ± 45.32	150.79 ± 41.49	0.181
Medium lateral segment	169.48 ± 41.77	149.67 ± 42.23	0.122
Roof lateral segment	161.67 ± 33.42	156.83 ± 41.26	0.671
Base anterior segment	151.71 ± 43.26	155.67 ± 34.38	0.734
Medium anterior segment	154.05 ± 41.87	154.54 ± 35.02	0.966
Roof anterior segment	157.05 ± 41.48	151.67 ± 49.59	0.697
Base inferior segment	159.52 ± 48.36	140.04 ± 30.32	0.108
Medium inferior segment	154.24 ± 51.01	144.42 ± 28.44	0.422
Roof inferior segment	161.43 ± 63.04	150.08 ± 33.65	0.447
Base inferior lateral segment	153.29 ± 49.10	145.38 ± 35.49	0.535
Medium inferior lateral segment	150.90 ± 44.43	148.04 ± 31.73	0.803
Roof inferior lateral segment	133.62 ± 45.81	151.54 ± 27.04	0.112
Right atria			
Base lateral segment	138.29 ± 62.95	135.17 ± 42.17	0.844
Medium lateral segment	131.24 ± 57.68	141.71 ± 35.19	0.460
Roof lateral segment	138.81 ± 62.89	143.88 ± 35.68	0.737

Data are expressed as mean and SD. *p* values for analysis by unpaired *t*-test.

This lateralization was not colocalized with the increased signal of tumor necrosis factor- α (TNF α) seen in the dyssynchronous group (Figure 6). The TNF α was mainly colocalized with Cx40 close to the intercalated discs.

Nitrotyrosine is a relatively stable marker of nitrooxidative stress that is formed by peroxynitrite interaction with tyrosine. The nitrotyrosine signal was clearly higher in the dyssynchronous group, especially around the blood vessels. However, it was diffusely observed in the tissue and the microvasculature (Figure 7). Cx43 increased in intercalated discs and also lateralized 14.6% (95% CI of difference 10.81-16.56) more in dyssynchronous patients (Figure 5), but both changes were unrelated to nitrotyrosine marks.

The expression of K_{ATP} channels assessed by the detection of its pore-forming unit Kir6.1 increased in atrial myocytes of dyssynchronous samples (Figure 8). K_{ATP} channels

usually aggregated at a vascular level in images of both synchronous and dyssynchronous patients. The action potential shortening and the hyperpolarization observed with the microelectrodes agrees with increased expression of this channel.

4. Discussion

Our study found that interatrial dyssynchrony assessed by echocardiography was associated with electrical and structural atrial remodeling and the incidence of postoperative atrial fibrillation. The innovative measurement interatrial dyssynchrony was suitable to estimate noninvasively nitrooxidative and inflammatory substrate, as well as, an electrophysiological arrhythmogenic remodeling.

TABLE 4: Comparative atrial strain measurements in both groups.

Atrial strain variables	Dyssynchronous	Synchronous	<i>p</i> value
Reservoir LA strain (%)	25.34 ± 8.7	31.30 ± 10.99	0.433
Conduit LA strain (%)	11.62 ± 5.08	15.61 ± 6.99	0.063
Contractile LA strain (%)	14.58 ± 5.8	16.37 ± 5.57	0.963
Strain rate LA reservoir (1/s)	1.16 ± 0.51	1.44 ± 0.58	0.867
Strain rate LA conduit (1/s)	-1.13 ± 0.60	1.63 ± 1.45	0.419
Strain rate LA contraction (1/s)	-1.01 ± 0.61	-1.15 ± 0.66	0.623
Reservoir RA strain (%)	46.81 ± 21.29	52.50 ± 19.13	0.623
Conduit RA strain (%)	20.62 ± 12.59	25.56 ± 14.26	0.787
Contractile RA strain (%)	17.92 ± 13.19	26.73 ± 14.69	0.598
Strain rate RA reservoir (1/s)	1.96 ± 0.83	2.04 ± 0.59	0.336
Strain rate RA conduit (1/s)	-1.52 ± 1.02	-2.10 ± 0.86	0.605
Strain rate RA contraction (1/s)	-1.22 ± 0.74	-1.68 ± 1.31	0.080

Data are expressed as mean and SD. *p* value values for analysis of *t*-test. LA: left atria; RA: right atria.

4.1. Atrial Dyssynchrony and Postoperative Atrial Fibrillation. Interatrial dyssynchrony is not a common risk factor for POAF. This is one of the first reports of a preoperative indicator of proarrhythmic tissue remodeling. Reservoir and contractile strain of the left atria have been previously related to the development of paroxysmal and chronic atrial fibrillation [25–27]. In this study, both were below the reference values agreed in the clinical guidelines [22]. This indicates more rigid atria, with less pump function, but without a difference between the two groups. One of the reasons for this absence of difference could be the way in which the patients were classified. We did not separate the groups according to the incidence of atrial fibrillation but to the presence of dyssynchrony determined by echocardiogram. Another reason for our patients having a better pump and reservoir function is that we did not include patients with mitral or tricuspid valve disease known for having larger atrial volumes, more rigid atria, and a clear tendency to develop atrial fibrillation. Also, one of our exclusion criteria was a previous history of atrial fibrillation. We found that interatrial dyssynchrony was a better predictor of postoperative atrial fibrillation than other atrial measurements.

Atrial structural and functional remodeling has many causal factors such as oxidative stress, inflammation, fibrosis, and the normal process of aging. Previous studies have shown that left and right atrial enlargement predicts postoperative atrial fibrillation [28, 29]. All our patients had left atrial size below the cutoff values for atrial enlargement. Moreover, the atrial size was preserved in the dyssynchronous patients despite the higher left ventricle index mass and the slightly reduced conduit strain. Left ventricular hypertrophy is associated with higher end-diastolic left ventricular pressures, explaining the difference in the conduit left atrial strain, but other markers of elevated end-diastolic pressures like E/e' relation showed no differences. Right atrial size had no significant difference between groups but was slightly bigger in the dyssynchronous group.

Evaluating the activation of the different segments of the atria did not show differences between the two groups. This supports the standardization guidelines that recommend

the longitudinal analysis of the atria as a whole [22]. Additionally, segment by segment analysis takes a longer time and requires a more experienced operator. Nevertheless, several studies have already shown that intra-atrial dyssynchrony is related to atrial fibrillation development [30, 31]. So, this analysis may be a useful tool for the prediction of arrhythmias. The omega approach, presented here for the first time, is an adaptation of the technique that not only introduces the evaluation of the right atria but it also reduces the time for analysis. This facilitates the interatrial dyssynchrony evaluation with significant potential for arrhythmogenic substrate identification in the preoperative setting.

Structural remodeling produces changes in atrial function. These changes can be accelerated in many disease processes, like hypertension, diabetes mellitus, and ischemic heart disease. These changes can reflect modifications in structural proteins that produce atrial electrical remodeling, which, in turn, could be the cause for longer times of atrial mechanical activation. The results of our study support that atrial dyssynchronous activation is related to both electrical and structural changes, without an apparent influence of other risk factors.

4.2. Atrial Dyssynchrony, Action Potentials, Connexins, and K_{ATP} Channels. Dyssynchronous patients presented abnormalities in the upstroke of the action potentials. In multicellular preparations, both Na^+ channels and connexins contribute to phase 0 of the action potentials. The foot and the delay in the upstroke observed in dyssynchronous patients have been previously associated with connexin alterations (see Figure 3(a)) [32]. Connexin expression, conductance, and location can influence the initial part of the electrical activation [33]. The lateralization of Cx40 and Cx43 shown in Figure 5 could support these findings at the beginning of the action potentials. Still, the concurrent increase in Cx43 at the intercalated discs goes against this idea, but agrees with previous reports that reduce the link with action potential morphology [34]. The reduced amplitude and maximal rate of depolarization indicate an impairment in the sodium currents. Therefore, both sodium channels and connexins can

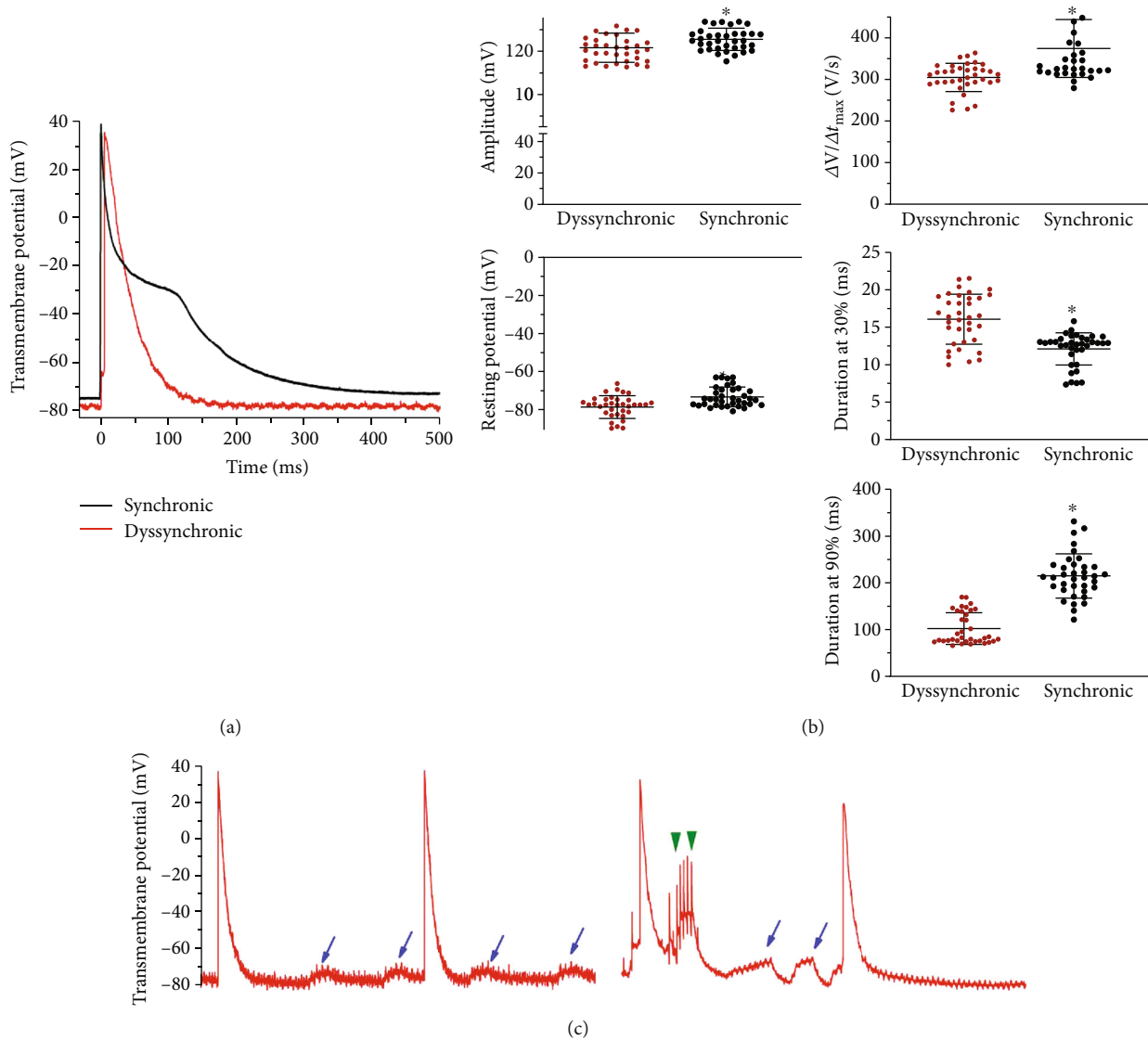


FIGURE 4: Action potentials and arrhythmic triggers in interatrial dyssynchronous patients. (a) Averaged action potentials from three different patients from each group; (b) quantification of action potential amplitude, resting membrane potential, maximum upstroke velocity ($\Delta V/\Delta t_{max}$), and the action potential duration at 30 and 90% of the repolarization from both groups. $*p < 0.01$ by *t*-test; (c) arrhythmogenic triggers in 2 seconds traces from two dyssynchronous patients. The blue arrows mark delayed afterdepolarizations, which are very frequent in dyssynchronous patients. Green arrowheads indicate triggered events from early afterdepolarizations.

contribute to interatrial dyssynchrony because they are the major determinants of electrical impulse propagation between cardiomyocytes.

K_{ATP} channels could explain the action potential shortening and the hyperpolarization, and these features can worsen under stressful situations like ischemia and reperfusion. Our results bring a new potential substrate to the complex electrophysiology of the atrial tissue. The subunit Kir6.1 is an inward rectifier current mainly expressed in the vasculature [16]. Here, we report the expression in human atrial cardiomyocytes of dyssynchronous patients. The activation of these channels reduces the refractory period, thus facilitating reentrant currents that could lead to postoperative atrial fibrillation. K_{ATP} channels are particularly sensitive to the

metabolic and oxidative cellular conditions [35]. In the context of cardiovascular surgery, their properties make them attractive candidates for potential preventive antiarrhythmic therapies.

The afterdepolarizations observed in the dyssynchronous group could be related to alterations in calcium handling and leaks from the sarcoplasmic reticulum through the ryanodine receptors. These alterations have already been described as associated with a more oxidized substrate in patients undergoing coronary artery bypass grafting [36]. Dyssynchrony can promote stretching of the cells during the repolarization phase of shortened action potentials, leading to mechanoelectric feedback capable of early afterdepolarization induction [37].

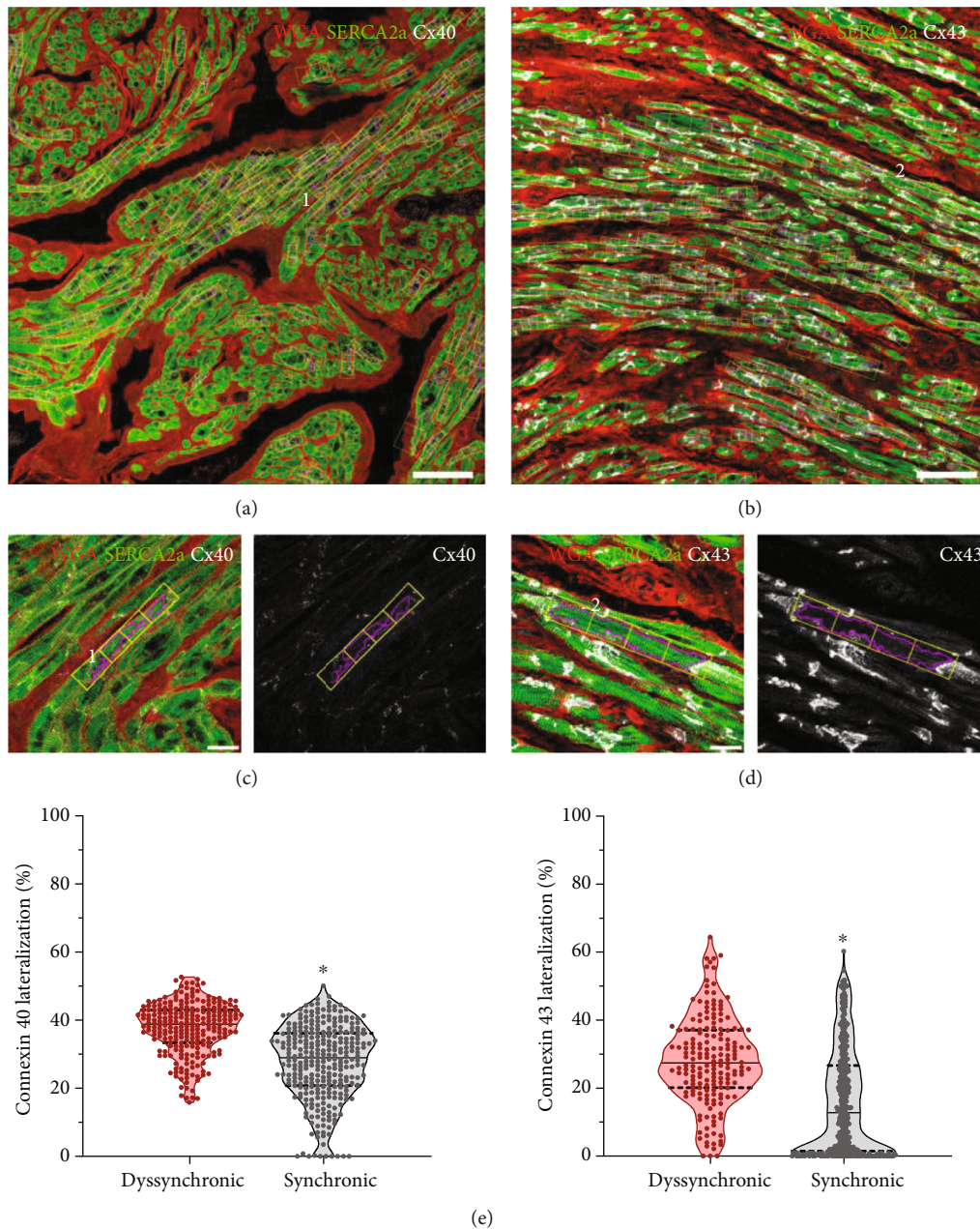


FIGURE 5: Automatic quantification of Cx40 and Cx43 lateralization. Cardiomyocyte detection in samples marked with wheat germ agglutinin (WGA) and antibodies anti-SERCA2a and anti-Cx40 in (a) or anti-Cx43 in (b). White bars correspond to 100 μm . The numbers 1 and 2 are used to trace the origin of the myocytes shown in (c) and (d). Each cell is divided into 4 rectangles to estimate the lateral-to-total ratio of connexins from the individual channel of the connexins marks. White bars correspond to 20 μm . (e) Median and quartiles of the percentage values for the lateralization of each connexin and $*p < 0.01$ by Mann-Whitney tests.

4.3. Atrial Dyssynchrony, Inflammation and Nitrooxidative Stress. The signal with nitrotyrosine was clearly higher in dyssynchronous patients, indicating an increased nitrooxidative state in this group. Accumulating data suggest that inflammation and oxidative stress are involved in the development, recurrence, and persistence of atrial fibrillation [38]. Myocardial oxidative injury can lead to an increased susceptibility to postoperative atrial fibrillation by impairing atrial contraction, altering myofibrillar energetics, and reducing atrial effective refractory period [5]. As a biomarker of oxidative damage, 3-nitrotyrosine has been widely studied.

The formation of 3-nitrotyrosine increases in various cardiovascular diseases, such as cardiac failure, hypertension, atherosclerosis, and cardiovascular complication of diabetes [39]. 3-Nitrotyrosine formation associates with atrial fibrillation in patients with mitral valve disease [14, 40]. Peroxynitrite has been suggested to participate in oxidative damage, which may contribute to atrial contractile dysfunction in atrial fibrillation [41]. Here, we found an increase of 3-nitrotyrosine in the dyssynchronous group, making the echocardiogram a potential oxidative stress indicator.

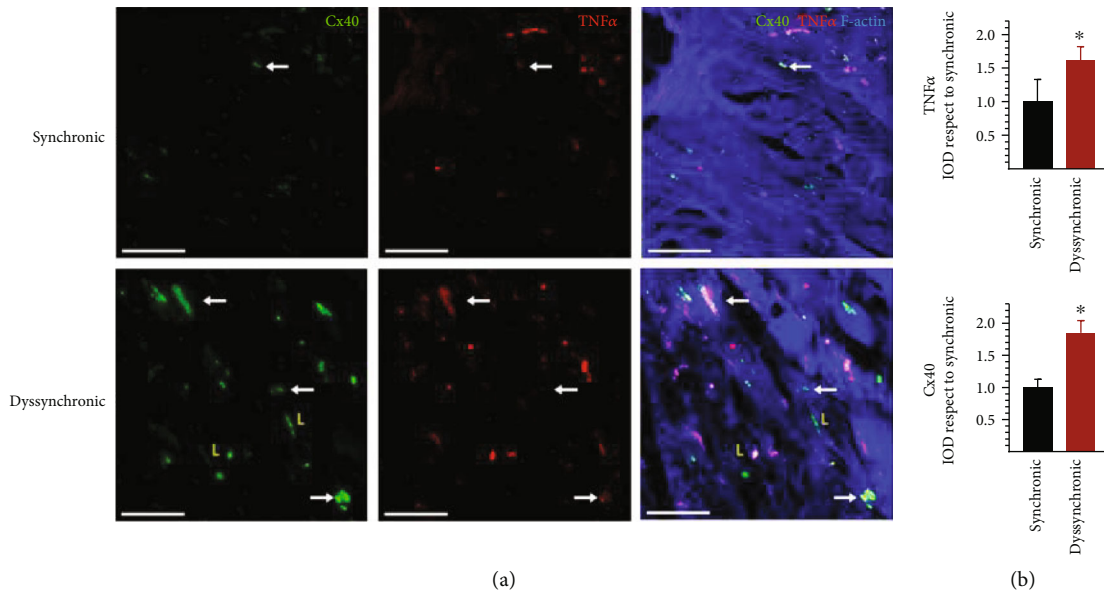


FIGURE 6: Analysis of Cx40 and TNF α localization and expression in atrial samples from synchronic and dyssynchronic patients. (a) White arrows indicate colocalization of both markers, while the yellow L letters indicate lateralized Cx40. F-Actin marks cellular structures. White bars correspond to 50 μ m. (b) Quantification of TNF α and Cx40 integrated optical density (IOD) displayed as mean and SD and * $p < 0.05$ by t -test.

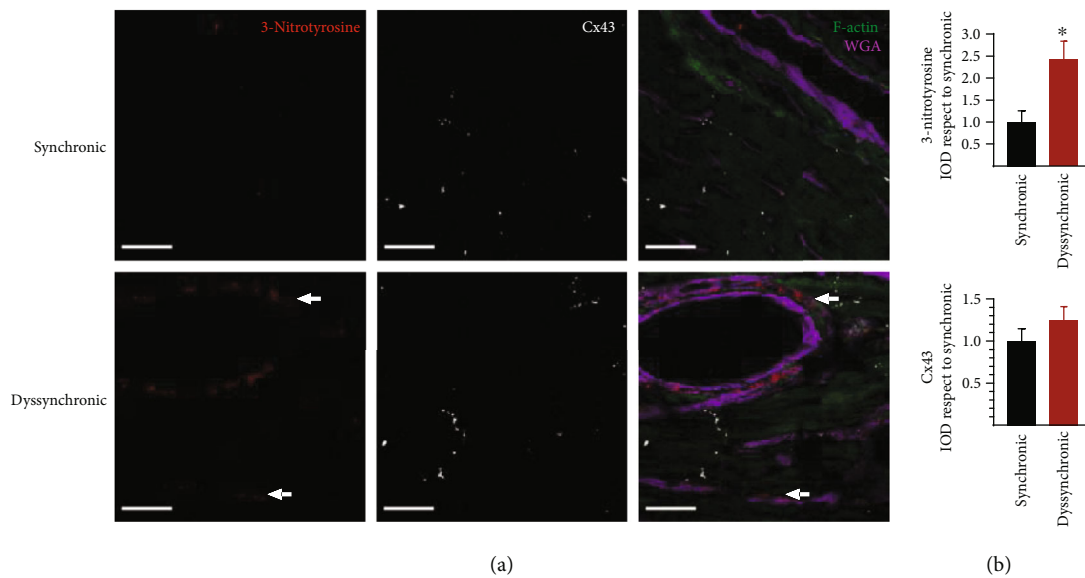


FIGURE 7: Detection of nitrooxidative stress levels and Cx43 expression in atrial samples from synchronic and dyssynchronic patients. (a) An increase in perivascular (indicated by the white arrows) and myocytic signals of 3-nitrotyrosine occurred in the dyssynchronic group. F-Actin marks the tissue in green, and wheat germ agglutinin (WGA) marks the membranes in purple to improve structural reference in the tissue. White bars correspond to 20 μ m. (b) Quantification of 3-nitrotyrosine and Cx43 integrated optical density (IOD) displayed as mean and SD and * $p < 0.05$ by t -test.

Inflammation levels were clearer in the dyssynchronic group. POAF is associated with a higher expression of NF- κ B, myocardial fibrosis, and impaired cardiomyocyte communication before the bypass surgery [11]. The histological results presented here show higher degree of colocalization between TNF α patches and the Cx40 close to the intercalated disc. Lateralized Cx40 did not show this association with TNF α . The latter weakens the relation between structural remodeling and inflammation. TNF α should be interpreted

with caution as the signal was disturbed by the fluorescence of red blood cells. An altered substrate of Cx40 can worsen the downregulation described during bypass surgery [42].

5. Conclusion

In conclusion, our results demonstrate that a novel noninvasive echocardiographic evaluation of interatrial dyssynchrony is better than the surface ECG to identify

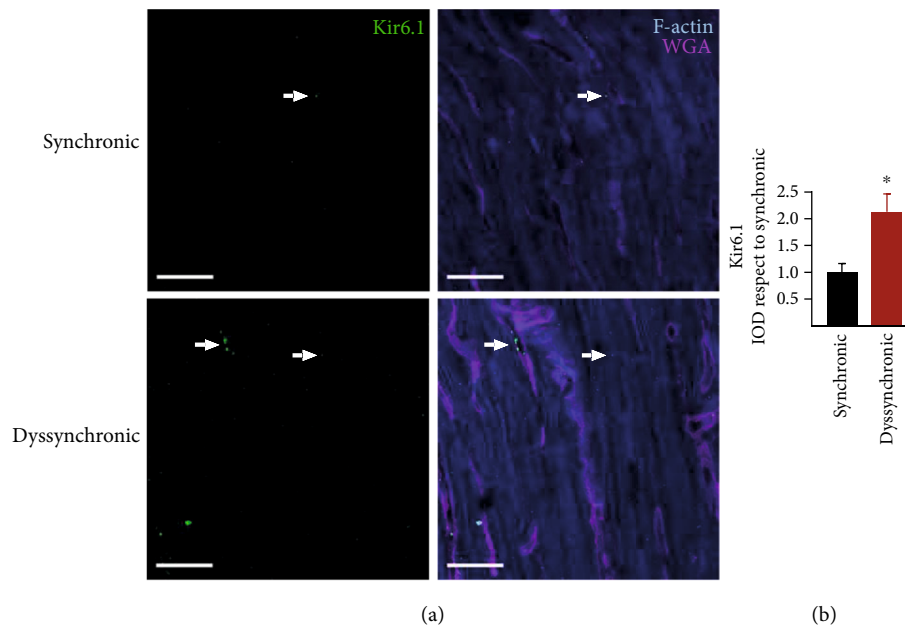


FIGURE 8: Characterization of K_{ATP} channel expression in atrial samples from synchronic and dyssynchronic patients. (a) The Kir6.1 subunit of the potassium channels was present perivascularly (white arrows) and in atrial cardiomyocytes (arrowheads). F-Actin marks the tissue with a blue staining and WGA cellular membranes to facilitate structural characterization. White bars correspond to $20\ \mu\text{m}$. (b) Quantification of Kir6.1 integrated optical density (IOD) displayed as mean and SD and $*p < 0.01$ by t -test.

proarrhythmic atrial electrical and structural remodeling, with increased susceptibility to POAF. The increase in the K_{ATP} channel and the lateralization of connexins observed in dyssynchronic atria could shorten action potential and predispose hearts to reentrant circuits. Inflammation and nitrooxidative stress can increase the proarrhythmic substrate. These factors were all estimated by a simple, noninvasive technique. Future research using this technique will help to further understand the potential role of atrial dyssynchrony as a preoperative predictor of atrial fibrillation in the context of cardiovascular surgery.

Data Availability

Data will be available on request because echocardiography video, electrophysiological records, and confocal images are all extremely big archives.

Conflicts of Interest

The authors declare that there is no conflict of interest regarding the publication of this paper.

Acknowledgments

The authors thank the following: Daniela Cornejo MD, from the Coronary Unit of Clinic of Cuyo for her support in patients' enrollment; Christian Martin MD and Gaston Hernandez MD from the Department of Cardiovascular Surgery of Clinic of Cuyo for the retrieval of the atrial sample; Adriana M. Carrión for her technical assistance. This work was supported by the European Research Council under grant agreement (ERC-StG 638284), by Ministerio de Ciencia e

Innovación (Spain) through project (PID2019-105674RB-I00) and by European Social Fund (EU) and Aragón Government through BSICoS group (T39_20R and project LMP124-18). Francisco J. Sánchez was supported by a scholarship from Universidad Nacional de Cuyo (SIIP project 06-J505). L. García-Mendivil was supported by a fellowship from Diputación General de Aragón (C150/2016), EMBO Short-Term Fellowship 7710, and Ibercaja-CAI Estancias de Investigación IT 18/18.

References

- [1] D. Dobrev, M. Aguilar, J. Heijman, J. B. Guichard, and S. Nattel, "Postoperative atrial fibrillation: mechanisms, manifestations and management," *Nature Reviews. Cardiology*, vol. 16, no. 7, pp. 417–436, 2019.
- [2] F. P. Júnior, G. F. T. Filho, J. R. M. Sant'anna et al., "Idade avançada e incidência de fibrilação atrial em pós-operatório de troca valvar aórtica," *Brazilian Journal of Cardiovascular Surgery*, vol. 29, no. 1, pp. 45–50, 2014.
- [3] Y. M. Kim, T. J. Guzik, Y. H. Zhang et al., "A myocardial Nox2 containing NAD(P)H oxidase contributes to oxidative stress in human atrial fibrillation," *Circulation Research*, vol. 97, no. 7, pp. 629–636, 2005.
- [4] E. J. Anderson, J. T. Efirid, S. W. Davies et al., "Monoamine oxidase is a major determinant of redox balance in human atrial myocardium and is associated with postoperative atrial fibrillation," *Journal of the American Heart Association*, vol. 3, no. 1, 2014.
- [5] M. M. Elahi, S. Flatman, and B. M. Matata, "Tracing the origins of postoperative atrial fibrillation: the concept of oxidative stress-mediated myocardial injury phenomenon," *European Journal of Preventive Cardiology*, vol. 15, no. 6, pp. 735–741, 2008.

- [6] S. I. Sarvari, K. H. Haugaa, T. M. Stokke et al., "Strain echocardiographic assessment of left atrial function predicts recurrence of atrial fibrillation," *European Heart Journal Cardiovascular Imaging*, vol. 17, no. 6, pp. 660–667, 2016.
- [7] F. Levy, N. Debry, A. L. Labescat et al., "Echocardiographic prediction of postoperative atrial fibrillation after aortic valve replacement for aortic stenosis: a two-dimensional speckle tracking left ventricular longitudinal strain multicentre pilot study," *Archives of Cardiovascular Diseases*, vol. 105, no. 10, pp. 499–506, 2012.
- [8] J. Imanishi, H. Tanaka, T. Sawa et al., "Left atrial booster-pump function as a predictive parameter for new-onset postoperative atrial fibrillation in patients with severe aortic stenosis," *The International Journal of Cardiovascular Imaging*, vol. 30, no. 2, pp. 295–304, 2014.
- [9] K. H. Haugaa, M. K. Smedsrud, T. Steen et al., "Mechanical dispersion assessed by myocardial strain in patients after myocardial infarction for risk prediction of ventricular arrhythmia," *JACC: Cardiovascular Imaging*, vol. 3, no. 3, pp. 247–256, 2010.
- [10] N. J. Severs, S. R. Coppen, E. Dupont, H. I. Yeh, Y. S. Ko, and T. Matsushita, "Gap junction alterations in human cardiac disease," *Cardiovascular Research*, vol. 62, no. 2, pp. 368–377, 2004.
- [11] J. Y. Li, Y. J. Lai, H. I. Yeh et al., "Atrial gap junctions, NF- κ B and fibrosis in patients undergoing coronary artery bypass surgery: the relationship with postoperative atrial fibrillation," *Cardiology*, vol. 112, pp. 81–88, 2009.
- [12] P. Saravanan, A. L. West, B. Bridgewater et al., "Omega-3 fatty acids do not alter P-wave parameters in electrocardiogram or expression of atrial connexins in patients undergoing coronary artery bypass surgery," *Europace*, vol. 18, no. 10, pp. 1521–1527, 2016.
- [13] T. Egan Benova, B. Szeiffova Bacova, C. Viczenczova, E. Diez, M. Barancik, and N. Tribulova, "Protection of cardiac cell-to-cell coupling attenuate myocardial remodeling and proarrhythmia induced by hypertension," *Physiological Research*, vol. 65 Suppl 1, pp. S29–S42, 2016.
- [14] Q. Yongjun, S. Huanzhang, Z. Wenxia, T. Hong, and X. Xijun, "Histopathological characteristics and oxidative injury secondary to atrial fibrillation in the left atrial appendages of patients with different forms of mitral valve disease," *Cardiovascular Pathology*, vol. 22, no. 3, pp. 211–218, 2013.
- [15] W. Han, S. Fu, N. Wei et al., "Nitric oxide overproduction derived from inducible nitric oxide synthase increases cardiomyocyte apoptosis in human atrial fibrillation," *International Journal of Cardiology*, vol. 130, no. 2, pp. 165–173, 2008.
- [16] M. N. Foster and W. A. Coetzee, "KATP channels in the cardiovascular system," *Physiological Reviews*, vol. 96, pp. 177–252, 2016.
- [17] F. J. Neumann, M. Sousa-Uva, A. Ahlsson et al., "2018 ESC/EACTS Guidelines on myocardial revascularization," *European Heart Journal*, vol. 40, no. 2, pp. 87–165, 2019.
- [18] H. Baumgartner, V. Falk, J. J. Bax et al., "2017 ESC/EACTS Guidelines for the management of valvular heart disease," vol. 38, no. 36, pp. 2739–2791.
- [19] A. Bayés De Luna, P. Platonov, F. G. Cosio et al., "Interatrial blocks. A separate entity from left atrial enlargement: a consensus report," *Journal of Electrocardiology*, vol. 45, no. 5, pp. 445–451, 2012.
- [20] L. P. Badano, T. J. Koliass, D. Muraru et al., "Standardization of left atrial, right ventricular, and right atrial deformation imaging using two-dimensional speckle tracking echocardiography: a consensus document of the EACVI/ASE/Industry Task Force to standardize deformation imaging," *European Heart Journal Cardiovascular Imaging*, vol. 19, no. 6, pp. 591–600, 2018.
- [21] A. Oliver-Gelabert, L. García-Mendivil, J. M. Vallejo-Gil et al., "Automatic quantification of cardiomyocyte dimensions and connexin 43 lateralization in fluorescence images," *Biomolecules*, vol. 10, no. 9, p. 1334, 2020.
- [22] F. Pathan, N. D'Elia, M. T. Nolan, T. H. Marwick, and K. Negishi, "Normal ranges of left atrial strain by speckle-tracking echocardiography: a systematic review and meta-analysis," *Journal of the American Society of Echocardiography*, vol. 30, no. 1, pp. 59–70.e8, 2017.
- [23] L. G. Rudski, W. W. Lai, J. Afilalo et al., "Guidelines for the echocardiographic assessment of the right heart in adults: a report from the American Society of Echocardiography. Endorsed by the European Association of Echocardiography, a registered branch of the European Society of Cardiology, and the Canadian Society of Echocardiography," *Journal of the American Society of Echocardiography*, vol. 23, no. 7, pp. 685–713, 2010.
- [24] R. M. Lang, L. P. Badano, M. A. Victor et al., "Recommendations for cardiac chamber quantification by echocardiography in adults: an update from the American Society of Echocardiography and the European Association of Cardiovascular Imaging," *Journal of the American Society of Echocardiography*, vol. 28, no. 1, pp. 1–39.e14, 2015.
- [25] M. Pernigo, G. Benfari, G. Geremia et al., "Atrial function as an independent predictor of postoperative atrial fibrillation in patients undergoing aortic valve surgery for severe aortic stenosis," *Journal of the American Society of Echocardiography*, vol. 30, no. 10, pp. 956–965.e1, 2017.
- [26] F. E. Fakuade, V. Steckmeister, F. Seibert et al., "Altered atrial cytosolic calcium handling contributes to the development of postoperative atrial fibrillation," *Cardiovascular Research*, 2020.
- [27] H. E. Verdejo, E. Becerra, R. Zalaquet et al., "Atrial function assessed by speckle tracking echocardiography is a good predictor of postoperative atrial fibrillation in elderly patients," *Echocardiography*, vol. 33, no. 2, pp. 242–248, 2016.
- [28] U. Aksu, K. Kalkan, O. Gulcu, E. Aksakal, M. Öztürk, and S. Topcu, "The role of the right atrium in development of postoperative atrial fibrillation: a speckle tracking echocardiography study," *Journal of Clinical Ultrasound*, vol. 47, no. 8, pp. 470–476, 2019.
- [29] T. Hirose, M. Kawasaki, R. Tanaka et al., "Left atrial function assessed by speckle tracking echocardiography as a predictor of new-onset non-valvular atrial fibrillation: results from a prospective study in 580 adults," *European Heart Journal Cardiovascular Imaging*, vol. 13, no. 3, pp. 243–250, 2012.
- [30] C. Xu, K. Chen, F. Yu et al., "Atrial dyssynchrony: a new predictor for atrial high-rate episodes in patients with cardiac resynchronization therapy," *Cardiology*, vol. 144, no. 1-2, pp. 18–26, 2019.
- [31] L. Ciuffo, S. Tao, E. Gucuk Ipek et al., "Intra-atrial dyssynchrony during sinus rhythm predicts recurrence after the first catheter ablation for atrial fibrillation," *JACC: Cardiovascular Imaging*, vol. 12, no. 2, pp. 310–319, 2019.
- [32] N. J. Prado, T. Egan Beňová, E. R. Diez et al., "Melatonin receptor activation protects against low potassium-induced ventricular fibrillation by preserving action potentials and

- connexin-43 topology in isolated rat hearts,” *Journal of Pineal Research*, vol. 67, no. 4, pp. e12605–e12614, 2019.
- [33] W. C. Cole, J. B. Picone, and N. Sperelakis, “Gap junction uncoupling and discontinuous propagation in the heart. A comparison of experimental data with computer simulations,” *Biophysical Journal*, vol. 53, no. 5, pp. 809–818, 1988.
- [34] E. R. Diez, J. A. Sánchez, N. J. Prado et al., “Ischemic postconditioning reduces reperfusion arrhythmias by adenosine receptors and protein kinase C activation but is independent of KATP channels or connexin 43,” *International Journal of Molecular Sciences*, vol. 20, no. 23, p. 5927, 2019.
- [35] Y. Chai, D. M. Zhang, and Y. F. Lin, “Activation of cGMP-dependent protein kinase stimulates cardiac ATP-sensitive potassium channels via a ROS/calmodulin/CaMKII signaling cascade,” *PLoS One*, vol. 6, no. 3, article e18191, 2011.
- [36] W. Xie, G. Santulli, S. R. Reiken et al., “Mitochondrial oxidative stress promotes atrial fibrillation,” *Scientific Reports*, vol. 5, no. 1, pp. 1–11, 2015.
- [37] E. R. Pfeiffer, J. R. Tangney, J. H. Omens, and A. D. McCulloch, “Biomechanics of cardiac electromechanical coupling and mechanoelectric feedback,” *Journal of Biomechanical Engineering*, vol. 136, no. 2, pp. 021007–021011, 2014.
- [38] P. Korantzopoulos, K. Letsas, N. Fragakis, G. Tse, and T. Liu, “Oxidative stress and atrial fibrillation: an update,” *Free Radical Research*, vol. 52, no. 11-12, pp. 1199–1209, 2018.
- [39] L. Zheng, M. Settle, G. Brubaker et al., “Localization of nitration and chlorination sites on apolipoprotein A-I catalysed by myeloperoxidase in human atheroma and associated oxidative impairment in ABCA1-dependent cholesterol efflux from macrophages,” *The Journal of Biological Chemistry*, vol. 280, pp. 38–47, 2005.
- [40] S. Liu, Z. Guan, X. Zheng et al., “Impaired left atrial systolic function and inter-atrial dyssynchrony may contribute to symptoms of heart failure with preserved left ventricular ejection fraction: a comprehensive assessment by echocardiography,” *International Journal of Cardiology*, vol. 257, pp. 177–181, 2018.
- [41] M. J. Mihm, F. Yu, C. A. Carnes et al., “Impaired Myofibrillar Energetics and Oxidative Injury During Human Atrial Fibrillation,” *Circulation*, vol. 104, no. 2, pp. 174–180, 2001.
- [42] E. Dupont, Y. S. Ko, S. Rothery et al., “The gap-junctional protein connexin 40 is elevated in patients susceptible to postoperative atrial fibrillation,” *Circulation*, vol. 103, no. 6, pp. 842–849, 2001.

Research Article

Cardioprotective Effects of Taurisolo® in Cardiomyoblast H9c2 Cells under High-Glucose and Trimethylamine N-Oxide Treatment *via De Novo* Sphingolipid Synthesis

Stefania Lama,¹ Vincenzo Monda,² Maria Rosaria Rizzo,³ Marco Dacrema,⁴ Maria Maisto,⁴ Giuseppa Annunziata,⁴ Gian Carlo Tenore ,⁴ Ettore Novellino,⁴ and Paola Stiuso ¹

¹Department of Precision Medicine, University of Campania “Luigi Vanvitelli”, Naples, Italy

²Department of Experimental Medicine, Section of Human Physiology, University of Campania “Luigi Vanvitelli”, Naples, Italy

³Department of Advanced Medical and Surgical Sciences, University of Campania “Luigi Vanvitelli”, Naples, Italy

⁴Department of Pharmacy, University of Naples Federico II, Naples, Italy

Correspondence should be addressed to Gian Carlo Tenore; giancarlo.tenore@unina.it and Paola Stiuso; paola.stiuso@unicampania.it

Received 18 June 2020; Revised 21 September 2020; Accepted 24 October 2020; Published 16 November 2020

Academic Editor: Laura Sartiani

Copyright © 2020 Stefania Lama et al. This is an open access article distributed under the Creative Commons Attribution License, which permits unrestricted use, distribution, and reproduction in any medium, provided the original work is properly cited.

In addition to high plasma glucose, increased levels of trimethylamine N-oxide (TMAO) have been found in obese subjects, where are considered as a novel risk factor for cardiovascular diseases. The present study aimed to investigate the effect of a novel nutraceutical formulation based on grape polyphenols (registered as Taurisolo®) in counteracting TMAO- and high glucose (HG)-induced cytotoxicity in cardiomyoblast H9c2 cells. Cell damage was induced with HG (HG-H9c2) and HG+TMAO (THG-H9c2); both experimental cell models were, thus, incubated for 72 h in the presence or absence of Taurisolo®. It was observed that Taurisolo® significantly increased the cell viability and reduced lactate dehydrogenase and aspartate transaminase release in both HG- and THG-H9c2 cells. Additionally, through its antioxidant activity, Taurisolo® modulated cell proliferation *via* ERK activation in THG-H9c2. Furthermore, Taurisolo® was able to induce autophagic process *via* increasing the expression of LC3II, a protein marker involved in formation of autophagosome and *ex novo* synthesis of sphingomyelin, ceramides, and their metabolites both in HG- and THG-H9c2 cells. Finally, Taurisolo® reduced hypertrophy and induced differentiation of HG-H9c2 cells into cardiomyocyte-like cells. These data suggest that Taurisolo® counteracts the toxicity induced by TMAO and HG concentrations increasing autophagic process and activating *de novo* sphingolipid synthesis, resulting in a morphological cell remodeling. In conclusion, our results allow speculating that Taurisolo®, combined with energy restriction, may represent a useful nutraceutical approach for prevention of cardiomyopathy in obese subjects.

1. Introduction

Obesity is a medical condition mainly characterized by increased body fat accumulation, which negative effects on health are well-known. Excessive adipose tissue is among the leading causes of chronic inflammation that, in turn, plays a pivotal role in developing or worsening the outcome of various pathologies such as metabolic, cardiovascular, respiratory, viral, and tumoral [1]. Obesity is a widely spread health problem in the world, and it has been recognized as a risk factor for the development of metabolic disorders, such

as type 2 diabetes, cardiovascular disease, or atherosclerosis [2, 3]. Diet-induced obesity (DIO) leads a significant increase of oxidative stress (OS) and reduced antioxidant defense, and it is associated with a typical chronic low-grade inflammation, which results in severe cardiovascular complications [4, 5]. Moreover, in cardiomyocytes, DIO induced many alterations, including mitochondria dysfunction [5], endoplasmic reticulum stress [6], apoptosis, and autophagy. Many studies suggest that enhanced autophagy acts as a protective mechanism against OS in the liver, adipose tissue, and skeletal muscle [7, 8]. Furthermore, when cardiac stresses are

sustained for a prolonged period, e.g., in high blood sugar levels, upregulation of autophagy promotes myocyte cellular architecture remodeling. Sphingolipids (SLs), a heterogeneous lipid class that includes ceramide (Cer), sphingosine-1-phosphate, and dihydroceramide present in all membrane structures, have been associated to mediate distinct autophagic pathways described as protective autophagy and autophagy-associated cell death [1, 9]. A recent study showed that Cer directly interacts with microtubule-associated protein light chain 3 (LC3) on mitochondrial membranes, inducing autophagy [10]. Therefore, Cer has been shown to reduce the nutrient transporters in plasma membrane resulting in autophagy activation. S1P has emerged as a cell-proliferative lipid messenger. It has been found to induce survival-mediated or protective autophagy under nutrient starvation, but it was shown to not be related to Beclin1 protein accumulation or class I PI3K or Akt suppression [11, 12]. The conversion of Cer to S1P simultaneously accumulates the survival effects and removes the death signals. This observation led to the concept of a so-called “SL rheostat” or “SL biostat,” based on the relative amounts and reciprocal roles of these antagonistic metabolites, which are critical in guiding the destiny of cells [12–14].

Circulating trimethylamine N-oxide (TMAO) levels has been recently highlighted as a potential prognostic marker for cardiovascular diseases (CVD). Increased TMAO concentrations have also been associated with impaired glucose tolerance and diabetes and were accompanied by other metabolic conditions such as low HDL cholesterol and phospholipids and hypomethylation [15]. Recently, Annunziata et al. demonstrated the ability of a novel nutraceutical formulation based on grape pomace polyphenolic extract (registered as Taurisol[®]) to reduce the serum levels of TMAO in healthy [16] and in overweight/obese subjects [17]. The authors have hypothesized two mechanisms of action by which Taurisol[®] may exert its TMAO-reducing effect: the antioxidant activity and the microbiota remodeling, both exerted by polyphenols. The goal of the present study was to investigate the *in vitro* effect and signaling mechanisms of Taurisol[®] on proliferation, OS, morphological remodeling, and autophagy, in trimethylamine TMAO and hyperglycemia damaged embryonic rat cardiomyoblast H9c2 cells.

2. Materials and Methods

2.1. Chemicals. All chemicals, standards, and reagents used were either analytical or mass grade reagents. The water was treated in a Milli-Q water purification system (Millipore, Bedford, MA, United States) before use. Bovine serum albumin (BSA) and 3-(4,5-dimethylthiazol-2-yl)-2,5-diphenyl tetrazolium bromide (MTT) and trimethylamine N-oxide (TMAO) were purchased from Sigma-Aldrich (St. Louis, MO, USA). Phosphate-buffered saline (PBS) and trypsin-EDTA were from Lonza (Milano, Italy). Fetal bovine serum (FBS) and Dulbecco's modified Eagle's medium (DMEM) were purchased from Gibco (Grand Island, NY, USA). Western blot analysis was performed using the following primary antibodies: polyclonal antibody (polyAb) p-ERK 44/42 and polyAb ERK 44/42 from Cell Signaling Technology (Beverly,

MA, USA); monoclonal Ab Mn-SOD was from Santa Cruz Biotechnology (San Diego, CA, USA). Blots were incubated with horseradish peroxidase (HRP)-conjugated goat anti-rabbit or HRP-conjugated goat anti-mouse (Immunoreagents Inc., Raleigh, NC, USA) secondary antibodies. Anti-mAb was purchased from Santa Cruz Biotechnology and secondary antibodies conjugated to Alexafluor 488 from Life Science, Portland, OR, USA, and 4',6-diamidino-2-phenylindole (DAPI) from Sigma-Aldrich.

2.2. Taurisol[®] Supplement. Taurisol[®] is a supplement consisting of a polyphenol extract obtained from *Aglianico* cultivar grape, collected during the autumn 2016 harvest. Firstly, the Department of Pharmacy, University of Naples Federico II (Naples, Italy), provided the supplement formulation; then, the large-scale production was accomplished by MBMed Company (Turin, Italy). For the polyphenol extract production, grapes were extracted with water (50°C), and the solution was filtrated and concentrated and underwent a spray-drying process with maltodextrins as support (40–70%) to obtain a fine microencapsulated powder. As previously reported, the High-Performance Liquid Chromatography-diodearray detector (HPLC-DAD, Jasco Inc., Easton, MD, USA) polyphenol profile of Taurisol[®] revealed the presence of: Ferulic acid 10.5 ± 0.70 µg/g, Resveratrol 13.6 ± 0.64 µg/g, Caffeic acid 20.7 ± 0.76 µg/g, Procyanidin B3 dimer 22.05 ± 6.61 µg/g, p-coumaric acid 27.9 ± 0.66 µg/g, Rutin 28.4 ± 0.70 µg/g, Quercetin 40.22 ± 7.11 µg/g, Procyanidin C2 trimer 44.6 ± 0.66 µg/g, Procyanidin B4 dimer 56.6 ± 0.88 µg/g, Procyanidin B1 dimer 62.8 ± 0.59 µg/g, Procyanidin B2 dimer 426.5 ± 5.92 µg/g, Syringic acid 539.2 ± 6.02 µg/g, Epicatechin 886.0 ± 7.82 µg/g, Gallic acid 1463.4 ± 65.5 µg/g, and Catechin 4087.0 ± 64.5 µg/g [18].

2.3. Cell Culture. Rat cardiomyocytes (H9c2) (ATCC, Manassas, VA) cells were cultured in DMEM, at two different glucose concentration 5.5 mM (NH-H9c2) and 44 mM (HG-H9c2), supplemented with 10% fetal bovine serum, 100 U/mL of penicillin, and 100 lg/mL of streptomycin in 150 cm² tissue culture flasks at 37°C in a humidified atmosphere of 5% CO₂. The cells were fed every 2–3 days and subcultured once they reached 70–80% of confluence. After 4 hr incubation, cells were washed with 1% PBS to remove unattached dead cells and treated with Tau (0.5 µg/µL), TMAO (50 µM), and TMAO/Tau combination.

2.4. Cell Proliferation Assay. The evaluation of cell proliferation was performed on NG-H9c2 and HG-H9c2 cell line after 24 and 72 hr incubation with Taurisol[®], TMAO, and TMAO/Tau combination. The cells were seeded in 96-well plates in a number of 30 × 10² per well. The growth was assessed by MTT viability assay as previously described [19]. Then, MTT assay was carried out by triplicate determination on at least three separate experiments. All data were expressed as mean ± SD. We have determined also the cell number and proliferation by TC10 automated cell counter (Bio-Rad, Milan, Italy).

2.5. Morphological Evaluation of Cardiomyocytes by Confocal Microscopy. After 72 hr incubation with Tau, TMAO, and TMAO/Tau combination, the HG-H9c2 cells were fixed for

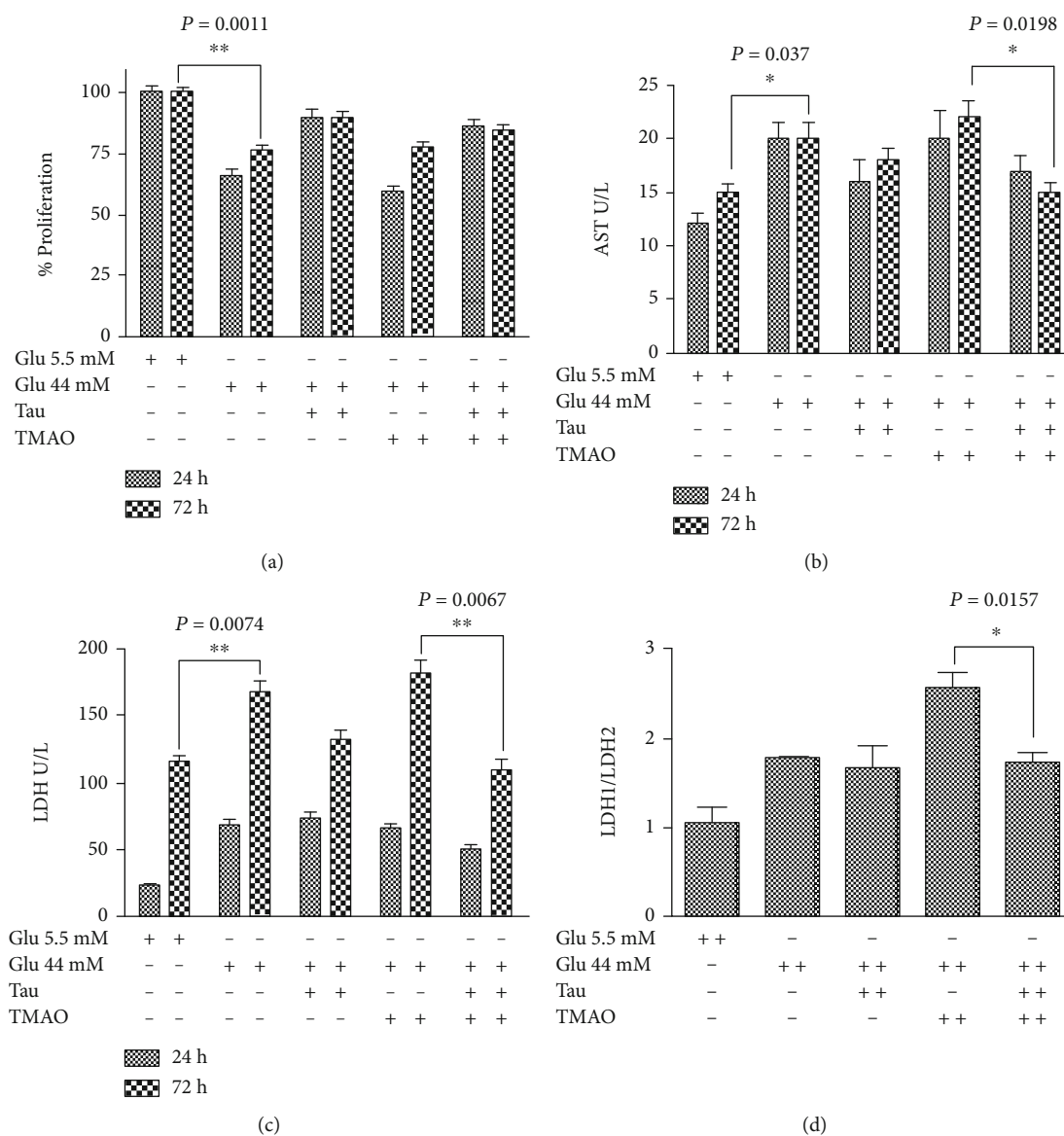


FIGURE 1: Taurisol® (Tau) counteracts the H9c2 cell injury induced from TMAO in hyperglycemic condition. H9c2 cells were grown in standard (5.5 mM Glu NG-H9c2) and high glucose (44 mM Glu, HG-H9c2) condition. The HG-H9c2 cells were treated, for 72 h with Tau (0,5 $\mu\text{g}/\mu\text{L}$), TMAO(50 μM), and TMAO-Tau combination. (a) The cell survival was performed with MTT assay. (b, c) AST and LDH as makers of cell injury were performed by the colorimetric assay. (d) LDH1/LDH2 isoenzymes ratio was evaluated at 72 h by the colorimetric assay. Each experiment was repeated at least three times. Results are expressed as mean \pm SD.

20 min with a 3% (*w/v*) paraformaldehyde (PFA) solution and permeabilized for 10 min with 0.1% (*w/v*) Triton X-100 in phosphate-buffered saline (PBS) at room temperature. To prevent nonspecific interactions of antibodies, cells were treated for 2 hr in 5% fetal bovine serum (FBS) in PBS; then, cells were incubated with a specific mouse monoclonal antibody raised against actin (1 : 500 Alexa Fluor®, BD Pharmingen™) for 24 hr at 37°C. The slides were mounted on microscope slides by Mowiol. The analyses were performed with a Zeiss LSM 510 microscope equipped with a plan-apochromat objective X 63 (NA 1.4) in oil immersion. Actin fluorescence was collected in a multitrack mode. Aggiungere dapi aggiungere nostra reference The nuclei were stained with 4',6-diamidino-2-phenylindole (DAPI) [20].

2.6. Nitrite Levels. Nitrite was measured by the Griess reaction. Briefly, 50 μL of medium was mixed with an equal volume of the Griess reagent (0.5% sulfanilamide, 2.5% H_3PO_4 , and 0.05% naphthylethylenediamine in H_2O) and incubated for 10 min at room temperature. Absorbance was assayed at 550 nm and compared with a standard curve obtained using sodium nitrite. [21]

2.7. Thiobarbituric Acid-Reactive Species (TBARS) Assay. Samples were incubated with 0.5 mL of 20% acetic acid, pH 3.5, and 0.5 mL of 0.78% aqueous solution of thiobarbituric acid. After heating at 95°C for 45 min, samples were centrifuged at 4000 rpm for 5 min. The TBARS were quantified by spectrophotometry at 532 nm. Results were expressed as

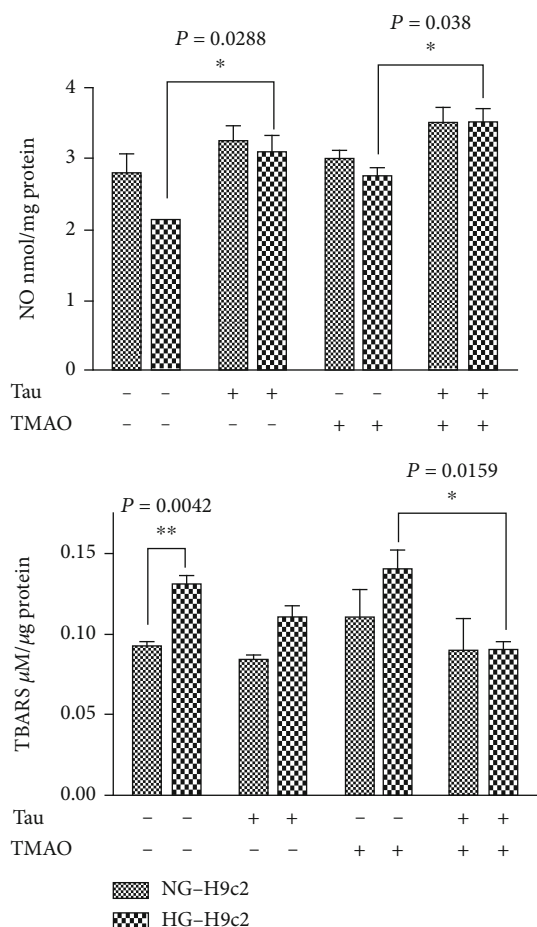


FIGURE 2: Taurisol[®] increased the nitric oxide values in the medium of THG-treated H9c2 cells. The values of NO were evaluated by the Griess assay. H9c2 cells were grown in standard (5.5 mM NG-H9c2) and high glucose (44 mM Glu, HG-H9c2) condition. The NG and HG-H9c2 cells were treated, for 72 h with Tau (0.5 μg/μL), TMAO (50 μM), and TMAO-Tau combination. Absorbance was assayed at 550 nm and compared with a standard curve obtained using sodium nitrite. TBARS were quantified by spectrophotometry at 532 nm. Results were expressed as TBARS M/g of serum proteins. Each data point is the average of triplicate measurements, with each experiment performed in triplicate. Results are expressed as mean ± SD.

TBARS μM/g of proteins. Each data point is the average of triplicate measurements, with each experiment performed in triplicate.

2.8. AST and LDH Assay. NG-H9c2 and HG-H9c2 cardiomyocytes (1×10^5 cells/well) after 24 and 72 hr incubation with Taurisol[®], TMAO, and TMAO/Tau combination were cultured in 6-well plates. The medium was collected for the measurement of the Aspartate transaminase (AST) and Lactate dehydrogenase (LDH) enzymes, including isoform 1 and 2 release. The enzyme activity was measured using an Abbott Aeroset fully automatic biochemical analyzer (Abbott Laboratories, USA). The levels of enzymes were assayed according to the instructions provided with the corresponding enzymatic kits.

2.9. Western Blots. We followed the methods of Vanacore et al. 2018 [22] for evaluation the protein expression by Western blot. Briefly, the cells were cultured at different condition for 72 hr, and then, cell pellets were lysed with 1 mL of lysis buffer (1% Triton, 0.5% sodium deoxycholate, 0.1 M NaCl, 1 mM Ethylenediamine tetra-acetic acid (EDTA), pH 7.5, 10 mM Na₂HPO₄, pH 7.4, 10 mM Phenylmethyl sulfonyl fluoride, 25 mM benzamidine, 1 mM leupeptin, and 0.025 units/mL aprotinin). The lysates were centrifuged at 12,000 rpm for 10 min at 4°C. Equal amounts of protein extracts were separated by SDS-PAGE, electrotransferred to nitrocellulose, and reacted with the different antibodies (ERK, pERK, LC3II, and Mn-SOD). All Western blots were repeated for three times. GAPDH was used as internal control. To quantify the results, the relative amount of each protein was determined.

2.10. Mass Spectrometry. LIPID MAPS Lipidomics Gateway and Human Metabolome Database queries were used to assign putative identities to mass features using based on mass accuracy within ±1 Da. (<http://www.lipidmaps.org/data/structure/index.html>.)

3. Results and Discussion

The present study was designed to test the ability of Taurisol[®] to counteract or reduce the high glucose and TMAO-induced cardiomyocytes damage. All experiments were performed utilizing H9c2 cardiomyoblast cells growth in DMEM with 5.5 mM glucose (NG-H9c2), 44 mM glucose (HG-H9c2); both NG and HG-H9c2 cells were treated with 50 μM TMAO (TNG-H9c2 THG-H9c2). We have set these concentrations of glucose and TMAO, because they produced moderate H9c2 cardiomyocyte toxicity and could be the conditions suitable for mimic in vitro diet-induced obesity (DIO) model.

3.1. Cardioprotective Effects of Taurisol[®] in H9c2 Cells under TMAO-/High Glucose-Induced Cytotoxicity. To gain an insight about the mechanism through which Taurisol[®] sustained the cardiomyocyte viability, we have damaged the H9c2 cardiomyoblastic cell line with high glucose concentration (44 mM) and TMAO, a molecule linked to obesity and energy metabolism [23, 24] (Figure 1). H9c2 vitality was detected *via* MTT assay, while LDH and AST release assays were performed for cellular injury. High glucose treatment of H9c2 (44 mM) significantly reduced cell viability (~25%; $P = 0.011$) and increased both AST and LDH release ($P = 0.037$ and $P = 0.0074$, respectively) compared with the NG-H9c2 growth in standard condition (5.5 mM glucose). In contrast, treatment with Taurisol[®] was able to counteract significantly the decrease of vitality and the AST and LDH release in both HG-H9c2 and THG-H9c2 cells, while at the same concentration, Tau-treated NG-H9c2 did not produce the same effect.

In Figure 1(d), we reported the LDH1 : LDH2 isoenzyme ratio, observing that increased of about 1,8 and 2,5 fold in HG-H9c2 and THG-H9c2, respectively, compared to NG-H9c2 (LDH1 : LDH2 ratio = 1). Interestingly, Taurisol[®]

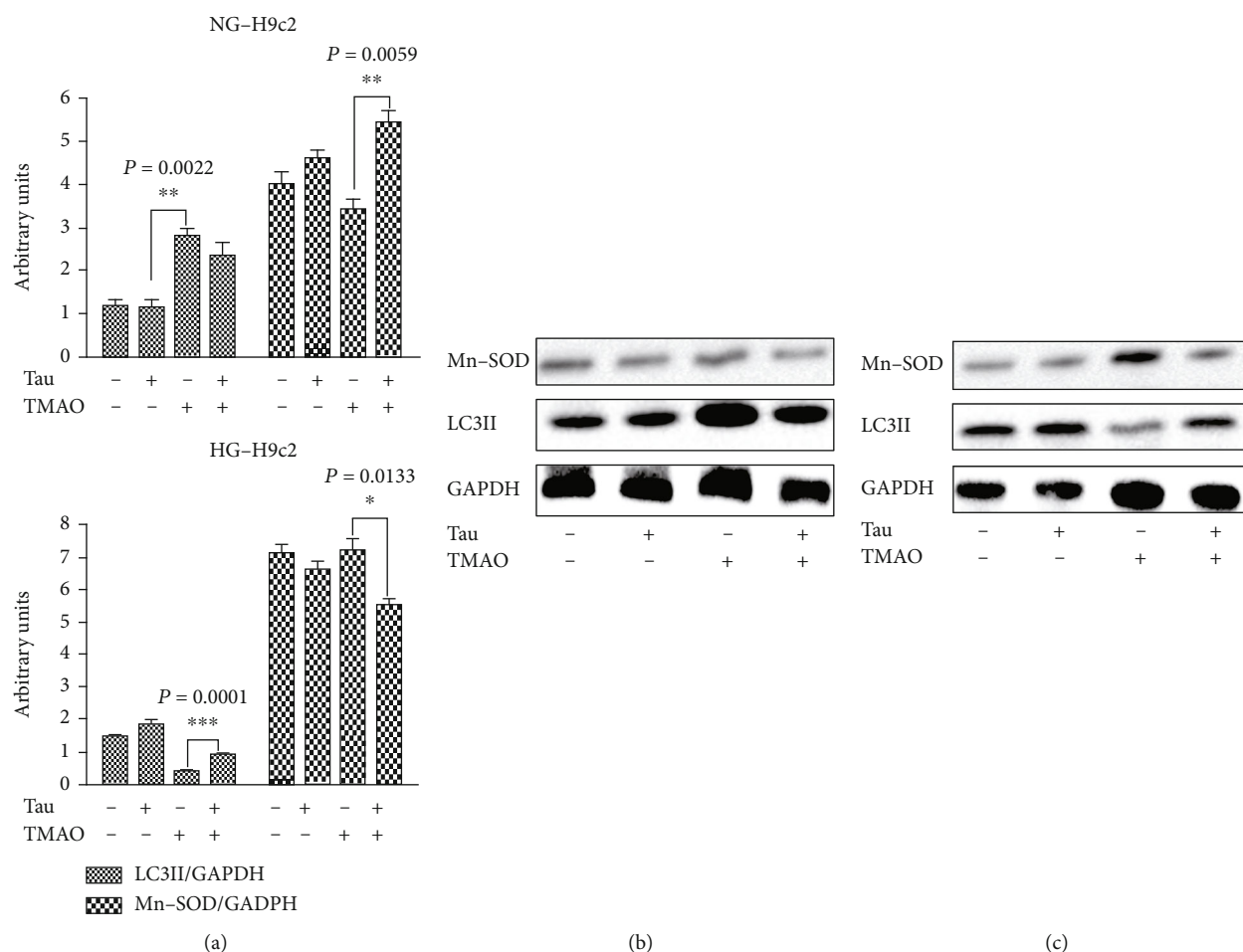


FIGURE 3: Taurisolo® (Tau) increase LC3II expression and counteract high levels of MnSOD. H9c2 cells were grown in standard (5.5 mM Glu NG-H9c2) and high glucose (44 mM Glu, HG9c2) condition. The NG and HG-H9c2 cells were treated, for 72 h with Tau (0.5 $\mu\text{g}/\mu\text{L}$), TMAO (50 μM), and TMAO-Tau combination. (a) Bar graphs show densitometrically quantified LC3II, MnSOD with respect to house-keeping GAPDH in NG (5.5 mM glucose) and HG-H9c2 cells. Representative immunoblots of Tau treated TNG-H9c2 (b) and THG-H9c2 cells (c). Each data point is the average of triplicate measurements, with each experiment performed in triplicate. Results are expressed as mean \pm SD.

treatment of THG-H9c2 counteracted the increase of LDH1/LDH2 ratio. To demonstrate that the effect of Taurisolo® on proliferation was related to the reduction of reactive oxygen species (ROS) production, we evaluated both lipid peroxidation by aldehyde reactive to thiobarbituric acids (TBARS) assay and endogenous free nitric oxide (as NO_2^-) by the Griess assay (Figure 2). We observed a significant increase of TBARS production in THG-H9c2 cells compared to Taurisolo®-treated THG-H9c2 cells ($P = 0.0159$) and an increase of NO production in the medium of Taurisolo®-treated THG-H9c2 ($P = 0.038$) compared with untreated THG-H9c2 cells. Furthermore, Taurisolo® treatment counteracted the higher expression of Manganese Superoxide dismutase (Mn-SOD) in THG-H9c2 cells (Figure 3).

Extracellular signal-regulated protein kinase (ERK) and its phosphorylated form (pERK) are important mediators of various cellular responses, such as proliferation, differentiation, and cell death. It is noting that chronic high glucose induced ERK phosphorylation and cell death. We detected ERK activation by evaluating the pERK/ERK ratio by West-

ern blot analysis using phospho-specific antibodies. ERK activation (Figure 4(a)) was elevated in HG-H9c2 cells compared to NG-H9c2 cells (Figure 4), while it was significantly reduced after TMAO treatment in both NG and HG-H9c2 cells. Of note, treatment with Tau modulated ERK activation in prosurvival manner both HG and THG-H9c2 cells.

Collectively, these data suggested that the association of 72 h-hyperglycemia and 72 h-TMAO treatment of H9c2 cells led to both cardiac cell cytotoxicity and increase in OS, as mainly indicated by the increases of both lipid peroxidation and antioxidant enzyme levels. Taurisolo® treatment mitigated the increases in AST and LDH levels and increased H9c2 cell viability, suggesting its protective effect on cardiomyocytes during both hyperglycemia- and TMAO-caused damage. Furthermore, these results showed that Taurisolo® reduced THG-induced H9c2 injury by reducing OS. Decreased levels of TBARS are combined with increase of free NO production, suggesting a potential involvement of Taurisolo® in regulating the balance between NO and peroxynitrite. A protective effect of NO has also been observed in

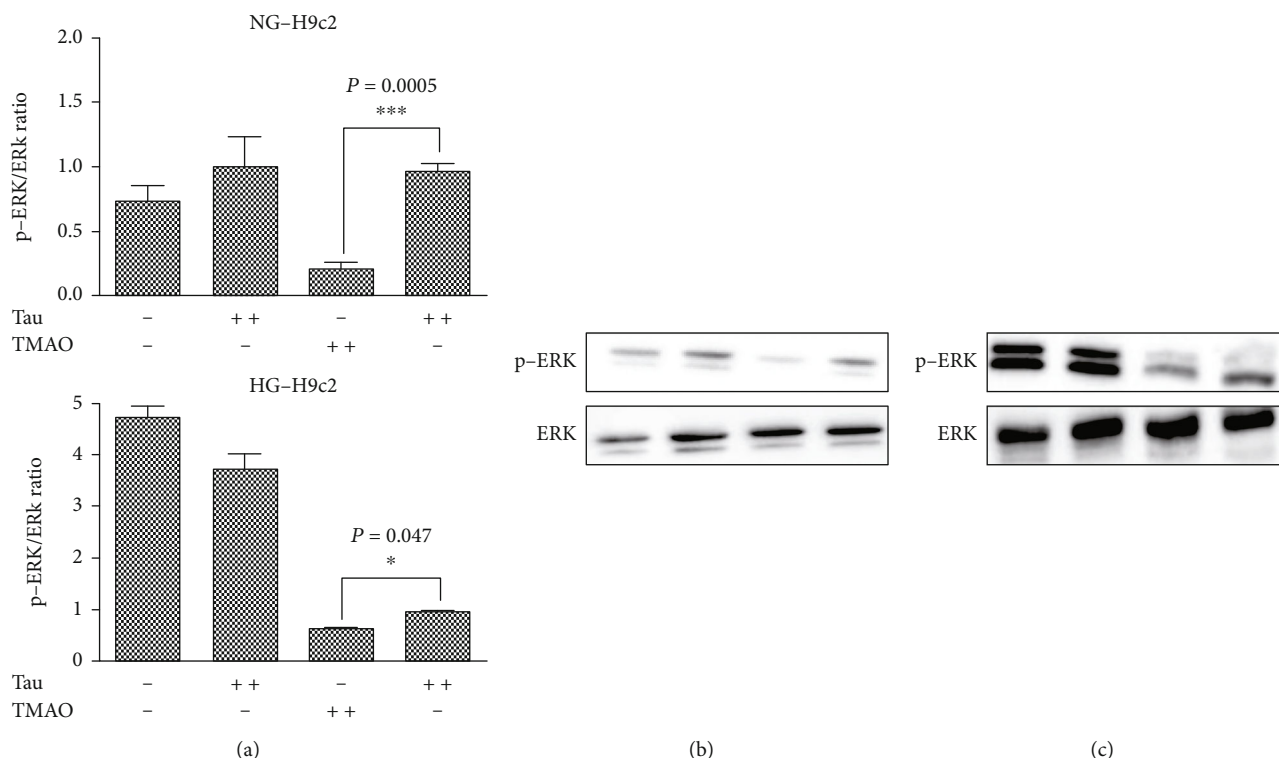


FIGURE 4: Taurisolo® modulated ERK activation. H9c2 cells were grown in standard (5.5 mM Glu NG-H9c2) and high glucose (44 mM Glu, HG9c2) condition. The NG and HG-H9c2 cells were treated, for 72 h with Tau (0.5 $\mu\text{g}/\mu\text{L}$), TMAO (50 μM), and TMAO-Tau combination. (a) Bar graphs show densitometrically quantified ratio of p-ERK/ERK in H9c2 cells. (b) Representative immunoblots of NG-H9c2 cells treated with Tau, TMAO, and Tau-TMAO combination. (c) Representative immunoblots of HG-H9c2 cells treated with Tau, TMAO, and Tau-TMAO combination. Each data point is the average of triplicate measurements, with each experiment performed in triplicate. Results are expressed as mean \pm SD.

endothelial cells, cardiomyocytes [25], and inflammatory cells [26]. When MnSOD is overexpressed, more superoxide radicals are converted to H_2O_2 , which acts as a cytotoxic agent, and therefore are removed from the physiological equilibrium, causing an increased production of membrane lipid peroxidation. To demonstrate that the cellular damage effect of high glucose and TMAO was related to increased oxidative stress, we assessed cell vitality after treatment for 24 h with 10 μM N-acetyl cysteine (NAC) widely used as a pharmacological antioxidant and cytoprotective compound. In this experimental condition, we did not observe growth inhibition in both HG and THG-H9c2 cells (data not shown). In conclusion, the protective effect of Taurisolo® on cell viability and cell injury is closely linked to the antioxidant activity of its polyphenol composition. To demonstrate that the antiproliferative effect induced in high glucose concentration was related to increased oxidative stress, we assessed cell vitality after treatment for 24 h with 10 μM NAC. In this experimental condition, we did not observe growth inhibition in both HG and THG-H9c2 cells (data not shown) compared to NG-H9c2 cells. In conclusion, the protective effect of Taurisolo® on cell viability and cell injury is closely linked to the antioxidant activity of its polyphenol composition. The antioxidant potential of Taurisolo® results in decreased both expression of MnSOD (Figures 3(a)–3(c)) and lipid peroxidation levels. Conversely, the increased release of NO leads to an ERK activation and a consequently

prosurvival effect against TMAO damage induced in the H9c2 cells.

3.2. Taurisolo® Increases Autophagic Process and Remodeling α -Actin Distribution under High Glucose- and TMAO-Induced H9c2 Injury. As autophagy is important for the maintenance of mitochondrial homeostasis, it was hypothesized that Taurisolo® may preserve the H9c2 from injury induced by TMAO and hyperglycemia *via* autophagy activation. To prove this hypothesis, we evaluated the autophagy marker protein microtubule-associated protein LC3II expression by western blot analysis. TMAO treatment of HG-H9c2 induced a downregulation of autophagy, as evidenced by a decrease in LC3II, compared with the HG-H9c2 cells. 72 h-treatment with TMAO/Taurisolo® combination of HG-H9c2 cells was able to reverse the decrease of LC3II expression in THG-H9c2 cells (Figures 3(a)–3(c)). Morphological changes induced by both HG and TMAO in H9c2 cells were detected by α -actin immunofluorescence by confocal microscopy; the representative results were shown in Figure 5. The α -actin protein (green signal) in Taurisolo®-treated HG-H9c2 cells was uniformly distributed in the cytoplasm, and cells presented a typical elongated form with respect to untreated HG-H9c2 cells where the shape appeared enlarged and rounded; in THG-H9c2 cells, α -actin accumulated, forming evident punctuated signals.

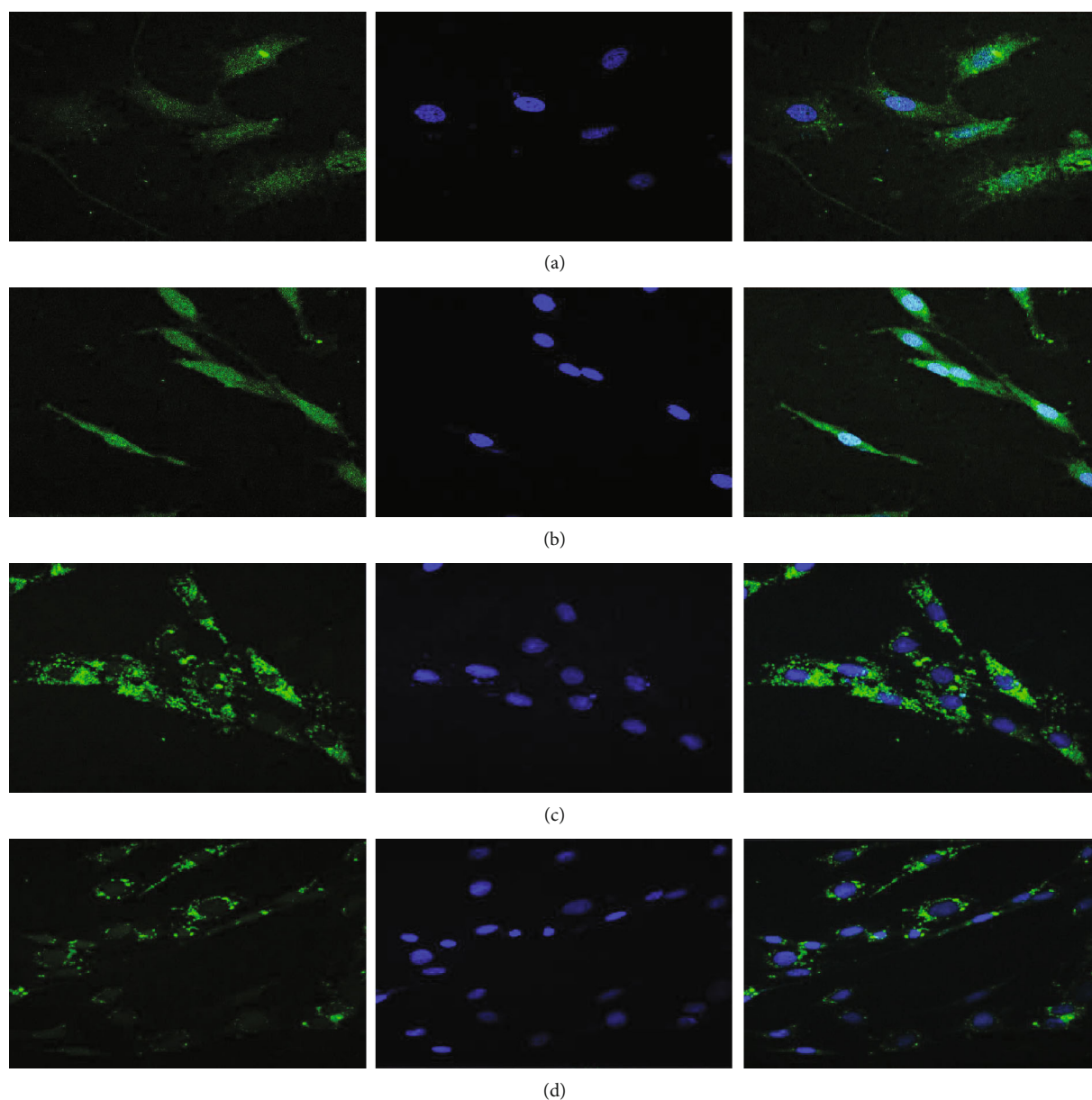


FIGURE 5: Representative microphotographs of HG-H9c2 cells. Cardiomyocyte was identified with α -actin antibody (green signal), and the nucleus was identified by DAPI (blue signal). (a) H9c2 cell growth with 44 mM glucose (HG-H9c2). (b) HG-H9c2 was treated for 72 h with Tau (0.5 $\mu\text{g}/\mu\text{L}$). (c) HG-H9c2 cell was treated for 72 h with TMAO (50 μM). (d) HG-H9c2 cell was treated for 72 h with TMAO/Tau combination.

Meanwhile, Taurisolo[®] treatment reduced actin aggregation in THG-H9c2 cells. These results demonstrate that exposure to Taurisolo[®] in both HG and THG-H9c2 cells induced α -actin spatial organization and a functional cell morphological conformation. The purpose of autophagy is to ensure quality control of organelles and proteins, as well as protection of intracellular homeostasis in stress and nutrient efficiency [27–32]. Autophagy is involved in the maintenance of organelle integrity, protein quality [33], and modulated and to participate in the pathogenesis of human diseases, such as DM, neurodegenerative diseases, aging, and vascular disease [7, 34, 35]. It has been reported that antioxidant molecules such as resveratrol by increasing autophagic flux ameliorates diabetic cardiomyopathy [36]. In THG-H9c2 damage cell model

cells, we demonstrated that Taurisolo[®], restoring the autophagic process, induces a reduction of the actin aggregation, restoring a normal cell morphology.

3.3. Taurisolo[®] Induces the Ex Novo Synthesis of Sphingomyelin, Ceramides, and Their Metabolites. SLs are molecules implicated in cell survival and autophagy. Bioactive lysolipids, including Cer and sphingosine-1-phosphate, may act as both extracellular and intracellular mediators. We used tandem mass spectrometry to investigate which sphingolipids were secreted in the cell medium in Taurisolo[®]-treated HG- and THG-H9c2 cells. In Figure 6, the positive ion mass spectrometry profile of lipid extract in the medium of the HG-H9c2, THG-

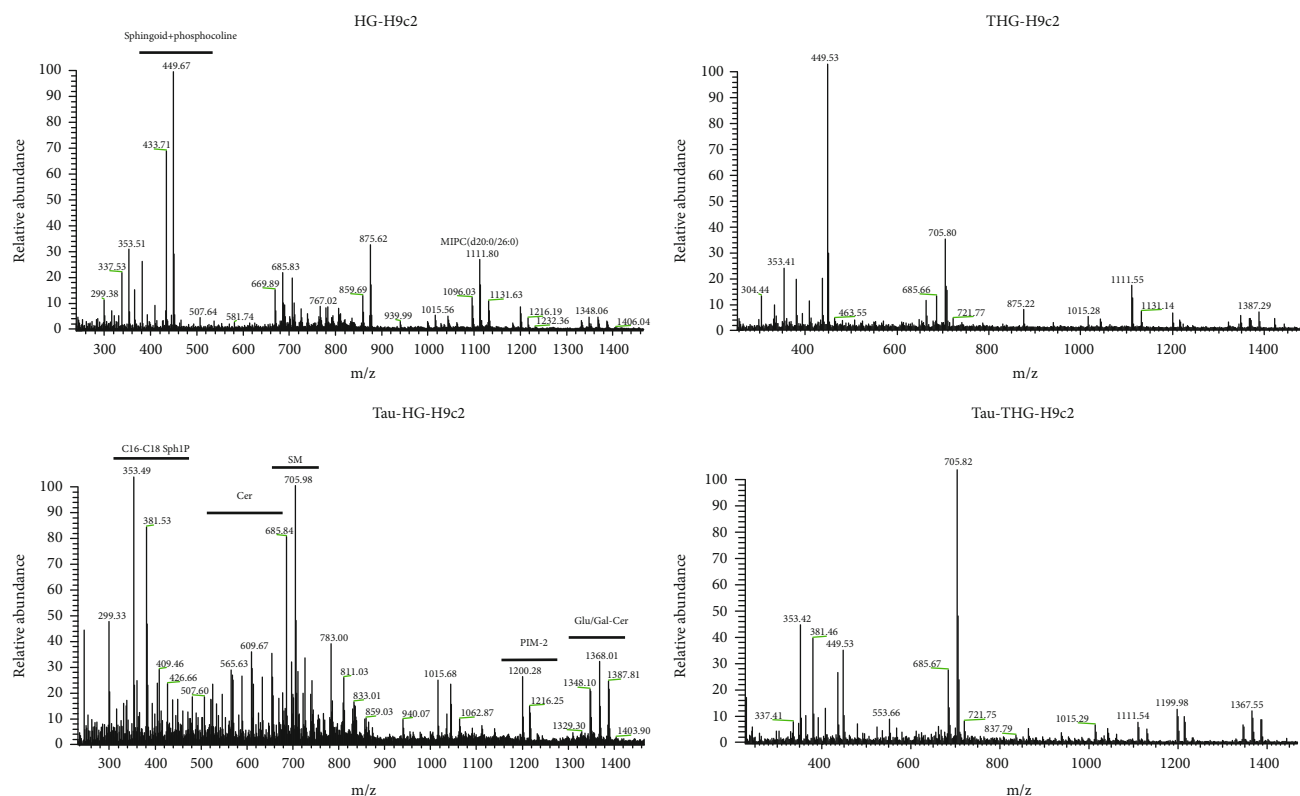


FIGURE 6: Positive mass spectra of lipid extracted from media of H9c2 cells. Positive ion electrospray mass spectra of lipid molecular species in lipid extracts from medium of the HG-H9c2 (44 mM glucose) and THG-H9c2 (44 mM glucose + 50 μ M TMAO) before and after Tau treatment (Tau-HG-H9c2; Tau-THG-H9c2). Aliquots of chloroform extracts were analyzed directly by electrospray as described in the Materials and Methods section. Selected peaks are indicated by their m/z values. For detailed peak assignments, see Table 1 (Supplementary Materials).

H9c2, and both Taurisol[®]-treated HG- and THG-H9c2 cells was reported. In both HG- and THG-H9c2 spectra, we identified the following peaks: d18: 1 sphingoid base and phosphocholine headgroup (449 m/z) [37] (Monounsaturated 18-carbon dihydroxylated sphingoid base linked to one chain of palmitic acid denominated 1-O-tricosanoyl-Cer (d18: 1/16: 0) (875 m/z) and N-(hexacosanoyl)-eicosasphinganine-1-O-[D-mannopyranosyl- α -1-2-myoinositol-1-phosphate] MIPC (d20:0/26:0) (1111 m/z). We observed in the lipid fingerprint profile of Tau-treated HG- and THG-H9c2 cells that the metabolite peaks were centered between 200 and 1500 m/z as sphingosine, C16-C18 sphinganine-1-phosphate, PE-Cer (d16:2/20:1), SM (d18:0/16:0), PI-Cer (d18:0/16:0), 1-O-stearoyl-Cer (d18:1/18:0)/Or 1-O-eicosanoyl-Cer (d18:1/16:0), MIPC (18:/20), PIM2 (16:0/18:1), and Glu/Gal-ceramide. Cer plays a central role in sphingolipid metabolism. Cer consists of sphingoid long-chain base linked to an acyl chain *via* an amide bond and synthesized *de novo* in the endoplasmic reticulum (ER); it can be modified into Golgi in sphingomyelin (SM), sphingosine, and glycosphingolipids (e.g., galactosylceramide) and are transported to the plasma membrane (PM). Cer can then be metabolized into ceramide-1-phosphate (C1P) and sphingosine-1-phosphate (S1P) or be resynthesized back into SM. Sphingosine was associated with growth arrest [38] (whereas SP1 promoted

cell proliferation and prevents programmed cell death [39]). In H9c2 cells, higher glucose concentration may block the Cer production and then promote transformation in SM and Sph1P, whereas Taurisol[®] treatment of HG and THG-H9c2 cells induced a reprogramming lipid metabolism and increased Cer, SM, and Sph1P productions that may protect the cardiomyocyte from glucose cytotoxicity. Further *in vivo* researches may serve to license Taurisol[®] as a useful nutraceutical approach in the prevention of heart damage in obese subjects.

4. Conclusion

It has been previously reported that polyphenols enhance glucose uptake, mainly in the muscular tissue, *via* increasing expression and/or translocation of GLUT4 transporters [40–42]. Moreover, studies demonstrated that polyphenols Resveratrol and Quercetin exert antioxidant and anti-inflammatory properties [43–46] and can ameliorate the diabetic complications [47]. However, the beneficial effects of polyphenolic compounds in functional foods and nutraceuticals are affected by several factors compromising their bioavailability. Notably, several strategies have been developed by the pharmaceutical and nutraceutical industries in order to counteract this crucial concern, including microencapsulation in various coating materials. Microencapsulation,

indeed, has been demonstrated to (i) protect polyphenols against degrading factors met during the transit in the gastrointestinal tract, including pH variations and digestive enzymes (increasing, thus, their bioaccessibility) and (ii) favor their absorption across the intestinal barrier (increasing their bioavailability) [48]. In this sense, Taurisol[®] is a nutraceutical formulation based on grape polyphenols microencapsulated in maltodextrins. In our previous studies [16], we demonstrated high bioavailability of Taurisol[®] polyphenols, leading to assume that also after oral administration, these bioactive compounds may reach high tissue concentrations.

Annunziata and colleagues [16, 17] have demonstrated the ability of the Taurisol[®] to reduce circulating levels of TMAO, a molecule related to metabolic syndrome and cardiovascular risk [49]. Moreover, the TMAO levels are inversely associated with the adherence to the Mediterranean diet [50]. The present study was designed to test the ability of Taurisol[®] to counteract or reduce the cardiomyocytes damage induced by high glucose concentration and TMAO. The hyperglycemia in ventricular cardiomyoblasts H9c2 cell induces cytotoxicity, OS, and cellular hypertrophy, whereas TMAO reduces autophagy and causes actin accumulation. Taurisol[®] exerted a protective effect on both hyperglycemia and TMAO-induced H9c2 cell injury by (1) modulation of OS through its direct scavenger action, (2) induction of morphological changes by α -actin redistribution, and (3) activation of the autophagic process by means of the *ex novo* synthesis of Cers and their metabolites [51]. Here, we demonstrated that Taurisol[®] improves *in vitro* HG- and TMAO-induced H9c2 dysfunction, suggesting that Taurisol[®], combined with energy restriction, may represent a useful nutraceutical approach for the prevention of cardiomyopathy in obese subjects.

Abbreviations

Sph:	Sphingosine
Sph1P:	Sphingosine 1-phosphate
Cer:	Ceramide
Cer1P:	Ceramide 1-phosphate
GalCer:	Galactosylceramide
GlcCer:	Glucosylceramide
LacCer:	Lactosylceramide
GM, GD, GT:	Gangliosides
SM:	Sphingomyelin
LC-MS/MS:	Liquid chromatography tandem mass spectrometry
Q:	Quadrupole
QQQ:	Triple quadrupole
QTrap:	Quadrupole linear ion trap
PI-P:	Phospho-(1'-myo-inositol)
LC3:	Microtubule-associated protein 1 light chain 3.

Data Availability

The data used to support the findings of this study are available from the corresponding author upon request.

Conflicts of Interest

The authors declare no conflicts of interest.

Acknowledgments

This study was supported by grants from the University of Campania Luigi Vanvitelli (grant number: B21B19000480008) and University of Naples Federico II (grant number: B61B19000530008). This work was supported by the Ministero dello Sviluppo economico National Operative Program 2014-2020 FESR.

Supplementary Materials

Assignments of the *m/z* ratios detected in the positive ion mass spectra of the lipid extracts in the growth medium of HG-H9c2 (44 mM glucose) and THG-H9c2 (44 mM glucose +TMAO 50 μ M) cells before and after treatment with Tau 0.5 μ g/ μ L. (*Supplementary Materials*)

References

- [1] G. Messina, R. Polito, V. Monda et al., "Functional role of dietary intervention to improve the outcome of COVID-19: a hypothesis of work," *International Journal of Molecular Sciences*, vol. 21, no. 9, article 3104, 2020.
- [2] P. Hossain, B. Kavar, and M. El Nahas, "Obesity and diabetes in the developing world—a growing challenge," *The New England Journal of Medicine*, vol. 356, no. 3, pp. 213–215, 2007.
- [3] J. Stock, "Gut microbiota: an environmental risk factor for cardiovascular disease," *Atherosclerosis*, vol. 229, no. 2, pp. 440–442, 2013.
- [4] C. Chrysohoou, D. B. Panagiotakos, C. Pitsavos et al., "The implication of obesity on total antioxidant capacity in apparently healthy men and women. The ATTICA study," *Nutrition, Metabolism, and Cardiovascular Diseases*, vol. 17, no. 8, pp. 590–597, 2007.
- [5] C. Patel, H. Ghanim, S. Ravishankar et al., "Prolonged reactive oxygen species generation and nuclear factor-kappaB activation after a high-fat, high-carbohydrate meal in the obese," *The Journal of Clinical Endocrinology and Metabolism*, vol. 92, no. 11, pp. 4476–4479, 2007.
- [6] J. D. Malhotra, H. Miao, K. Zhang et al., "Antioxidants reduce endoplasmic reticulum stress and improve protein secretion," *Proceedings of the National Academy of Sciences*, vol. 105, no. 47, pp. 18525–18530, 2008.
- [7] Q. He, S. Sha, L. Sun, J. Zhang, and M. Dong, "GLP-1 analogue improves hepatic lipid accumulation by inducing autophagy via AMPK/mTOR pathway," *Biochemical and Biophysical Research Communications*, vol. 476, no. 4, pp. 196–203, 2016.
- [8] J. Yan, Z. Feng, J. Liu et al., "Enhanced autophagy plays a cardinal role in mitochondrial dysfunction in type 2 diabetic Goto-Kakizaki (GK) rats: ameliorating effects of (-)-epigallocatechin-3-gallate," *The Journal of Nutritional Biochemistry*, vol. 23, no. 7, pp. 716–724, 2012.
- [9] W. Zheng, J. Kollmeyer, H. Symolon et al., "Ceramide and other bioactive sphingolipid backbones in health and disease: lipidomic analysis, metabolism and roles in membrane

- structure, dynamics, signaling and autophagy," *Biochimica et Biophysica Acta*, vol. 1758, no. 12, pp. 1864–1884, 2006.
- [10] R. D. Sentelle, C. E. Senkal, W. Jiang et al., "Ceramide targets autophagosomes to mitochondria and induces lethal mitophagy," *Nature Chemical Biology*, vol. 8, no. 10, pp. 831–838, 2012.
- [11] G. Lavieu, F. Scarlatti, G. Sala et al., "Regulation of autophagy by sphingosine kinase 1 and its role in cell survival during nutrient starvation," *The Journal of Biological Chemistry*, vol. 281, no. 13, pp. 8518–8527, 2006.
- [12] Y. Li, S. Li, X. Qin et al., "The pleiotropic roles of sphingolipid signaling in autophagy," *Cell Death & Disease*, vol. 5, no. 5, article e1245, 2014.
- [13] O. Cuvillier, G. Pirianov, B. Kleuser et al., "Suppression of ceramide-mediated programmed cell death by sphingosine-1-phosphate," *Nature*, vol. 381, no. 6585, pp. 800–803, 1996.
- [14] J. R. Van Brocklyn and J. B. Williams, "The control of the balance between ceramide and sphingosine-1-phosphate by sphingosine kinase: oxidative stress and the seesaw of cell survival and death," *Comparative Biochemistry and Physiology Part B: Biochemistry & Molecular Biology*, vol. 163, no. 1, pp. 26–36, 2012.
- [15] R. Obeid, H. M. Awwad, Y. Rabagny, S. Graeber, W. Herrmann, and J. Geisel, "Plasma trimethylamine N-oxide concentration is associated with choline, phospholipids, and methyl metabolism," *The American Journal of Clinical Nutrition*, vol. 103, no. 3, pp. 703–711, 2016.
- [16] G. Annunziata, M. Maisto, C. Schisano et al., "Effects of Grape Pomace Polyphenolic Extract (Taurisolo®) in reducing TMAO serum levels in humans: preliminary results from a randomized, placebo-controlled, cross-over study," *Nutrients*, vol. 11, no. 1, p. 139, 2019.
- [17] G. Annunziata, M. Maisto, C. Schisano et al., "Effect of grape pomace polyphenols with or without pectin on TMAO serum levels assessed by LC/MS-based assay: a preliminary clinical study on overweight/obese subjects," *Frontiers in Pharmacology*, vol. 10, p. 575, 2019.
- [18] D. Lapi, M. Stornaiuolo, L. Sabatino et al., "The pomace extract taurisolo protects rat brain from ischemia-reperfusion injury," *Frontiers in Cellular Neuroscience*, vol. 14, p. 3, 2020.
- [19] I. Gomez-Monterrey, P. Campiglia, C. Aquino et al., "Design, synthesis, and cytotoxic evaluation of acyl derivatives of 3-aminonaphtho[2,3-b]thiophene-4,9-dione, a quinone-based system," *Journal of Medicinal Chemistry*, vol. 54, no. 12, pp. 4077–4091, 2011.
- [20] C. G. Tenore, E. Pagano, S. Lama et al., "Intestinal anti-inflammatory effect of a peptide derived from gastrointestinal digestion of buffalo (*Bubalus bubalis*) mozzarella cheese," *Nutrients*, vol. 11, no. 3, p. 610, 2019.
- [21] G. C. Tenore, M. Manfra, P. Stiuso et al., "Antioxidant profile and in vitro cardiac radical-scavenging versus pro-oxidant effects of commercial red grape juices (*Vitis vinifera* L. cv. Aglianico N.)," *Journal of Agricultural and Food Chemistry*, vol. 60, no. 38, pp. 9680–9687, 2012.
- [22] D. Vanacore, G. Messina, S. Lama et al., "Effect of restriction vegan diet's on muscle mass, oxidative status, and myocytes differentiation: a pilot study," *Journal of Cellular Physiology*, vol. 233, no. 12, pp. 9345–9353, 2018.
- [23] J. Miao, A. V. Ling, P. V. Manthena et al., "Flavin-containing monooxygenase 3 as a potential player in diabetes-associated atherosclerosis," *Nature Communications*, vol. 6, no. 1, article 6498, 2015.
- [24] D. M. Shih, Z. Wang, R. Lee et al., "Flavin containing monooxygenase 3 exerts broad effects on glucose and lipid metabolism and atherosclerosis," *Journal of Lipid Research*, vol. 56, no. 1, pp. 22–37, 2015.
- [25] L. Santucci, A. Mencarelli, B. Renga et al., "Nitric oxide modulates proapoptotic and antiapoptotic properties of chemotherapy proapoptotic and antiapoptotic properties of chemotherapy agents: the case of NO-pegylated epirubicin," *The FASEB Journal*, vol. 20, no. 6, pp. 765–767, 2006.
- [26] D. Ronchetti, V. Borghi, G. Gaitan, J. F. Herrero, and F. Impagnatiello, "NCX 2057, a novel NO-releasing derivative of ferulic acid, suppresses inflammatory and nociceptive responses in in vitro and in vivo models," *British Journal of Pharmacology*, vol. 158, no. 2, pp. 569–579, 2009.
- [27] A. Salminen, K. Kaarniranta, and A. Kauppinen, "AMPK and HIF signaling pathways regulate both longevity and cancer growth: the good news and the bad news about survival mechanisms," *Biogerontology*, vol. 17, no. 4, pp. 655–680, 2016.
- [28] S. Kume and D. Koya, "Autophagy: a novel therapeutic target for diabetic nephropathy," *Diabetes and Metabolism Journal*, vol. 39, no. 6, pp. 451–460, 2015.
- [29] S. Cetrullo, S. D'Adamo, B. Tantini, R. M. Borzi, and F. Flamigni, "mTOR, AMPK, and Sirt1: key players in metabolic stress management," *Critical Reviews in Eukaryotic Gene Expression*, vol. 25, no. 1, pp. 59–75, 2015.
- [30] E. A. Dunlop and A. R. Tee, "mTOR and autophagy: a dynamic relationship governed by nutrients and energy," *Seminars in Cell & Developmental Biology*, vol. 36, pp. 121–129, 2014.
- [31] S. Sridharan, K. Jain, and A. Basu, "Regulation of autophagy by kinases," *Cancers*, vol. 3, no. 2, pp. 2630–2654, 2011.
- [32] N. Mizushima and M. Komatsu, "Autophagy: renovation of cells and tissues," *Cell*, vol. 147, no. 4, pp. 728–741, 2011.
- [33] K. Zientara-Rytter and S. Subramani, "Autophagic degradation of peroxisomes in mammals," *Biochemical Society Transactions*, vol. 44, no. 2, pp. 431–440, 2016.
- [34] M. Lippai and Z. Szatmari, "Autophagy from molecular mechanisms to clinical relevance," *Cell Biology and Toxicology*, vol. 33, no. 2, pp. 145–168, 2017.
- [35] B. Wang, Q. Yang, Y. Y. Sun et al., "Resveratrol-enhanced autophagic flux ameliorates myocardial oxidative stress injury in diabetic mice," *Journal of Cellular and Molecular Medicine*, vol. 18, no. 8, pp. 1599–1611, 2014.
- [36] X. X. Lv, S. S. Liu, and Z. W. Hu, "Autophagy-inducing natural compounds: a treasure resource for developing therapeutics against tissue fibrosis," *Journal of Asian Natural Products Research*, vol. 19, no. 2, pp. 101–108, 2017.
- [37] M. C. Sullards, Y. Liu, Y. Chen, and A. H. Merrill Jr., "Analysis of mammalian sphingolipids by liquid chromatography tandem mass spectrometry (LC-MS/MS) and tissue imaging mass spectrometry (TIMS)," *Biochimica et Biophysica Acta*, vol. 1811, no. 11, pp. 838–853, 2011.
- [38] L. R. Ballou, C. P. Chao, M. A. Holness, S. C. Barker, and R. Raghov, "Interleukin-1-mediated PGE2 production and sphingomyelin metabolism. Evidence for the regulation of cyclooxygenase gene expression by sphingosine and ceramide," *Journal of Biological Chemistry*, vol. 267, no. 28, pp. 20044–20050, 1992.

- [39] S. Spiegel and S. Milstien, "Sphingosine-1-phosphate: signaling inside and out," *FEBS Letters*, vol. 476, no. 1-2, pp. 55–57, 2000.
- [40] N. Kim, J. O. Lee, H. J. Lee et al., "AMPK, a metabolic sensor, is involved in isoeugenol-induced glucose uptake in muscle cells," *The Journal of Endocrinology*, vol. 228, no. 2, pp. 105–114, 2016.
- [41] S. Momtaz, A. Salek-Maghsoudi, A. H. Abdolghaffari et al., "Polyphenols targeting diabetes via the AMP-activated protein kinase pathway; future approach to drug discovery," *Critical Reviews in Clinical Laboratory Sciences*, vol. 56, no. 7, pp. 472–492, 2019.
- [42] F. Vlavcheski, D. Baron, I. A. Vlachogiannis, R. MacPherson, and E. Tsiani, "Carnosol increases skeletal muscle cell glucose uptake via AMPK-dependent GLUT4 glucose transporter translocation," *International Journal of Molecular Sciences*, vol. 19, no. 5, article 1321, 2018.
- [43] D. M. Breen, T. Sanli, A. Giacca, and E. Tsiani, "Stimulation of muscle cell glucose uptake by resveratrol through sirtuins and AMPK," *Biochemical and Biophysical Research Communications*, vol. 374, no. 1, pp. 117–122, 2008.
- [44] E. Conte, E. Fagone, M. Fruciano, E. Gili, M. Iemmolo, and C. Vancheri, "Anti-inflammatory and antifibrotic effects of resveratrol in the lung," *Histology and Histopathology*, vol. 30, no. 5, pp. 523–529, 2015.
- [45] M. Suwalsky, F. Villena, and M. J. Gallardo, "In vitro protective effects of resveratrol against oxidative damage in human erythrocytes," *Biochimica et Biophysica Acta (BBA) - Biomembranes*, vol. 1848, no. 1, pp. 76–82, 2015.
- [46] F. C. Huang, H. C. Kuo, Y. H. Huang, H. R. Yu, S. C. Li, and H. C. Kuo, "Anti-inflammatory effect of resveratrol in human coronary arterial endothelial cells via induction of autophagy: implication for the treatment of Kawasaki disease," *BMC Pharmacology and Toxicology*, vol. 18, no. 1, p. 3, 2017.
- [47] G. J. Shi, Y. Li, Q. H. Cao et al., "In vitro and in vivo evidence that quercetin protects against diabetes and its complications: a systematic review of the literature," *Biomedicine & Pharmacotherapy*, vol. 109, pp. 1085–1099, 2019.
- [48] G. Annunziata, M. Jimenez-Garcia, X. Capo et al., "Microencapsulation as a tool to counteract the typical low bioavailability of polyphenols in the management of diabetes," *Food and Chemical Toxicology*, vol. 139, article 111248, 2020.
- [49] L. Barrea, G. Annunziata, G. Muscogiuri et al., "Trimethylamine-N-oxide (TMAO) as novel potential biomarker of early predictors of metabolic syndrome," *Nutrients*, vol. 10, no. 12, article 1971, 2018.
- [50] L. Barrea, G. Annunziata, G. Muscogiuri et al., "Trimethylamine N-oxide, Mediterranean diet, and nutrition in healthy, normal-weight adults: also a matter of sex?," *Nutrition*, vol. 62, pp. 7–17, 2019.
- [51] C. Bedia, T. Levade, and P. Codogno, "Regulation of autophagy by sphingolipids," *Anti-Cancer Agents in Medicinal Chemistry*, vol. 11, no. 9, pp. 844–853, 2011.

Research Article

Chicoric Acid Ameliorates Nonalcoholic Fatty Liver Disease via the AMPK/Nrf2/NFκB Signaling Pathway and Restores Gut Microbiota in High-Fat-Diet-Fed Mice

Xiaoqin Ding ¹, Tunyu Jian ¹, Jiawei Li ¹, Han Lv ¹, Bei Tong ¹, Jing Li ²,
Xiuhua Meng ¹, Bingru Ren ¹ and Jian Chen ^{1,2}

¹Institute of Botany, Jiangsu Province and Chinese Academy of Sciences, Nanjing 210014, China

²Department of Food Science and Technology, College of Light Industry and Food Engineering, Nanjing Forestry University, Nanjing 210037, China

Correspondence should be addressed to Jian Chen; chenjian80@aliyun.com

Received 1 July 2020; Revised 29 September 2020; Accepted 8 October 2020; Published 4 November 2020

Academic Editor: Massimo Collino

Copyright © 2020 Xiaoqin Ding et al. This is an open access article distributed under the Creative Commons Attribution License, which permits unrestricted use, distribution, and reproduction in any medium, provided the original work is properly cited.

This study examines the effects of chicoric acid (CA) on nonalcoholic fatty liver disease (NAFLD) in high-fat-diet- (HFD-) fed C57BL/6 mice. CA treatment decreased body weight and white adipose weight, mitigated hyperglycemia and dyslipidemia, and reduced hepatic steatosis in HFD-fed mice. Moreover, CA treatment reversed HFD-induced oxidative stress and inflammation both systemically and locally in the liver, evidenced by the decreased serum malondialdehyde (MDA) abundance, increased serum superoxide dismutase (SOD) activity, lowered *in situ* reactive oxygen species (ROS) in the liver, decreased serum and hepatic inflammatory cytokine levels, and reduced hepatic inflammatory cell infiltration in HFD-fed mice. In addition, CA significantly reduced lipid accumulation and oxidative stress in palmitic acid- (PA-) treated HepG2 cells. In particular, we identified AMPK as an activator of Nrf2 and an inactivator of NFκB. CA upregulated AMPK phosphorylation, the nuclear protein level of Nrf2, and downregulated NFκB protein level both in HFD mice and PA-treated HepG2 cells. Notably, AMPK inhibitor compound C blocked the regulation of Nrf2 and NFκB, as well as ROS overproduction mediated by CA in PA-treated HepG2 cells, while AMPK activator AICAR mimicked the effects of CA. Similarly, Nrf2 inhibitor ML385 partly blocked the regulation of antioxidative genes and ROS overproduction by CA in PA-treated HepG2 cells. Interestingly, high-throughput pyrosequencing of 16S rRNA suggested that CA could increase *Firmicutes*-to-*Bacteroidetes* ratio and modify gut microbial composition towards a healthier microbial profile. In summary, CA plays a preventative role in the amelioration of oxidative stress and inflammation via the AMPK/Nrf2/NFκB signaling pathway and shapes gut microbiota in HFD-induced NAFLD.

1. Introduction

Nonalcoholic fatty liver disease (NAFLD), characterized by hepatic fat accumulation in patients without consumption of excessive alcohol, is the manifestation of metabolic syndrome in the liver. NAFLD ranges from simple hepatic steatosis to steatohepatitis (NASH), fibrosis, and cirrhosis [1]. The prevalence of NAFLD is increasing rapidly worldwide, which has become the major cause of chronic liver disease consistent with the increasing incidence of obesity [2]. The underlying mechanism in the development of NAFLD is complicated. The increase of free fatty acid (FFA) levels could

cause fat accumulation, along with consequent oxidative stress and insulin resistance to activate proinflammatory cytokine production and release systemically and locally in the liver [3]. Hepatic oxidative stress and inflammation have been revealed to play critical roles in the progression of NAFLD in recent studies [3, 4]. It is reported that anti-inflammatory therapy can effectively improve the NAFLD/NASH [5]. Besides, gut microbiota was also considered to play an important role in the pathophysiology of NAFLD, through the gut-liver axis [6].

Adenosine monophosphate-activated protein kinase (AMPK) has been proposed to be a potential therapeutic

target of NAFLD [7]. As a key energy sensor to alter metabolic pathways, previous studies largely focused on its role on regulation of energy metabolism in related diseases [8, 9]; however, AMPK also took part in the modulation of inflammatory signaling pathways [10]. Recently, attention has shifted toward the role of AMPK on influence of inflammatory degree in metabolic disorders [11], yet its action on alleviating the progression of NAFLD has not been attracted sufficiently. In response to chronic low-grade inflammation induced by high-fat diet (HFD), AMPK activity was found to be reduced in the liver [12]. Moreover, liver-specific AMPK activation would decrease the expression of inflammation genes, which gain improvements in obesity [13]. Besides, it is believed that AMPK exerts a positive influence on Kelch-like ECH-associated protein 1/nuclear factor-related factor 2 (keap1/Nrf2) signaling [14], thus increasing the cellular defense against oxidative and other harmful insults. Accumulating evidence suggests the functional crosstalk between Nrf2 and nuclear factor- κ B (NF κ B) [15], since the latter is a key transcription factor regulating the cellular response to inflammation. Nevertheless, the related association among AMPK, Nrf2, and NF κ B signaling in the liver has not been well investigated in NAFLD. Therefore, we started to examine the crosstalk among AMPK, Nrf2, and NF κ B in the alleviation of hepatic oxidative and inflammatory injury in high-fat-induced NAFLD.

Chicoric acid (CA), a major nutraceutical component of chicory (*Cichorium intybus* L.), exhibited a wide range of pharmacological effects including antioxidant, antiviral, anti-inflammatory, and antihyperglycemic activities [16–19]. Although there are few reports revealing the protective effects of chicory seed extract on diabetes- and oleic acid-induced NAFLD [20], information concerning the specific molecular mechanism of CA on HFD-induced NAFLD is rarely available. Growing scientific evidence has demonstrated the regulation of gut microbiota by natural compounds in metabolic disorders which also include NAFLD [21, 22], while the effect of CA on gut microbiota still remains unclear. Overall, the aim of the present study was to investigate the effect and its underlying mechanism of CA on oxidative stress and inflammation in the liver of HFD mice and palmitic acid- (PA-) incubated human hepatoma cell line (HepG2), in addition, to further explore the potential crosstalk among the AMPK, keap1/Nrf2, and NF κ B pathways, and to evaluate whether its effects are related to modulations in the gut microbiota of HFD mice.

2. Results

2.1. CA Mitigated Hyperglycemia, Dyslipidemia, and Systemic Inflammation in Mice Fed with a High-Fat Diet. As illustrated in Figures 1(a) and 1(b), significant higher body weight and white adipose weight were observed in the HFD group in comparison with the ND group ($p < 0.001$). CA (15 and 30 mg/kg) administration significantly reduced body weight and white adipose weight in comparison with the HFD group ($p < 0.01$, $p < 0.001$). Compared with the ND mice, the HFD mice exhibited a significant increase in fasting blood glucose level ($p < 0.001$). Consequently, CA significantly reduced

fasting blood level in mice fed with a high-fat diet (Figure 1(c); $p < 0.001$). In addition, compared with the ND mice, serum total cholesterol (TC), triglyceride (TG), and low-density lipoprotein cholesterol (LDL-C) levels were significantly increased, and high-density lipoprotein cholesterol (HDL-C) level was decreased in the HFD mice ($p < 0.001$), while CA administration significantly downregulated TC, TG, and LDL-C levels, as well as upregulated HDL-C level (Figures 1(d)–1(g); $p < 0.05$, $p < 0.001$). Furthermore, the serum levels of interleukin- (IL-) 2, IL-6, IL-1 β , and tumor necrosis factor- (TNF-) α were all increased in the HFD group in comparison with the ND group ($p < 0.001$). Consequently, CA (15 and 30 mg/kg) administration led to the reduction of IL-2 ($p < 0.01$), IL-6 ($p < 0.001$), IL-1 β ($p < 0.001$), and TNF- α ($p < 0.01$, $p < 0.05$). These results suggested that CA could ameliorate HFD-induced hyperglycemia, dyslipidemia, and inflammation in mice.

2.2. CA Alleviated Hepatic Lipid Accumulation, Oxidative Stress, and Liver Injury in Mice Fed with a High-Fat Diet. Lipid accumulation in the liver is a sign of NAFLD. As observed in Figure 2(a), Oil Red O- (ORO-) stained lipid droplets were more prominent in sections from the HFD mice in comparison with those of the ND mice, while CA-treated mice had a relative healthier liver tissue ($p < 0.001$). Moreover, large areas of steatosis, cytoplasmic vacuolation (red arrow), and inflammatory cell infiltration (black arrow) were seen in hepatic hematoxylin and eosin (H&E) staining of the HFD mice; all of which were ameliorated after CA treatment (Figure 2(b)). NAFLD activity score analysis also showed the decrease of NAFLD lesion severity by CA (Figure 2(c); $p < 0.001$, $p < 0.001$). The serum MDA level was prominently increased, while the SOD activity was decreased in the HFD group in comparison with those of the ND group ($p < 0.001$), and these parameters were all reversed after CA administration (Figures 2(d) and 2(e); $p < 0.01$, $p < 0.001$). As showed in Figure 2(f), dihydroethidium (DHE) staining of the liver in HFD mice established a distinct higher *in situ* ROS in comparison with the ND mice ($p < 0.001$). However, both two doses of CA treatment notably restored ROS overproduction in the liver ($p < 0.001$). Furthermore, the enzymatic activities of serum pyruvic transaminase/alanine aminotransferase (GPT-ALT) and glutamic oxaloacetic transaminase/aspartate aminotransferase (GOT-AST) were dramatically increased in HFD mice ($p < 0.001$). These two markers of liver injury were both reversed after CA treatment (Figures 2(g) and 2(h); $p < 0.01$, $p < 0.001$). All above data suggested that CA could ameliorate HFD-induced lipid accumulation, oxidative stress, and liver injury.

2.3. CA Suppressed the Hepatic NF κ B Pathway and Liver Inflammation in HFD Mice. The inflammatory reaction is one of the major features of liver injury in NAFLD [23]. To determine whether CA could inhibit hepatic inflammatory responses in NAFLD, we assessed the hepatic levels of inflammatory cytokines. As showed in Figure 3(a), the hepatic levels of inflammatory cytokines were all increased in the HFD group in comparison with the ND group

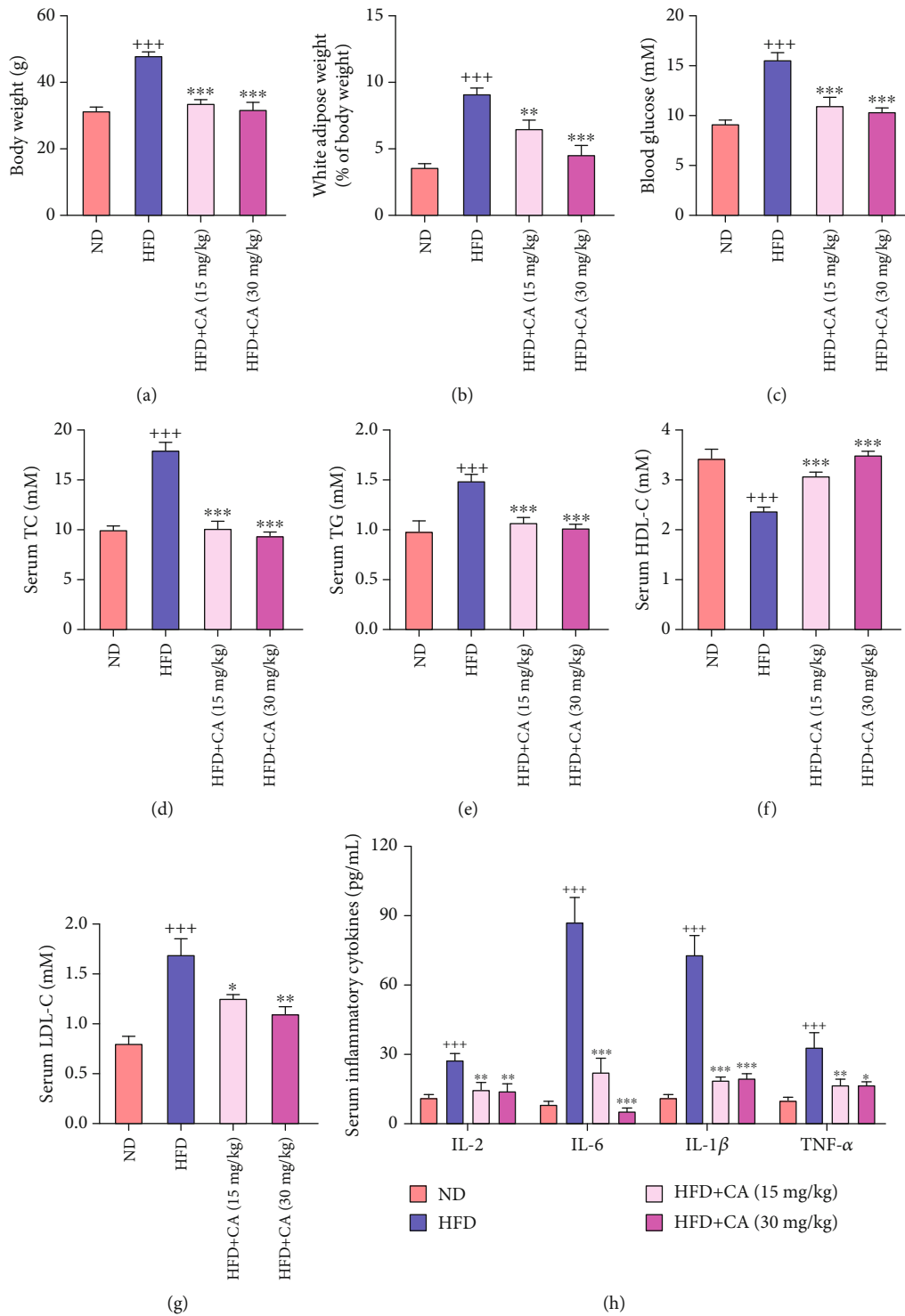


FIGURE 1: Effects of CA on hyperglycemia, dyslipidemia, and inflammation in HFD mice. CA affected body weight (a), white adipose (b), blood glucose (c), serum TC (d), TG (e), HDL-C (f), LDL-C (g), and serum inflammatory cytokines (h) in HFD-fed mice. C57BL/6 mice were randomly divided into four groups: in the ND group, mice were fed with a ND and received 0.9% NaCl solution. In the HFD group, mice were fed with a HFD diet and received 0.9% NaCl solution. In the two HFD+CA groups, mice were fed with a HFD and received 15 mg/kg or 30 mg/kg of CA once daily by oral gavage. Data represent the mean \pm SEM, $n = 8$ per group. ⁺⁺⁺ $p < 0.001$ vs. ND group. ^{*} $p < 0.05$, ^{**} $p < 0.01$, and ^{***} $p < 0.001$ vs. HFD group.

($p < 0.001$). Consequently, CA administration reduced IL-2 ($p < 0.01$), IL-6 ($p < 0.01$, $p < 0.001$), IL-1 β ($p < 0.01$), and TNF- α ($p < 0.05$, $p < 0.05$) levels in the liver. As a transcrip-

tion factor that plays a crucial role in inflammation, NF κ B can facilitate the occurrence and development of NAFLD [24]. In parallel with the elevated levels of these inflammatory

cytokines, the hepatic protein expression levels of p-IKK α/β ($p < 0.01$), p-I κ B α ($p < 0.01$), and p-NF κ B ($p < 0.001$) were all significantly increased in HFD mice in comparison with those of ND mice, while CA administration led to a remarkable reduction of these parameters (Figure 3(b); $p < 0.01$). These findings demonstrated the significant anti-inflammatory effect of CA in NAFLD.

2.4. CA Ameliorated Lipid Accumulation and Oxidative Stress and Inhibited the NF κ B Pathway in PA-Treated HepG2 Cells. To further investigate the role of CA in the amelioration of NAFLD, we constructed an *in vitro* NAFLD model by using HepG2 cells as previously described [25]. As shown in Figure 4(a), there was no significant growth inhibition of HepG2 cells after CA treatment even up to the concentration of 250 μ M, indicating the well safety of CA. Significantly more lipid droplets were observed in PA-treated HepG2 cells than those of the normal group (Figure 4(b); $p < 0.001$). And the results showed that the intracellular TC and TG levels were significantly increased in PA-treated HepG2 cells in comparison with the normal group (Figure 4(c); $p < 0.001$). Interestingly, the accumulation of lipids induced by PA treatment was significantly decreased by CA (10 and 20 μ M) administration ($p < 0.01$, $p < 0.001$). As showed in Figure 4(d), using DHE and MitoSOX Red staining, we observed that CA reduced the intracellular O $_2^{\cdot-}$ and mitochondrial oxidative stress in PA-treated HepG2 cells ($p < 0.001$). To further confirm the antioxidant effect of CA in NAFLD, we assessed intracellular ROS through the 2',7'-dichlorofluorescein diacetate (DCFH-DA) detector. PA treatment significantly elevated ROS production in HepG2 cells, but it was prevented after CA administration (Figure 4(e); $p < 0.001$). In addition, the protein levels of p-IKK α/β ($p < 0.01$), p-I κ B α ($p < 0.001$), and p-NF κ B ($p < 0.01$) were significantly increased in PA-treated HepG2 cells, which were remarkably decreased after CA administration (Figure 4(f); $p < 0.01$, $p < 0.001$). These data suggested the lipid regulation, antioxidant activity, and the inhibition of the NF κ B pathway of CA *in vitro* evaluation.

2.5. CA Activated Keap1/Nrf2 Signaling Both in the Liver of HFD Mice and PA-Treated HepG2 Cells. The keap1/Nrf2 pathway is one of the most important defense mechanisms against oxidative stress. It has been shown that Nrf2 $^{-/-}$ mice fed with a high-carbohydrate diet failed to induce antioxidant enzymes resulting in oxidative liver damage [26]. In the present study, high keap1 protein level ($p < 0.01$) and low nuclear Nrf2 protein level ($p < 0.001$) were both observed in the liver of HFD mice. In accordance with the inhibition of nuclear Nrf2, significant decreases of protein levels of HO-1 ($p < 0.001$), SOD1 ($p < 0.01$), and SOD2 ($p < 0.001$) were also detected in the liver of HFD mice in comparison with those in ND mice. However, treatment with CA significantly decreased keap1 protein expression level ($p < 0.05$), upregulated nuclear Nrf2 protein level ($p < 0.001$, $p < 0.01$), and increased the protein levels of HO-1 ($p < 0.01$, $p < 0.001$), SOD1 ($p < 0.001$, $p < 0.01$), and SOD2 ($p < 0.01$) in the liver of mice fed with a high-fat diet (Figure 5(a)). In accordance with the suppression of keap1/Nrf2 signaling in the liver of

HFD mice, we also observed the elevated keap1 ($p < 0.05$), downregulated nuclear Nrf2 ($p < 0.001$), and decreased HO-1 ($p < 0.05$), SOD1 ($p < 0.001$), and SOD2 ($p < 0.05$) protein levels in PA-treated HepG2 cells, and all of these parameters were reversed to normal after CA administration (Figure 5(b)).

2.6. CA Suppressed Oxidative Stress and Inflammation via AMPK Activation. AMPK is a key energy sensor of cellular metabolism, including oxidative stress and inflammation [27, 28]. Both in the liver of HFD mice and PA-treated HepG2 cells, decreased AMPK phosphorylation at threonine 183/172 levels ($p < 0.01$) could be observed in the present study. However, the protein level of p-AMPK was significantly elevated after CA administration both *in vivo* and *in vitro* (Figures 6(a) and 6(b); $p < 0.05$, $p < 0.01$). To further investigate whether CA activates keap1/Nrf2 and inhibits NF κ B via AMPK to suppress oxidative stress and inflammation in NAFLD, AMPK activator AICAR and AMPK inhibitor compound C were used as a pair in the CA-mediated action of PA-treated HepG2 cells. The results showed that AICAR (0.5 mmol/L) partly mimicked, while compound C (CC, 10 μ mol/L) partly abolished, the downregulative effect of CA on keap1, the upregulative effect of CA on nuclear Nrf2 protein level, and the downregulative effect of CA on NF κ B phosphorylation level in PA-treated HepG2 cells (Figures 6(c)). These results suggested that the AMPK pathway was involved in the CA-induced keap1-dependent activation of Nrf2 and suppression of NF κ B in PA-treated HepG2 cells.

Moreover, both AICAR and CC were used to investigate whether the AMPK pathway was also involved in the CA-mediated antioxidant effect in PA-treated HepG2 cells. Our data showed that AICAR partly mimicked, while compound C partly abolished the downregulation of CA on ROS production in PA-treated HepG2 cells (Figure 6(d)).

In addition, the Nrf2 inhibitor ML385 (5 μ M) partly blocked the upregulation of SOD1, SOD2, and HO-1 and the downregulation of ROS production by CA in PA-induced HepG2 cells. These results indicate Nrf2 as a key factor in the regulation of oxidative stress by CA. Likewise, we investigated whether ML385 blocked the role of CA-mediated NF κ B inactivation. The result showed that ML385 diminished CA-induced NF κ B suppression, suggesting that Nrf2 plays a key role in CA-mediated amelioration of inflammation (Figures 6(e) and 6(f)).

All these data above demonstrated that CA might suppress oxidative and inflammation via AMPK-mediated keap1/Nrf2 activation and NF κ B inhibition in NAFLD.

2.7. CA Shaped the Gut Microbiota in HFD Mice. Gut microbiota dysbiosis has been repeatedly observed in NAFLD and NASH [29]. To reveal the possible contribution of gut microbiota in the therapeutic action of CA, we analyzed the fecal microbiota composition using the 16S rRNA pyrosequencing based on V3-V4 region. After size filtering, quality control, and chimera removal, we totally detected 1953854 raw tags from 24 fecal samples with 1953854 clean sequences for further analysis, from which were clustered into operational

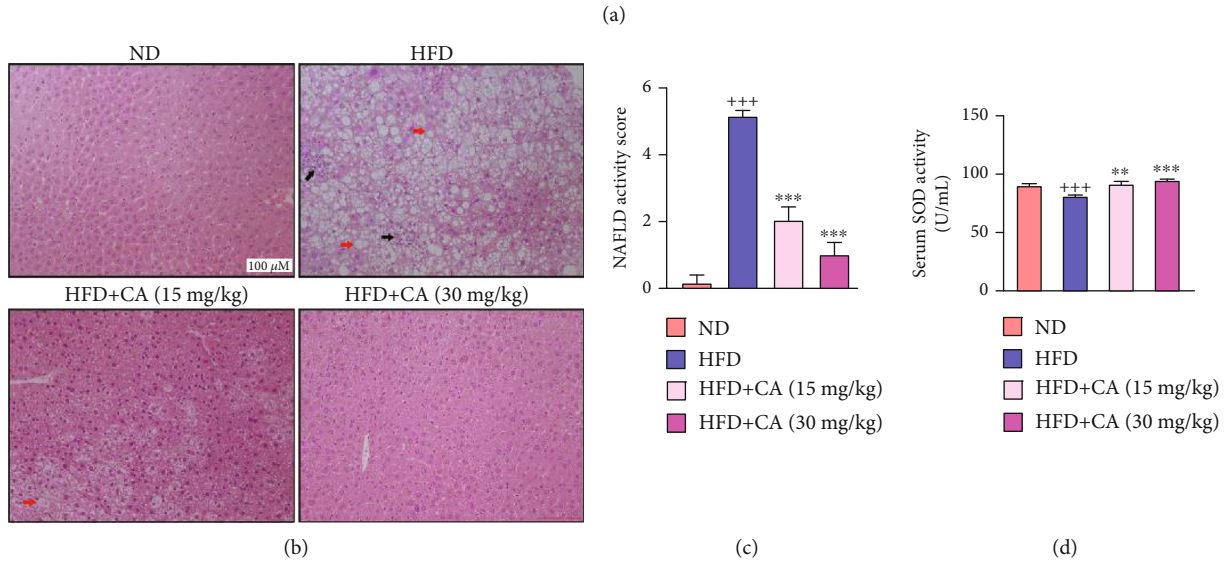
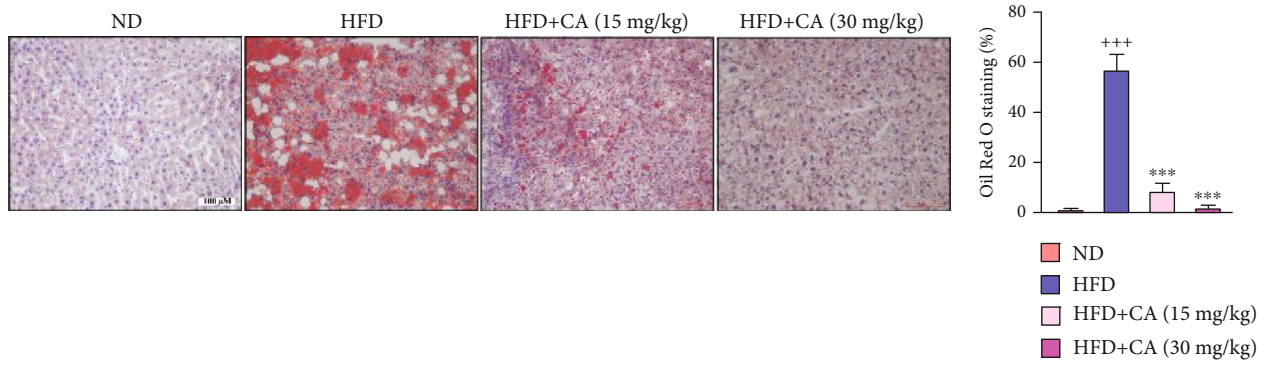


FIGURE 2: Continued.

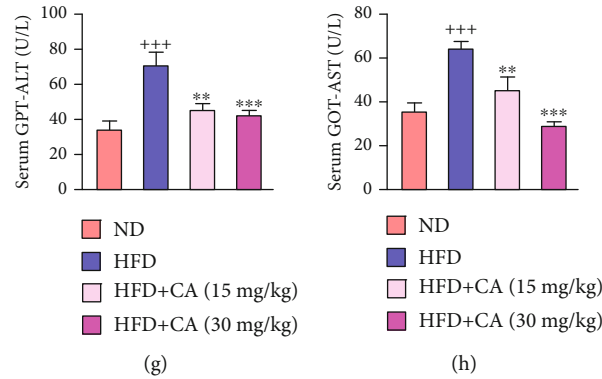


FIGURE 2: CA alleviated hepatic lipid accumulation, oxidative stress, inflammation, and liver injury in HFD-fed mice. (a) Hepatic ORO staining (scale bar: 100 μ M) and quantitative analysis of lipid content ($n = 6$). (b) Histological analysis of liver tissues by H&E staining (scale bar: 100 μ M); red arrow: cytoplasmic vacuolation; black arrow: inflammatory cell infiltration. (c) NAFLD activity score determined according to the liver section histology analysis ($n = 6$). (d, e) Serum SOD and MDA activity levels in mice ($n = 8$). (f) The *in situ* ROS of the liver detected by DHE staining (scale bar: 50 μ M) and the fluorescence intensity analysis ($n = 4$). (g, h) Serum GPT-ALT and GOT-AST levels in mice ($n = 8$). Data represent the mean \pm SEM. $^{++}p < 0.01$ and $^{+++}p < 0.001$ vs. ND group. $^{**}p < 0.01$ and $^{***}p < 0.001$ vs. HFD group.

taxonomic unit (OTU) with similarity higher than 97%. According to the rarefaction curve analysis (Figure 7(a)), the OTU rarefaction curves reached a steady level, indicating that the libraries were large enough to obtain the major information of the bacterial diversity in all samples. A Venn diagram displaying 593 OTUs was shared among 3 groups, and each group owned unique OTUs (Figure 7(b)). Alpha analyses with *chao1* ($p < 0.05$), *observed_species*, *PD_whole_tree*, and Shannon indexes indicated that the HFD mice had decreased microbial species richness, while CA administration increased the diversity of gut bacteria (Figures 7(c) and 7(d)). The nonmetric multidimensional scaling (NMDS) analysis and principal component analysis (PCA) revealed a separated clustering of gut microbiota among ND, HFD, and CA-treated mice (Figures 7(e) and 7(f)).

The microbial community bar plot analyses on top phylum and genus levels exhibited different bacterial community structures among the groups. The microbial community structure at phylum level was dominated by *Firmicutes* and *Bacteroidetes*. The increased level of the phylum *Firmicutes* and decreased level of the phylum *Bacteroidetes* were observed in HFD mice, which were reversed by CA administration (Figure 8(a)). Thus, *Firmicutes*-to-*Bacteroidetes* ratio (F/B ratio) was significantly increased ($p < 0.01$) in the HFD group compared with the ND group, and after CA administration, this ratio was significantly decreased (Figure 8(b); $p < 0.05$). Among the dominant microbial communities at the genus level, the relative abundance of *Lactobacillus* ($p < 0.05$), *Turicibacter* ($p < 0.05$), *Bacteroides*, *Faecalibaculum* ($p < 0.001$), and *Candidatus_Saccharimonas* was higher, while the proportion of *Lachnospiraceae*, *Allobaculum*, *Ruminococcaceae_UCG-014*, and *Alloprevotella* was decreased in HFD mice compared with the ND mice. However, CA administration reversed the proportion of *Lactobacillus* ($p < 0.05$), *Turicibacter* ($p < 0.05$), *Ruminococcaceae_UCG-014*, *Alloprevotella*, and *Candidatus_Saccharimonas* in HFD mice (Figure 8(c)). The community heat map analysis

confirmed these changes (Figure 8(d)). All these suggested that CA enhanced the diversity of gut microbiota and restored the alert microbiota to a state more similar to ND mice.

3. Discussion

Oxidative stress, inflammatory response, and gut microbiota are critical factors in the progression of NAFLD. Due to its potential antioxidant and anti-inflammatory activities, CA may contribute to the intervention of NAFLD. In the present study, we evaluated the effects of CA treatment on NAFLD both in HFD mice and PA-induced HepG2 cells. The amelioration of oxidative stress and inflammation was observed. Moreover, CA greatly shaped the composition of gut microbiota into a status more similar to ND mice. Collectively, the therapeutic effect of CA on NAFLD has been proven through the present investigation.

As an important cellular sensor to restore cellular energy homeostasis and a central regulator of multiple metabolic pathways, AMPK has been proposed as a therapeutic target for metabolic diseases [7, 30, 31]. The ability to control the energy balance equation through defined metabolic pathways heavily pursues AMPK as a golden target against obesity [31]. Activation of AMPK by the E3 ubiquitin ligase makorin ring finger protein 1 (MKRN1) represses diet-induced metabolic syndrome [8]. Lipid metabolism abnormal and insulin resistance are two typical features of NAFLD, so the regulative effects of lipid and glucose metabolism of AMPK have got the most attention in NAFLD. Liver-specific reduction of AMPK activity inhibits acetyl-CoA carboxylase (ACC) phosphorylation and leads to lipogenesis increases in hepatocytes [9]. Liver AMPK activator PF-06409577 decreases both hepatic and systemic lipids in the high-fat-diet-induced NAFLD models of the rodent and monkey preclinical models [32]. Activation of AMPK suppresses hepatic glucose release and enhances insulin sensitivity in dexamethasone-induced fatty liver disease in C57BL/6 mice [33]. In this study, the

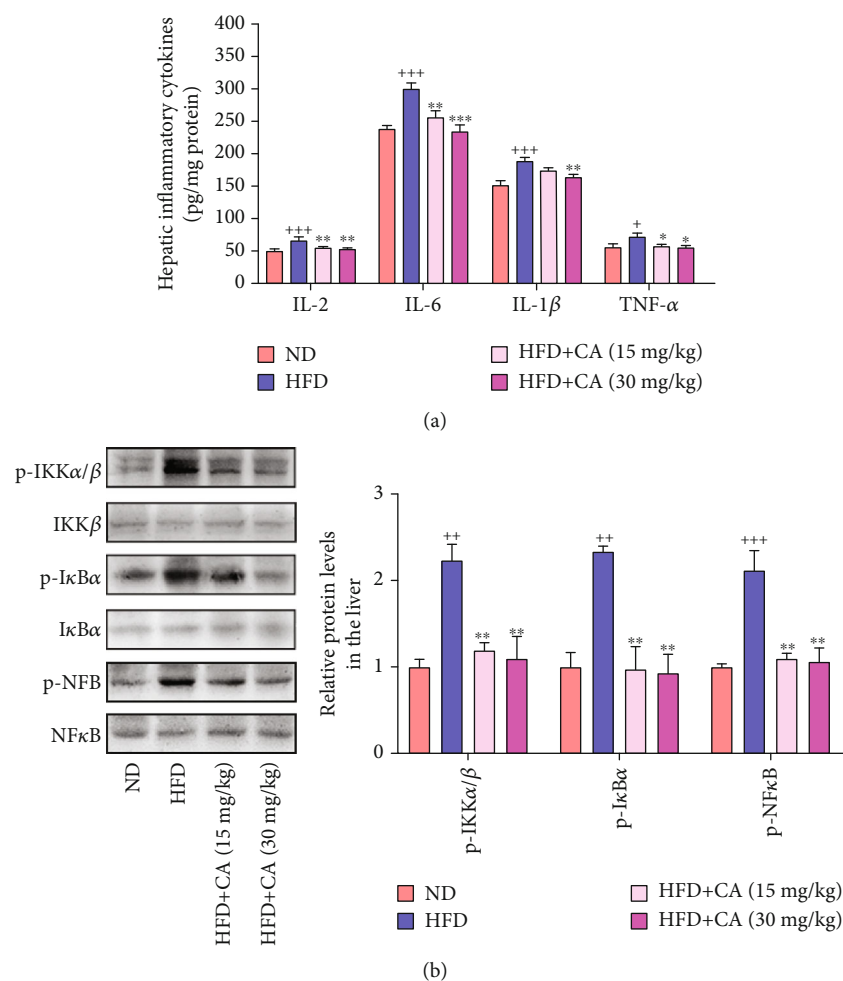


FIGURE 3: CA suppressed the hepatic NF κ B pathway and liver inflammation in HFD mice. (a) Hepatic levels of IL-2, IL-6, IL-1 β , and TNF- α ($n = 8$). (b) Hepatic p-IKK α/β , p-I κ B α , and p-NF κ B protein levels in mice ($n = 3$). Data represent the mean \pm SEM. ⁺⁺ $p < 0.01$ and ⁺⁺⁺ $p < 0.001$ vs. ND group. ^{*} $p < 0.05$, ^{**} $p < 0.01$, and ^{***} $p < 0.001$ vs. HFD group.

reduction of AMPK phosphorylation was observed both in the liver of HFD mice and PA-treated HepG2 cells, in company with elevated body weight, serum glucose, and lipid metabolism disorders. It has been surmised that numerous polyphenols are capable of activating AMPK via the elevation of AMP levels by inhibiting mitochondrial ATP production, which serves as indirect AMPK activators [34]. CA has been found to restore insulin signaling and dyslipidemia [19, 35]. Our results indicated that CA alleviated HFD-induced hyperglycemia and dyslipidemia in mice, as well as reduced lipid accumulation in the liver. In addition to these, CA could also restore PA-induced lipid drop deposition and decrease TC and TG levels in HepG2 cells. Importantly, decreased AMPK phosphorylation levels in the liver of HFD mice and PA-treated HepG2 cells were both reversed by CA.

Moreover, oxidative metabolism also contributes to oxidative stress and inflammation during NAFLD [36]. Recent researches demonstrated that suppression of oxidative stress and inflammation contributed to the amelioration of NAFLD or NASH [5, 37, 38]. Not only as a key sensor of energy balance but also a factor of redox balance improvement and inflammation reduction, the antioxidation and anti-

inflammatory effect of AMPK activation has gained more attention [39, 40]. Activation of AMPK could alleviate mitochondrial oxidative damage and apoptosis [40]. AMPK was also reported to prevent oxidative stress-induced senescence by improving autophagic flux and NAD(+) homeostasis [41]. Furthermore, stimulation of AMPK phosphorylation prevented HFD-induced insulin resistance and inflammation in adipose tissue through anti-inflammatory effects in obesity and attenuated lipopolysaccharide-induced secretion of pro-inflammatory cytokines such as TNF- α and MCP-1 [11]. In this study, we observed oxidative stress and inflammation, including elevated MDA and suppressed SOD activity in HFD mice, overproduction of O₂^{•-} in the liver and ROS in PA-treated HepG2 cells, and increased serum IL-2, IL-6, IL-1 β , and TNF- α levels in HFD mice. It has been noted that the antioxidant and anti-inflammatory effects of CA have already been documented in metabolic diseases, including obesity and atherosclerosis [16, 42]. Consistent with these reports, in our experiments, CA treatment dramatically decreased ROS production and inflammatory cytokines. Taken together, our data demonstrated that CA could mitigate high-fat-induced inflammation and oxidative damage

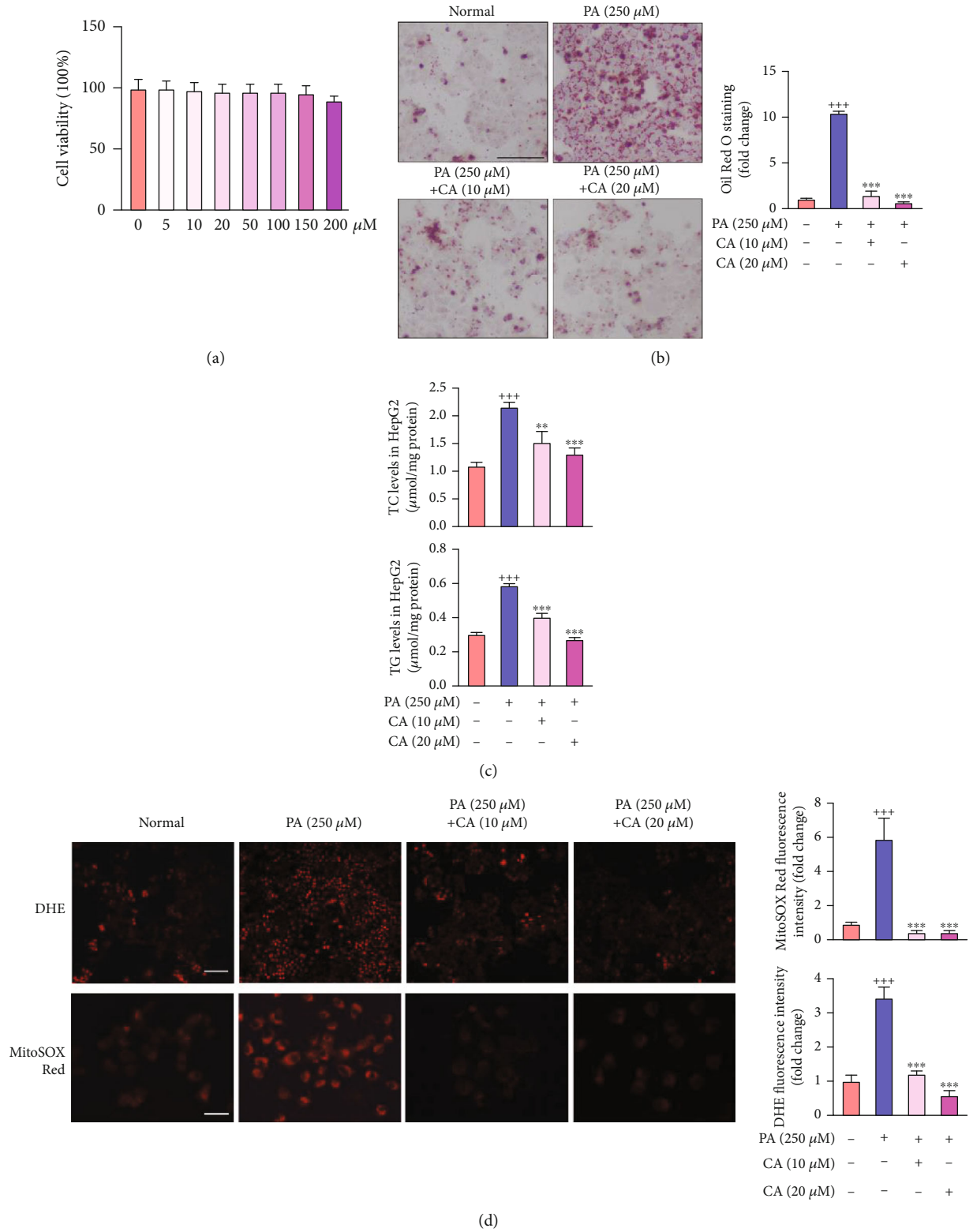


FIGURE 4: Continued.

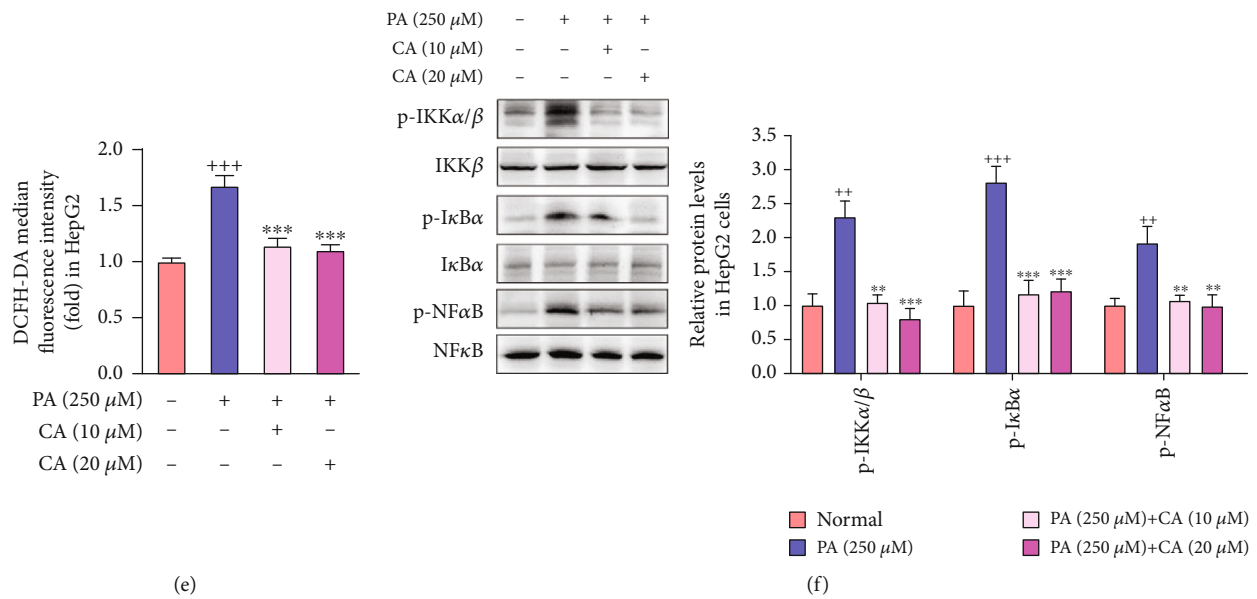


FIGURE 4: CA ameliorated lipid accumulation and oxidative stress, as well as inhibited the NFκB pathway in PA-induced HepG2 cells. (a) Cell viability after treatment with different concentrations of CA from 0 to 250 μM for 24 h ($n = 8$). (b) lipid droplets detected by ORO staining (scale bar: 100 μM) and quantitative analysis of lipid content in HepG2 cells ($n = 4$). (c) Intracellular TC and TG levels in HepG2 cells ($n = 8$). (d) The intracellular O_2^- and mitochondrial ROS detected by DHE (scale bar: 100 μM), MitoSOX Red staining (scale bar: 50 μM), and the fluorescence intensity analyses in PA-treated HepG2 cells ($n = 8$). (e) ROS production detected by DCFH-DA detector ($n = 8$). (f) The protein levels of p-IKKα/β, p-IκBα, and p-NFκB in HepG2 cells ($n = 3$). Data represent the mean ± SEM. $^{++}p < 0.01$ and $^{+++}p < 0.001$ vs. normal group. $^{**}p < 0.01$ and $^{***}p < 0.001$ vs. PA group.

in vivo and *in vitro* probably via AMPK phosphorylation activation.

Importantly, those benefits of antioxidative and anti-inflammation were also observed in previous studies on Nrf2 activation [43–45]. Keap1/Nrf2 system forms the cellular defense against oxidative and electrophilic stresses, which has been known to attenuate inflammation [44, 45]. Activation of Nrf2 has also been confirmed to reduce hepatic lipid accumulation in bisphenol A-induced mouse model of NAFLD [46]. It has been demonstrated that Nrf2-dependent antioxidant genes contain almost all the antioxidant enzymes, including SOD, catalase, glutathione S-transferase (GST), glutathione peroxidase-1 (GPX-1), and HO-1 [47]. Activation of Nrf2 in hepatocytes inhibited inflammatory and oxidative stress, suppressed hepatic steatosis, and mitigated liver fibrosis in NASH [48, 49], while inactivation of Nrf2 led to aggravation of liver injury in NASH; thus, impairment of Nrf2 activity represented a major risk factor for the evolution of NAFLD to NASH [50]. We surmised that activation of Nrf2 functions attributed to ROS elimination in NAFLD. Likewise, we observed keap1 and Nrf2 alteration both in the liver of HFD mice and PA-treated HepG2 cells. Activation of Nrf2 by CA increased the expression of downstream antioxidant genes, including SOD1, SOD2, and HO-1, thereby functionally attenuated hepatocyte injury *in vivo* and *in vitro*. What is interesting, recent researches have revealed the crosstalk between AMPK and Nrf2 [14, 39, 51]. Nrf2 signaling was revealed as the downstream signal of AMPK in oxidative stress and inflammation [39], and AMPK activation promotes autophagic degradation of keap1 to induce Nrf2 dissociate from keap1

and translocate to the nucleus [52]. However, whether Nrf2 is the downstream signal of AMPK in HFD-induced NAFLD still remains unclear. To confirm the crosstalk between AMPK and Nrf2 in NAFLD and whether CA could regulate Nrf2 via AMPK, we conducted AMPK activator AICAR and inhibitor compound C in PA-induced HepG2 cell. Our results showed that both PA-induced elevation of keap1 and reduction of nuclear Nrf2 protein level and ROS overproduction in HepG2 cells were reversed by either CA or partly reversed by AMPK activator AICAR. Importantly, the downregulative effect on keap1 level and upregulative effect on Nrf2 level of CA and the decrease of ROS production were partly eliminated by adding AMPK inhibitor compound C. These results indicated that the AMPK pathway was involved in the keap1-dependent regulation of CA on Nrf2 level in PA-treated HepG2 cells. Likewise, the upregulative effect on SOD1, SOD2, and p-NFκB protein levels, and the downregulative effect of ROS production of CA were partly diminished by Nrf2 inhibitor ML385. These results further indicated that Nrf2 was involved in CA-mediated amelioration of oxidative stress in PA-treated HepG2 cells.

On the one hand, inflammation results in a stress response of hepatocytes and may lead to lipid accumulation and precede steatosis [53]. On the other hand, increased FFA levels, insulin resistance, and adipose tissue dysfunction activate the production and release of proinflammatory cytokines, both systemically and locally in the liver [3]. NFκB has been recognized as a key proinflammatory transcription factor in inflammation and immune response. Persistent NFκB pathway activation has been shown in animal models or patients with

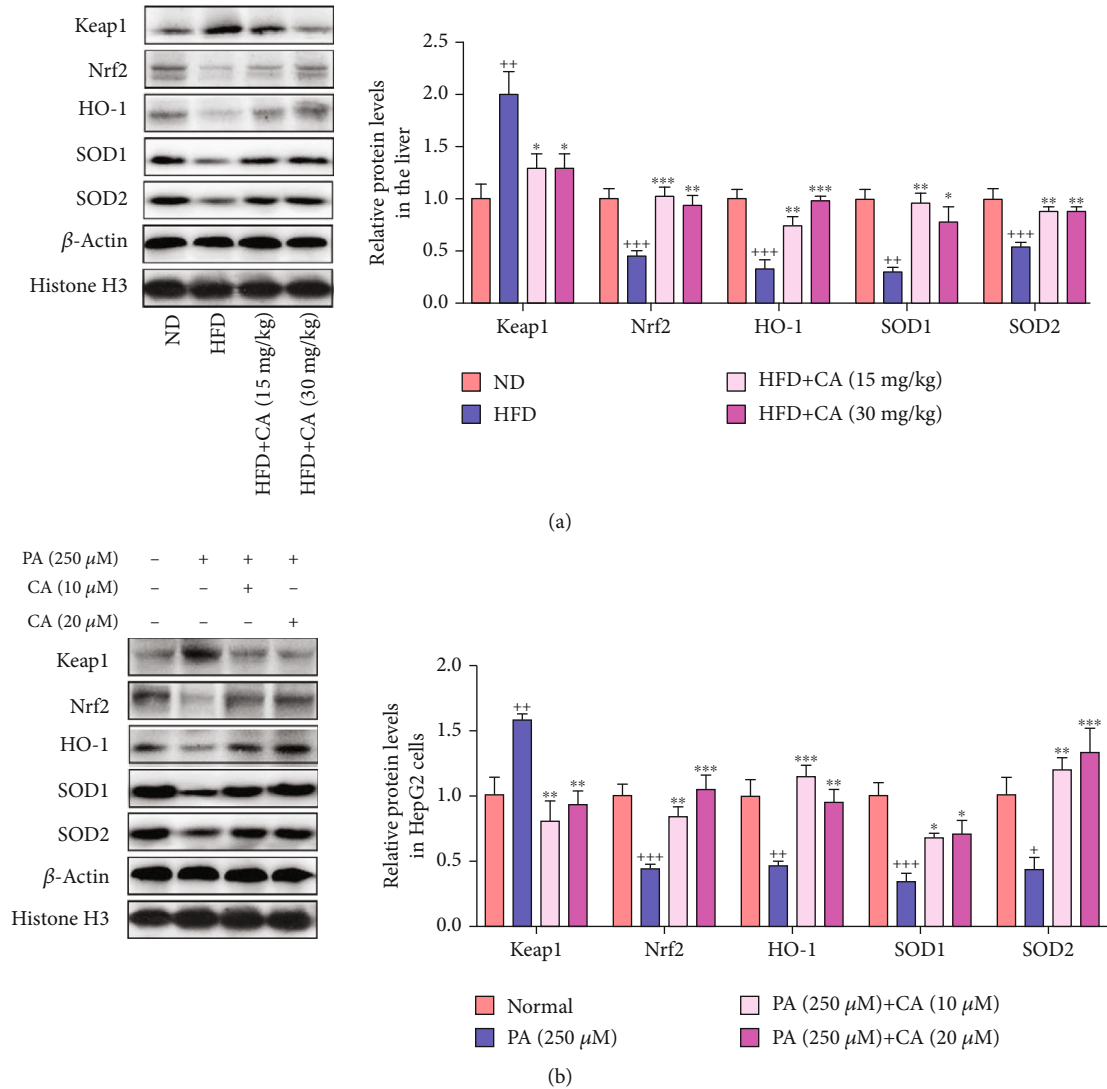


FIGURE 5: CA regulated keap1/Nrf2 signaling in the liver of HFD mice and PA-treated HepG2 cells. (a, b) The protein levels of keap1, nuclear Nrf2, SOD1, SOD2, and HO-1 in the liver or HepG2 cells. Data represent the mean \pm SEM, $n = 3$ per group. ⁺⁺ $p < 0.01$ and ⁺⁺⁺ $p < 0.001$ vs. ND or normal group. ^{**} $p < 0.01$ and ^{***} $p < 0.001$ vs. HFD or PA group.

NAFLD and NASH [54–57]. To further characterize the mechanism of inhibitory effect of CA on inflammatory cytokine production, we investigated the effect of CA on the NF κ B pathways and serum inflammatory cytokines in HFD mice. It was well noted that the increase of serum IL-2, IL-6, IL-1 β , and TNF- α was confirmed in HFD mice, as well as the inflammatory cell infiltration detected by liver H&E staining. CA treatment significantly downregulated inflammation systemically and in the liver. Studies have shown that the NF κ B pathway could be regulated by AMPK and Nrf2 [15, 58]. Herewith, we showed many degrees of upregulation on NF κ B phosphorylation by AICAR in PA-treated HepG2 cells. Moreover, the upregulative effect of CA on NF κ B phosphorylation level was partly eliminated by compound C. Similarly, the suppression on p-NF κ B of CA was partly diminished by ML385. These results indicated that the AMPK-Nrf2 pathway was involved in the regulation of CA on NF κ B suppression in PA-treated HepG2 cells.

Growing evidences indicate the gut microbiota alteration in metabolic disorders, including NAFLD [29]. In the present study, the composition and proportion of gut microbiota were changed in HFD mice. Our 16S rRNA sequencing experiment revealed that CA treatment increased the OTU numbers and upregulated *chao1*, *observed_species*, *PD_whole_tree*, and *Shannon* indexes in HFD mice. Based on the NMDS and PCoA, HFD changed the overall gut microbiota composition in NAFLD mice, and it was reversed by CA treatment. *Bacteroidetes* and *Firmicutes* are two dominant bacterial divisions in the gut, and numerous studies have observed that the ratio of *Firmicutes* to *Bacteroidetes* in gut microbiota, characteristic of “obese microbiota”, was associated with metabolic disorders including obesity and NAFLD [22, 59, 60]. In the current study, HFD induced relative increase of *Firmicutes* and decrease of *Bacteroidetes* in the gut in comparison with the ND mouse group, causing the significantly elevation of F/B ratio, in parallel with body weight gain and adiposity in HFD mice. CA treatment significantly

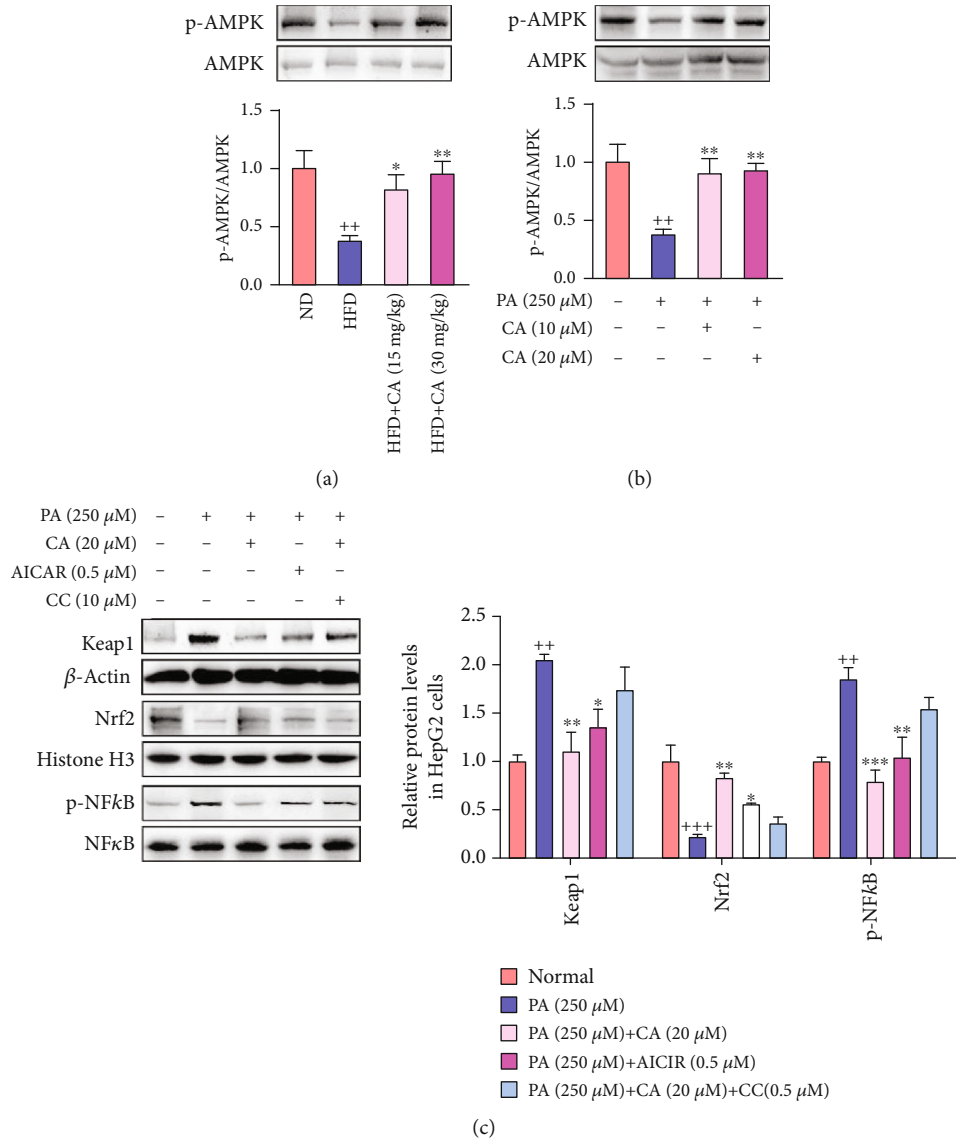


FIGURE 6: Continued.

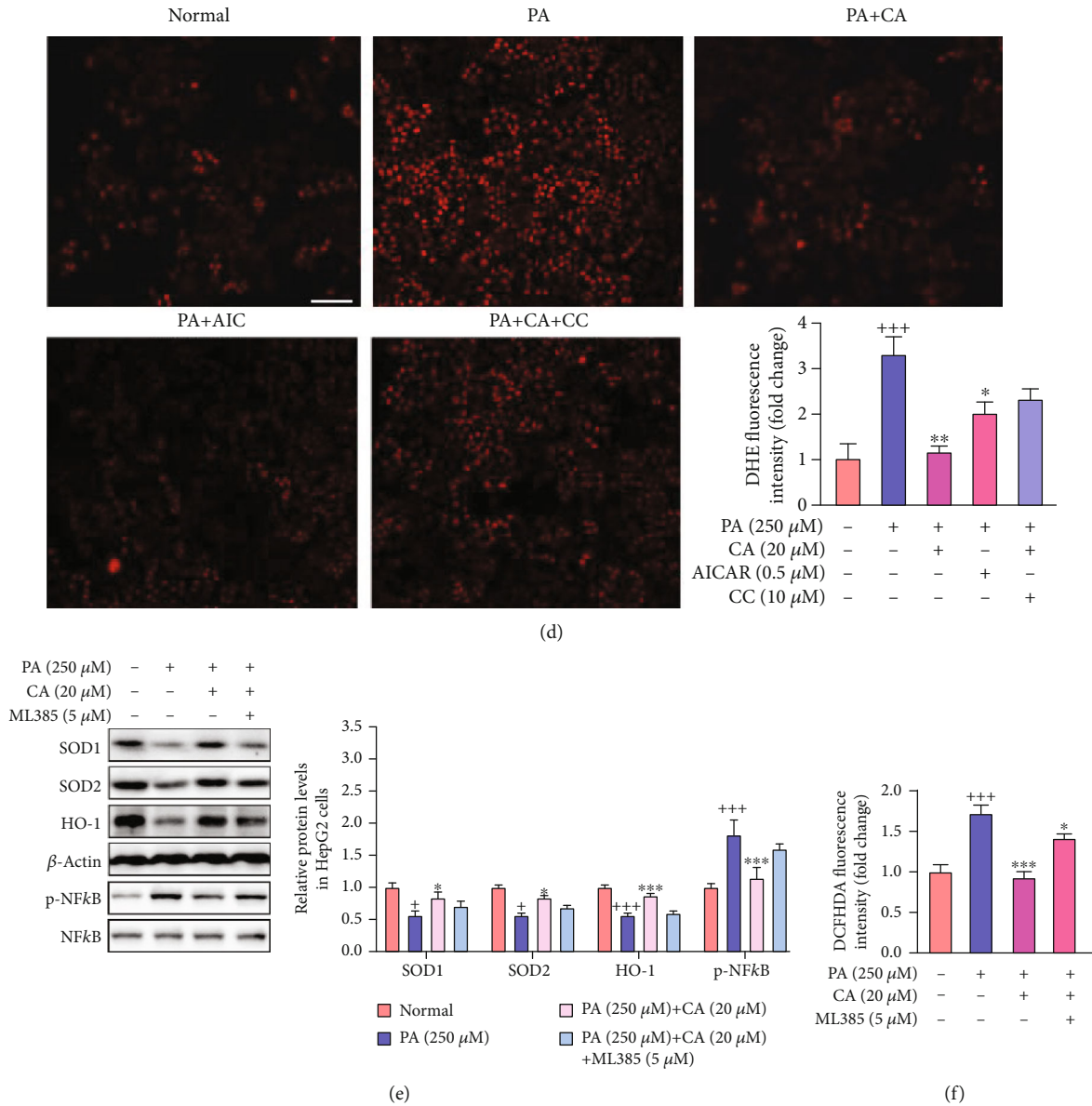


FIGURE 6: CA suppressed oxidative stress and inflammation via AMPK activation. (a, b) Effects of CA on the phosphorylation of APMK in the liver and HepG2 cells ($n = 3$). (c) The protein levels of keap1, nuclear Nrf2, and p-NF κ B in HepG2 cells ($n = 3$). (d) ROS production of cells detected by DHE staining (scale bar: 100 μ M) and the fluorescence intensity analysis ($n = 4$). (e) The protein levels of SOD1, SOD2, HO-1, and p-NF κ B in HepG2 cells ($n = 3$). (f) ROS production in HepG2 cells detected by DCFH-DA detector ($n = 8$). Data represent the mean \pm SEM. $^{++}p < 0.01$ and $^{+++}p < 0.001$ vs. ND or normal group. $^*p < 0.05$ and $^{**}p < 0.01$ vs. HFD or PA group.

reversed F/B ratio in HFD mice, as well as decreased HFD-induced body weight gain and adiposity. Although *Lactobacillus* is recognized as a probiotic bacterium in metabolic disorders including NAFLD, some studies showed the contrary results [61–63]. Elevated *Lactobacillus* in the gut may correlate with decreased insulin sensitivity and increased plasma inflammatory cytokine [61]. Similar increase of *Lactobacillus* was also observed in NAFLD patient and mice [62, 63]. Furthermore, some species of *Lactobacillus* such as *L. reuteri* also had a redundant role associated with increased body fat and insulin levels [64]. In the current study, the proportion of *Lactobacillus* was increased almost 3 folds (from 5.3% to 14%) in HFD mice in comparison of ND mice and lowered to 6.1% after CA administration. NAFLD severity associates

with gut dysbiosis and a shift in metabolic function of the gut microbiota. We conjectured that overmuch or disproportionate *Lactobacillus* might cause adverse reactions. *Bacteroides* abundance was significantly increased in NASH and has been defined as independently associated with NASH [65]. In this study, *Bacteroides* was increased in the HFD group, indicating the high severity of NAFLD in the mice. *Turicibacter*, a genus of the *Firmicutes* phylum *Firmicutes*, has been primary confirmed to alter gut microbiota of healthy and be associated with hyperlipidemia and body gain [66]. Compared with the HFD group, the abundance of *Turicibacter* was decreased in the CA group. *Faecalibaculum* belonging to *Erysipelotrichaceae*, enriched in HFD mice, was closely related to adiposity and found as biomarker

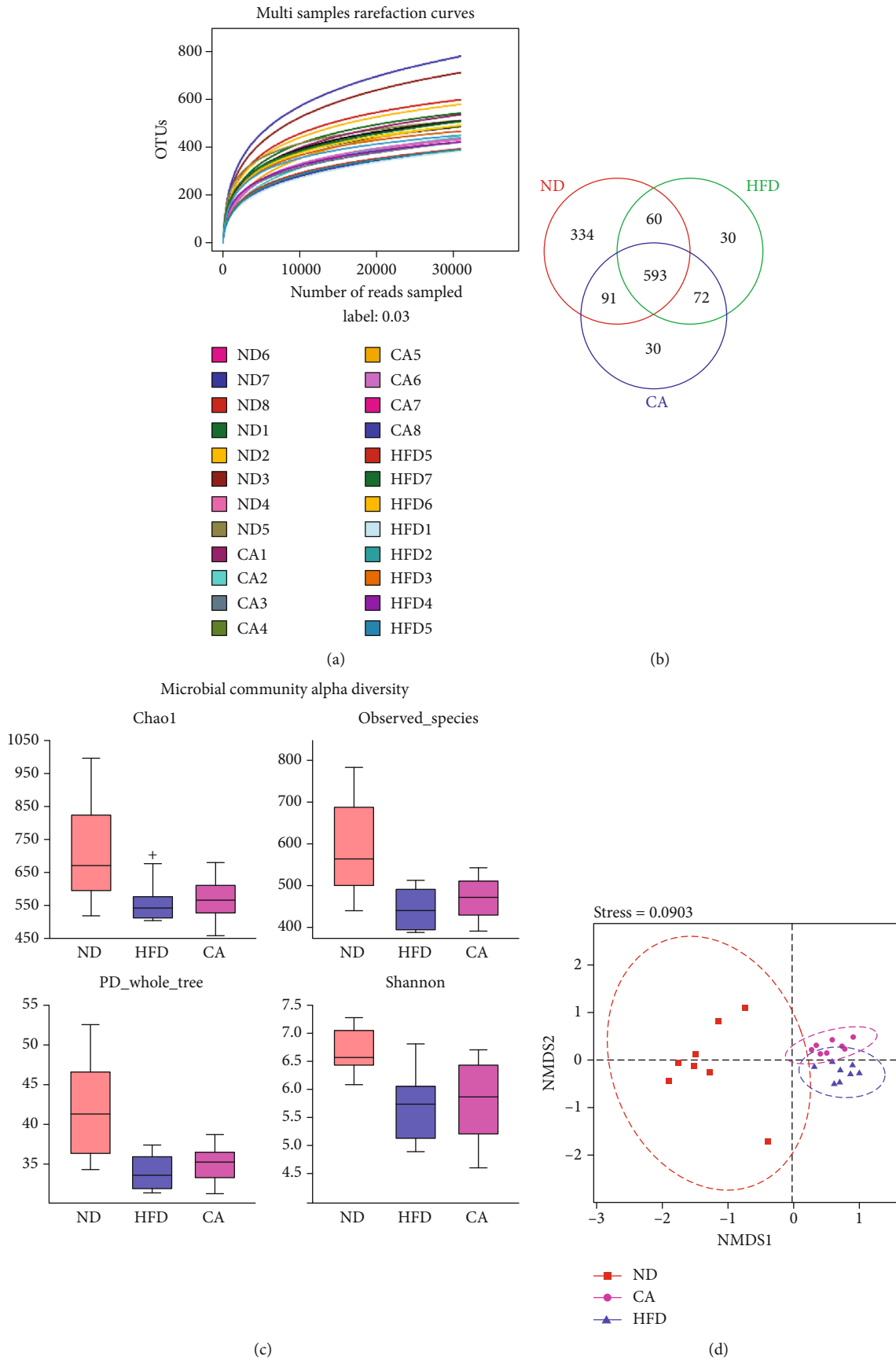
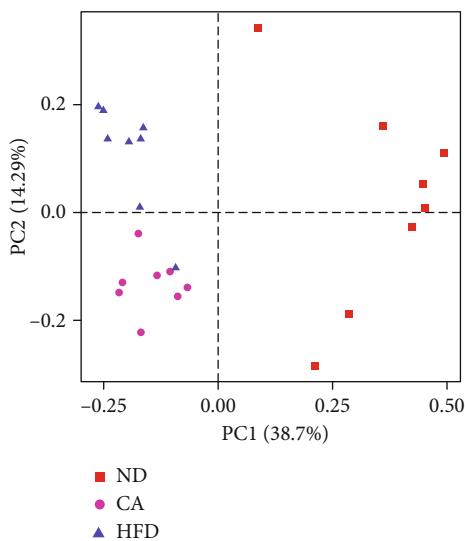


FIGURE 7: Continued.



(e)

FIGURE 7: Effect of CA (30 mg/kg) treatment on the relative abundance of gut microbial community in HFD mice. (a) Rarefaction curve for each sample (ND1-ND8: mice fed with a ND and received 0.9% NaCl solution; HFD1-8: mice fed with a HFD diet and received 0.9% NaCl solution; CA1-8: mice fed with a HFD and received 30 mg/kg of CA once daily by oral gavage). (b) Venn diagram of the overlap of the OTUs in the gut microbiota in different treatments. (c) The bacterial richness in gut estimated by alpha-diversity of chao1, observed_species, PD_whole_tree, and Shannon indexes. The β -diversity analysis of nonmetric multidimensional scaling (NMDS) (d) and principle coordinate analysis (PCoA) (e). Data represent the mean \pm SEM, $n = 8$. $^*p < 0.05$ vs. ND group.

correlated with oxidative stress [67]. In this study, the amount of *Faecalibaculum* was increased in HFD mice and reversed to normal after CA administration. CA also contributed to an increase in the abundance of *Alloprevotella*, which was associated with health benefits in short-chain fatty acids producing and anti-inflammatory [68]. We primary infer that the amelioration of NAFLD by CA may be associated with the alleviation on the dysbiosis of gut microbial, and further investigation is needed to support this hypothesis.

We noticed that previous studies also tried to explore the therapeutic effect of CA on NAFLD or NASH, and many researches had been well done. Using methionine and choline deficiency-induced mouse model and cell models, Kim et al. revealed the improvement of NASH by CA [69]. Xiao et al. placed emphasis on the antiobesity effect of CA by the regulation of COX-2, p-JNK, PPAR γ , and C/EBP α in high-fat-diet mice [70]. Here, using high-fat-diet-induced NAFLD mouse model and PA-induced cell model, we focused on the antioxidant and anti-inflammation effect of CA and tried to connect and explain the crosstalk among AMPK, keap1/Nrf2, and NF κ B system in HFD-induced NAFLD for the first time. These results of the study formed a completed signal path loop, which clearly figured out the mechanism of CA on HFD-induced NAFLD. Additionally, we applied high-throughput pyrosequencing of 16S rRNA to observe the changes of related gut microbial composition, and the results suggested that high-fat-diet-induced decrease of *Firmicutes*-to-*Bacteroidetes* ratio and dysbiosis of NAFLD mice could be reversed by CA treatment. Ziamajidi et al. observed that chicory seed extract improved diabetes- and oleic acid-induced NAFLD and NASH by PPAR α and SREBP-1 [20]. Chicory seed extract contains a variety of compounds, yet the precise ingredient is not clear. Here, in this study, we con-

firmed the amelioration of NAFLD by CA, as a single active compound. Mohammadi et al. paid the attention on the improvement of lipid accumulation by CA and fish oil through a NAFLD cell model via the AMPK-mediated SREBP-1/FAS and PPAR α /UCP2 pathways [71]. Here, we investigated the improvement of oxidative stress and inflammation in both NAFLD animal and cell models via the AMPK/Nrf2/NF κ B pathway and this might be associated with the restored gut microbiota. The pathogenesis of NAFLD is very complex, and CA may serve as a multitargeting pharmacologically active compound. Combined with these previous studies, CA would be an attractive agent for the amelioration of NAFLD.

In conclusion, CA treatment displays an effect against lipid dysregulation, oxidative stress, inflammation, and gut microbiota in NAFLD. The action of CA in upregulating AMPK phosphorylation and nuclear Nrf2 level, as well as suppression of NF κ B in hepatocytes, may contribute to the protective effect of the liver in NAFLD. It is conceivable that CA may be able to protect hepatocytes from oxidative damage and inflammation via regulating AMPK-mediated Nrf2 activation and NF κ B inactivation and shaping gut microbiota. Our findings provide strong scientific basis of CA for amelioration of NAFLD and its related metabolic diseases.

4. Materials and Methods

4.1. Reagents and Chemical. CA (purity > 98%), palmitic acid, and fatty acid-free bovine serum albumin (BSA) were purchased from Nanjing Spring & Autumn Biological Engineering Corporation (Nanjing, China), Macklin (Shanghai, China), and YEASEN (Shanghai, China), respectively. AIA-CAR, Compound C, and ML385 were obtained from

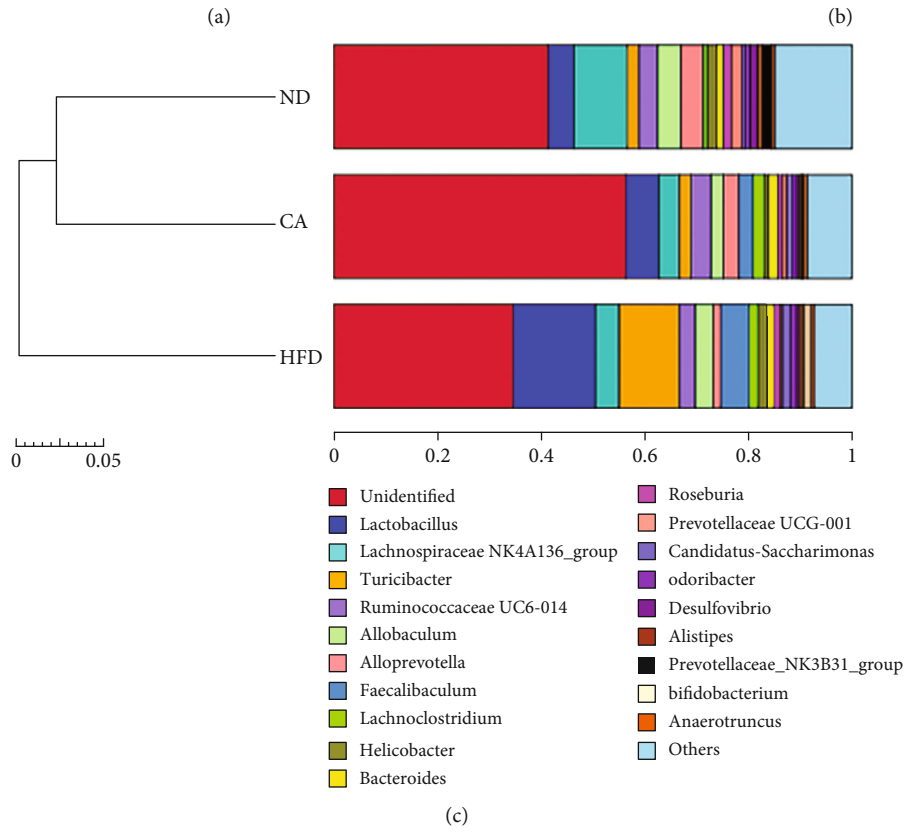
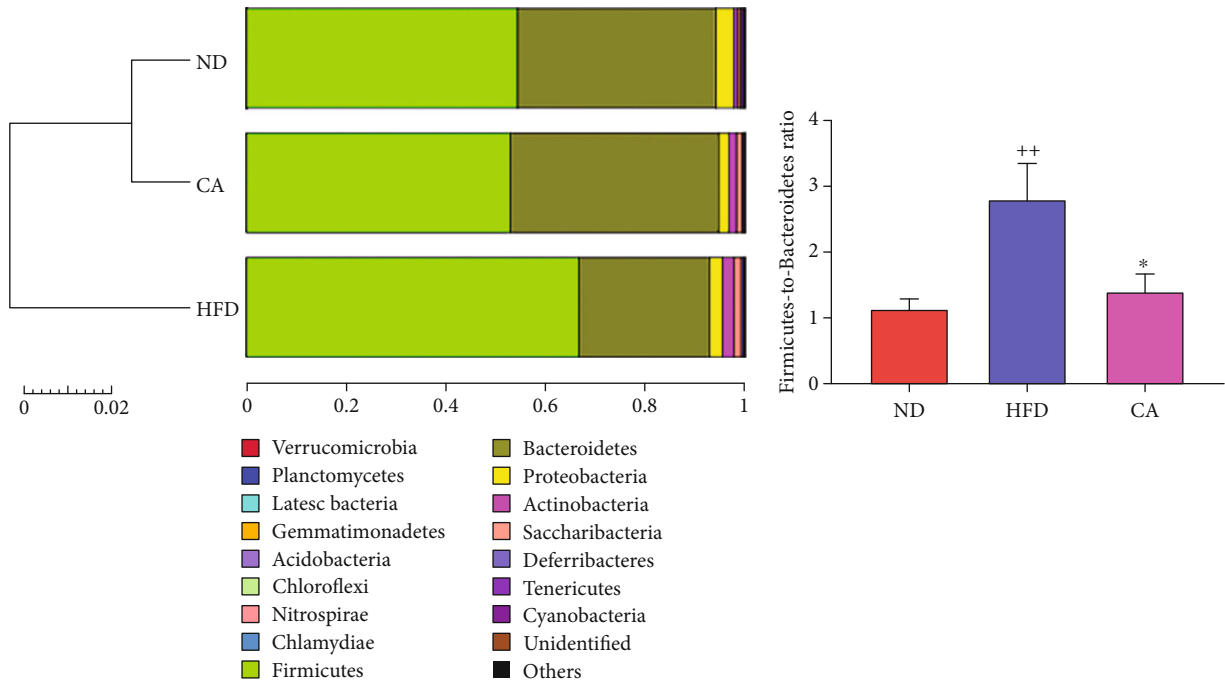


FIGURE 8: Continued.

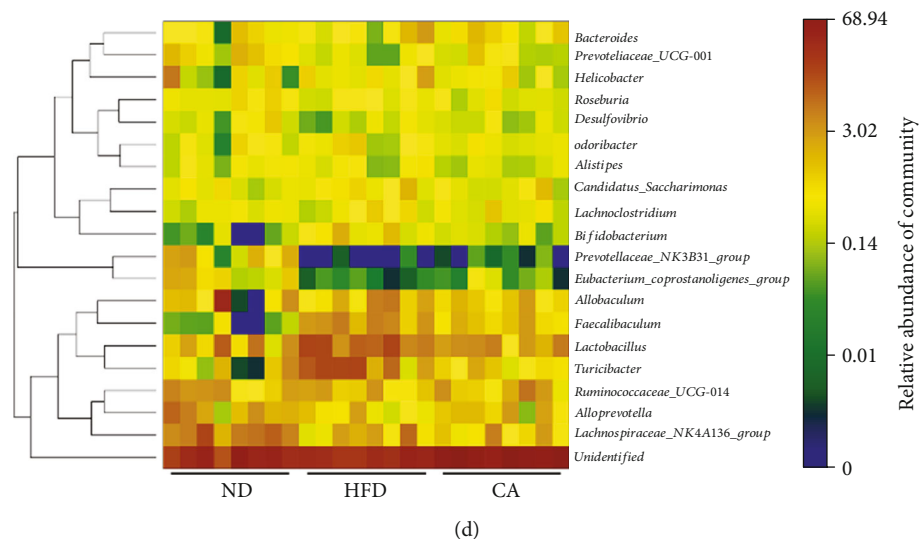


FIGURE 8: Effect of CA treatment on the population structure of gut microbiota in HFD mice. (a) Bar plot analysis of microbial community at the phylum level in mice. (b) The alteration in the Firmicutes-to-Bacteroidetes ratio in mice. Bar plot analysis (c) and heat map analysis (d) of microbial community at the genus level in mice. Data represent the mean \pm SEM, $n = 8$ per group. $^{**}p < 0.001$ vs. ND group. $^{*}p < 0.05$ vs. HFD group.

Beyotime Institute of Biotechnology (Haimen, China), Selleck (Houston, TX, USA), and MedChemExpress (NJ, USA), respectively. Dulbecco's modified Eagle's medium (DMEM), penicillin-streptomycin, and fetal bovine serum (FBS) were all obtained from Invitrogen-Gibco (Grand Island, NY). Cell Counting Kit-8 (CCK-8) assay and bicinchoninic acid (BCA) Protein Quantification Kit were purchased from Biosharp (Hefei, China). Biochemical indexes including glucose, TC, TG, LDL-C, HDL-C, GPT-ALT, and GOT-AST assay kits were purchased from Nanjing Jiancheng Bioengineering Institute (Jiangsu, China). MDA and SOD assay kits, DHE and DCFH-DA probes, and the nuclear protein extraction kit were offered by Beyotime Institute of Biotechnology (Jiangsu, China). ORO staining kit was purchased from Nanjing Jiancheng Bioengineering Institute (Jiangsu, China). MitoSOX Red probe was obtained from Yeasen (Shanghai, China). Serum and hepatic inflammatory cytokines including IL-2 (EK202HS-96), IL-6 (EK206/3-96), IL-1 β (EK201B/3-96), and TNF- α (EK282HS-96) enzyme-linked immunosorbent assay (ELISA) kits were purchased from MultiSciences (Lianke) Biotech Co., Ltd (Zhejiang, China). Antibodies against Nrf2, NF κ B, p-NF κ B, I κ B α , p-I κ B α , IKK β , p-IKK α/β , and the HRP-linked secondary antibodies were obtained from Cell Signaling (Boston, MA, USA); antibodies against keap1, SOD1, and HO-1 were obtained from Santa Cruz Biotechnology (CA, USA); antibodies against SOD2 and AMPK were purchased from Proteintech Group (Chicago, USA). p-AMPK (T183/172) was purchased from Bioworld Technology (MN, USA).

4.2. Animal Model and the Treatment. All animal experiments were in strict accordance with the *Guide for the Care and Use of Laboratory Animals* approved by the Animal Ethics Committee of China Pharmaceutical University (certificate number: SYXK2016-0011, approval date: 27 January 2016 to 26 January 2021). Male C57BL/6 mice (20 to 25 g

body weight) were housed with food and water available *ad libitum* in light, temperature, and humidity-controlled environments. The normal control group was fed with normal diet (ND), while the others were fed with HFD (18% lard stearin (*w/w*), 5% egg powder, 1% cholesterol, 20% sucrose, 0.1% bile salt, and 55.9% normal diet) [72] for 9 weeks. Then, the HFD mice received either CA (15 or 30 mg/kg/d, dissolved in water) or saline solution daily for 9 weeks by gavage ($n = 8$). Mice were sacrificed, and then the blood samples were collected from the carotid artery and centrifuged to obtain serum, and the livers were harvested for the following biochemical analysis. The serum and liver tissues were stored at -80°C .

4.3. Detection of Serum Biomarkers. The levels of serum glucose, TC, TG, LDL-C, HDL-C, MDA, SOD activity, GPT-ALT, and GOT-AST were determined by commercial assay kits in accordance with the manufacturer's instructions. The inflammatory cytokines including IL-2, IL-6, IL-1 β , and TNF- α were measured using ELISA kits in accordance with the manufacturer's instructions.

4.4. Histological Assessment. Pieces of the liver were fixed in 4% paraformaldehyde and processed to paraffin wax then stained with hematoxylin and eosin (H&E). In addition, lipid droplets in the liver were observed by ORO staining in the frozen liver sections and quantified by ImageJ software. Histopathological changes of the livers were observed and photographed under a light microscope (Olympus, Tokyo, Japan).

4.5. Measurement of Hepatic Inflammatory Cytokines. Liver tissues were homogenized in lysis buffer (pH 7.2, Tris with 1% Triton X-100 and 0.1% protease inhibitor) and centrifuged at 12,000 g for 15 min. The supernatants were collected for determination of IL-2, IL-6, IL-1 β , and TNF- α by ELISA

kits according to the manufacturer's instructions adjusted for protein content.

4.6. Cell Culture and Treatment. HepG2 cells were obtained from FuHeng Cell Center, Shanghai, China. Cells were cultured in low-glucose DMEM supplemented with 5% FBS and 1% penicillin-streptomycin and incubated at 37°C and 5% CO₂. PA was dissolved in 50% ethanol by heating at 50°C, then conjugated with 10.5% fatty acid-free BSA (volume ratio 1:25) under agitation at 40°C for 2 h, and finally diluted in culture media. HepG2 cells were pretreated with or without 250 μM PA for 24 h and then incubated in the culture media with or without 250 μM PA or CA (10 and 20 μM, dissolved in PBS) for another 24 h. To clarify the involved signaling pathways, AICAR (0.5 mM) or compound C (10 μM) was used to treat HepG2 cells.

4.7. Cell Viability Analysis. The cell viabilities were assessed using CCK-8 assay. In brief, HepG2 cells were plated into 96-well plates with 2 × 10⁵ per well and incubated overnight. Afterwards, the cells were incubated with different concentrations (0–250 μM) of CA for 24 h. Subsequently, CCK-8 working solution was added to each well and cultivated for another 1 h. The absorbance was recorded on a microplate reader at 450 nm (Molecular Devices, Sunnyvale, USA).

4.8. Measurement of Lipid Uptake in HepG2 Cells. The cells were homogenized in lysis buffer. The intracellular TC and TG contents were measured using commercially assay kits according to the manufacturer's instructions. The protein concentration was assayed using BCA protein quantitative kit. The intracellular TC and TG contents were presented as μmol/mg protein.

The lipid deposition in HepG2 cells was measured by ORO staining [73]. Briefly, after fixed in 4% formaldehyde for 15 min fixation and then cleaned with PBS, ORO working solution was injected into cells for 30 min. The cells were immediately washed with 60% isopropanol, incubated with hematoxylin for 5 minutes, washed by PBS and immediately imaged using microscopy (Olympus, Tokyo, Japan), and quantified by ImageJ software.

4.9. Detection of ROS. Liver in situ O₂^{•−} production was determined by fluorescence probe DHE labeling. Frozen liver sections were prepared for immediate DHE staining. Thawed sections were incubated with 2 μM DHE at 37°C for 30 minutes (avoiding light). After washed 3 times by PBS, sections were immediately imaged using fluorescence microscopy (Olympus, Tokyo, Japan) and quantified by ImageJ software.

Intracellular O₂^{•−} levels were detected using the DHE staining. Cells were incubated with PBS diluted DHE (10 μM) at 37°C for 20 min (avoiding light), washed with PBS for 3 times, and then imaged using fluorescence microscopy (Olympus, Tokyo, Japan). Mitochondrial ROS in HepG2 cells was measured by MitoSOX Red at a concentration of 4 μM for 20 min at 37°C, imaged using fluorescence microscopy (Olympus, Tokyo, Japan), and quantified by ImageJ software.

DCFH-DA fluorescent probe was used to detect intracellular ROS generation. Cells were washed with PBS after incubation with DCFH-DA (10 μM) at 37°C for 30 min (avoiding light). Fluorescence intensity was measured at 530 nm with an excitation wavelength of 485 nm using a fluorescence microscope (Tecan, Crailsheim, Germany).

4.10. Western Blot. The liver tissues and HepG2 cell cultures were lysed in RIPA buffer and then centrifuged again at 12,000 g for 15 min at 4°C, following the supernatant collection. The nuclear protein was obtained using a nuclear protein extraction kit. The concentration of protein was measured using a BCA protein assay kit, and then the protein level was normalized and the 5× loading buffer was added, following boiled at 100°C.

The proteins (equal amount) were electrophoresed on 10% SDS-PAGE at 85 V (stacking gel) and 135 V (separating gel), transferred onto a 2.2 μM PVDF membrane in a 4°C refrigerator at 300 mA for 1.5 h, blocked with 5% skim milk for 2 h at room temperature, and incubated with primary antibodies overnight at 4°C. The membranes were washed three times with TBST (8 min each time) and then probed with horseradish peroxidase- (HRP-) conjugated anti-rabbit or anti-mouse secondary antibody for 1 h followed by six washes with TBST (8 min each time). The blot bands were visualized using enhanced chemiluminescence, and band intensities were analyzed using ImageJ gel analysis software. β-Actin and histone H3 were used as the loading controls.

4.11. Gut Microbiota Analysis. At the end of the intervention period, fresh fecal samples were collected and stored at -80°C immediately. The DNA of fecal samples was extracted using an EZNA Stool DNA kit (Omega Bio-tek, Norcross, GA, USA) according to the manufacturer's instructions. Purity and quality of the genomic DNA were checked on 0.8% agarose gels. Amplification was performed targeting the variable regions V3-4 of bacterial 16S rRNA gene with the primers 338F (ACTCCTACGGGAGGCAGCAG) and 806R (GGAC TACHVGGGTWTCTAAT). The PCR was carried out on a Mastercycler Gradient (Eppendorf, Germany) in triplicate: 25 μL mixture containing 12.5 μL of KAPA 2G Robust Hot Start Ready Mix, 1 μL of forward primer (5 μM), 1 μL of reverse primer (5 μM), 5 μL of DNA sample (30 ng), and 5.5 μL of H₂O. Cycling parameters were 95°C for 5 min, followed by 28 cycles of 95°C for 45 s, 55°C for 50 s, and 72°C for 45 s with a final extension at 72°C for 10 min. The PCR products were purified using a QIAquick Gel Extraction Kit (QIAGEN, Germany) and quantified using real-time PCR. Deep sequencing was performed at Beijing Allwegene Technology Inc. (Beijing, China) using Illumina Miseq PE300 sequencing platform (Illumina, San Diego, CA, USA) as described previously [74].

4.12. Statistical Analysis. All statistical analyses were performed using GraphPad Prism 8 (San Diego, CA). All data were expressed as the mean ± standard error of the mean (SEM). Statistical analysis was performed by one-way ANOVA analysis followed by Dunnett's post hoc test. Statistical significance was set at $p < 0.05$.

Data Availability

The data used to support the findings of this study are available from the corresponding author upon request.

Conflicts of Interest

The authors declare that they have no conflict of interest.

Authors' Contributions

Xiaoqin Ding and Tunyu Jian contributed equally to this work.

Acknowledgments

This study was supported by the grants from the National Natural Science Foundation of China (81973463, 82004018, and 32000279), the Open Fund of Jiangsu Key Laboratory for the Research and Utilization of Plant Resources (JSPKLB202050), and the Jiangsu Agricultural Science and Technology Innovation Fund (CX(20)3167). Support was also received from the Jiangsu Scientific and Technological Innovations Platform named Jiangsu Provincial Service Center for Antidiabetic Drug Screening.

References

- [1] G. Musso, M. Cassader, and R. Gambino, "Non-alcoholic steatohepatitis: emerging molecular targets and therapeutic strategies," *Drug Discovery*, vol. 15, no. 4, pp. 249–274, 2016.
- [2] Z. Younossi, Q. M. Anstee, M. Marietti et al., "Global burden of NAFLD and NASH: trends, predictions, risk factors and prevention," *Gastroenterology & Hepatology*, vol. 15, no. 1, pp. 11–20, 2018.
- [3] E. Buzzetti, M. Pinzani, and E. A. Tsochatzis, "The multiple-hit pathogenesis of non-alcoholic fatty liver disease (NAFLD)," *Metabolism*, vol. 65, no. 8, pp. 1038–1048, 2016.
- [4] I. R. Wanless and K. Shiota, "The pathogenesis of nonalcoholic steatohepatitis and other fatty liver diseases: a four-step model including the role of lipid release and hepatic venular obstruction in the progression to cirrhosis," *Seminars in Liver Disease*, vol. 24, no. 1, pp. 99–106, 2004.
- [5] Y. Sumida and M. Yoneda, "Current and future pharmacological therapies for NAFLD/NASH," *Journal of Gastroenterology*, vol. 53, no. 3, pp. 362–376, 2018.
- [6] J. Aron-Wisnewsky, M. V. Warmbrunn, M. Nieuwdorp, and K. Clément, "Nonalcoholic fatty liver disease: modulating gut microbiota to improve severity?," *Gastroenterology*, vol. 158, no. 7, pp. 1881–1898, 2020.
- [7] E. A. Day, R. J. Ford, and G. R. Steinberg, "AMPK as a therapeutic target for treating metabolic diseases," *Trends Endocrinol. Metab.*, vol. 28, no. 8, pp. 545–560, 2017.
- [8] M. S. Lee, H. J. Han, S. Y. Han et al., "Loss of the E3 ubiquitin ligase MKRN1 represses diet-induced metabolic syndrome through AMPK activation," *Nature Communications*, vol. 9, no. 1, p. 3404, 2018.
- [9] N. Dzamko, B. J. W. van Denderen, A. L. Hevener et al., "AMPK β 1 deletion reduces appetite, preventing obesity and hepatic insulin resistance," *The Journal of Biological Chemistry*, vol. 285, no. 1, pp. 115–122, 2009.
- [10] C. Lyons and H. Roche, "Nutritional modulation of AMPK-impact upon metabolic-inflammation," *International Journal of Molecular Sciences*, vol. 19, no. 10, p. 3092, 2018.
- [11] T. W. Jung, H. S. Park, G. H. Choi, D. Kim, and T. Lee, " β -aminoisobutyric acid attenuates LPS-induced inflammation and insulin resistance in adipocytes through AMPK-mediated pathway," *Journal of Biomedical Science*, vol. 25, no. 1, p. 27, 2018.
- [12] C. R. Lindholm, R. L. Ertel, J. D. Bauwens, E. G. Schmuck, J. D. Mulligan, and K. W. Saupe, "A high-fat diet decreases AMPK activity in multiple tissues in the absence of hyperglycemia or systemic inflammation in rats," *Journal of Physiology and Biochemistry*, vol. 69, no. 2, pp. 165–175, 2013.
- [13] D. Garcia, K. Hellberg, A. Chaix et al., "Genetic liver-specific AMPK activation protects against diet-induced obesity and NAFLD," *Cell Reports*, vol. 26, no. 1, pp. 192–208.e6, 2019.
- [14] K. Zimmermann, J. Baldinger, B. Mayerhofer, A. G. Atanasov, V. M. Dirsch, and E. H. Heiss, "Activated AMPK boosts the Nrf2/HO-1 signaling axis—a role for the unfolded protein response," *Free Radical Biology & Medicine*, vol. 88, Part B, pp. 417–426, 2015.
- [15] J. D. Wardyn, A. H. Ponsford, and C. M. Sanderson, "Dissecting molecular cross-talk between Nrf2 and NF- κ B response pathways," *Biochemical Society Transactions*, vol. 43, no. 4, pp. 621–626, 2015.
- [16] Q. B. Lu, M. Y. Wan, P. Y. Wang et al., "Chicoric acid prevents PDGF-BB-induced VSMC dedifferentiation, proliferation and migration by suppressing ROS/NF κ B/mTOR/P70S6K signaling cascade," *Redox Biology*, vol. 14, pp. 656–668, 2018.
- [17] D. J. Lee and W. E. Robinson, "Human immunodeficiency virus type 1 (HIV-1) integrase: resistance to diketo acid integrase inhibitors impairs HIV-1 replication and integration and confers cross-resistance to L-chicoric acid," *Journal of Virology*, vol. 78, no. 11, pp. 5835–5847, 2004.
- [18] J. Lee and C. F. Scagel, "Chicoric acid: chemistry, distribution, and production," *Frontiers in Chemistry*, vol. 1, p. 40, 2013.
- [19] K. Ferrare, L. P. R. Bidel, A. Awwad et al., "Increase in insulin sensitivity by the association of chicoric acid and chlorogenic acid contained in a natural chicoric acid extract (NCRAE) of chicory (*Cichorium intybus* L.) for an antidiabetic effect," *Journal of Ethnopharmacology*, vol. 215, pp. 241–248, 2018.
- [20] N. Ziamajidi, S. Khaghani, G. Hassanzadeh et al., "Amelioration by chicory seed extract of diabetes- and oleic acid-induced non-alcoholic fatty liver disease (NAFLD)/non-alcoholic steatohepatitis (NASH) via modulation of PPAR α and SREBP-1," *Food and Chemical Toxicology*, vol. 58, pp. 198–209, 2013.
- [21] J. Guo, X. Han, H. Tan, W. Huang, Y. You, and J. Zhan, "Blueberry extract improves obesity through regulation of the gut microbiota and bile acids via pathways involving FXR and TGR5," *iScience*, vol. 19, pp. 676–690, 2019.
- [22] W. Li, K. Zhang, and H. Yang, "Pectin alleviates high fat (lard) diet-induced nonalcoholic fatty liver disease in mice: possible role of short-chain fatty acids and gut microbiota regulated by pectin," *Journal of Agricultural and Food Chemistry*, vol. 66, no. 30, pp. 8015–8025, 2018.
- [23] J. T. Haas, S. Francque, and B. Staels, "Pathophysiology and mechanisms of nonalcoholic fatty liver disease," *Annual Review of Physiology*, vol. 78, no. 1, pp. 181–205, 2016.
- [24] B. Xu, M. Jiang, Y. Chu et al., "Gasdermin D plays a key role as a pyroptosis executor of non-alcoholic steatohepatitis in

- humans and mice,” *Journal of Hepatology*, vol. 68, no. 4, pp. 773–782, 2018.
- [25] S. K. Das, W. S. Chu, A. K. Mondal et al., “Effect of pioglitazone treatment on endoplasmic reticulum stress response in human adipose and in palmitate-induced stress in human liver and adipose cell lines,” *American Journal of Physiology-Endocrinology and Metabolism*, vol. 295, no. 2, pp. E393–E400, 2008.
- [26] S. H. Bae, S. H. Sung, S. Y. Oh et al., “Sestrins activate Nrf2 by promoting p62-dependent autophagic degradation of Keap1 and prevent oxidative liver damage,” *Cell Metabolism*, vol. 17, no. 1, pp. 73–84, 2013.
- [27] S. Herzig and R. J. Shaw, “AMPK: guardian of metabolism and mitochondrial homeostasis,” *Nature Reviews Molecular Cell Biology*, vol. 19, no. 2, pp. 121–135, 2018.
- [28] D. G. Hardie, B. E. Schaffer, and A. Brunet, “AMPK: an energy-sensing pathway with multiple inputs and outputs,” *Trends in Cell Biology*, vol. 26, no. 3, pp. 190–201, 2016.
- [29] J. Aron-Wisniewsky, C. Vigliotti, J. Witjes et al., “Gut microbiota and human NAFLD: disentangling microbial signatures from metabolic disorders,” *Nature Reviews Gastroenterology & Hepatology*, vol. 17, no. 5, pp. 279–297, 2020.
- [30] D. Garcia and R. J. Shaw, “AMPK: mechanisms of cellular energy sensing and restoration of metabolic balance,” *Molecular Cell*, vol. 66, no. 6, pp. 789–800, 2017.
- [31] M. López, “EJE PRIZE 2017: hypothalamic AMPK: a golden target against obesity?,” *European Journal of Endocrinology*, vol. 176, no. 5, pp. R235–r246, 2017.
- [32] R. M. Esquejo, C. T. Salatto, J. Delmore et al., “Activation of liver AMPK with PF-06409577 corrects NAFLD and lowers cholesterol in rodent and primate preclinical models,” *EBio-Medicine*, vol. 31, pp. 122–132, 2018.
- [33] A. P. Gupta, P. Singh, R. Garg et al., “Pancreastatin inhibitor activates AMPK pathway via GRP78 and ameliorates dexamethasone induced fatty liver disease in C57BL/6 mice,” *Biomedicine & Pharmacotherapy*, vol. 116, article 108959, 2019.
- [34] J. Kim, G. Yang, Y. Kim, J. Kim, and J. Ha, “AMPK activators: mechanisms of action and physiological activities,” *Experimental & Molecular Medicine*, vol. 48, no. 4, article e224, 2016.
- [35] R. Guo, B. Zhao, Y. Wang et al., “Cholic acid prevents free-fatty-acid-induced lipid metabolism disorders via regulating Bmal1 in HepG2 cells,” *Journal of Agricultural and Food Chemistry*, vol. 66, no. 37, pp. 9667–9678, 2018.
- [36] S. Satapati, B. Kucejova, J. A. G. Duarte et al., “Mitochondrial metabolism mediates oxidative stress and inflammation in fatty liver,” *The Journal of Clinical Investigation*, vol. 125, no. 12, pp. 4447–4462, 2015.
- [37] X. Feng, W. Yu, X. Li et al., “Apigenin, a modulator of PPAR γ , attenuates HFD-induced NAFLD by regulating hepatocyte lipid metabolism and oxidative stress via Nrf2 activation,” *Biochemical Pharmacology*, vol. 136, pp. 136–149, 2017.
- [38] A. K. S. Silva and C. A. Peixoto, “Role of peroxisome proliferator-activated receptors in non-alcoholic fatty liver disease inflammation,” *Cellular and Molecular Life Sciences*, vol. 75, no. 16, pp. 2951–2961, 2018.
- [39] C. Mo, L. Wang, J. Zhang et al., “The crosstalk between Nrf2 and AMPK signal pathways is important for the anti-inflammatory effect of berberine in LPS-stimulated macrophages and endotoxin-shocked mice,” *Antioxidants & Redox Signaling*, vol. 20, no. 4, pp. 574–588, 2014.
- [40] D. Liu, Z. Ma, S. Di et al., “AMPK/PGC1 α activation by melatonin attenuates acute doxorubicin cardiotoxicity via alleviating mitochondrial oxidative damage and apoptosis,” *Free Radical Biology & Medicine*, vol. 129, pp. 59–72, 2018.
- [41] X. Han, H. Tai, X. Wang et al., “AMPK activation protects cells from oxidative stress-induced senescence via autophagic flux restoration and intracellular NAD(+) elevation,” *Aging Cell*, vol. 15, no. 3, pp. 416–427, 2016.
- [42] Q. Liu, Y. Chen, C. Shen et al., “Chicoric acid supplementation prevents systemic inflammation-induced memory impairment and amyloidogenesis via inhibition of NF- κ B,” *The FASEB Journal*, vol. 31, no. 4, pp. 1494–1507, 2016.
- [43] M. Yamamoto, T. W. Kensler, and H. Motohashi, “The KEAP1-NRF2 system: a thiol-based sensor-effector apparatus for maintaining redox homeostasis,” *Physiological Reviews*, vol. 98, no. 3, pp. 1169–1203, 2018.
- [44] E. H. Kobayashi, T. Suzuki, R. Funayama et al., “Nrf2 suppresses macrophage inflammatory response by blocking pro-inflammatory cytokine transcription,” *Nature Communications*, vol. 7, no. 1, article 11624, 2016.
- [45] J. D. Belcher, C. Chen, J. Nguyen et al., “Control of oxidative stress and inflammation in sickle cell disease with the Nrf2 activator dimethyl fumarate,” *Antioxidants & Redox Signaling*, vol. 26, no. 14, pp. 748–762, 2017.
- [46] P. C. Shimpi, V. R. More, M. Paranjpe et al., “Hepatic lipid accumulation and Nrf2 expression following perinatal and peripubertal exposure to bisphenol A in a mouse model of nonalcoholic liver disease,” *Environmental Health Perspectives*, vol. 125, no. 8, article 087005, 2017.
- [47] L. Guariguata, “Contribute data to the 6th edition of the IDF Diabetes Atlas,” *Diabetes Research and Clinical Practice*, vol. 100, no. 2, pp. 280–281, 2013.
- [48] P. Ramadori, H. Drescher, S. Erschfeld et al., “Hepatocyte-specific Keap1 deletion reduces liver steatosis but not inflammation during non-alcoholic steatohepatitis development,” *Free Radical Biology & Medicine*, vol. 91, pp. 114–126, 2016.
- [49] R. S. Sharma, D. J. Harrison, D. Kisilewski et al., “Experimental nonalcoholic steatohepatitis and liver fibrosis are ameliorated by pharmacologic activation of Nrf2 (NF-E2 p45-related factor 2),” *Cellular and Molecular Gastroenterology and Hepatology*, vol. 5, no. 3, pp. 367–398, 2018.
- [50] S. Chowdhry, M. H. Nazmy, P. J. Meakin et al., “Loss of Nrf2 markedly exacerbates nonalcoholic steatohepatitis,” *Free Radical Biology & Medicine*, vol. 48, no. 2, pp. 357–371, 2010.
- [51] Y. Wang, Y. Huang, Y. Xu et al., “A dual AMPK/Nrf2 activator reduces brain inflammation after stroke by enhancing microglia M2 polarization,” *Antioxidants & Redox Signaling*, vol. 28, no. 2, pp. 141–163, 2018.
- [52] Z. Wang, Z. Chen, Z. Jiang et al., “Cordycepin prevents radiation ulcer by inhibiting cell senescence via NRF2 and AMPK in rodents,” *Nature Communications*, vol. 10, no. 1, p. 2538, 2019.
- [53] H. Tilg and A. R. Moschen, “Evolution of inflammation in nonalcoholic fatty liver disease: the multiple parallel hits hypothesis,” *Hepatology*, vol. 52, no. 5, pp. 1836–1846, 2010.
- [54] A. R. Mridha, A. Wree, A. A. B. Robertson et al., “NLRP3 inflammasome blockade reduces liver inflammation and fibrosis in experimental NASH in mice,” *Journal of Hepatology*, vol. 66, no. 5, pp. 1037–1046, 2017.
- [55] T. Zhang, J. Hu, X. Wang et al., “MicroRNA-378 promotes hepatic inflammation and fibrosis via modulation of the NF-

- κ B-TNF α pathway,” *Journal of Hepatology*, vol. 70, no. 1, pp. 87–96, 2019.
- [56] C. X. Li, J. G. Gao, X. Y. Wan et al., “Allyl isothiocyanate ameliorates lipid accumulation and inflammation in nonalcoholic fatty liver disease via the Sirt1/AMPK and NF- κ B signaling pathways,” *World Journal of Gastroenterology*, vol. 25, no. 34, pp. 5120–5133, 2019.
- [57] Z. Darabi, M. Darand, Z. Yari et al., “Inflammatory markers response to citrulline supplementation in patients with non-alcoholic fatty liver disease: a randomized, double blind, placebo-controlled, clinical trial,” *BMC Research Notes*, vol. 12, no. 1, p. 89, 2019.
- [58] A. Salminen and K. Kaarniranta, “AMP-activated protein kinase (AMPK) controls the aging process via an integrated signaling network,” *Ageing Research Reviews*, vol. 11, no. 2, pp. 230–241, 2012.
- [59] H. J. Flint, K. P. Scott, P. Louis, and S. H. Duncan, “The role of the gut microbiota in nutrition and health,” *Gastroenterology & Hepatology*, vol. 9, no. 10, pp. 577–589, 2012.
- [60] W. Tang, X. Yao, F. Xia et al., “Modulation of the gut microbiota in rats by Hugin Qingzhi tablets during the treatment of high-fat-diet-induced nonalcoholic fatty liver disease,” *Oxidative Medicine and Cellular Longevity*, vol. 2018, Article ID 7261619, 14 pages, 2018.
- [61] L. C. Kong, P. H. Wuillemin, J. P. Bastard et al., “Insulin resistance and inflammation predict kinetic body weight changes in response to dietary weight loss and maintenance in overweight and obese subjects by using a Bayesian network approach,” *The Journal of Clinical Nutrition*, vol. 98, no. 6, pp. 1385–1394, 2013.
- [62] M. Raman, I. Ahmed, P. M. Gillevet et al., “Fecal microbiome and volatile organic compound metabolome in obese humans with nonalcoholic fatty liver disease,” *Clinical Gastroenterology and Hepatology*, vol. 11, no. 7, pp. 868–875.e3, 2013.
- [63] Y. F. Bai, S. W. Wang, X. X. Wang et al., “The flavonoid-rich Quzhou Fructus Aurantii extract modulates gut microbiota and prevents obesity in high-fat diet-fed mice,” *Nutrition & Diabetes*, vol. 9, no. 1, p. 30, 2019.
- [64] E. Org, B. W. Parks, J. W. J. Joo et al., “Genetic and environmental control of host-gut microbiota interactions,” *Genome Research*, vol. 25, no. 10, pp. 1558–1569, 2015.
- [65] J. Boursier, O. Mueller, M. Barret et al., “The severity of nonalcoholic fatty liver disease is associated with gut dysbiosis and shift in the metabolic function of the gut microbiota,” *Hepatology*, vol. 63, no. 3, pp. 764–775, 2016.
- [66] W. L. Guo, Y. Y. Pan, L. Li, T. T. Li, B. Liu, and X. C. Lv, “Ethanol extract of *Ganoderma lucidum* ameliorates lipid metabolic disorders and modulates the gut microbiota composition in high-fat diet fed rats,” *Food & Function*, vol. 9, no. 6, pp. 3419–3431, 2018.
- [67] H. Ma, B. Zhang, Y. Hu et al., “Correlation analysis of intestinal redox state with the gut microbiota reveals the positive intervention of tea polyphenols on hyperlipidemia in high fat diet fed mice,” *Journal of Agricultural and Food Chemistry*, vol. 67, no. 26, pp. 7325–7335, 2019.
- [68] X. Wei, J. Tao, S. Xiao et al., “Xiexin Tang improves the symptom of type 2 diabetic rats by modulation of the gut microbiota,” *Scientific Reports*, vol. 8, no. 1, article 3685, 2018.
- [69] M. Kim, G. Yoo, A. Randy, H. S. Kim, and C. W. Nho, “Chicoric acid attenuate a nonalcoholic steatohepatitis by inhibiting key regulators of lipid metabolism, fibrosis, oxidation, and inflammation in mice with methionine and choline deficiency,” *Molecular Nutrition & Food Research*, vol. 61, no. 5, 2017.
- [70] H. Xiao, G. Xie, J. Wang et al., “Chicoric acid prevents obesity by attenuating hepatic steatosis, inflammation and oxidative stress in high-fat diet-fed mice,” *Food Research International*, vol. 54, no. 1, pp. 345–353, 2013.
- [71] M. Mohammadi, R. Abbasalipourkabir, and N. Ziamajidi, “Fish oil and chicoric acid combination protects better against palmitate-induced lipid accumulation via regulating AMPK-mediated SREBP-1/FAS and PPAR α /UCP2 pathways,” *Archives of Physiology and Biochemistry*, vol. 11, pp. 1–9, 2020.
- [72] T. Jian, X. Ao, Y. Wu et al., “Total sesquiterpene glycosides from loquat (*Eriobotrya japonica*) leaf alleviate high-fat diet induced non-alcoholic fatty liver disease through cytochrome P450 2E1 inhibition,” *Biomedicine & Pharmacotherapy*, vol. 91, pp. 229–237, 2017.
- [73] Q. Ma, Y. Cui, S. Xu, Y. Zhao, H. Yuan, and G. Piao, “Synergistic inhibitory effects of acacetin and 11 other flavonoids isolated from *Artemisia sacrorum* on lipid accumulation in 3T3-L1 cells,” *Journal of Agricultural and Food Chemistry*, vol. 66, no. 49, pp. 12931–12940, 2018.
- [74] J. Zheng, J. Zhang, Y. Guo et al., “Improvement on metabolic syndrome in high fat diet-induced obese mice through modulation of gut microbiota by Sangguayin decoction,” *Journal of Ethnopharmacology*, vol. 246, article 112225, 2020.

Research Article

Saikosaponin A-Induced Gut Microbiota Changes Attenuate Severe Acute Pancreatitis through the Activation of Keap1/Nrf2-ARE Antioxidant Signaling

Jing Li,¹ Jinfeng Han,¹ Juan Lv,¹ Shiji Wang,¹ Lai Qu,¹ and Yanfang Jiang^{ID}²

¹Department of Intensive Care Unit, The First Hospital of Jilin University, Changchun 130021, China

²Genetic Diagnosis Center, The First Hospital of Jilin University, Changchun 130021, China

Correspondence should be addressed to Yanfang Jiang; jiangyfjl@126.com

Received 1 April 2020; Revised 11 July 2020; Accepted 21 July 2020; Published 2 November 2020

Academic Editor: Carlo Gabriele Tocchetti

Copyright © 2020 Jing Li et al. This is an open access article distributed under the Creative Commons Attribution License, which permits unrestricted use, distribution, and reproduction in any medium, provided the original work is properly cited.

Objective. Severe acute pancreatitis (SAP) is a serious and life-threatening disease associated with multiple organ failure and a high mortality rate and is accompanied by distinct oxidative stress and inflammatory responses. Saikosaponin A has strong antioxidant properties and can affect the composition of gut microbiota. We sought to determine the effects of Saikosaponin A interventions on SAP by investigating the changes of gut microbiota and related antioxidant signaling. **Methods.** A SAP model was established in Sprague-Dawley (SD) rats through the injection of sodium taurocholate into the biliopancreatic duct and confirmed by elevated levels of serum lipase and amylase. The model was fed a standard diet either with saline solution or with Saikosaponin A. Fecal microbiota transplantation (FMT) from Saikosaponin A-induced rats into the rat model was performed to test the effects of gut microbiota. The composition of gut microbiota was analyzed by using 16S rRNA gene sequencing. We measured apoptotic status, inflammatory biomarkers, and Keap1-Nrf2-ARE ((Kelch-like ECH-associated protein 1) nuclear factor erythroid 2-related factor 2-antioxidant response element) antioxidant signaling. **Results.** Saikosaponin A intervention attenuated SAP lesions and reduced the levels of serum amylase and lipase, oxidative stress, and inflammatory responses by reducing pathological scores and affecting the serum level of oxidative and inflammatory factors. Meanwhile, the expression of Keap1-Nrf2-ARE was increased. Saikosaponin A intervention improved microbiota composition by increasing the relative abundance of Lactobacillus and Prevotella species. FMT resulted in similar results as those caused by the Saikosaponin A intervention, suggesting Saikosaponin A may exert its function via the improvement of gut microbiota composition. **Conclusions.** Saikosaponin A-induced gut microbiota changes attenuate SAP progression in the rat model and may be a potential natural drug for adjuvant treatment of SAP. Further work is needed to clear up the points.

1. Introduction

Pancreatitis is a leading complication of gastrointestinal diseases, and often initiates and exacerbates systemic inflammatory responses. The mortality rate of pancreatitis is between 1.5% and 4.2% according to the previous report [1]. Pancreatitis development will lead to the release of inflammatory indicators and cytokines, which lead to intestinal barrier damage [2]. Pancreatitis increases intestinal permeability and facilitates bacterial infection, resulting in the damage of intestinal barrier [3]. Pancreatitis is often involved with lung injury [4, 5], liver disease [6], and other organ failure [7, 8].

Natural products have been found to be effective in the prevention of pancreatitis risk [9, 10]. *Radix bupleuri* is a common Chinese herb and shows anti-inflammatory properties in the prevention of SAP progression [11]. Saikosaponin A is one of the most effective components of *Radix bupleuri* roots [12, 13]. The previous work indicated that Saikosaponin A attenuated hyperlipidemic pancreatitis in an animal model by improving lipid metabolism and preventing the release of proinflammatory cytokines via the NF-kappaB signaling [14]. However, its function on SAP remains unclear. SAP is often characterized by recurrent episodes of inflammation and loss of tissue integrity in the intestine

[15]. Gut microbiota is thought to be important for maintaining the balance of proinflammatory cytokines, which is closely associated with SAP progression. The knowledge for gut microbiota and its metabolites on intestinal barrier function in SAP will help us to understand the mechanism of gut failure in the pathogenesis of SAP [16]. Early dysbiosis of the gut microbiota is associated with the SAP risk, and the modulation of the gut microbiota is a potential approach in the prevention of SAP development [17].

Keap1-Nrf2-ARE ((Kelch-like ECH-associated protein 1) nuclear factor erythroid 2-related factor 2-antioxidant response element) are widely reported antioxidant signaling molecules [18, 19]. Pancreatitis is usually accompanied by the increase in the oxidative stress and inflammatory responses [20, 21]. Free radicals play an important role in the pathophysiology of SAP, and increased free radical activities and increased concentrations of lipid peroxides have been found in both SAP patients [22] and animal models [20, 23]. Xanthine oxidase (XO) [24] and nitric oxide synthase (NOS) [25] may be the individual contribution of possible sources of free radicals. Cellular oxidative stress contributes to pancreas injury and the improvement of antioxidant capacity by increasing the levels of the reduced glutathione (GSH) level, and catalase (CAT) activity will reduce the injury [26]. The enhancement of antioxidants superoxidase dismutase (SOD) and glutathione peroxidases (GPx) and the reduction of lipid oxidation product malondialdehyde (MDA) contribute to the recovery of SAP-induced intestinal barrier injury [27]. Therefore, the improvement of the expression of antioxidant signaling molecules will be a potential approach in the therapy of pancreatitis [28, 29]. Therefore, the aim of present work is to explore the protective effects of Saikosaponin A on SAP and delineate the underlying mechanisms of functional Saikosaponin A by investigating the composition of gut microbiota and related molecules.

2. Materials and Methods

2.1. Extracts of Saikosaponin A and Analysis of HPLC. Saikosaponin A standard (purity > 99%) was bought from Sigma (St. Louis, MO, USA) and dissolved in PBS buffer (20 mM, pH 7.4) with 0.1% BSA at room temperature. Sodium taurocholate was purchased from Sigma and dissolved in 0.9% NaCl to final concentration 1 mg/ml. All other reagents were analytical grade.

Radix bupleuri rhizomes were purchased from Shanghai State-owned Changning Pharmacy (Shanghai, China); Saikosaponin A was isolated and characterized according to a previous report with slight modification [30]. 1000-g rhizomes of *Radix bupleuri* were taken, crushed, sieved through a 20-30-mesh sieve, soaked with 100% ethanol for three days, filtered, combined with the soaking solution, and evaporated under reduced pressure on a rotary evaporator to recover ethanol. The sample was concentrated to obtain the total extracts of *Radix bupleuri*. The extracts were suspended in water and further extracted with petroleum ether, chloroform, and ethyl acetate to obtain a petroleum ether portion, a chloroform portion, an ethyl acetate portion, and a water-soluble portion, respectively. One thousand grams of macro-

porous resin H802 was packed into a column (10 × 60 cm). After pretreatment, ethyl acetate raffinate was added (50 g of the concentrated solution was dissolved in water, and insoluble matter was filtered off). After the sample loading, the column was washed with 3000 ml of water and then eluted with 50% ethanol, concentrated under reduced pressure on a rotary evaporator, and then dried in a vacuum oven. A total of 1500 g of 200~300 mesh silica gel was suspended in CHCl₃ and equilibrated the column with CHCl₃ in a column. The sample was dissolved in 200 ml of ethanol, mixed with 100 mesh silica gel, and dried at room temperature. After the column was equilibrated, the sample was loaded. CHCl₃ : MeOH = 5 : 1 was used as the mobile phase to elute the sample successively. The eluted samples were collected (250 ml/bottle), numbered, and analyzed via high-pressure liquid chromatography (HPLC) (apparatus: HPLC-SCL-10 Avp; mobile phase: MeOH:H₂O (4:6); detection wavelength: 265 nm; column size: Luna C18 250 × 4.6 mm; column temperature: 40°C; flow rate: 1 ml/min; and injection volume: 10 μl). Thirty-nine grams of Saikosaponin was obtained. Finally, about 10 g of Saikosaponin A was finally purified on semipreparative HPLC (Beckman, Brea, CA, USA).

2.2. Establishment of the Model with SAP. Before the present study, all experimental processes were ensured to be consistent with the guidance for the care and use of laboratory animals from NIH and approved by the Animal Ethics Committee of The First Hospital of Jilin University (2017JLU0298). Eighty male Sprague-Dawley (SD) rats (8 weeks, 220–240 g) were purchased from the Animal Center of The First Hospital of Jilin University (Changchun, China). All rats were housed in separated cages (two rats in a cage) under either a 12:12 light:dark cycle (LD 12:12) and 22 ± 1°C with 65% humidity [2]. The rats had free access to standard food pellets and tap water ad libitum. SAP was established via the injection of 0.2 ml of 5% sodium taurocholate into the biliopancreatic duct according to the previous report [31]. SAP was induced by sodium taurocholate that resulted in acinar cell calcium overload, zymogen activation, cytokine activities, and cell death [32]. The SAP model was confirmed by the evaluated levels of blood lipase or amylase [33]. Fifty microliters blood was obtained from each rat tail vein before and after 3-day model establishment, and serum was prepared via centrifugation at 2000 × *g* for 10 min. Rat serum amylase and lipase were measured by using the rat pancreatic amylase (PAMY) ELISA Kit (Cat. No. MBS269618) and rat pancreatic lipase ELISA Kit (Cat. No. MBS453575) from MyBioSource (San Diego, CA, USA) according to the manufacturer's instructions. For the controls, the rats were injected with 0.9% NaCl solution. The animal model establishment was performed for twice as Figure 1 shows.

2.3. Animal Grouping. The dose range of Saikosaponin was referred to a report that the concentration of Saikosaponin A was from 6.25 mg/kg to 25.00 mg/kg [34], and a wider range of the dose (10, 20, and 40 mg/kg) was used in the present study. According to a previous report, pancreatic tissues

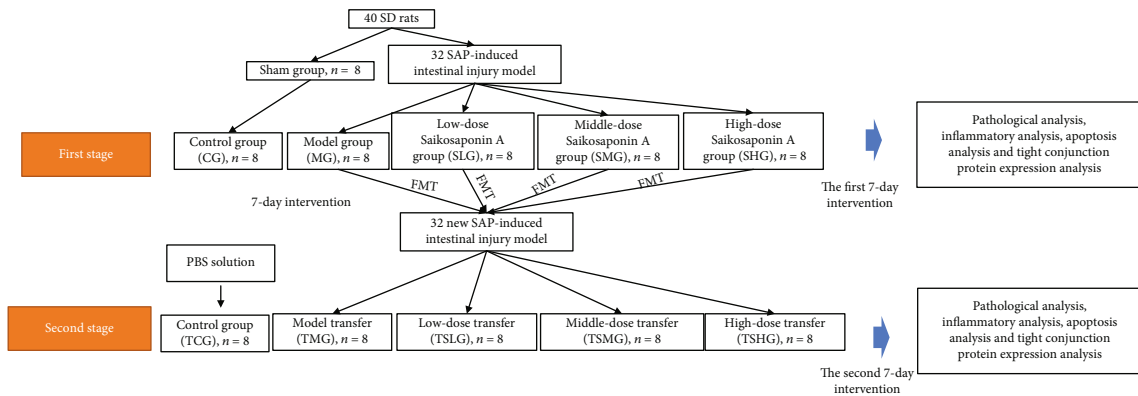


FIGURE 1: Study flow chart of the present experiment. There were 7 days for each stage, and the second stage was performed following the first stage.

were collected after 1-, 3-, and 5-day SAP model establishment. Most inflammatory cytokines had significant changes after 3- and 5-day SAP model establishment [35]. On the other hand, considering the effects of the Saikosaponin A on gut microbiota, a longer time (7 d) may be used [36]. There were two stages for the whole experiment as Figure 1 shows. After 12-hour sodium taurocholate injection, 24 SAP rats were administrated with different concentrations of Saikosaponin A (10, 20, and 40 mg/kg) in 0.2 ml 0.9% saline solution via the tail vein. Meanwhile, 0.2 ml 0.9% saline solution was injected in the control or animal group ($n = 8$ for each group) without Saikosaponin A. In the first stage, all rats were divided into CG (control group), MG (model group), SLG (low-dose Saikosaponin A), SMG (middle-dose Saikosaponin A), and SHG (high-dose Saikosaponin) groups according to different treatments (Figure 1). Rats were monitored daily for weight and disease activity index (DAI, including weight loss, presence of blood in feces, and stool consistency). The feces and urine samples were collected at 7 days. After 7 days, the rats were anesthetized with pentobarbital (40 mg/kg i.p.), blood samples were drawn, colon length was measured, and the animals were killed. Pancreas tissues were quickly removed and frozen at -80°C until use.

After 7-day Saikosaponin A intervention, fecal sample (1.0 g) was obtained from each rat in the MG, SLG, SMG, and SHG groups, suspended with 5 ml of sterile PBS buffer, and used to colonize the newly SAP rats. In the second stage, fecal microbiota transplantation (FMT) was transferred according to the previous study [37]. For the control group, the rats were treated with PBS buffer. Briefly, the fecal samples in the PBS solution (0.01 M, pH 7.4) were vortexed for 5 min, homogenized, and centrifuged for 10 min (1,000 g), and the pools were divided into equal volumes for 7 d. The model rats were colonized with pooled samples for another 7 d. These rats were divided into TCG, TMG, TSLG, TSMG, and TSHG groups according to the fecal microbiota were from MG, SLG, SMG, and SHG groups, respectively (Figure 1).

2.4. DAI. The DAI was evaluated according to the previous report, and the DAI score was presented as mean scores of

body weight loss, fecal consistency, and fecal blood test scores [38].

2.5. Histological Evaluation. Colon tissues were washed in PBS buffer. The pancreas tissues were fixed by using 4% formalin, embedded in paraffin, cut in 4 m sections, and stained with hematoxylin and eosin (H&E) [39]. The inflammatory and injury of pancreas were observed in 5 fields per sections. The pathological grades were calculated according to Park's classification [40, 41] with slight modification: Grade 0, the lowest grade of injury with normal pancreas cell structure and without inflammation; Grade 1, the normal pancreas morphology was with a small number of mononuclear cell infiltration; Grade 2, the pancreas tissues were with middle number of mononuclear cell infiltration; Grade 3, the pancreas tissues were characterized with high-number of mononuclear cell infiltration; and Grade 4, pancreas structure was damaged with the significant number of mononuclear cell infiltration.

2.6. Serum Oxidative Assay. Blood sample was collected via abdominal aorta and centrifuged at $4000 \times g$ for 10 min at 4°C . The serum was separated and stored at -80°C for subsequent biochemical testing. Sera MDA, CAT, SOD, and GPx were measured by using corresponding assay kits from Northwest Life Science Specialties (Vancouver, WA, USA), Cayman Chemical Company (MI, USA), Calbiochem (San Diego, CA, USA), and Nanjing Jiancheng Bio-Tek Co. (Nanjing, China) on an automatic blood chemical analyzer (CIBA Corning, OH, USA), respectively.

2.7. Serum Inflammatory Cytokines Analysis. The levels of TNF- α (SKU: BC-ER141303), IL-1 β (SKU: BC-EH101933), IL-6 (SKU: BC-ER140741), and IL-10 (SKU: BC-ER140711) in serum were assessed by using ELISA kits following the manufacturer's scheme from Biocodon Technologies (Mission, KS, USA) and an automatic blood chemical analyzer (CIBA Corning, OH, USA). Serum C-reactive protein (CRP) was measured using the ELISA kit from DRG Instrument GmbH (Marburg, Germany) on a microplate reader from Thermo Scientific (Waltham, MA, USA).

Serum procalcitonin (PCT) was measured with the ELISA kit from EIAab Science Co., Ltd. (Wuhan, China).

2.8. Reverse Transcription-Quantitative PCR (RT-qPCR). RNA was isolated from 5 mg pancreas using TRIzol reagent (Shanghai Shenggong Co., Ltd., Shanghai, China). cDNA was made by using a reverse transcription kit (Shanghai Shenggong Co., Ltd., Shanghai, China). The following primers were used: Keap1 forward primer 5'-TTCGCCTACACGGCCTC-3' and reverse primer 5'-GAAGTTGGC GATGCCGATG-3'; Nrf2, forward primer 5'-CCTCAACTATAGCGATGCTGAATCT-3' and reverse primer 5'-AGGAGTTGGGCATGAGTGAGTAG-3'; ARE, forward primer 5'-CTGTCCTCAAATGAACCTGCCTCCTC-3' and reverse primer 5'-GAGGAGGCAGGTTCCATTGAGGACAG-3'; and β -actin, forward primer 5'-AAGTCCCTCACCTCCCAAAG-3' and reverse primer 5'-AAGCAATGCTGTCACCTTCCC-3'. RT-qPCR was performed on GeneAmp PCR System 9700 (Applied Biosystems, Foster City, CA, USA). The levels of target genes were detected and the relative mRNA levels were normalized to β -actin using the $2^{-\Delta\Delta Ct}$ method.

2.9. Western Blot. Pancreas tissues were used to measure the expression of Keap1, Nrf2, and ARE. Ten milligrams of pancreatic tissue was ground in liquid nitrogen, and total protein was extracted by using the Protein Isolation Kit (Invitrogen, CA, USA) according to the manufacture's instruction. Protein concentration was determined by using the BCA kit (Invitrogen, Carlsbad, CA, USA). HRP-conjugated goat anti-rabbit IgG H&L (ab6721) secondary antibodies were from Abcam (Abcam, San Francisco, CA, USA). The proteins were separated by SDS-PAGE and transferred to the PVDF membrane. The membrane was blocked for 1 hour at ambient room temperature in 10% nonfat milk and incubated with primary antibody (Anti-Keap1 antibody/Anti-Nrf2 antibody/Anti-ARE antibody from Abcam (1:1,000; Cambridge, MA, USA) overnight at 4°C. The membrane was rinsed 3 times with PBTB, incubated 2 hours at 37°C in secondary antibodies. Image was obtained on an infrared scanner (Odyssey, Lincoln, NE, USA). Relative protein levels were calculated by using internal reference β -actin.

2.10. Analysis of Gut Microbiota. Fecal pellets were collected and weighed, homogenized with 1 ml of sterile PBS. Bacterial DNA was extracted from the samples by using the QIAamp Fast DNA Stool Mini Kit (catalog number: 51604, QIAGEN, CA, USA). The isolated DNA was amplified using primers for the target gene 16S rRNA (V3-4 regions: forward 5'-CCTACGGGNGGCWGCAG-3' and reverse 5'-GACTAC HVGGGTATCTAATCC-3') according to the previous report [42]. The gut microbiota of rats was analyzed by using 16S rRNA sequencing of bacterial genomes.

2.11. Statistical Analysis. All data were presented as the mean \pm standard deviation (S.D.). The variables were analyzed by using unpaired two tailed Student's *t*-test. A normal distribution of variance was confirmed by the Kolmogorov

and Smirnov test [43]. Homogeneity of variance was confirmed by using Bartlett's test [44]. *p* values were corrected for multiple comparisons by using the Bonferroni adjustment [45]. The statistical data were analyzed by one-way ANOVA followed by Tukey's post hoc test. The statistical difference was considered if *p* < 0.5.

3. Results

3.1. HPLC Analysis of Saikosaponin A. Comparing with the standard of Saikosaponin A (Figure 2(a)), HPLC analysis showed that the main extracts of *Radix bupleuri* was Saikosaponin A (Figure 2(b)) and the eluting time was 19.9 min. *Radix bupleuri* may exert its function via its main component Saikosaponin A.

3.2. Saikosaponin A Intervention Reduced SAP Symptoms. The present results showed that the levels of serum amylase (Figure 3(a)) and serum lipase (Figure 3(b)) significantly increased in the MG group when compared with the CG group (*p* < 0.05). The results suggested that SAP was established with the significantly increased levels of serum amylase and lipase. On the other hand, Saikosaponin A treatment reduced the level of serum amylase (Figure 3(a)) and serum lipase (Figure 3(b)) in a dose-dependent way (*p* < 0.05). The results suggest that Saikosaponin A intervention reduces serum levels of amylase and lipase in the SAP model.

To explore the effects of Saikosaponin A on pancreas damage, an SAP model was established in rats. The DAI was 0 in the CG group, and the scores were highest in the MG group. Saikosaponin A intervention reduced the DAI value in a dose-dependent way (Figure 4(a), *p* < 0.05). Pathological change was assessed by using the H&E stain. There was no pathological character in the CG group with Grade 0. In contrast, the rats had a significant pathological character in the MG group with grade 4, including acinar cell edema, widened intercellular spaces, hemorrhage, necrosis, inflammatory cell infiltration, and cell destruction (Figures 4(b) and 3(c), *p* < 0.05). The pathological characters were significantly reduced in Saikosaponin A-treated group in a dose-dependent way (Figures 4(b) and 3(c), *p* < 0.05). These results suggest that Saikosaponin A intervention ameliorates SAP lesions.

3.3. Saikosaponin A Had Antioxidant and Anti-Inflammatory Effects on the Rats with SAP. Antioxidant analysis showed that serum levels of SOD (Figure 5(a)), CAT (Figure 5(b)), and GPx (Figure 5(c)) were highest in the CG group and significantly reduced in the MG group while the MDA level was lowest in the CG group and highest in the MG group (Figure 5(d), *p* < 0.05). Saikosaponin A intervention increased the serum levels of SOD (Figure 5(a)), CAT (Figure 5(b)), and GPx (Figure 5(c)) and reduced the MDA level (Figure 5(d), *p* < 0.05). The administration of Saikosaponin A suppressed oxidative stress in the rats with SAP.

Anti-inflammatory analysis showed that serum levels of TNF- α (Figure 5(e)), IL-1 β (Figure 5(f)), and IL-6 (Figure 5(g)) were lowest in the CG group and significantly

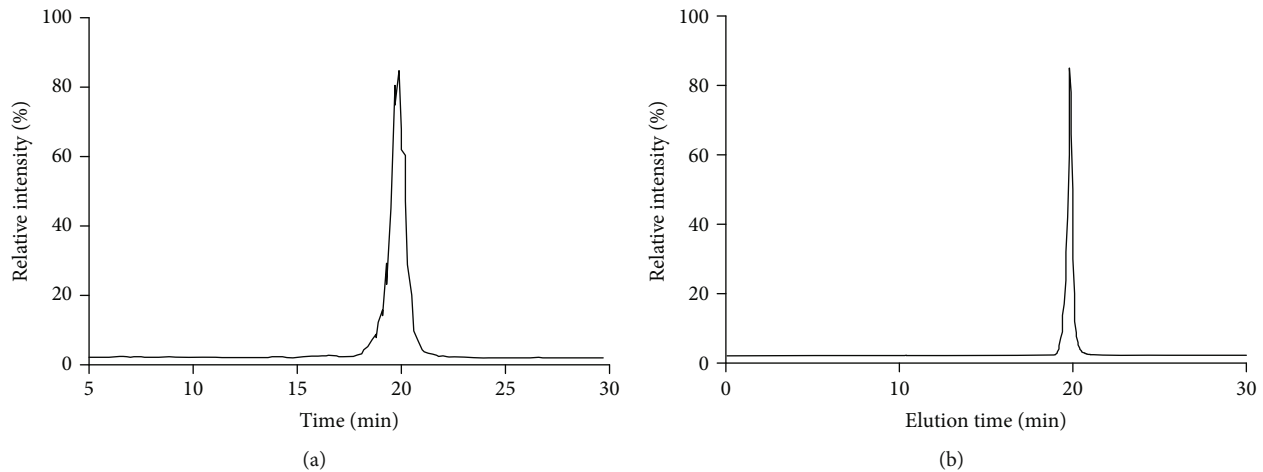


FIGURE 2: High-performance liquid chromatography (HPLC) analysis for the extracts of *Radix bupleuri*. (a) The standard of Saikosaponin A. (b) Purified Saikosaponin A.

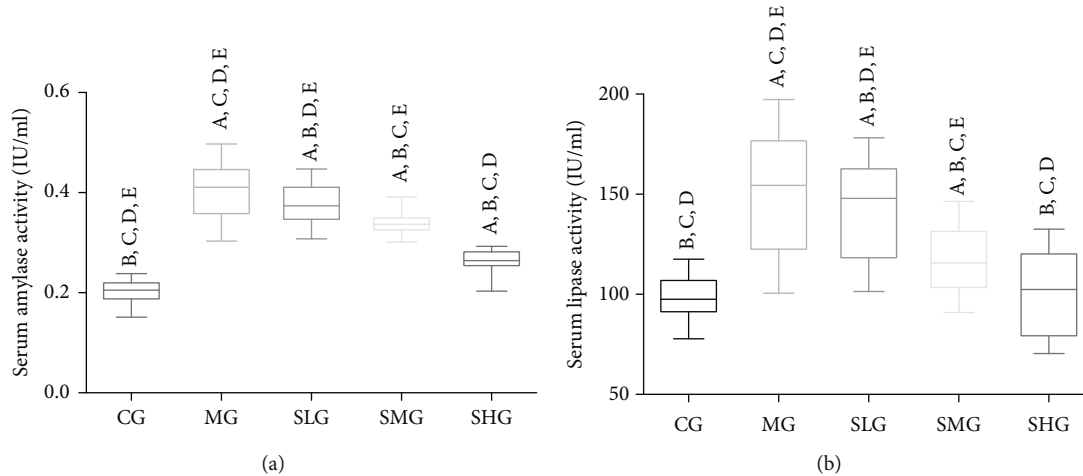


FIGURE 3: The effects of Saikosaponin A on serum lipase and amylase among different groups. Data were presented as means \pm S.D. (standard deviation) and $n = 8$ for each group. ^a $p < 0.05$ vs. the CG group, ^b $p < 0.05$ vs. the MG group, ^c $p < 0.05$ vs. the SLG group, ^d $p < 0.05$ vs. the SMG group, and ^e $p < 0.05$ vs. the SHG group.

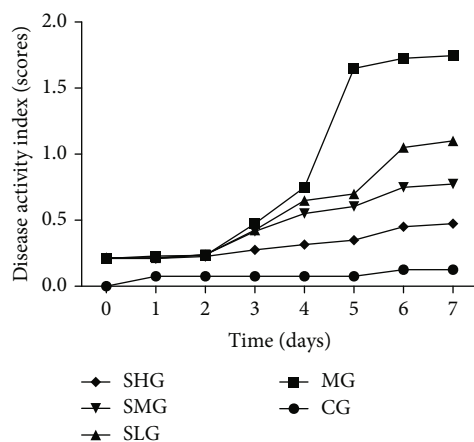
increased in the MG group while the IL-10 level was highest in the CG group and lowest in the MG group (Figure 5(h), $p < 0.05$). Saikosaponin A intervention reduced the serum levels of TNF- α (Figure 5(e)), IL-1 β (Figure 5(f)), and IL-6 (Figure 5(g)) and increased the IL-10 level (Figure 5(h), $p < 0.05$). The levels of serum CRP (Figure 5(i)) and serum PCT (Figure 5(j)) significantly increased in the MG group when compared with the CG group ($p < 0.05$). The results suggested that SAP was established with the significantly increased levels of serum CRP and PCT. On the other hand, Saikosaponin A treatment reduced the level of serum CRP (Figure 5(i)) and serum PCT (Figure 5(j)) in a dose-dependent way ($p < 0.05$). The results suggest that Saikosaponin A intervention reduces serum levels of inflammatory indicators in the SAP model. Saikosaponin A increased anti-inflammatory properties in the rats with SAP.

3.4. Saikosaponin A Increased the Relative mRNA Levels of Antioxidant Signaling Molecules. Keap1-Nrf2-ARE are impor-

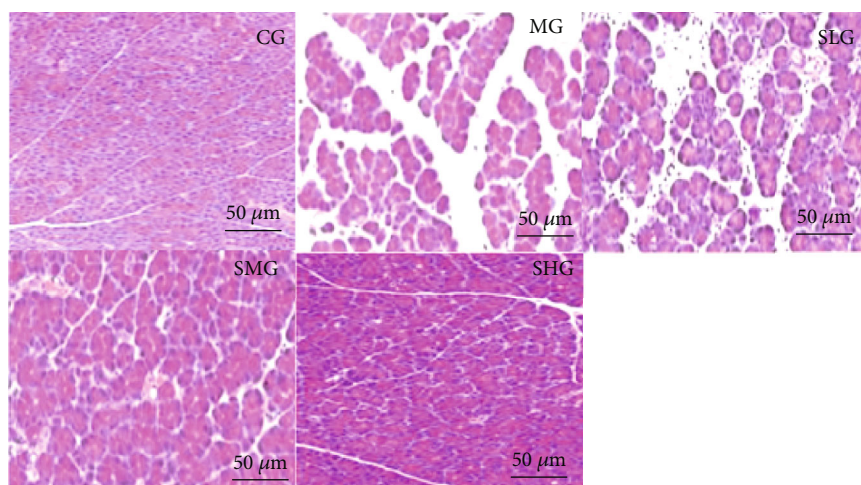
tant antioxidant signaling molecules to maintain antioxidant properties and pancreas integrity [46]. Thus, we explored the protective function by investigating the effects of Saikosaponin A on the relative mRNA levels of the antioxidant signaling. The levels of Keap1 (Figure 6(a)), Nrf2 (Figure 6(b)), and ARE (Figure 6(c)) were obviously decreased in the MG group when compared with those in the CG group ($p < 0.05$). However, the administration of Saikosaponin A increased the level of Keap1 (Figure 6(a)), Nrf2 (Figure 6(b)), and ARE (Figure 6(c)). The experiment result demonstrated that Saikosaponin A ameliorated the SAP by increasing the relative mRNA levels of antioxidant signaling molecules.

3.5. Saikosaponin A Increased the Protein Levels of Antioxidant Signaling Molecules.

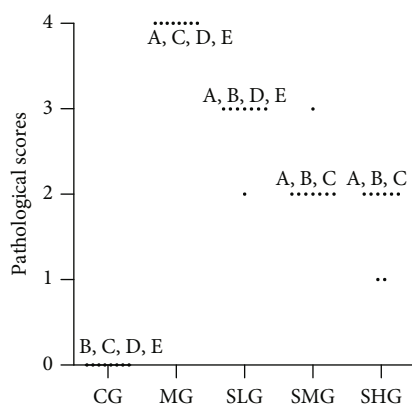
We further explored the protective function by investigating the effects of Saikosaponin A on the protein levels of the antioxidant signaling molecules. The expression levels of Keap1 (Figure 7(a)), Nrf2 (Figure 7(b)), and ARE (Figure 7(c)) obviously decreased in



(a)



(b)



(c)

FIGURE 4: Saikosaponin A ameliorated pathological character of SAP in rats. (a) Disease activity index. (b) Hematoxylin and eosin (H&E) staining of pancreas in each group. (c) Histopathological scores. Data were presented as means \pm S.D. (standard deviation) and $n = 8$ for each group. ^a $p < 0.05$ vs. the CG group, ^b $p < 0.05$ vs. the MG group, ^c $p < 0.05$ vs. the SLG group, ^d $p < 0.05$ vs. the SMG group, and ^e $p < 0.05$ vs. the SHG group.

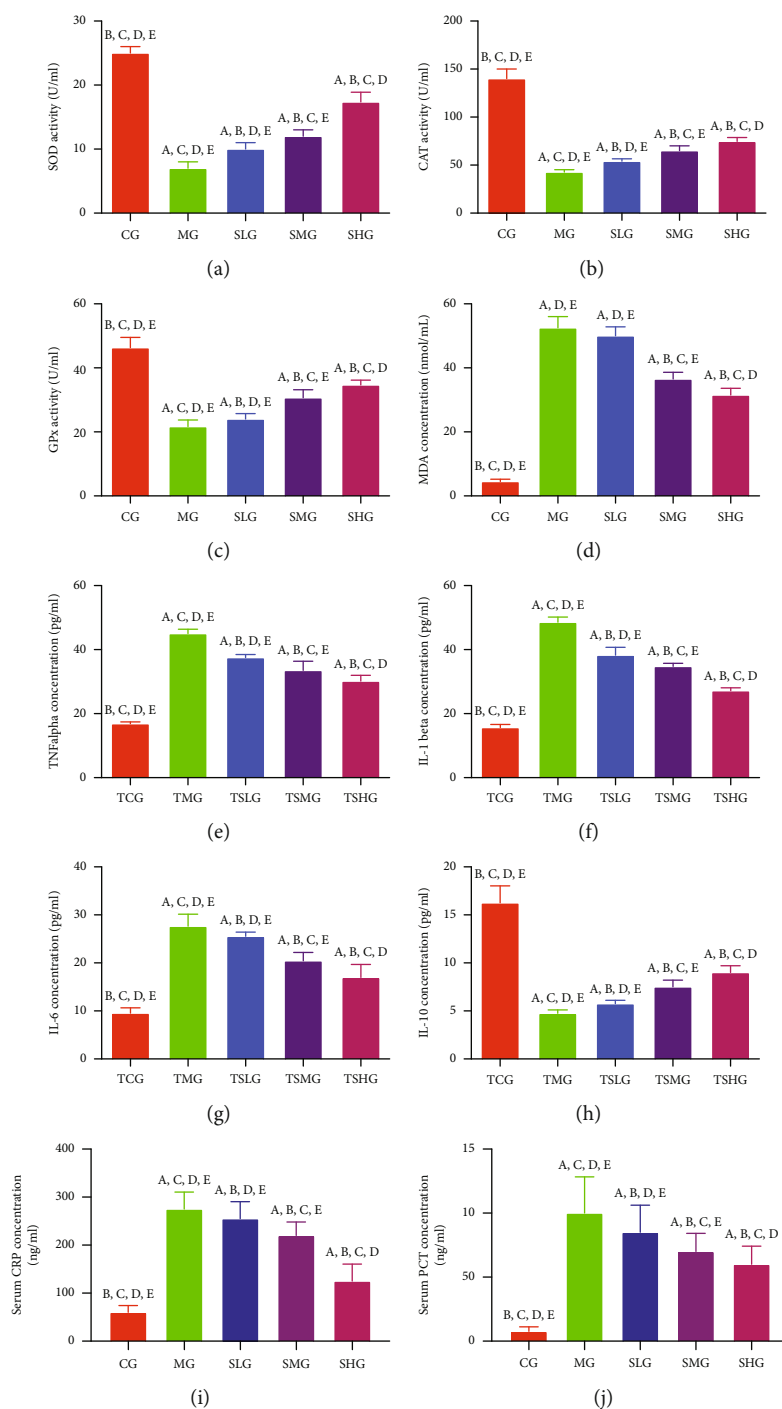


FIGURE 5: The effects of administration of Saikosaponin A on serum level of oxidative stress, inflammatory responses, and apoptosis status in the rats with severe acute pancreatitis (SAP). (a) Superoxide dismutase (SOD). (b) Catalase (CAT). (c) Oxidized glutathione (GPx). (d) Malondialdehyde (MDA). (e) Tumor necrosis factor- (TNF-) α . (f) Interleukin- (IL-) 1β . (g) IL-6. (h) IL-10. (i) C-reactive protein (CRP). (j) Procalcitonin (PCT). Data were presented as means \pm S.D. (standard deviation) and $n = 8$ for each group. ^a $p < 0.05$ vs. the CG group, ^b $p < 0.05$ vs. the MG group, ^c $p < 0.05$ vs. the SLG group, ^d $p < 0.05$ vs. the SMG group, and ^e $p < 0.05$ vs. the SHG group.

the MG group when compared with those in the CG group ($p < 0.05$). However, the administration of Saikosaponin A increased the expression levels of Keap1 (Figure 7(a)), Nrf2 (Figure 7(b)), and ARE (Figure 7(c)). The experiment result demonstrated that Saikosaponin A ameliorated the SAP

status by increasing the expression of antioxidant signaling proteins.

3.6. Saikosaponin A Intervention Improved Gut Microbiota Composition. Dysbiosis of gut microbiota is closely

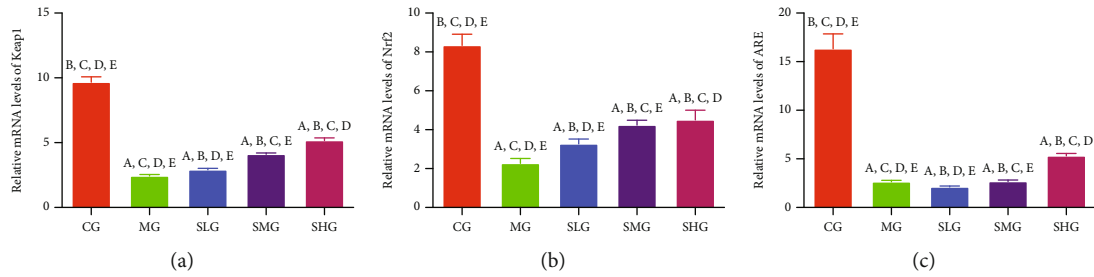


FIGURE 6: The real-time reverse transcription polymerase chain reaction (RT-PCR) analysis of the effects of Saikosaponin A on the relative mRNA levels of antioxidant signaling proteins. (a) Kelch-like ECH-associated protein 1 (Keap1). (b) Nuclear factor erythroid 2-related factor 2 (NRF2). (c) Antioxidant response element (ARE). Data were presented as mean values \pm S.D. (standard deviation) and $n = 8$ for each group. ^a $p < 0.05$ vs. the CG group, ^b $p < 0.05$ vs. the MG group, ^c $p < 0.05$ vs. the SLG group, ^d $p < 0.05$ vs. the SMG group, and ^e $p < 0.05$ vs. the SHG group.

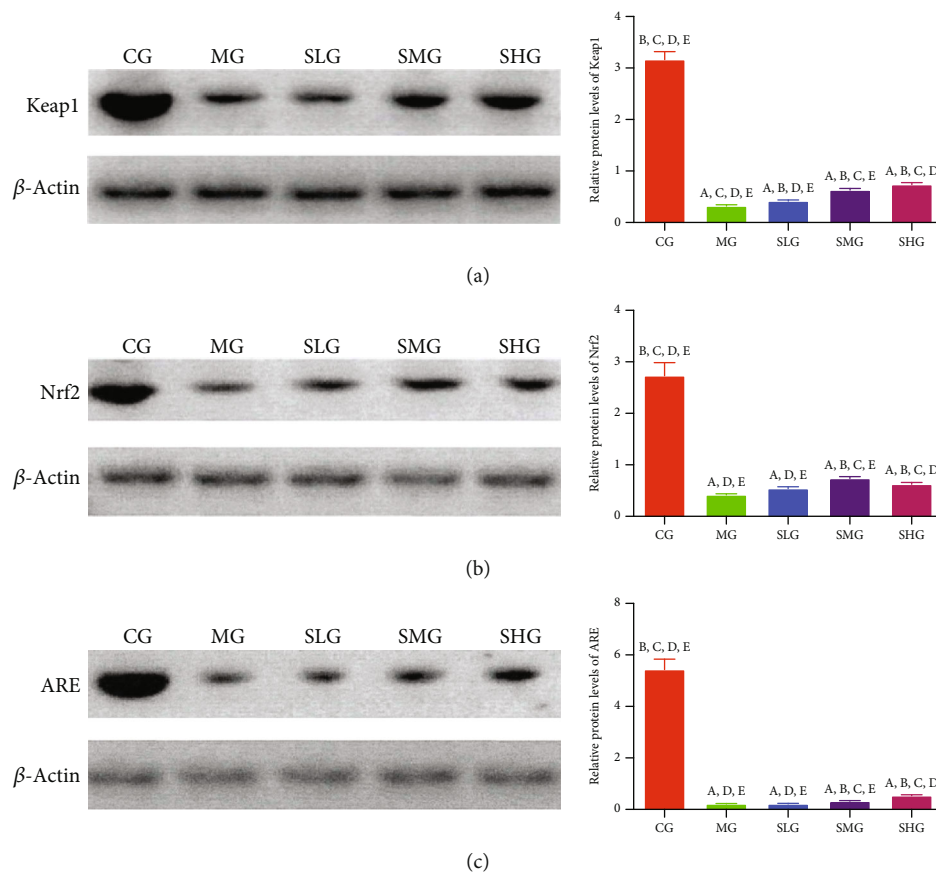


FIGURE 7: Western blot analysis of the effects of Saikosaponin A on the expression of antioxidant signaling proteins. (a) Kelch-like ECH-associated protein 1 (Keap1). (b) Nuclear factor erythroid 2-related factor 2 (NRF2). (c) Antioxidant response element (ARE). Data were presented as mean values \pm S.D. (standard deviation) and $n = 8$ for each group. ^a $p < 0.05$ vs. the CG group, ^b $p < 0.05$ vs. the MG group, ^c $p < 0.05$ vs. the SLG group, ^d $p < 0.05$ vs. the SMG group, and ^e $p < 0.05$ vs. the SHG group.

associated with pancreas dysfunction and damage. To investigate the impact of Saikosaponin A on gut microbiota composition, 16S rRNA gene sequencing was conducted by using the different fecal specimens from all groups. The relative abundance of Lactobacillus species was highest in the CG, and lowest in the MG group (Figure 8(a)). Saikosaponin A treatment increased the relative abundance of Lactobacillus species in a dose-dependent way (Figure 8(a)). The abun-

dance of Prevotella species was similar between the CG and MG groups (Figure 8(a)). Saikosaponin A treatment increased the relative abundance of Prevotella species in a dose-dependent way (Figure 8(a)). Heatmap analysis showed the similar results as those in the barplots (Figure 8(b)).

3.7. FMT of Saikosaponin A-Treated Rats Ameliorated SAP Lesions. To explore whether the gut microbiota of

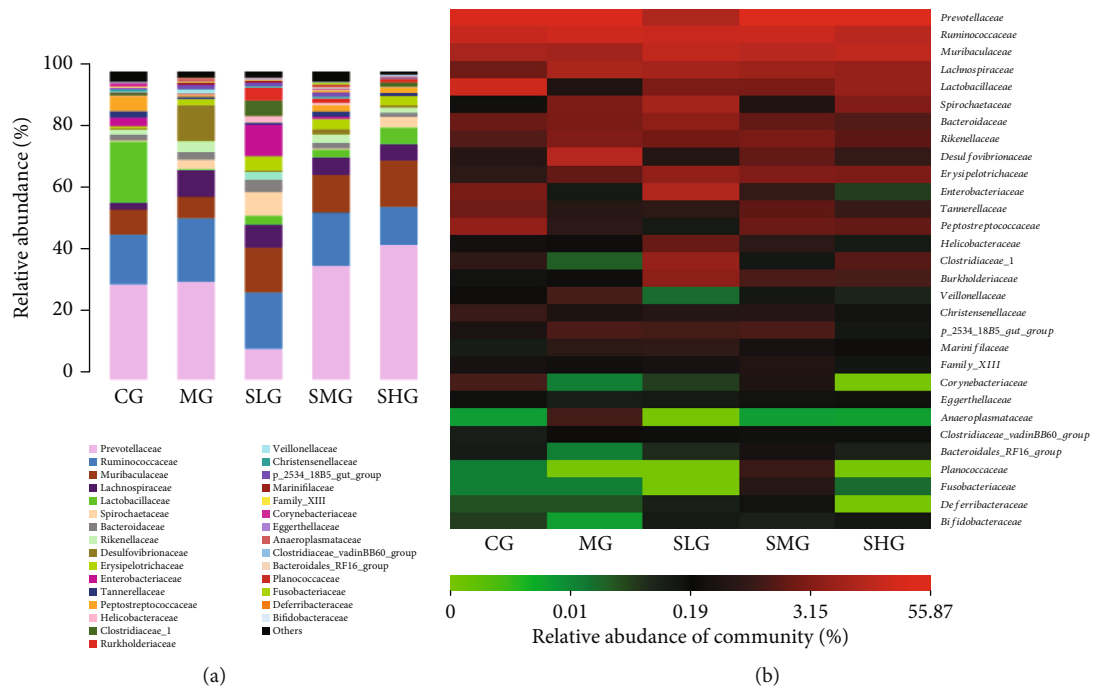


FIGURE 8: The composition of gut microbiota among different groups. (a) The proportion of gut microbiota. (b) Heatmap analysis of gut microbiota changes from different treatments.

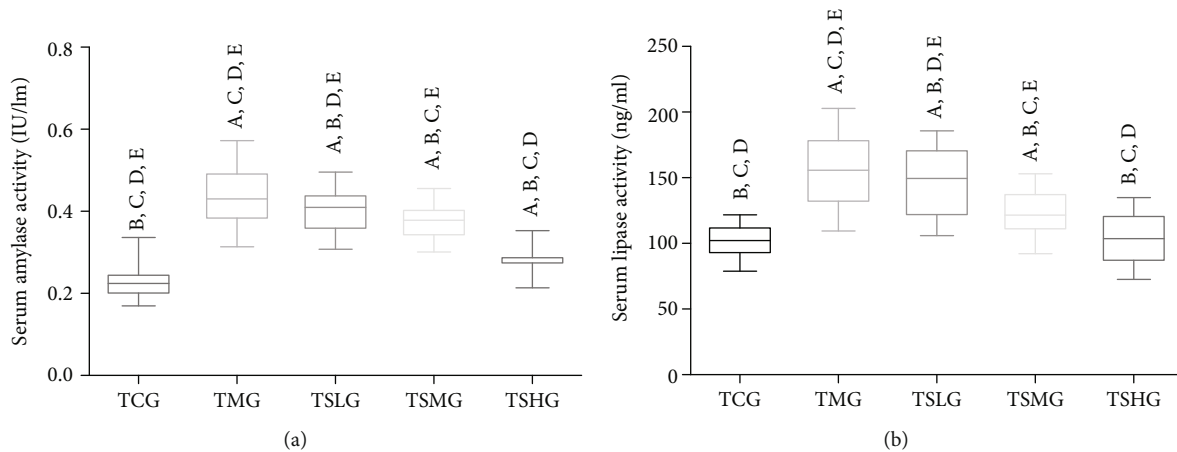
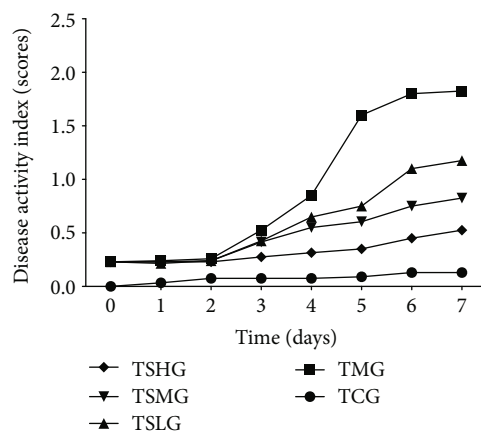


FIGURE 9: The effects of fecal microbiota transplantation (FMT) of Saikosaponin A-treated rats on serum lipase and amylase among different groups. Data were presented as means \pm S.D. (standard deviation) and $n = 8$ for each group. ^a $p < 0.05$ vs. the TCG group, ^b $p < 0.05$ vs. the TMG group, ^c $p < 0.05$ vs. the TSLG group, ^d $p < 0.05$ vs. the TSMG group, and ^e $p < 0.05$ vs. the TSHG group.

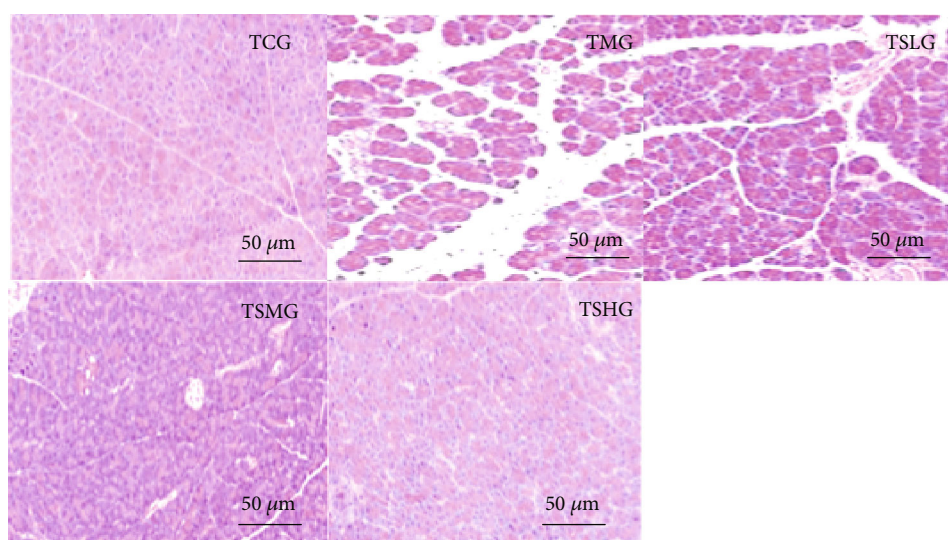
Saikosaponin A-treated animals improve the SAP rats, the gut microbiota of Saikosaponin A-treated SAP rats (the model was established within the first 7 days) was transferred to another SAP rats (the model was established within the second 7 days). All the previous parameters were repeated analyzed. The levels of serum amylase (Figure 9(a)) and serum lipase (Figure 9(b)) significantly increased in the TMG group when compared with the TCG group ($p < 0.05$). The results suggested that FMT of the SAP model rats significantly increased the levels of serum amylase and lipase. On the other hand, FMT of Saikosaponin A-treated rats reduced the level of serum amylase (Figure 9(a)) and serum lipase (Figure 9(b), $p < 0.05$). The

results suggest that FMT of Saikosaponin A-treated rats reduces serum levels of amylase and lipase in the SAP model. FMT of model rat increased disease activity index scores (Figure 10(a)) and pathological scores (Figures 10(b) and 10(c)). In contrast, the FMT of Saikosaponin A-treated rats reduced disease activity index scores (Figure 10(a)) and pathological scores (Figures 10(b) and 10(c)). These results suggest that Saikosaponin A ameliorates SAP lesions by improving gut microbiota.

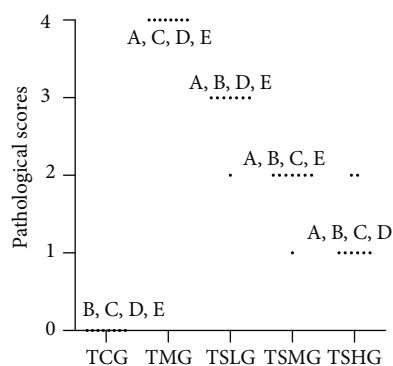
3.8. FMT of Saikosaponin A-Treated Rats Had Antioxidant and Anti-Inflammatory Effects on the Rats with SAP. Antioxidant analysis showed that serum levels of SOD



(a)



(b)



(c)

FIGURE 10: Fecal microbiota transplantation (FMT) of Saikosaponin A-treated rats ameliorated pathological character of severe acute pancreatitis (SAP) in rats. (a) Disease activity index. (b) Hematoxylin and eosin (H&E) staining of pancreas in each group. (c) Histopathological scores. Data were presented as means \pm S.D. (standard deviation) and $n = 8$ for each group. ^a $p < 0.05$ vs. the TCG group, ^b $p < 0.05$ vs. the TMG group, ^c $p < 0.05$ vs. the TSLG group, ^d $p < 0.05$ vs. the TSMG group, and ^e $p < 0.05$ vs. the TSHG group.

(Figure 11(a)), CAT (Figure 11(b)), and GPx (Figure 11(c)) were highest in the TCG group and significantly reduced in the TMG group while the MDA level was lowest in the

TCG group and highest in the TMG group (Figure 11(d), $p < 0.05$). FMT of Saikosaponin A-treated rats increased the serum levels of SOD (Figure 11(a)), CAT (Figure 11(b)),

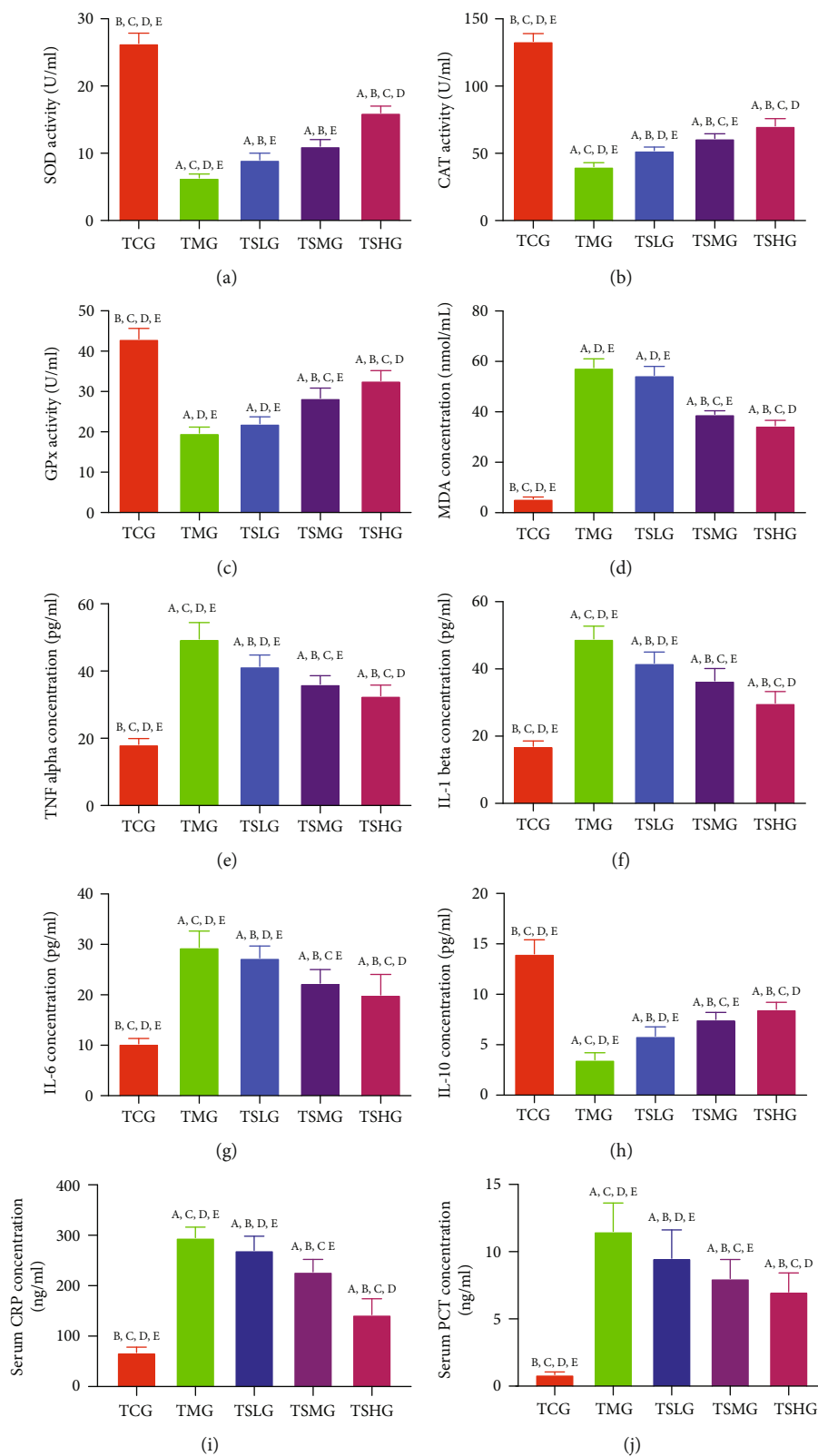


FIGURE 11: The effects of Saikosaponin A-treated rats on serum level of oxidative stress, inflammatory responses, and apoptosis status in the rats with severe acute pancreatitis (SAP). (a) Superoxide dismutase (SOD). (b) Catalase (CAT). (c) Oxidized glutathione (GPx). (d) Malondialdehyde (MDA). (e) Tumor necrosis factor- (TNF-) α . (f) Interleukin- (IL-) 1β . (g) IL-6. (h) IL-10. (i) C-reactive protein (CRP). (j) Procalcitonin (PCT). Data were presented as means \pm S.D. (standard deviation) and $n = 8$ for each group. ^a $p < 0.05$ vs. the TCG group, ^b $p < 0.05$ vs. the TMG group, ^c $p < 0.05$ vs. the TSLG group, ^d $p < 0.05$ vs. the TSMG group, and ^e $p < 0.05$ vs. the TSHG group.

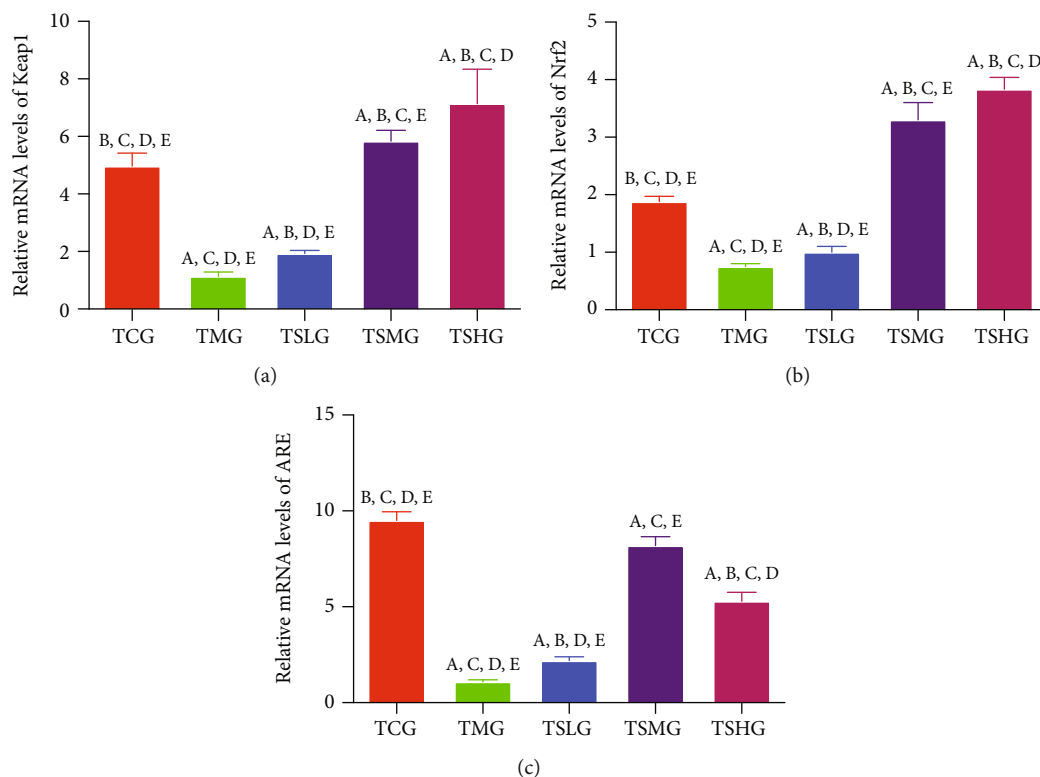


FIGURE 12: The real-time reverse transcription polymerase chain reaction (RT-PCR) analysis of the effects of fecal microbiota transplantation (FMT) of Saikosaponin A on relative mRNA levels of antioxidant signaling proteins. (a) Kelch-like ECH-associated protein 1 (Keap1). (b) Nuclear factor erythroid 2-related factor 2 (NRF2). (c) Antioxidant response element (ARE). Data were presented as means \pm S.D. (standard deviation) and $n=8$ for each group. ^a $p < 0.05$ vs. the TCG group, ^b $p < 0.05$ vs. the TMG group, ^c $p < 0.05$ vs. the TSLG group, ^d $p < 0.05$ vs. the TSMG group, and ^e $p < 0.05$ vs. the TSHG group.

and GPx (Figure 11(c)) and reduced the MDA level (Figure 11(d), $p < 0.05$). FMT of Saikosaponin A-treated rats suppressed oxidative stress in the rats with SAP.

Anti-inflammatory analysis showed that serum levels of TNF- α (Figure 11(e)), IL-1 β (Figure 11(f)), and IL-6 (Figure 11(g)) were lowest in the TCG group and significantly increased in the TMG group while the IL-10 level was highest in the TCG group and lowest in the TMG group (Figure 11(h), $p < 0.05$). FMT of Saikosaponin A-treated rats reduced the serum levels of serum levels of TNF- α (Figure 11(e)), IL-1 β (Figure 11(f)), and IL-6 (Figure 11(g)) and increased the IL-10 level (Figure 11(h), $p < 0.05$). The levels of serum CRP (Figure 11(i)) and serum PCT (Figure 11(j)) significantly increased in the TMG group when compared with the TCG group ($p < 0.05$). The results suggested that FMT of SAP model rats significantly increased the levels of serum CRP and PCT. On the other hand, FMT of Saikosaponin A-treated rats reduced the level of serum CRP (Figure 11(i)) and serum PCT (Figure 11(j), $p < 0.05$). FMT of Saikosaponin A-treated rats increased anti-inflammatory properties in the rats with SAP.

3.9. FMT of Saikosaponin A-Treated Rats Increased the Relative mRNA Levels of Antioxidant Signaling Protein. The relative mRNA levels of Keap1 (Figure 12(a)), Nrf2 (Figure 12(b)), and ARE (Figure 12(c)) was obviously decreased in the TMG group when compared with those

in the TCG group ($p < 0.05$). However, FMT of Saikosaponin A-treated rats increased the relative mRNA levels of Keap1 (Figure 12(a)), Nrf2 (Figure 12(b)), and ARE (Figure 12(c)). The experiment result demonstrated that FMT of Saikosaponin A-treated rats ameliorated the SAP by increasing the relative mRNA levels of antioxidant signaling molecules.

3.10. FMT of Saikosaponin A-Treated Rats Increased the Expression of Antioxidant Signaling Protein. Western blot analysis showed that the expression levels of Keap1 (Figure 13(a)), Nrf2 (Figure 13(b)), and ARE (Figure 13(c)) obviously decreased in the TMG group when compared with the TCG group ($p < 0.05$). However, FMT of Saikosaponin A-treated rats increased the expression levels of Keap1 (Figure 13(a)), Nrf2 (Figure 13(b)), and ARE (Figure 13(c)). The experiment result demonstrated that FMT of Saikosaponin A-treated rats ameliorated the SAP by increasing the expression of antioxidant signaling protein.

3.11. FMT of Saikosaponin A-Treated Rats Improved Gut Microbiota Composition. The abundance of Lactobacillus species was highest in the TCG, and lowest in the TMG group (Figure 14(a)). FMT of Saikosaponin A-treated rats increased the relative abundance of Lactobacillus species (Figure 14(a)). The abundance of Prevotella species was similar between the TCG and TMG groups (Figure 14(a)).

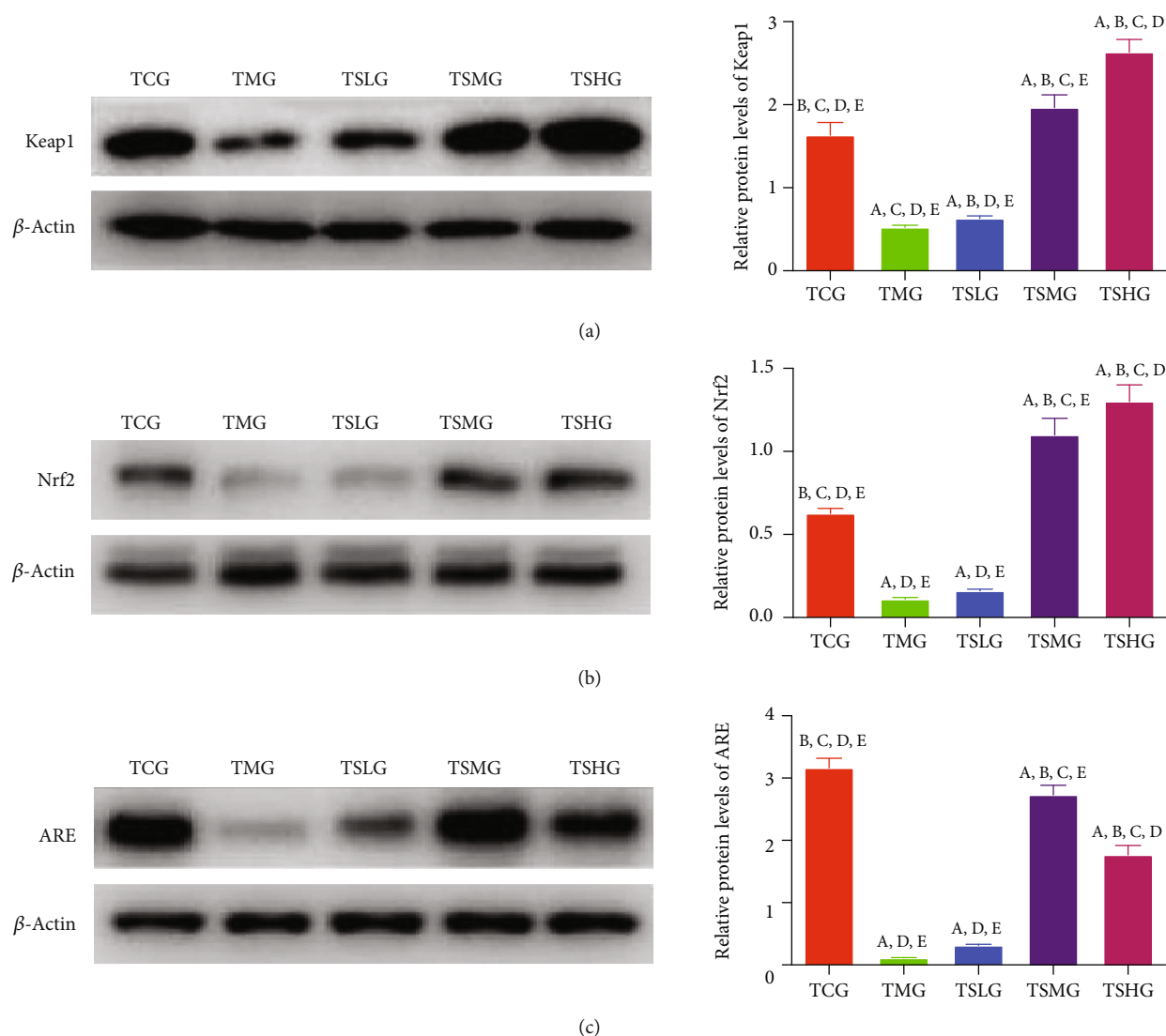


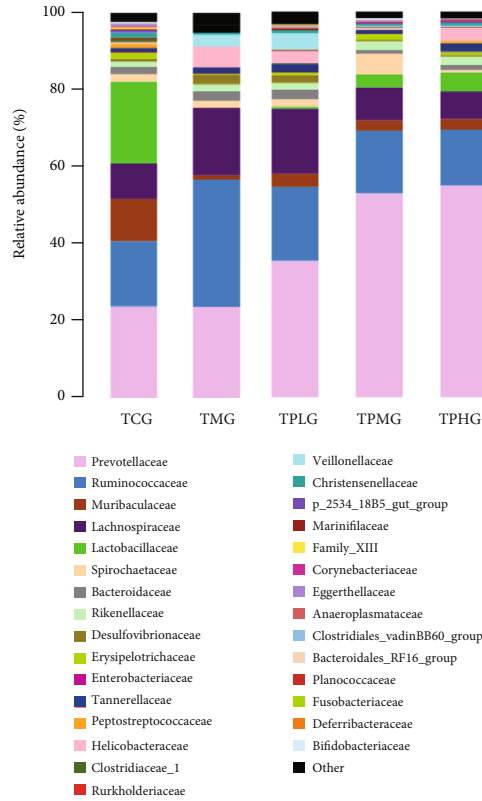
FIGURE 13: Western blot analysis of the effects of FMT of Saikosaponin A on the expression of antioxidant signaling proteins. (a) Kelch-like ECH-associated protein 1 (Keap1). (b) Nuclear factor erythroid 2-related factor 2 (NRF2). (c) Antioxidant response element (ARE). Data were presented as means \pm S.D. (standard deviation) and $n = 8$ for each group. ^a $p < 0.05$ vs. the TCG group, ^b $p < 0.05$ vs. the TMG group, ^c $p < 0.05$ vs. the TSLG group, ^d $p < 0.05$ vs. the TSMG group, and ^e $p < 0.05$ vs. the TSHG group.

FMT of Saikosaponin A-treated rats increased the relative abundance of Prevotella species in a dose-dependent way (Figure 14(a)). Heatmap analysis showed the similar results as the barplots (Figure 14(b)). Therefore, FMT of Saikosaponin A-treated rats improved the gut microbiota by increasing the proportion of Lactobacillus and Prevotella species (Figure 14). The results indicated that FMT of Saikosaponin A-treated rats improved gut microbiota in the SAP model.

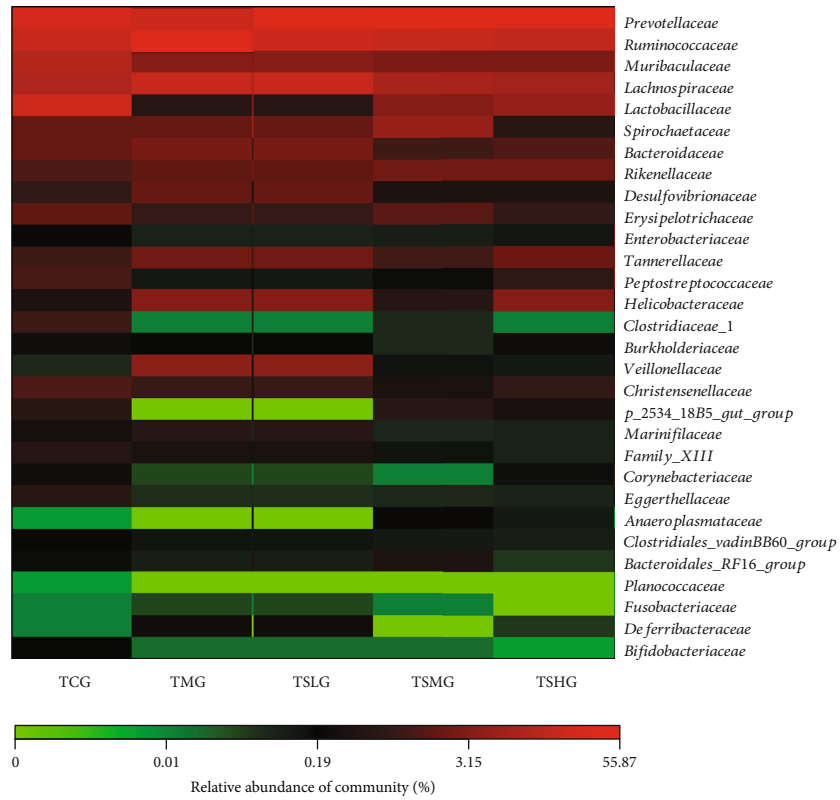
4. Discussion

SAP lesions are linked with sepsis, infected pancreatic necrosis, and multiorgan failure [47]. SAP is a relapsing complication of digestive system and can lead to chronic inflammatory disease [48]. Many drugs are used for the treatment of SAP but most of them have unwanted adverse effects [49]. The present work showed that Saikosaponin A exerted

protective effects against SAP risk by reducing pathological scores (Figure 4) and increasing antioxidant and anti-inflammation (Figure 5) properties. We next examined the effects of Saikosaponin A on the expression of antioxidant signaling molecules. Saikosaponin A administration significantly improved the expression of Keap1, Nrf2, and ARE (Figures 7 and 8). Furthermore, Saikosaponin A intervention also increased anti-inflammatory capacity by reducing the levels of IL-6, IL-1 β , and TNF- α and increased the level of IL-10 (Figure 5). The results were consistent with the previous reports that Saikosaponin A treatment reduced the IL-6, IL-1 β , and TNF- α levels [50] and increased IL-10 level [50, 51]. Saikosaponin A treatment also reduced the levels of main inflammatory factors of SAP, CRP, and PCT (Figure 5), but the related report was not found yet. These results suggest that Saikosaponin A is a potential drug in the prevention of SAP progression.



(a)



(b)

FIGURE 14: The effects of FMT on composition of gut microbiota among different groups. (a) The proportion of gut microbiota. (b) Heatmap analysis of gut microbiota changes from different FMT.

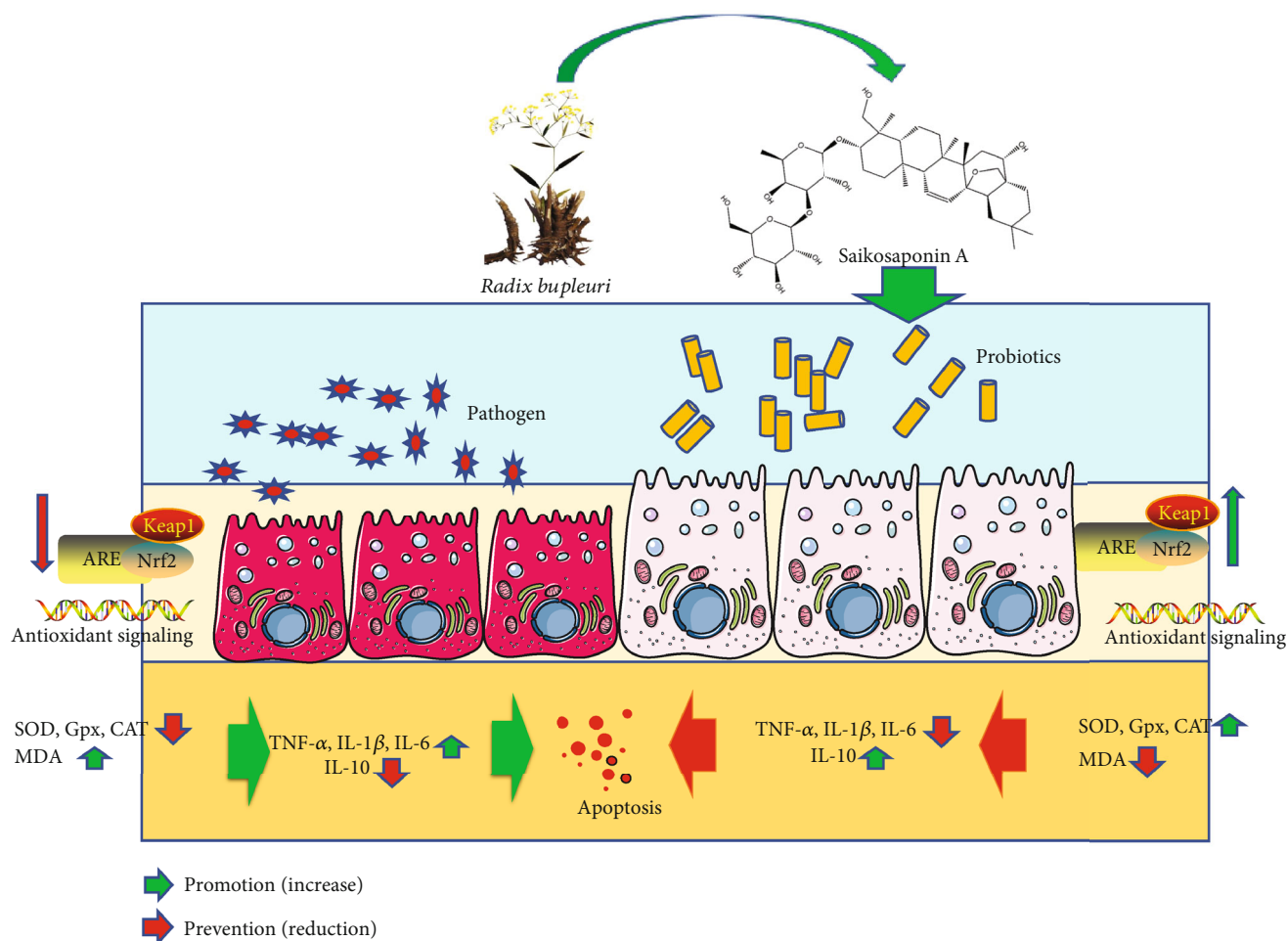


FIGURE 15: Saikosaponin A from *Radix bupleuri* prevented severe acute pancreatitis. Saikosaponin A intervention improved gut microbiota composition, which reduces inflammation responses and improves antioxidant properties via Kelch-like ECH-associated protein 1-nuclear factor erythroid 2-related factor 2-antioxidant response element (Keap1-Nrf2-ARE) signaling.

Saikosaponin A treatment improved antioxidant capacity by increasing the serum levels of SOD, CAT, and GPx and reducing the MDA level. Free radicals and reactive oxygen species (ROS) and reactive nitrogen species (RNS) contribute to many pancreatitis processes by inducing oxidative stress and oxidative damage [29, 52, 53]. The increase in the ROS level induces DNA damage and potential cytotoxicity [54]. SOD shows its antioxidant role by directly scavenging excess intracellular free radicals and reducing MDA level and enhancing total antioxidant capacity (T-AOC) [55]. Decreased antioxidant SOD activity will induce the increase in the levels of oxidative stress biomarkers (MDA) in the SAP model [56]. GPx is a selenium-dependent enzyme that prevents intracellular hydrogen peroxide and lipid peroxides [57]. CAT widely exists in mammalian cells and shows the protection against from ROS, which is produced through the decomposition of H_2O_2 [58]. Serum activity of GPx and SOD is closely associated with the removal of ROS [59]. SOD, CAT, and GPx are indispensable in the defense against oxidative species into bloodstream, especially super oxide anion radical (O_2^-), which is continuously produced in human body metabolism via the mitochondrial energy production pathway [60].

The ROS superoxide anion radical is mainly generated by NADPH oxidase (NOX) in the SAP model and usually converted into H_2O_2 with the participation of SOD, as well as NO generated by inducible nitric oxide synthase. The latter ROS generated from XO plays a crucial role in SAP injury [29]. The previous reports showed that Saikosaponin A reduced the expression of NOX [61]. The extracts with Saikosaponin A inhibited the superoxide anion formation by XO [62].

Nrf2-ARE pathway also attenuates oxidative stress-induced DNA damage in pancreatic beta cells [63]. Keap1-Nrf2-ARE are important antioxidant signaling and exerts protective function against SAP. The expression of Keap1-Nrf2-ARE was significantly downregulated in SAP rats. The change was inhibited via Saikosaponin A administration. Many antioxidant enzyme systems are expressed by activating the Keap1-Nrf2-ARE signaling pathway [64]. These results indicate that Saikosaponin A may exert an important protective effect on pancreas integrity by affecting the expression of Keap1-Nrf2-ARE antioxidant signaling.

On the other hand, the treatment of Saikosaponin A treatment improved gut microbiota composition (Figure 8).

Saikosaponin A may show its function via the improvement of gut microbiota composition, and the results of FMT further confirmed such a proposal. To explore the effects of FMT on pancreatitis, histology analysis was also performed. FMT of Saikosaponin A-treated rats increased colon length and reduced DAI and pathological scores. FMT of Saikosaponin A-treated rats also increased antioxidant and anti-inflammation properties (Figure 11). Meanwhile, the FMT of Saikosaponin A-treated rats increased the expression of antioxidant signaling molecules of Keap1-Nrf2-ARE (Figure 13).

Additionally, Saikosaponin A intervention improved gut microbiota and showed significant increases in the probiotics, including *Lactobacillus* and *Prevotella* species (Figure 8). Similarly, FMT of Saikosaponin A-treated rats also improved gut microbiota. FMT-treated samples showed significant increases in the probiotics, including *Lactobacillus* and *Prevotella* species (Figure 14). *Lactobacillus* species suppressed and repair *E. coli*-impaired SAP by increasing the expression and distribution of antioxidant proteins and can be served as an essential food additive to solve health complications. *Lactobacillus* as a new generation of probiotics plays an important role in maintaining intestinal epithelial homeostasis and exerting health-promoting function [65]. *Prevotella* species may exert their function by fermenting carbohydrate and releasing short-chain fatty acid (SCFA) to protect pancreas integrity [66]. Notably, *Prevotella copri* is potential harmful bacterium which can be inhibited by *Lactobacillus* bacteria [67]. Surprisingly, the abundance of *Lactobacillus* and *Prevotella* species was increased after supplementation with Saikosaponin A or gavage with FMT. These results suggest that Saikosaponin A-induced gut microbiota reduces SAP by reducing inflammatory responses and improving antioxidant signaling through gut microbiota (Figure 15).

There were some limitations in the present study. The redox homeostasis was only analyzed in the blood sample although it is more important to measure the redox homeostasis in pancreatic tissues for better understanding the effects of Saikosaponin A on the SAP risk. The serum concentrations of ROS and RNS were not measured although ROS and RNS levels are closely associated with oxidative stress. Albumin is a very abundant and important circulating antioxidant with ligand binding and strong DPPH (1,1-diphenyl-2-picrylhydrazyl) radical scavenging activity properties [68, 69]. However, serum albumin was not measured in the present experiment. Furthermore, only the activities of selected redox biomarkers were evaluated without considering other critical redox protein, DNA oxidation products, ROS production rate, etc. The effects of FMT on healthy rats were not evaluated. Finally, the rat models could not adequately imitate the clinical scenarios of human SAP. The effects of Saikosaponin A treatment on microbiota-depleted rats were not explored in the present work, and thus, the function of Saikosaponin A may be affected by the preexisting gut microbiota. Saikosaponin A intervention may induce the production of an antimicrobial peptide (AMP), which can change the composition of gut microbiota by reducing the bacterial translocation. The decrease in the AMP levels

will result in the dysbiosis of gut microbiota in the AP model [70]. The FMT may contain such AMP and affect the distribution of gut microbiota. Therefore, the effect of FMT in normal animals should be studied if AMP can be identified and used to treat AP. Further work is needed to address these important issues.

In conclusion, this study indicates that administration of Saikosaponin A intervention attenuates SAP lesions. Saikosaponin A treatment not only increased antioxidant and anti-inflammatory properties but also improved SAP lesions in the rat model. These findings indicate that Saikosaponin A-induced gut microbiota changes may have a potential protective effect on SAP and are useful in the prevention of the inflammatory disease as SAP.

Data Availability

All data are available from the corresponding author (Yanfeng Jiang, Email: jiangyfjl@126.com) upon reasonable request.

Conflicts of Interest

There is no conflict of interest.

Authors' Contributions

J. L., J. H., and S. W. conceived and designed the experiments. J. L., S. W., and L. Q. performed the experiments and analyzed data. L. Q. and Y. J. wrote the paper. Jing Li and Jinfeng Han contributed equally to this work.

Acknowledgments

The project was supported by the creative project of Jilin University. We are very grateful to Professor Jie Liu for his technical support and experimental design.

References

- [1] L. Medina Andrade, A. Delgado, L. Perez Corona, O. Moreno, and D. Rodríguez, "Acute pancreatitis, actualization and evidence based management," *Archives of Clinical Gastroenterology*, vol. 3, no. 1, pp. 1–8, 2017.
- [2] W. Deng, A. Abliz, S. Xu et al., "Severity of pancreatitis-associated intestinal mucosal barrier injury is reduced following treatment with the NADPH oxidase inhibitor apocynin," *Molecular Medicine Reports*, vol. 14, no. 4, pp. 3525–3534, 2016.
- [3] M. Schietroma, B. Pessia, F. Carlei, P. Mariani, F. Sista, and G. Amicucci, "Intestinal permeability and systemic endotoxemia in patients with acute pancreatitis," *Annali Italiani di Chirurgia*, vol. 87, no. 1, pp. 138–144, 2016.
- [4] J. Samanta, S. Singh, S. Arora et al., "Cytokine profile in prediction of acute lung injury in patients with acute pancreatitis," *Pancreatology*, vol. 18, no. 8, pp. 878–884, 2018.
- [5] C. Skouras, Z. A. Davis, J. Sharkey et al., "Lung ultrasonography as a direct measure of evolving respiratory dysfunction and disease severity in patients with acute pancreatitis," *HPB*, vol. 18, no. 2, pp. 159–169, 2016.
- [6] N. R. Thiruvengadam, K. A. Forde, V. Chandrasekhara et al., "Tacrolimus and indomethacin are safe and effective at

- reducing pancreatitis after endoscopic retrograde cholangio-pancreatography in patients who have undergone liver transplantation,” *Clinical Gastroenterology and Hepatology*, vol. 18, pp. 1224–1232.e1, 2020.
- [7] X. Chai, H. B. Huang, G. Feng et al., “Baseline serum cystatin C is a potential predictor for acute kidney injury in patients with acute pancreatitis,” *Disease Markers*, vol. 2018, Article ID 8431219, 7 pages, 2018.
 - [8] T. P. Fitzgibbons, J. Paolino, J. C. Dagorn, and T. E. Meyer, “Usefulness of pancreatitis-associated protein, a novel biomarker, to predict severity of disease in ambulatory patients with heart failure,” *The American Journal of Cardiology*, vol. 113, no. 1, pp. 123–126, 2014.
 - [9] Y. Zhou, L. Wang, X. Huang, H. Li, and Y. Xiong, “Add-on effect of crude rhubarb to somatostatin for acute pancreatitis: a meta-analysis of randomized controlled trials,” *Journal of Ethnopharmacology*, vol. 194, pp. 495–505, 2016.
 - [10] J. Li, S. Zhang, R. Zhou, J. Zhang, and Z. F. Li, “Perspectives of traditional Chinese medicine in pancreas protection for acute pancreatitis,” *World Journal of Gastroenterology*, vol. 23, no. 20, pp. 3615–3623, 2017.
 - [11] H. Wang, H. Zheng, Z. Zhao, and P. Chen, “Effect of Chaihu Shihuang soup on blood serum level TNF, IL-6 and IL-10 of severe acute pancreatitis (SAP),” *Zhongguo Zhong Yao Za Zhi*, vol. 34, no. 12, pp. 1582–1584, 2009.
 - [12] Y. Wang, L. Zhao, X. Han et al., “Saikosaponin A inhibits triple-negative breast cancer growth and metastasis through downregulation of CXCR4,” *Frontiers in Oncology*, vol. 9, article 1487, 2019.
 - [13] J. Guo, F. Zhang, J. Gao et al., “Proteomics-based screening of the target proteins associated with antidepressant-like effect and mechanism of Saikosaponin A,” *Journal of Cellular and Molecular Medicine*, vol. 24, no. 1, pp. 174–188, 2020.
 - [14] P. Feng, Y. Xu, B. Tong et al., “Saikosaponin a attenuates hyperlipidemic pancreatitis in rats via the PPAR- γ /NF- κ B signaling pathway,” *Experimental and Therapeutic Medicine*, vol. 19, no. 2, pp. 1203–1212, 2020.
 - [15] V. Cifarelli, S. Ivanov, Y. Xie et al., “CD36 deficiency impairs the small intestinal barrier and induces subclinical inflammation in mice,” *Cellular and Molecular Gastroenterology and Hepatology*, vol. 3, no. 1, pp. 82–98, 2017.
 - [16] X. Y. Li, C. He, Y. Zhu, and N. H. Lu, “Role of gut microbiota on intestinal barrier function in acute pancreatitis,” *World Journal of Gastroenterology*, vol. 26, no. 18, pp. 2187–2193, 2020.
 - [17] X. Li, C. He, N. Li et al., “The interplay between the gut microbiota and NLRP3 activation affects the severity of acute pancreatitis in mice,” *Gut Microbes*, vol. 11, no. 6, pp. 1774–1789, 2020.
 - [18] G. Zhang, R. Cui, Y. Kang et al., “Testosterone propionate activated the Nrf2-ARE pathway in ageing rats and ameliorated the age-related changes in liver,” *Scientific Reports*, vol. 9, no. 1, article 18619, 2019.
 - [19] M. C. Lu, J. A. Ji, Z. Y. Jiang, and Q. D. You, “The Keap1-Nrf2-ARE pathway as a potential preventive and therapeutic target: an update,” *Medicinal Research Reviews*, vol. 36, no. 5, pp. 924–963, 2016.
 - [20] H. H. Hagar, S. A. Almubrik, N. M. Attia, and S. N. Aljasser, “Mesna alleviates cerulein-induced acute pancreatitis by inhibiting the inflammatory response and oxidative stress in experimental rats,” *Digestive Diseases and Sciences*, 2020.
 - [21] R. Ma, F. Yuan, S. Wang, Y. Liu, T. Fan, and F. Wang, “Calycosin alleviates cerulein-induced acute pancreatitis by inhibiting the inflammatory response and oxidative stress via the p38 MAPK and NF- κ B signal pathways in mice,” *Biomedicine & Pharmacotherapy*, vol. 105, pp. 599–605, 2018.
 - [22] G. Marek, M. Ściskalska, Z. Grzebieniak, and H. Milnerowicz, “Decreases in paraoxonase-1 activities promote a pro-inflammatory effect of lipids peroxidation products in non-smoking and smoking patients with acute pancreatitis,” *International Journal of Medical Sciences*, vol. 15, no. 14, pp. 1619–1630, 2018.
 - [23] S. Cao, Y. Bian, X. Zhou et al., “A small-molecule activator of mitochondrial aldehyde dehydrogenase 2 reduces the severity of cerulein-induced acute pancreatitis,” *Biochemical and Biophysical Research Communications*, vol. 522, no. 2, pp. 518–524, 2020.
 - [24] M. Sajadian, M. Hashemi, S. Salimi, and A. Nakhaee, “The effect of experimental thyroid dysfunction on markers of oxidative stress in rat pancreas,” *Drug Development Research*, vol. 77, no. 4, pp. 199–205, 2016.
 - [25] N. E. El-Ashmawy, N. F. Khedr, H. A. El-Bahrawy, and O. B. Hamada, “Suppression of inducible nitric oxide synthase and tumor necrosis factor-alpha level by lycopene is comparable to methylprednisolone in acute pancreatitis,” *Digestive and Liver Disease*, vol. 50, no. 6, pp. 601–607, 2018.
 - [26] E. M. El Morsy and M. A. E. Ahmed, “Carvedilol attenuates l-arginine induced acute pancreatitis in rats through modulation of oxidative stress and inflammatory mediators,” *Chemico-Biological Interactions*, vol. 327, article 109181, 2020.
 - [27] X. Piao, B. Liu, X. Sui et al., “Picoside II improves severe acute pancreatitis-induced intestinal barrier injury by inactivating oxidative and inflammatory TLR4-dependent PI3K/AKT/NF- κ B signaling and improving gut microbiota,” *Oxidative Medicine and Cellular Longevity*, vol. 2020, Article ID 3589497, 12 pages, 2020.
 - [28] G. G. Kojayan, R. F. Alizadeh, S. Li, and H. Ichii, “Reducing pancreatic fibrosis using antioxidant therapy targeting Nrf2 antioxidant pathway: a possible treatment for chronic pancreatitis,” *Pancreas*, vol. 48, no. 10, pp. 1259–1262, 2019.
 - [29] M. Maciejczyk, A. Skutnik-Radziszewska, I. Zieniewska et al., “Antioxidant defense, oxidative modification, and salivary gland function in an early phase of cerulein pancreatitis,” *Oxidative Medicine and Cellular Longevity*, vol. 2019, Article ID 8403578, 14 pages, 2019.
 - [30] Z. Y. Xiao, X. R. Li, W. Y. Shao, and S. H. Wu, “Purification and concentration of the Total saikosaponins extracted from radix bupleurium using foam fractionation,” *Separation Science and Technology*, vol. 49, no. 3, pp. 469–475, 2014.
 - [31] H. Aho, T. Nevalainen, R. Lindberg, and A. Aho, “Experimental pancreatitis in the rat: the role of phospholipase A in sodium taurocholate-induced acute haemorrhagic pancreatitis,” *Scandinavian Journal of Gastroenterology*, vol. 15, no. 8, pp. 1027–1031, 2010.
 - [32] R. Mukherjee, O. A. Mareninova, I. V. Odinkova et al., “Mechanism of mitochondrial permeability transition pore induction and damage in the pancreas: inhibition prevents acute pancreatitis by protecting production of ATP,” *Gut*, vol. 65, no. 8, pp. 1333–1346, 2016.
 - [33] D. Liu, G. Song, Z. Ma et al., “Resveratrol improves the therapeutic efficacy of bone marrow-derived mesenchymal stem cells in rats with severe acute pancreatitis,” *International Immunopharmacology*, vol. 80, article 106128, 2020.

- [34] X. Zhou, H. Cheng, D. Xu et al., "Attenuation of neuropathic pain by saikosaponin a in a rat model of chronic constriction injury," *Neurochemical Research*, vol. 39, no. 11, pp. 2136–2142, 2014.
- [35] H. B. Meng, J. Gong, B. Zhou, J. Hua, L. Yao, and Z. S. Song, "Therapeutic effect of human umbilical cord-derived mesenchymal stem cells in rat severe acute pancreatitis," *International Journal of Clinical and Experimental Pathology*, vol. 6, no. 12, pp. 2703–2712, 2013.
- [36] J. Ali, A. U. Khan, F. A. Shah et al., "Mucoprotective effects of Saikosaponin-A in 5-fluorouracil-induced intestinal mucositis in mice model," *Life Sciences*, vol. 239, article 116888, 2019.
- [37] W.-W. Wang, Y. Zhang, X.-B. Huang, N. You, L. Zheng, and J. Li, "Fecal microbiota transplantation prevents hepatic encephalopathy in rats with carbon tetrachloride-induced acute hepatic dysfunction," *World Journal of Gastroenterology*, vol. 23, no. 38, pp. 6983–6994, 2017.
- [38] P. Shen, Z. Zhang, K. Zhu et al., "Evodiamine prevents dextran sulfate sodium-induced murine experimental colitis via the regulation of NF- κ B and NLRP3 inflammasome," *Biomedicine & Pharmacotherapy*, vol. 110, pp. 786–795, 2019.
- [39] X. Fu, P. Li, W. Yin et al., "Overexpression of Nrf2 protects against lipopolysaccharide and cerulein-induced pancreatitis in vitro and in vivo," *Pancreas*, vol. 49, no. 3, pp. 420–428, 2020.
- [40] X. Song, J. Li, Y. Wang et al., "Clematichinenoside AR ameliorated spontaneous colitis in Il-10^{-/-} mice associated with improving the intestinal barrier function and abnormal immune responses," *Life Sciences*, vol. 239, article 117021, 2019.
- [41] F. A. N. K. and L. D., "DSC examination of intestinal tissue following cold preservation," *Thermochimica Acta*, vol. 497, pp. 41–45, 2010.
- [42] F. Zhao, Z. Huang, G. Zhou, H. Li, X. Xu, and C. Li, "Dietary proteins rapidly altered the microbial composition in rat caecum," *Current Microbiology*, vol. 74, no. 12, pp. 1447–1452, 2017.
- [43] T. Strate, O. Mann, H. Kleinhans et al., "Systemic intravenous infusion of bovine hemoglobin significantly reduces microcirculatory dysfunction in experimentally induced pancreatitis in the rat," *Annals of Surgery*, vol. 238, no. 5, pp. 765–771, 2003.
- [44] R. K. McNamara, R. Jandacek, T. Rider, P. Tso, A. Cole-Strauss, and J. W. Lipton, "Atypical antipsychotic medications increase postprandial triglyceride and glucose levels in male rats: relationship with stearoyl-CoA desaturase activity," *Schizophrenia Research*, vol. 129, no. 1, pp. 66–73, 2011.
- [45] C. D'Ambrosio, T. Bowman, and V. Mohsenin, "Quality of life in patients with obstructive sleep apnea: effect of nasal continuous positive airway pressure—a prospective study," *Chest*, vol. 115, no. 1, pp. 123–129, 1999.
- [46] Y. Gao, J. Li, S. Chu et al., "Ginsenoside Rg1 protects mice against streptozotocin-induced type 1 diabetic by modulating the NLRP3 and Keap1/Nrf2/HO-1 pathways," *European Journal of Pharmacology*, vol. 866, article 172801, 2020.
- [47] I. K. Uchendu, C. E. Agu, O. C. Orji, M. C. Offor, and T. F. Nwosu, "Review on diagnosis of acute pancreatitis," *Journal of Medical & Allied Sciences*, vol. 7, no. 2, p. 76, 2017.
- [48] A. Garcia Garcia de Paredes, E. Rodriguez de Santiago, C. Rodriguez-Escaja et al., "Idiopathic acute pancreatitis in patients with inflammatory bowel disease: a multicenter cohort study," *Pancreatology*, vol. 20, no. 3, pp. 331–337, 2020.
- [49] H. Vargas-Robles, K. F. Castro-Ochoa, A. F. Citalán-Madrid, and M. Schnoor, "Beneficial effects of nutritional supplements on intestinal epithelial barrier functions in experimental colitis models in vivo," *World Journal of Gastroenterology*, vol. 25, no. 30, pp. 4181–4198, 2019.
- [50] J. Zhu, C. Luo, P. Wang, Q. He, J. Zhou, and H. Peng, "Saikosaponin A mediates the inflammatory response by inhibiting the MAPK and NF- κ B pathways in LPS-stimulated RAW 264.7 cells," *Experimental and Therapeutic Medicine*, vol. 5, no. 5, pp. 1345–1350, 2013.
- [51] M. Q. Huang, X. Y. Cao, X. Y. Chen et al., "Saikosaponin a increases interleukin-10 expression and inhibits scar formation after sciatic nerve injury," *Neural Regeneration Research*, vol. 13, no. 9, pp. 1650–1656, 2018.
- [52] L. Wen, T. A. Javed, A. K. Dobbs et al., "The protective effects of calcineurin on pancreatitis in mice depend on the cellular source," *Gastroenterology*, vol. 159, no. 3, pp. 1036–1050.e8, 2020.
- [53] J. E. Fishman, G. Levy, V. Alli, X. Zheng, D. J. Mole, and E. A. Deitch, "The intestinal mucus layer is a critical component of the gut barrier that is damaged during acute pancreatitis," *Shock*, vol. 42, no. 3, pp. 264–270, 2014.
- [54] M. Cal, I. Matyjaszczyk, I. Litwin et al., "The anticancer drug 3-Bromopyruvate induces DNA damage potentially through reactive oxygen species in yeast and in human cancer cells," *Cell*, vol. 9, no. 5, p. 1161, 2020.
- [55] J. Pan, L. Li, L. Liang et al., "Cytoprotective effects of cell-permeable bifunctional antioxidant enzyme, GST-TAT-SOD, against cisplatin-induced cell damage," *Oxidative Medicine and Cellular Longevity*, vol. 2017, Article ID 9530791, 7 pages, 2017.
- [56] A. M. Abdel-Aziz, R. A. Rifaai, and S. A. Abdel-Gaber, "Possible mechanisms mediating the protective effect of cilostazol in L-arginine induced acute pancreatitis in rats: role of cGMP, cAMP, and HO-1," *Naunyn-Schmiedeberg's Archives of Pharmacology*, vol. 393, no. 10, pp. 1859–1870, 2020.
- [57] J.-Q. Huang, J.-C. Zhou, Y.-Y. Wu, F.-Z. Ren, and X. G. Lei, "Role of glutathione peroxidase 1 in glucose and lipid metabolism-related diseases," *Free Radical Biology & Medicine*, vol. 127, pp. 108–115, 2018.
- [58] A. Reale, R. G. Ianniello, F. Ciocia et al., "Effect of respiratory and catalase-positive *Lactobacillus casei* adjuncts on the production and quality of Cheddar-type cheese," *International Dairy Journal*, vol. 63, pp. 78–87, 2016.
- [59] J. Dworzański, M. Strycharz-Dudziak, E. Kliszczewska et al., "Glutathione peroxidase (GPx) and superoxide dismutase (SOD) activity in patients with diabetes mellitus type 2 infected with Epstein-Barr virus," *PLoS One*, vol. 15, no. 3, article e0230374, 2020.
- [60] O. Ighodaro and O. Akinloye, "First line defence antioxidants-superoxide dismutase (SOD), catalase (CAT) and glutathione peroxidase (GPX): their fundamental role in the entire antioxidant defence grid," *Alexandria Journal of Medicine*, vol. 54, no. 4, pp. 287–293, 2018.
- [61] J. Li, S. Biswas, Y. Niu et al., "P23 Saikosaponin a ameliorate learning and memory impairment via anti-inflammation effect in an AD mouse model," *Biochemical Pharmacology*, vol. 139, p. 132, 2017.
- [62] C.-T. Liu, C.-Y. Wu, Y.-M. Weng, and C.-Y. Tseng, "Ultrasound-assisted extraction methodology as a tool to improve the antioxidant properties of herbal drug Xiao-Chia-Hu-Tang," *Journal of Ethnopharmacology*, vol. 99, no. 2, pp. 293–300, 2005.

- [63] P. Vanitha, S. Senthilkumar, S. Dornadula, S. Anandhakumar, P. Rajaguru, and K. M. Ramkumar, "Morin activates the Nrf2-ARE pathway and reduces oxidative stress-induced DNA damage in pancreatic beta cells," *European Journal of Pharmacology*, vol. 801, pp. 9–18, 2017.
- [64] M.-C. Lu, J. Zhao, Y.-T. Liu et al., "CPUY192018, a potent inhibitor of the Keap1-Nrf2 protein-protein interaction, alleviates renal inflammation in mice by restricting oxidative stress and NF- κ B activation," *Redox Biology*, vol. 26, article 101266, 2019.
- [65] Q. Liu, Z. Yu, F. Tian et al., "Surface components and metabolites of probiotics for regulation of intestinal epithelial barrier," *Microbial Cell Factories*, vol. 19, no. 1, article 23, 2020.
- [66] C. le Bourgot, S. Ferret-Bernard, E. Apper et al., "Perinatal short-chain fructooligosaccharides program intestinal microbiota and improve enteroinular axis function and inflammatory status in high-fat diet-fed adult pigs," *The FASEB Journal*, vol. 33, no. 1, pp. 301–313, 2018.
- [67] W. Ou, H. Hu, P. Yang et al., "Dietary daidzein improved intestinal health of juvenile turbot in terms of intestinal mucosal barrier function and intestinal microbiota," *Fish & Shellfish Immunology*, vol. 94, pp. 132–141, 2019.
- [68] S. Minic, D. Stanic-Vucinic, M. Radomirovic et al., "Characterization and effects of binding of food-derived bioactive phycocyanobilin to bovine serum albumin," *Food Chemistry*, vol. 239, pp. 1090–1099, 2018.
- [69] S. Wu, X. Wang, Y. Bao et al., "Molecular insight on the binding of monascin to bovine serum albumin (BSA) and its effect on antioxidant characteristics of monascin," *Food Chemistry*, vol. 315, article 126228, 2020.
- [70] J. Chen, C. Huang, J. Wang et al., "Dysbiosis of intestinal microbiota and decrease in paneth cell antimicrobial peptide level during acute necrotizing pancreatitis in rats," *PLoS One*, vol. 12, no. 4, article e0176583, 2017.

Research Article

ROS-Mediated Necroptosis Is Involved in Iron Overload-Induced Osteoblastic Cell Death

Qing Tian,¹ Bo Qin,² Yufan Gu,¹ Lijun Zhou,³ Songfeng Chen,¹ Song Zhang,¹ Shuhao Zhang,¹ Qicai Han ,¹ Yong Liu,³ and Xuejian Wu¹

¹Department of Orthopaedics, The First Affiliated Hospital of Zhengzhou University, Zhengzhou 450052, China

²Department of Translational Medical Center, First Affiliated Hospital of Zhengzhou University, Zhengzhou 450052, China

³Department of Orthopaedics, Union Hospital, Tongji Medical College, Huazhong University of Science and Technology, Wuhan 430022, China

Correspondence should be addressed to Qicai Han; fcchanqc@zzu.edu.cn

Received 24 June 2020; Revised 15 September 2020; Accepted 28 September 2020; Published 17 October 2020

Academic Editor: Claudia Penna

Copyright © 2020 Qing Tian et al. This is an open access article distributed under the Creative Commons Attribution License, which permits unrestricted use, distribution, and reproduction in any medium, provided the original work is properly cited.

Excess iron has been reported to lead to osteoblastic cell damage, which is a crucial pathogenesis of iron overload-related osteoporosis. However, the cytotoxic mechanisms have not been fully documented. In the present study, we focused on whether necroptosis contributes to iron overload-induced osteoblastic cell death and related underlying mechanisms. Here, we showed that the cytotoxicity of iron overload in osteoblastic cells was mainly due to necrosis, as evidenced by the Hoechst 33258/PI staining, Annexin-V/PI staining, and transmission electronic microscopy. Furthermore, we revealed that iron overload-induced osteoblastic necrosis might be mediated via the RIPK1/RIPK3/MLKL necroptotic pathway. In addition, we also found that iron overload was able to trigger mitochondrial permeability transition pore (mPTP) opening, which is a critical downstream event in the execution of necroptosis. The key finding of our experiment was that iron overload-induced necroptotic cell death might depend on reactive oxygen species (ROS) generation, as N-acetylcysteine effectively rescued mPTP opening and necroptotic cell death. ROS induced by iron overload promote necroptosis via a positive feedback mechanism, as on the one hand N-acetylcysteine attenuates the upregulation of RIPK1 and RIPK3 and phosphorylation of RIPK1, RIPK3, and MLKL and on the other hand Nec-1, siRIPK1, or siRIPK3 reduced ROS generation. In summary, iron overload induced necroptosis of osteoblastic cells in vitro, which is mediated, at least in part, through the RIPK1/RIPK3/MLKL pathway. We also highlight the critical role of ROS in the regulation of iron overload-induced necroptosis in osteoblastic cells.

1. Introduction

Iron, an essential micronutrient, plays a crucial role in a wide scale of biological processes like DNA synthesis, energy metabolism, and oxygen transport; however, excess iron is toxic to cells as leading to organ dysfunction and diseases [1, 2]. As reported, excess iron stored in the bone tissue is linked with higher rates of bone loss at proximal femur sites even in healthy people [3]. Moreover, patients with iron overload associated diseases like hemochromatosis, thalassemia, and sickle cell disease are much more prone to suffer from osteoporosis [4, 5]. Nevertheless, the fundamental mechanisms by which iron overload causes osteoporosis remain poorly understood.

Recently, substantial evidence has accumulated to demonstrate that oxidative stress caused by iron overload is the major contributor to the pathogenesis of osteoporosis [6–8]. In our previous study, we have demonstrated that reactive oxygen species was essential for iron overload-induced apoptosis in the osteoblastic cells [9]. More importantly, an in vivo study of iron overload documented that elimination of ROS by antioxidants largely prevented the bone abnormalities and inhibited detrimental inflammatory cytokine production [10, 11]. However, it has been documented that apoptosis is generally considered to be nonimmunogenic [11, 12]. Meanwhile, we also noticed that osteoblastic cell death was only partially mediated by apoptosis under iron overload conditions [9]. Based on previous

related studies and this phenomenon, we hypothesized that other types of cell death might account for the underlying mechanisms.

Necroptosis is another type of programmed cell death characterized by cellular organelle swelling and membrane rupture, induced by multiple death receptors, oxidative stress, or mitochondrial dysfunction, which is mainly mediated by the RIPK1/RIPK3/MLKL pathway [13–15]. Recent studies have suggested that necroptosis plays an important role in the regulation of tissue homeostasis and disorders [16–18]. It has also been established that activation by stimuli leads to RIPK1 autophosphorylation, recruitment of RIPK3 to RIPK1 to form the necrosome complex, then oligomerization of MLKL, and finally translocation to the plasma membrane to execute necroptotic cell death [19]. However, it is unknown whether necroptosis was implicated in iron overload-induced osteoblastic cell death.

In our current study, for the first time, we systematically confirm that the necroptosis pathway is involved in iron overload-induced death of osteoblastic cells. The key finding of this study is that ROS is essential for iron overload-induced necroptosis. We then further discover that ROS contribute to necroptosis of osteoblastic cells through a positive feedback loop involving RIPK1/RIPK3. These findings suggest targeted antioxidants as an alternative therapy for the prevention and treatment of iron overload relevant osteoblastic cell injury.

2. Materials and Methods

2.1. Cell Culture. MC3T3-E1 (subclone 4; ATCC® CRL-2593™), an osteoblast cell line, was obtained from American Type Culture Collection [20, 21]. Cells were maintained in modified α -Minimum Essential Medium Eagle (α -MEM) (HyClone, Logan, USA) which contains 10% fetal bovine serum (FBS) (Gibco, Invitrogen, NY, USA) and 1% antibiotics (penicillin and streptomycin) in a humidified atmosphere at 37°C. The culture medium was replaced every 2 or 3 days.

2.2. Treatment Groups. Ferric ammonium citrate (FAC) (Sigma, St. Louis, MO, USA), a source of iron, was utilized to mimic iron overload conditions in vivo and in vitro [7, 9, 22]. To evaluate the cytotoxic effect of iron overload, the MC3T3-E1 osteoblastic cells were exposed to FAC (50, 100, and 200 μ M) for 24, 72, and 120 h, respectively. The control groups were treated with 0.9% saline solution. According to our previous experiments, the cell viability of osteoblastic cells significantly decreased from 24 to 120 h [9]. More importantly, with iron overload exposure time prolonged, the osteoblastic cell necrosis peaked at 120 h. Thus, 120 h FAC-treated time periods were chosen throughout the following study. N-acetyl-cysteine (NAC) (Beyotime Biological Technology, Shanghai, China) was dissolved in phosphate-buffered saline (PBS). The RIPK1 inhibitor Necrostatin-1 (Nec-1) (Selleck, Houston, TX), MLKL inhibitor Necrosulfonamide (NSA) (Selleck, Houston, TX), and RIPK3 inhibitor GSK872 (Selleck, Houston, TX) were dissolved in DMSO solution. Before exposure to FAC, the MC3T3-E1 osteoblastic cells were incubated

with or without NAC (1 mM), Nec-1 (20 μ M), GSK872 (4 μ M), or NSA (4 μ M) [9, 23–25]. Then, after FAC (200 μ M) treatment for 120 h, all samples were collected and analyzed by a microplate reader, flow cytometry, western blots, and confocal microscopy.

2.3. Cell Counting Kit-8 Assay. The cytotoxicity of iron on osteoblastic cells was determined by the cell counting kit-8 assay kit (Dojindo Biotechnology, Japan) as described in instruments [9]. The osteoblastic cells were collected and seeded in a 96-well plate. After culture for 24 h, the osteoblastic cells were treated with FAC as described above. Then, the culture medium was removed and replaced with 100 μ l mixture solution containing 10 μ l of CCK-8 reactant. After reaction for 2 h at room temperature in the dark, the absorbance value at 450 nm was detected in a microplate reader (Thermo, Waltham, MA, USA).

2.4. Evaluation of Cell Death by Annexin-V-FITC/Propidium Iodide Staining. After exposure as mentioned above, the osteoblastic cells were stained using Annexin-V-FITC/propidium iodide (PI) kit (KeyGen Biotech, Nanjing, China) [9]. Then, the osteoblastic cells underwent trypsinization and centrifugation. Subsequently, cells were gently washed twice by PBS and resuspended in 500 μ l binding buffer containing 5 μ l Annexin-V and 5 μ l PI. After incubating for 15 min in the dark, the samples were detected using flow cytometry (Becton Dickinson, NJ, USA).

2.5. Hoechst 33258/Propidium Iodide Staining. Cell death was evaluated by the confocal laser scanning microscope (OLYMPUS FV1000, Japan) using Hoechst 33258/PI staining kit (Sigma, St. Louis, MO, USA) [26]. The osteoblastic cells were seeded and treated in 24-well culture plates as described above. Then, the culture medium was discarded, and the plates were washed twice with PBS. Hoechst 33258 (10 mg/ml) and PI (5 mg/ml) were used to stain osteoblastic cells. After incubating for 10 min in the dark, the osteoblastic cells were washed with phosphate-buffered saline and observed under the confocal laser scanning microscope.

2.6. Transmission Electron Microscopy (TEM). The cellular ultrastructure of osteoblasts after treatment with FAC was observed by TEM as previously described [23]. Briefly, the osteoblastic cells were collected, centrifuged, and rinsed twice with PBS. Next, all samples were fixed in 2.5% glutaraldehyde for 2 h and subsequently postfixated with 1% osmium tetroxide for 2 h at 37°C. Then, after being dehydrated with ethanol and embedded in Epon-812, the ultrathin sections were stained with lead citrate and uranyl acetate and were used to evaluate ultrastructure changes with TEM (Tecnai 200 kV, FEI Company, Holland).

2.7. Western Blot Analysis. When the cells reached an 80–90% confluence, they were then seeded at 6×10^4 cells/cm² density onto appropriate culture plates for western blot. After treatment as described above, the osteoblastic cells were harvested and lysed in the RIPA lysis buffer (Boster Biological Technology, Wuhan, China). After centrifugation at 12,000 * g for 10 min at 4°C, the protein concentrations were determined

by an Enhanced BCA Protein Assay Kit (Beyotime Biological Technology, Shanghai, China). Then, the total lysates of each sample were separated by 12% SDS-PAGE and then transferred to the nitrocellulose membranes, which was blocked in blocking solution for 2 h at room temperature and incubated with primary antibodies overnight at 4°C [27]. All the primary antibodies used in this experiment were the following: anti-RIPK1 (1:500, CST, USA), anti-Phospho-RIPK1 (1:1000, CST, USA), anti-RIPK3 (1:1000, Abcam, USA), anti-Phospho-RIPK3 (1:1000, Abcam, USA), anti-MLKL (1:1000, CST, USA), anti-Phospho-MLKL (1:1000, CST, USA), anti-VDAC1 (1:1000, CST, USA), anti-PGAM5 (1:1000, Abcam, USA), anti-Drp-1 (1:1000, Abcam, USA), anti-Phospho-Drp-1 (ser637) (1:1000, Abcam, USA), and anti- β -Actin (1:1000, Abcam, USA). Following three washes by TBST solution, membranes were incubated with horseradish peroxidase-conjugated secondary antibodies for 2 h at room temperature. Finally, the protein levels were determined by the enhanced chemiluminescence kit (Boster Biological Technology, Wuhan, China) as described in the manufacturer's instructions.

2.8. Estimation of Mitochondrial Membrane Potential (MMP). MMP was quantified by flow cytometry after stained in 5,5',6,6'-tetrachloro-1,1',3,3'-tetraethyl-benzimidazolyl-carbocyanine iodide (JC-1) (Beyotime Biological Technology, Shanghai, China). When the mitochondrial membrane potential is high, JC-1 aggregates in the matrix which can produce red fluorescence. When MMP is low, JC-1 disperses which can exhibit green fluorescence. In this study, the osteoblastic cells were subjected as described above and stained according to the manufacturer's instructions [28]. The levels of MMP in osteoblastic cells were analyzed by flow cytometry and determined by the ratio of red to green fluorescence intensity. Additionally, a laser scanning confocal microscopy (OLYMPUS FV1000, Japan) was utilized to visualize the changes of MMP in situ.

2.9. Evaluation of Mitochondrial Permeability Transition Pore (mPTP). The mPTP of the osteoblastic cells was analyzed by mPTP Assay Kit (Beyotime Biological Technology, Shanghai, China) as previously described [24]. Finally, the relative fluorescence intensity (RFI) in different groups was determined by flow cytometry.

2.10. Detection of Reactive Oxygen Species. 2',7'-Dichlorofluorescein diacetate (H2DCF-DA) (Sigma, St. Louis, MO, USA) is a special and commonly used fluorescent probe to detect the intracellular ROS level. Briefly, after being treated as described above, the culture medium was discarded and the osteoblastic cells were harvested and washed thrice by PBS. Then, cells were resuspended and incubated with 20 μ M H2DCF-DA at 37°C for 20 min in the dark [25]. Subsequently, serum-free medium was used to rinse the cells in order to remove the residual dyes. Finally, the mean fluorescence intensity (MFI) in different groups was determined by flow cytometry. In addition, in order to estimate the production of intracellular ROS levels in situ, a fluorescence microscope (Carl Zeiss, German) was utilized to visualize each sample.

2.11. siRNA Knockdown. siRIPK1 and siRIPK3 were synthesized by Ribo Biological Technology (Ribo, Guangzhou, China) according to the current guidelines [23, 24, 29, 30]. The sequences of each are shown in Table 1.

Nonspecific siRNA was treated as a negative control group (siControl).

The osteoblastic cells were transfected with effective sequence at a concentration of 100 pmol/10⁵ cell using Lipofectamine™ RNAi MAX reagent (Invitrogen, Life Technologies) according to the manufacturer's protocol [23, 24]. After 24 h transfection with siRNAs, the osteoblastic cells were used for subsequent experiments. The knockdown efficiency of the siRNAs was assessed by western blotting.

2.12. Statistical Analysis. All data were derived from at least three separate experiments and were given as the mean \pm standard deviation (SD). Statistical analyses were performed with SPSS software package 18.0 by the method one-way analysis of variance (ANOVA) to compare different samples. Student's *t*-tests were also performed to analyze the differences between the two groups. A probability of $p < 0.05$ was considered statistically significant.

3. Results

3.1. Iron Overload Impair the Viability of Osteoblastic Cells. To explore the cytotoxic effects of iron overload on the osteoblastic cells, CCK-8 assays were used to quantitate cell viability. The results showed the dose-dependent cytotoxicity as evidenced by the decrease of absorbance in the osteoblastic cells with increasing FAC treatment for 72 h and 120 h (Figure 1). However, there is no statistical difference between control groups and treatment groups for 24 h, suggesting iron exerts cytotoxic effects through a long-term accumulation in the osteoblastic cells. Thus, the osteoblastic cells were subjected to FAC (50-200 μ M) for 120 h in the following experiments.

3.2. Characterization of Osteoblastic Cell Death Induced by Iron Overload. In order to analyze the type of osteoblastic cell death induced by iron overload, Annexin-V/PI staining and Hoechst 33258/PI staining were used to detect cell death. In our study, after incubating with FAC (50-200 μ M) for 120 h, the increase of osteoblastic cell death was mainly caused by the PI-positive cells (Figures 2(a)). Meanwhile, as shown in Figures 2(b), there is a definitive increase in the ratio of PI-positive cells with elevated dose of FAC ($p < 0.05$). Consistently, the Hoechst 33258/PI staining demonstrated that the ratio of necrosis (PI-positive cells) was elevated greatly in osteoblastic cells after treatment with FAC (50-200 μ M) (Figures 2(c)). To further identify that cellular necrosis was induced by iron overload in the osteoblastic cells, TEM was applied to observe morphological changes. With the detection by TEM, after treatment with 200 μ M FAC for 120 h, the osteoblastic cells presented typical necrotic morphological features including severe vacuolation, organelle swelling, and subsequent cellular lysis (Figure 3). Taken together, our results of experiments demonstrated that iron overload-induced osteoblastic cell death might be mainly due to cellular necrosis.

TABLE 1

Genes	The special sequences of siRNA
RIPK1	5'-AUGAUCUCCACGAUUAUCCdTdT-3'
RIPK3	5'-GCAGUUGUAUAUGUUAAGGAGCGGUCGdTdT-3'

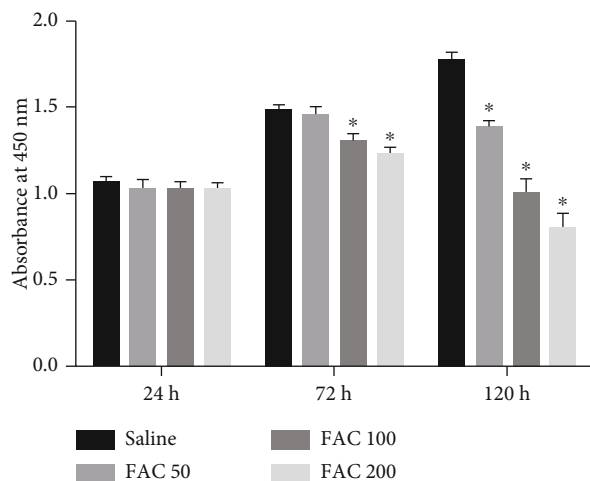


FIGURE 1: The influence of iron overload on the osteoblastic cell viability. After subjecting to FAC (50-200 μ M) for 24, 72, and 120 h, the viability of osteoblasts was detected by CCK-8 assays. The histogram showed the statistical significance only in the 72 h and 120 h groups. Values are expressed as the means \pm SD from three independent experiments (* $p < 0.05$ vs. saline control, ANOVA test).

3.3. Implication of the Necroptotic Pathway in Iron-Induced Osteoblastic Necrosis. Necroptosis, one form of programmed cellular necrosis, recently has been demonstrated to play an essential role in several pathologies [11]. To explore whether iron-induced osteoblastic cell death is associated with necroptosis, we detected the expression of RIPK1, RIPK3, and MLKL, three crucial regulating molecules of the necroptosis pathway. As shown in Figures 4(a) and 4(b), after exposure to FAC (50-200 μ M) for 120 h, the expression levels of RIPK1 and RIPK3 were upregulated in a dose-dependent manner. However, FAC had no significant modulatory effect on the expression of MLKL. Interestingly, the phosphorylation of RIPK1, RIPK3, and MLKL in the osteoblastic cells was increased in response to FAC treatment. To further confirm whether the RIPK1-RIPK3-MLKL pathway was involved in the necroptosis induced by iron overload, the osteoblastic cells were pretreated with and without the Nec-1 (20 μ M) (Supplementary Figure 1), GSK872 (4 μ M) (Supplementary Figure 2), and NSA (4 μ M) (Supplementary Figure 3), respectively. As shown in Figures 4(c) and 4(d), the ratio of PI-positive cells was effectively decreased by Nec-1, GSK872, or NSA. Meanwhile, the data of CCK-8 assays demonstrated that the osteoblastic cell viability was effectively improved by GSK872, Nec-1, or NSA (Figure 4(e)). Taken together, these findings illustrate that RIPK1, RIPK3, and MLKL are required for iron overload-induced necrotic cell death in osteoblastic cells.

3.4. Iron Overload Induces the Opening of Mitochondrial Permeability Transition Pore (mPTP) in Osteoblastic Cells. Mitochondrial dysfunctions have been considered a crucial step during iron overload-induced cell death [31]. Various pathologic factors could trigger the opening of mitochondrial permeability transition pore, result in the loss of mitochondrial membrane potential, and eventually lead to necroptosis. To illustrate the fundamental mechanisms of iron overload-caused necroptosis, we explored its possible effects on mitochondria. Firstly, we detected the opening of mPTP by flow cytometry in osteoblastic cells. As shown in Figure 5(a), the value of RFI was markedly decreased in osteoblastic cells after treatment with FAC (50-200 μ M) for 120 h. Meanwhile, we also estimated the changes of mitochondrial membrane potential by JC-1 staining. The collapse of the mitochondrial membrane potential was defined as the decline in the ratio of red fluorescence (JC-1 aggregates) to green fluorescence (JC-1 monomers). After exposure to FAC (50-200 μ M) for 120 h, compared with the saline group, a dose-dependent decrease of the ratio of red to green fluorescence in osteoblastic cells was detected by flow cytometry (Figure 5(b)). To further evaluate the loss of mitochondrial membrane potential caused by iron overload, after JC-1 staining, the osteoblastic cells were detected by the confocal microscopy in situ. In the saline group, the osteoblastic cells exhibited primarily red fluorescence, indicating that the mitochondrial membrane potential was normal. However, after treatment with FAC (50-200 μ M) for 120 h, the red fluorescence in the osteoblastic cells was dramatically decreased and the green fluorescence was increased (Figure 5(c)).

Next, to further explore the molecular pathway underlying iron overload-induced mitochondrial permeability transition pore opening, we determined the alteration of PGAM5 and DRP1, two important molecules in maintaining mitochondrial homeostasis, which have been uncovered to act as a substrate of RIPK3. PGAM5, once activated by RIPK3, will be recruited to mitochondrial membrane, which then activates DRP1 by dephosphorylation of serine 637 site and ultimately results in mPTP opening and necroptosis [32]. As shown in Figures 5(d) and 5(e), following 50-200 μ M treatment, the total protein expression of PGAM5 and DRP1 was obviously increased in a dose-dependent manner, accompanied by a decrease in DRP1 serine 637 site phosphorylation in mitochondria.

Collectively, these results suggested that mPTP opening might involve iron overload-induced necroptosis in osteoblastic cells.

3.5. ROS Are Required for Iron Overload-Induced Necroptotic Cell Death in Osteoblastic Cells. ROS caused by iron overload have long been considered the principal factor in regulating cell death [2]. To investigate whether ROS formation is

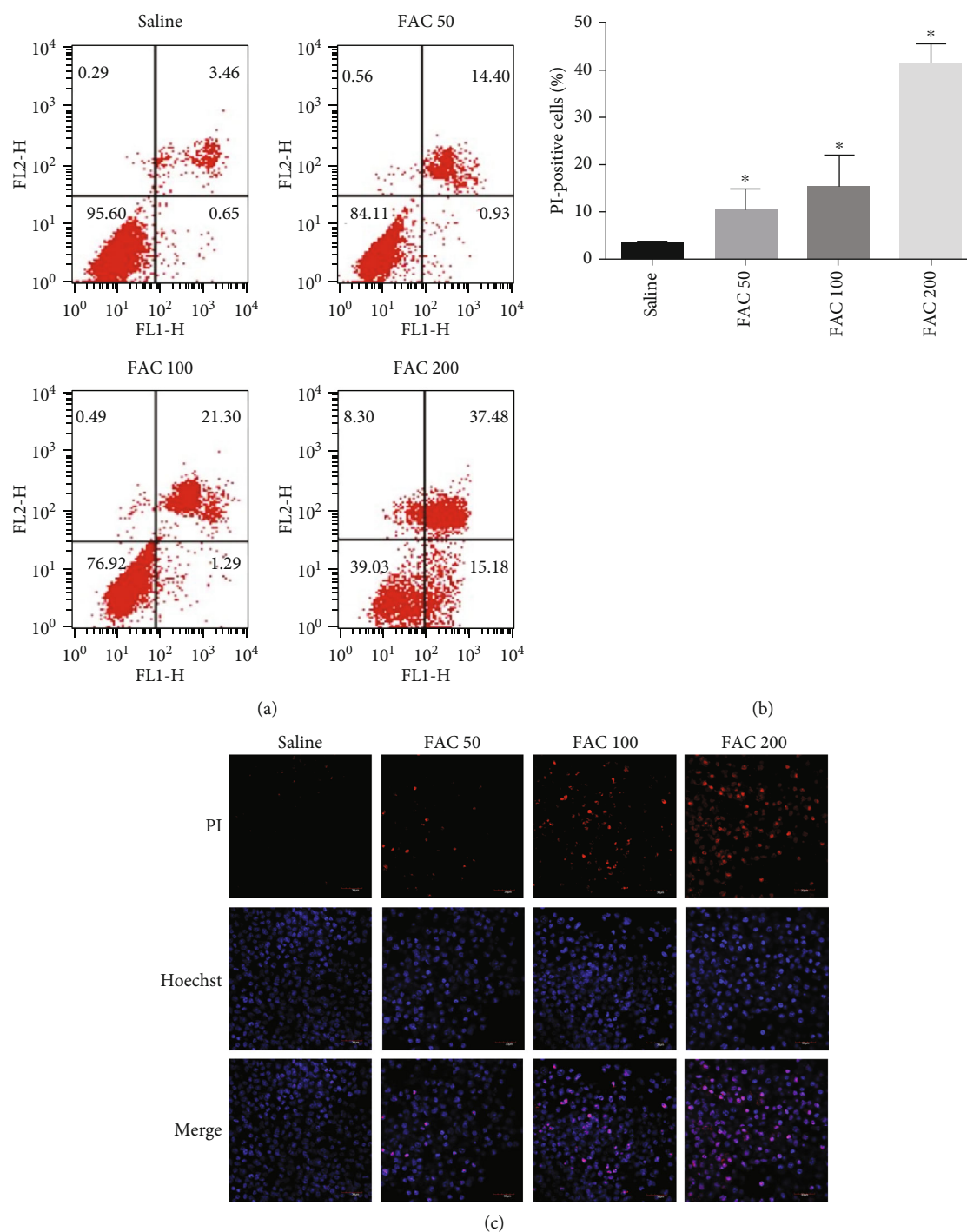


FIGURE 2: Iron overload-induced necrotic cell death in the osteoblastic cells. (a) Representative data were analyzed using the flow cytometer after Annexin-V/PI staining in osteoblastic cells after exposure to 50-200 μ M FAC for 120 h. In each plot, the lower left quadrant (Annexin-V-/PI-) corresponds to live cells, the lower right quadrant (Annexin-V+/PI-) corresponds to apoptosis, and the upper left and right quadrants (Annexin-V-/PI+ and Annexin-V+/PI+) correspond to necrotic cell. (b) Histogram statistical analysis illustrated the dose-dependent increase of PI-positive osteoblasts. Values are expressed as the means \pm SD from three independent experiments (* $p < 0.05$ vs. saline control, ANOVA test). (c) Representative confocal photomicrograph of Hoechst 33258/PI staining. After treatment with FAC (50-200 μ M) for 120 h, the osteoblastic cells were counterstained with Hoechst 33258 and PI. PI positive represents necrotic cells. Scale bar = 30 μ m.

required for iron overload-induced necroptosis in osteoblastic cells, we first measured the effect of iron overload on the intracellular ROS levels by flow cytometry. As shown in

Figures 6(a) and 6(b), FAC increased the intracellular ROS levels in a dose-dependent manner. Furthermore, observation using fluorescence microscopy, the green fluorescence

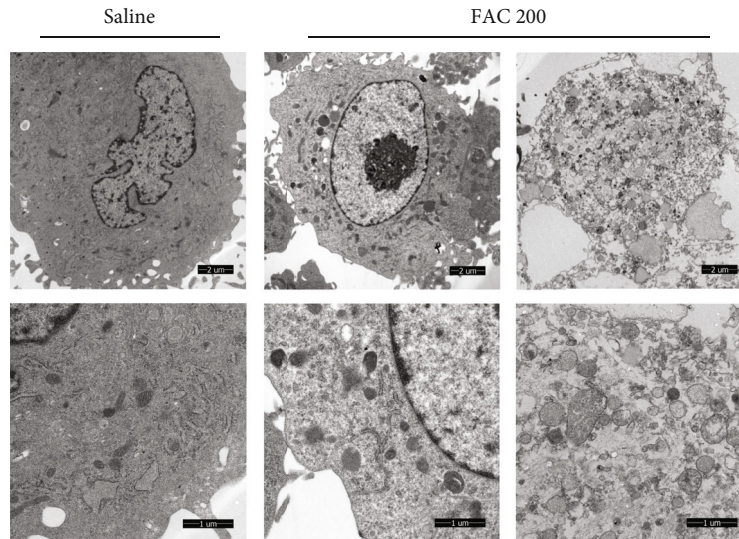


FIGURE 3: Typical TEM images of morphological ultrastructural changes in the osteoblastic cells. In the saline control group, the osteoblastic cells exhibited a normal cell morphology as manifested by intact plasma membrane and organelles. After exposure to 200 μM FAC for 120 h, the osteoblastic cells displayed typical necrotic ultrastructural changes including losing integrity of the plasma membrane, swelling of organelles, and eventually cellular lysis. Scale bar = 1 μm and 2 μm .

spots were dramatically increased in osteoblastic cells following FAC (50–200 μM) treatment, indicating the generation of intracellular ROS induced by iron overload (Figure 6(c)).

Next, we explored whether ROS are indispensable for iron overload-induced necroptosis, using radical scavengers to inhibit the production of ROS. In our study, the antioxidant NAC significantly diminished the generation of ROS induced by iron overload in osteoblastic cells (Figure 7(a)). Notably, addition of NAC obviously reduced iron overload-induced necroptotic cell death of the osteoblastic cells (Figure 7(b)).

As the RIPK1-RIPK3-MLKL pathway represents an essential mechanism mediating necroptosis, we then analyzed whether ROS drive the necroptotic cell death through the RIPK1-RIPK3-MLKL pathway in osteoblastic cells. Intriguingly, we found that the increased phosphorylation of RIPK1, RIPK3, and MLKL induced by iron overload was abrogated by NAC. Besides, NAC also abolished the upregulated expression of the total protein of RIPK1 and RIPK3 (Figures 7(c) and 7(d)).

Together, this set of results confirms that ROS are required for iron overload-induced necroptotic cell death and might mediate the necroptosis through the RIPK1-RIPK3-MLKL pathway.

3.6. ROS Are Required for Iron Overload-Induced mPTP in Osteoblastic Cells. ROS has been confirmed as one of the principal factors triggering mPTP opening in multiple necrotic death pathways [33]. Once activating mPTP opening directly results in the loss of mitochondrial membrane potential, it eventually leads to necroptotic cell death [30]. To explore whether ROS generation is required for iron overload-induced mPTP, we used NAC to neutralize ROS stimulated by iron overload. As shown in Figure 8(a), FAC (200 μM) promoted the opening of mPTP in osteoblastic cells, which

was attenuated by NAC. Similarly, JC-1 staining revealed that NAC also could reverse the depolarization of MMP induced by iron overload in osteoblastic cells (Figures 8(b) and 8(c)). Furthermore, NAC inhibited the upregulation of PGAM5 and activation of DRP1 in mitochondria caused by iron overload (Figures 8(d) and 8(e)). Therefore, our results verified that ROS contributed to the mPTP opening under iron overload-induced necroptosis in osteoblastic cells.

3.7. RIPK1 And RIPK3 Contribute to Iron Overload-Induced ROS Generation in Osteoblastic Cells. RIPK1 has been identified to contribute to the production of ROS and also play essential roles in the regulation of cell survival and death [34]. To analyze the roles of RIPK1 in iron overload-induced ROS production and cell death, RIPK1 was silenced with RIPK1siRNA or inhibited its kinase activity by Nec-1. First, we silenced RIPK1 as confirmed by western blot (Figure 9(a)). The generation of ROS in response to iron overload was significantly suppressed in the RIPK1-silenced and Nec-1-treated groups (Figures 9(c) and 9(e)). Interestingly, knockdown of RIPK1 significantly increased iron overload-induced necrotic cell death, which implied that RIPK1 deficiency in osteoblastic cells was highly sensitive to iron toxicity (Figure 9(d)). By comparison, Nec-1, described as the kinase activity inhibitor of RIPK1, significantly decreased iron overload-induced necrotic cell death (Figure 9(f)). Considering kinase-dependent and kinase-independent functions of RIPK1, our findings indicated that the kinase activity of RIPK1 might partly contribute to iron overload-induced ROS production and is required for iron overload-induced necroptosis in osteoblastic cells.

Next, we explored the role of RIPK3 in iron overload-triggered ROS generation, which has recently been considered a central regulator of necroptosis. To clarify the requirement of RIPK3 for iron overload-induced ROS generation, the

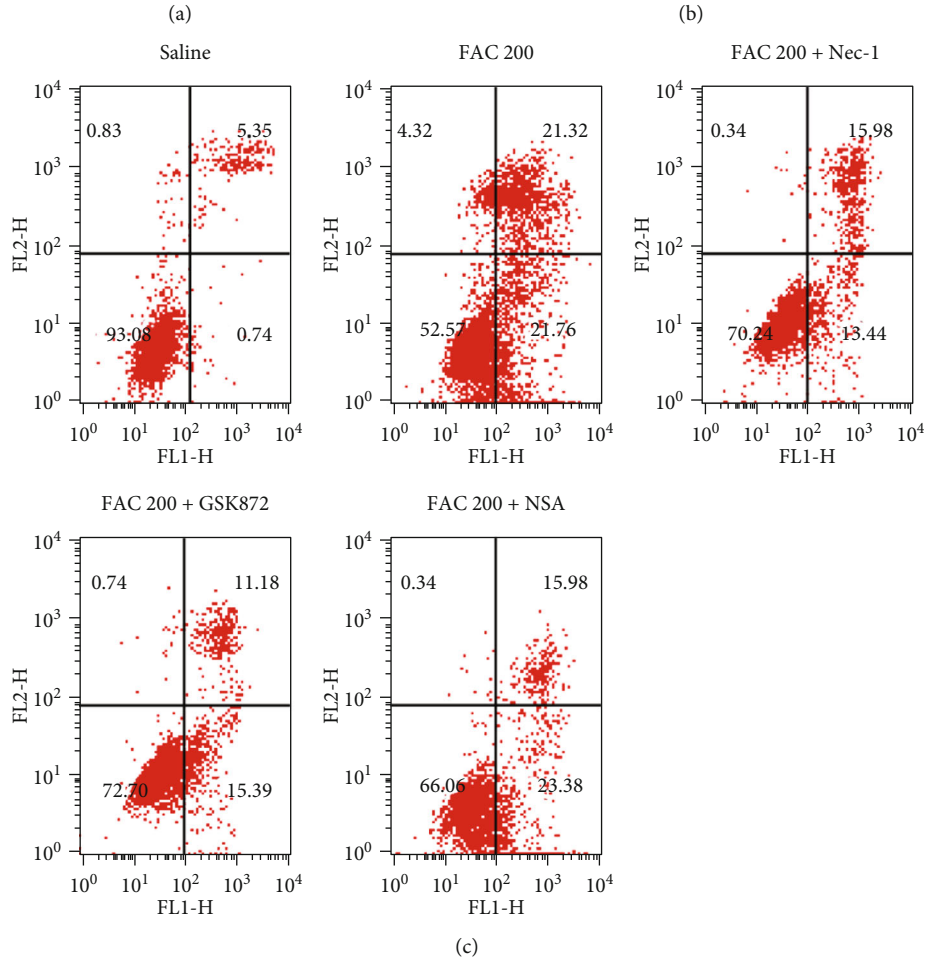
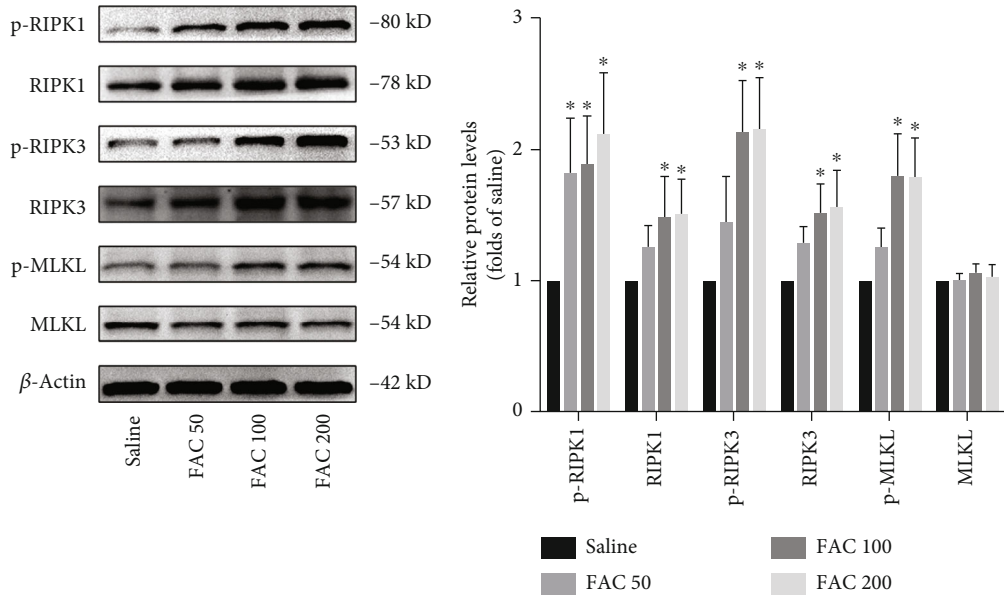


FIGURE 4: Continued.

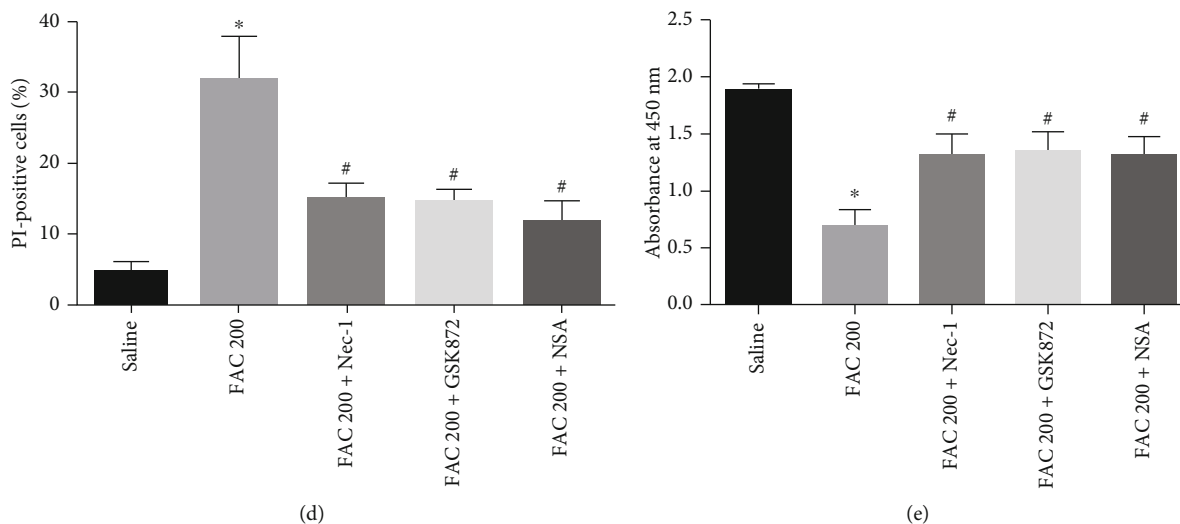


FIGURE 4: Implication of the necroptosis pathway in iron-induced osteoblastic necrosis. (a) Total protein levels of phosphorylated RIPK1, RIPK3, MLKL, and corresponding total protein. After exposure to FAC (50-200 μ M) for 120 h, western blot was used to detect the expression of phosphorylated RIPK1, RIPK3, MLKL, and corresponding total protein in osteoblastic cells. (b) Histogram analysis showing the relative protein levels of phosphorylated RIPK1, RIPK3, MLKL, and corresponding total protein. Data are presented as the means \pm SD from three independent experiments ($*p < 0.05$ vs. saline control, ANOVA test). (c) Representative data were analyzed using the flow cytometer after Annexin-V/PI staining in osteoblastic cells after exposure to 50-200 μ M FAC for 120 h. (d) Histogram statistical analysis demonstrating the ratio of PI positive cells. Values are expressed as the means \pm SD from three independent experiments ($*p < 0.05$ vs. saline control, $#p < 0.05$ vs. FAC 200, ANOVA test). (e) The protective effects of Nec-1, GSK872, or NSA on the osteoblastic cell viability were evaluated by the CCK-8 assay. Values are expressed as the means \pm SD from three independent experiments ($*p < 0.05$ vs. saline control, $#p < 0.05$ vs. FAC 200, ANOVA test).

osteoblastic cells were treated with RIPK3 siRNA. Knockdown efficacy of RIPK3 was confirmed by western blot analysis (Figure 9(b)). As shown in Figures 9(g) and 9(h), silencing of RIPK3 substantially attenuated iron overload-induced ROS production and also protected against iron overload-induced necrotic cell death. Meanwhile, inhibition of RIPK3 by GSK872 abrogated iron overload-stimulated necrotic cell death in the osteoblastic cells (Figures 4(c) and 4(d)). Based on our results, we conclude that RIPK3, at least in part, contributes to iron overload-induced ROS generation and is indispensable for iron overload-induced necroptosis in the osteoblastic cells.

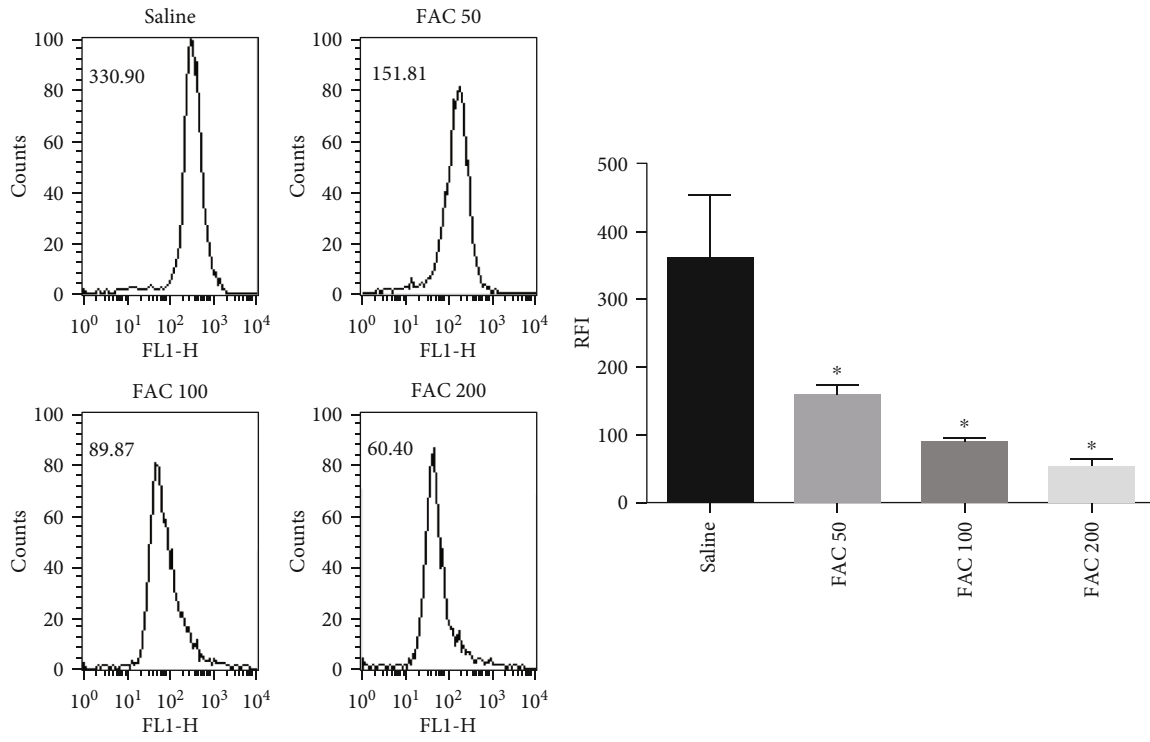
4. Discussion

Osteoporosis is an age-related degenerative disorder that connected with a higher risk of fragility fractures. Iron gradually accumulates in the course of aging, and excess iron could accelerate bone loss in physically fit postmenopausal women and old men [35]. As numerous studies have confirmed iron overload as an independent risk contributor for the development of aging-associated osteoporosis, it is imperative to explore the precise iron toxicity in osteoblastic cells and elucidate the underlying mechanism. In the present study, we first demonstrated that iron overload could induce necroptosis of osteoblastic cells in vitro, which is mediated, at least in part, through the RIPK1/RIPK3/MLKL pathway. More interestingly, we revealed the critical regulation of ROS in iron overload-induced necroptosis. Notably, ROS

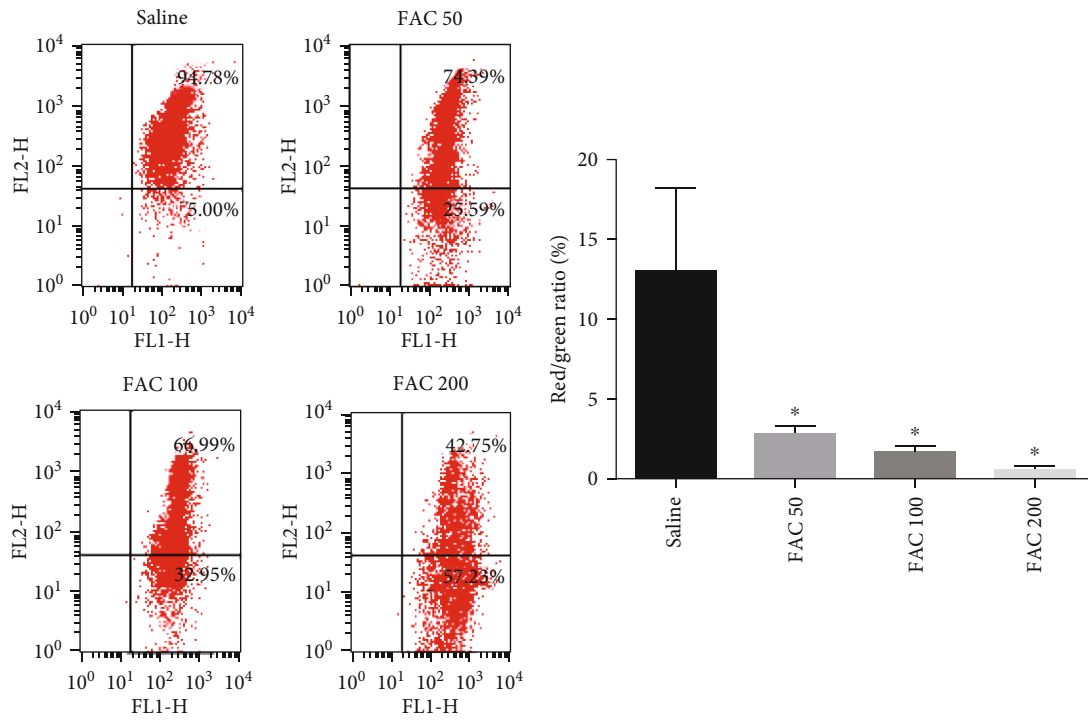
induced by iron overload promote necroptosis via the formation positive feedback loop involving RIPK1/RIPK3.

Excessive iron can be toxic to many cell types, and it seems that the mechanism of iron toxicity is closely associated with cell death in the iron overload-related disorders [36, 37]. Historically, there are two mainly fundamental pathways of cell death: apoptosis and necrosis [38]. Apoptosis is marked by cytosolic shrinkage, nuclear condensation, apoptotic body formation, and activation of caspases [37]. The typical characteristics of necrosis, as opposed to apoptosis, are cellular swelling, plasma membrane disintegration, cellular contents release, and inflammation induction [14, 39]. Previous studies indicated that apoptosis mediated by the mitochondrial pathway was involved in iron overload-induced osteoblastic cell death [9]. However, our data suggested that the characteristics of osteoblastic cell death induced by iron overload seem to be closely related to necrosis, as proved by the higher PI-positive rate of cells and the typical necrotic morphological features obtained by TEM. Similar phenomena have also been found by previous work, which implied that necrosis might be the primary type of cell death for the osteoblastic cells in the iron overload-associated bone diseases [7, 40].

The exact mechanisms by which iron overload induced necrosis in osteoblastic cells have not been well established. Necrosis is traditionally considered to be an unregulated type of cell death, but growing evidence has shown that it is a type of programmed cell death carried out by multiple signaling transduction mechanisms [41]. Necroptosis, one type of programmed necrosis, was characterized by morphological changes of necrosis, which is critically dependent on the



(a)



(b)

FIGURE 5: Continued.

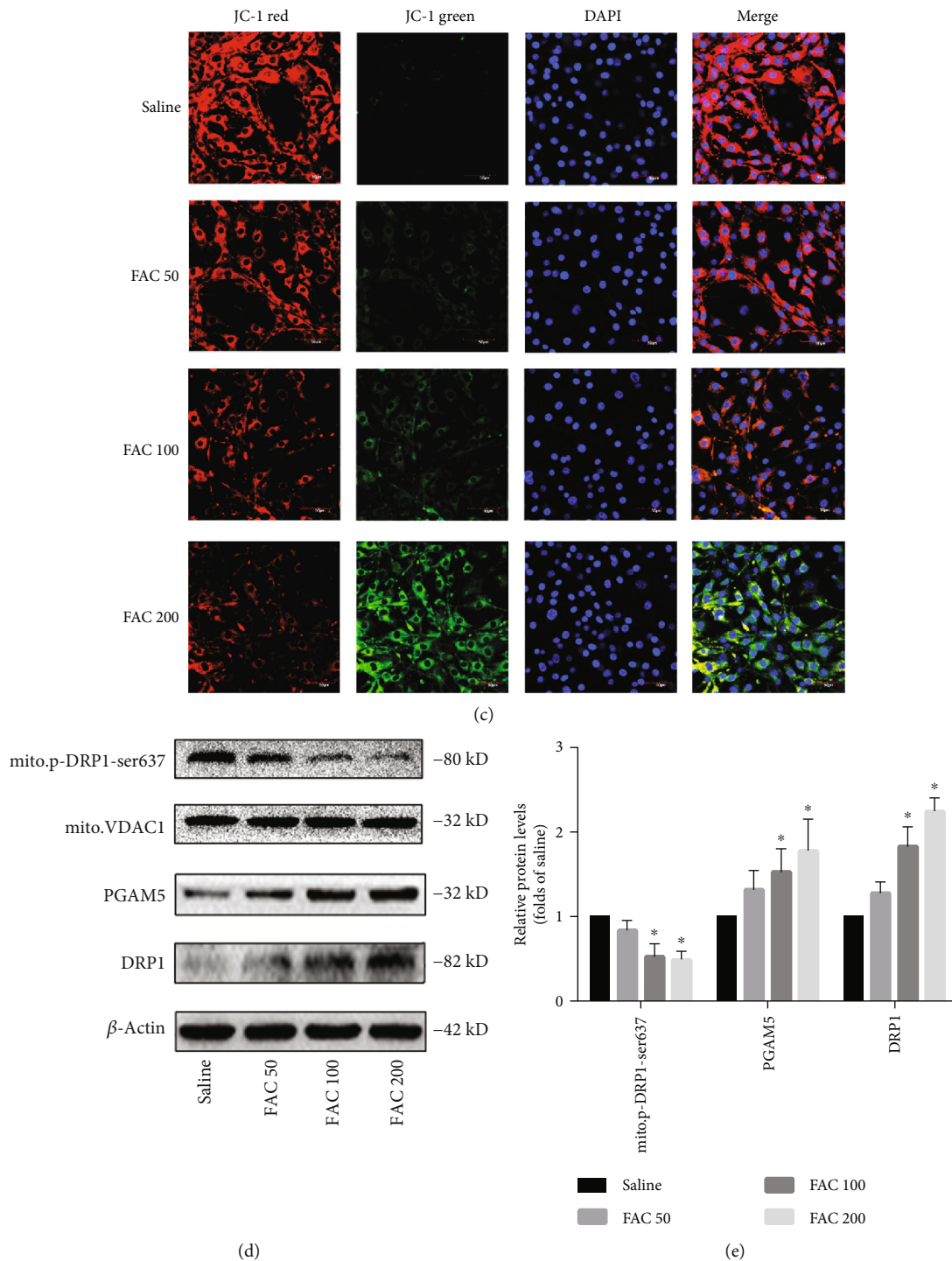


FIGURE 5: Iron overload induces the opening of mitochondrial permeability transition pore in osteoblastic cells. The opening of mitochondrial permeability transition pore results in the loss of mitochondrial membrane potential. After exposure to FAC (50–200 μ M) for 120 h, the flow cytometry was used to detect the opening of mPTP and changes of MMP. (a) Representative dot plot of the flow cytometry results illustrated the increase of mPTP opening. The quantitative mPTP in osteoblasts is shown by RFI. Values are expressed as the means \pm SD from three independent experiments ($*p < 0.05$ vs. saline control, ANOVA test). (b) Representative dot plot of the flow cytometry results illustrated the decrease MMP. The quantitative MMP in osteoblasts is shown by red/green ratio. Values are expressed as the means \pm SD from three independent experiments ($*p < 0.05$ vs. saline control, ANOVA test). (c) Representative fluorescence images were obtained in situ JC-1 staining by confocal microscopy. Scale bar = 50 μ m. (d) Representative western blots of the total protein expression of PGAM5, DRP1, and mitochondrial protein expression of phosphorylated DRP1 (Ser637). (e) Histogram analysis showing the relative protein levels of PGAM5, DRP1, and mitochondrial protein expression of phosphorylated DRP1 (Ser637). Data are presented as the means \pm SD from three independent experiments ($*p < 0.05$ vs. saline control, ANOVA test).

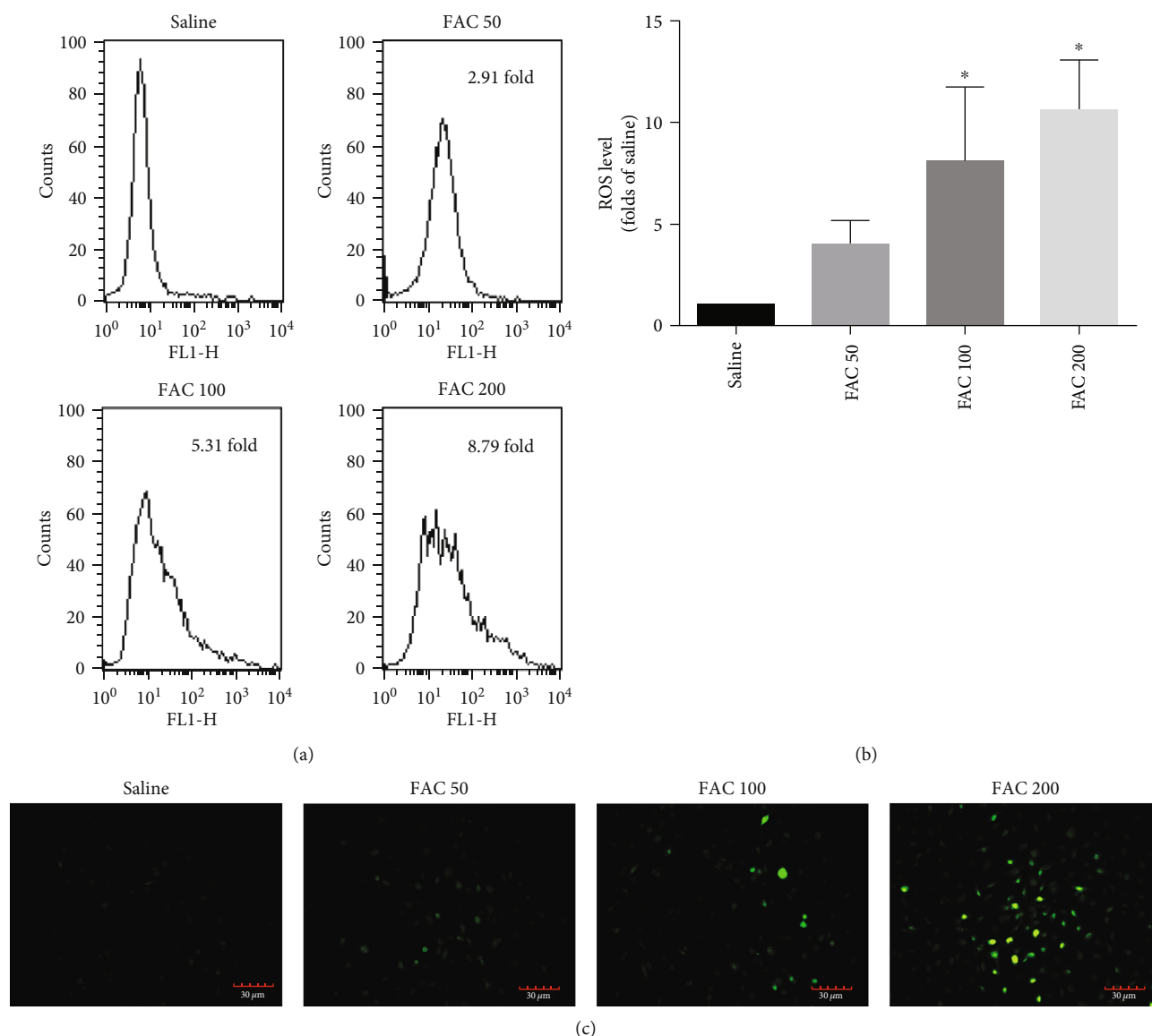
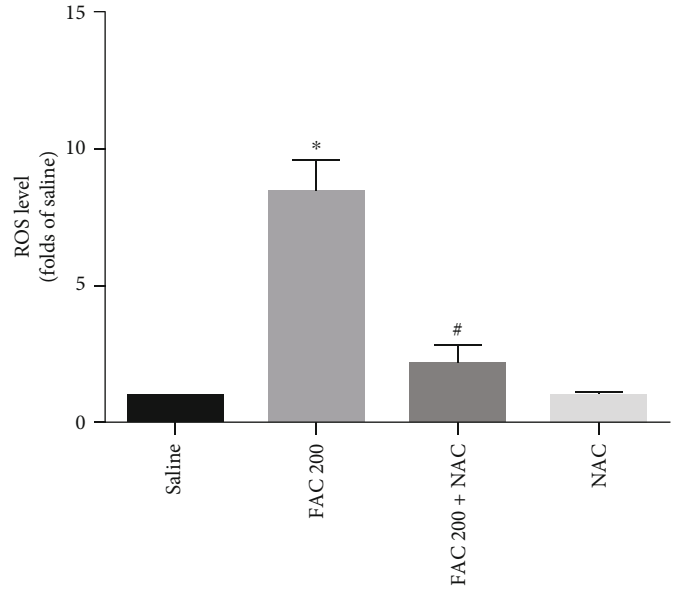
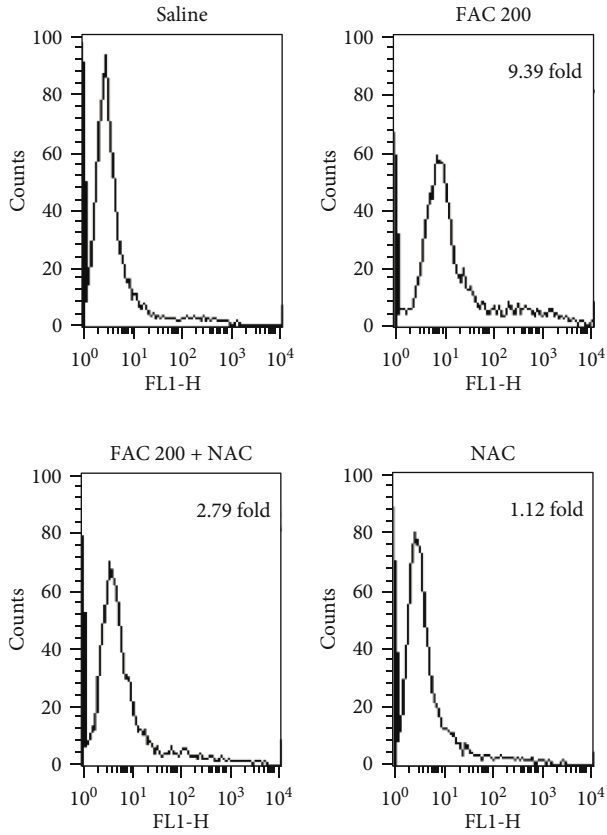


FIGURE 6: Iron overload induces the production of ROS in osteoblastic cells. (a) Representative data were analyzed using a flow cytometer after H2DCF-DA staining in osteoblasts after exposure to FAC (50–200 μ M) for 120 h. (b) Histogram statistical analysis illustrated the production of ROS in osteoblasts. Values are expressed as the means \pm SD from three independent experiments (**p* < 0.05 vs. saline control, ANOVA test). (c) Representative fluorescence photomicrograph was obtained in situ H2DCF-DA staining by the fluorescence microscope. Scale bar = 30 μ m.

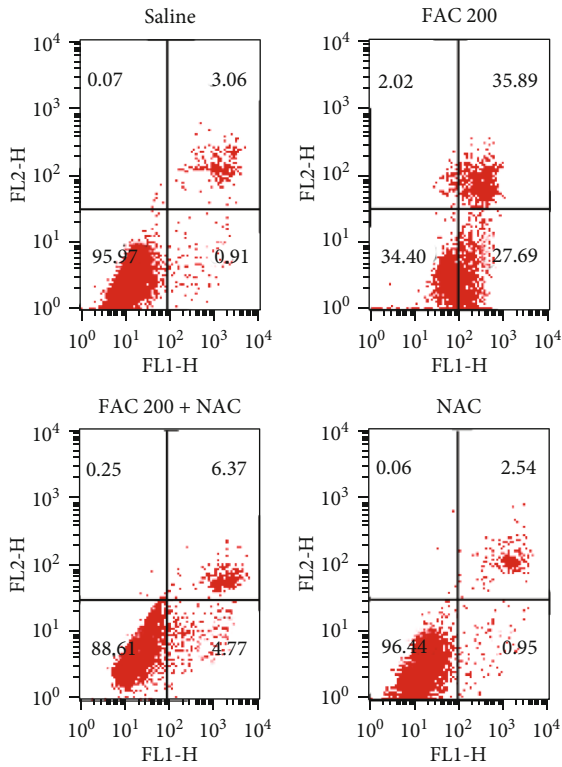
regulation of RIPK1, RIPK3, and MLKL. During activation of necroptosis, the phosphorylated RIPK1 recruits RIPK3 to form the RIPK1/RIPK3 necrosome complex. Then, RIPK3 recruits and phosphorylates MLKL [19]. Eventually, the phosphorylated MLKL undergoes oligomerization and translocates to the plasma membrane to execute necroptotic cell death [18, 29]. In this study, our data showed a dose-dependent increase in the total protein expression and phosphorylation of RIPK1 and RIPK3 in the osteoblastic cells after exposure to FAC. However, the protein expression of MLKL has no significant change in the osteoblastic cells after treatment with FAC. Considering RIPK3-dependent MLKL phosphorylation is the more critical step for necroptosis execution; we next detected the phosphorylation levels of

MLKL in osteoblastic cells. In line with the changes of RIPK3 expression, we found that iron overload induced the increase of MLKL phosphorylation, indicating that phosphorylated MLKL is involved in the execution of necroptotic cell death. Furthermore, addition of Nec-1, GSK872, or NSA reduced iron overload-induced necrotic cell death in osteoblastic cells. Taken these results and previous research together, we could possibly conclude that iron overload promotes necroptosis in osteoblastic cells, at least in part, via the RIPK1/RIPK3/MLKL pathway.

RIPK1 and RIPK3 have been identified as two major executive molecules of necroptosis [11, 42]. Nevertheless, the exact mechanisms of RIPK1 and RIPK3 underlying osteoblastic necroptosis under iron overload condition are



(a)



(b)

(b)

(b)

FIGURE 7: Continued.

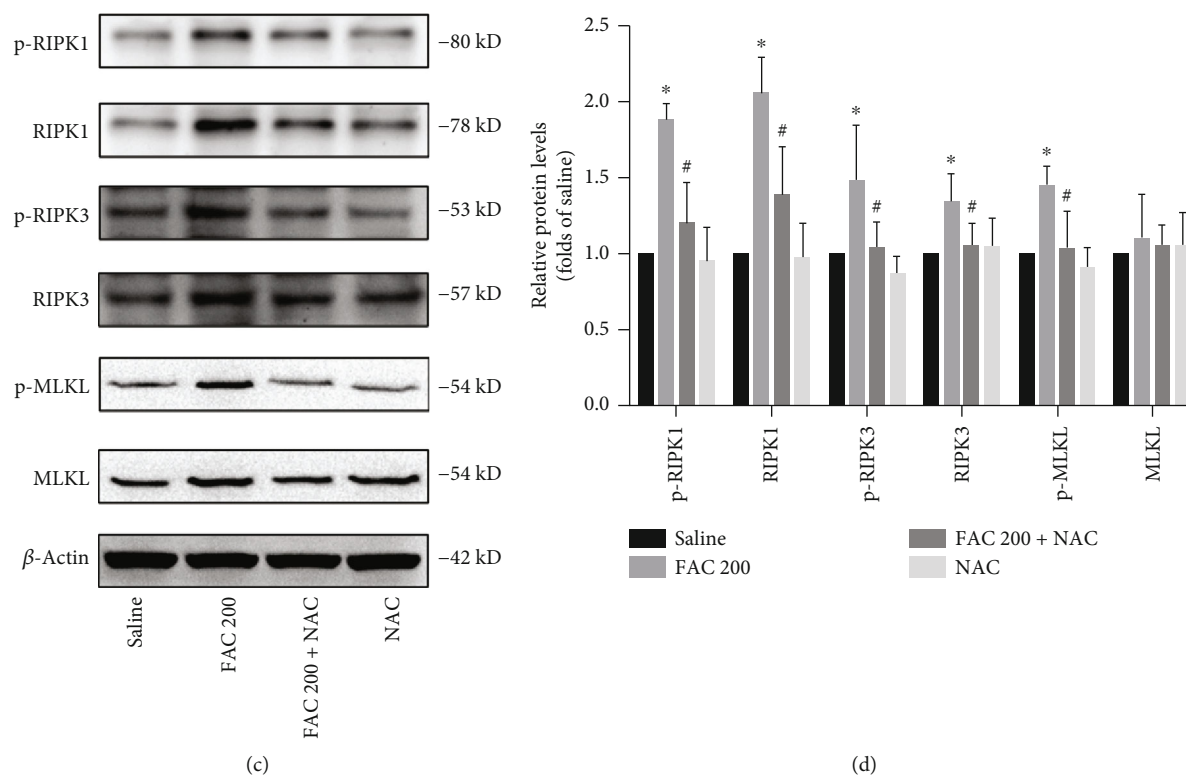


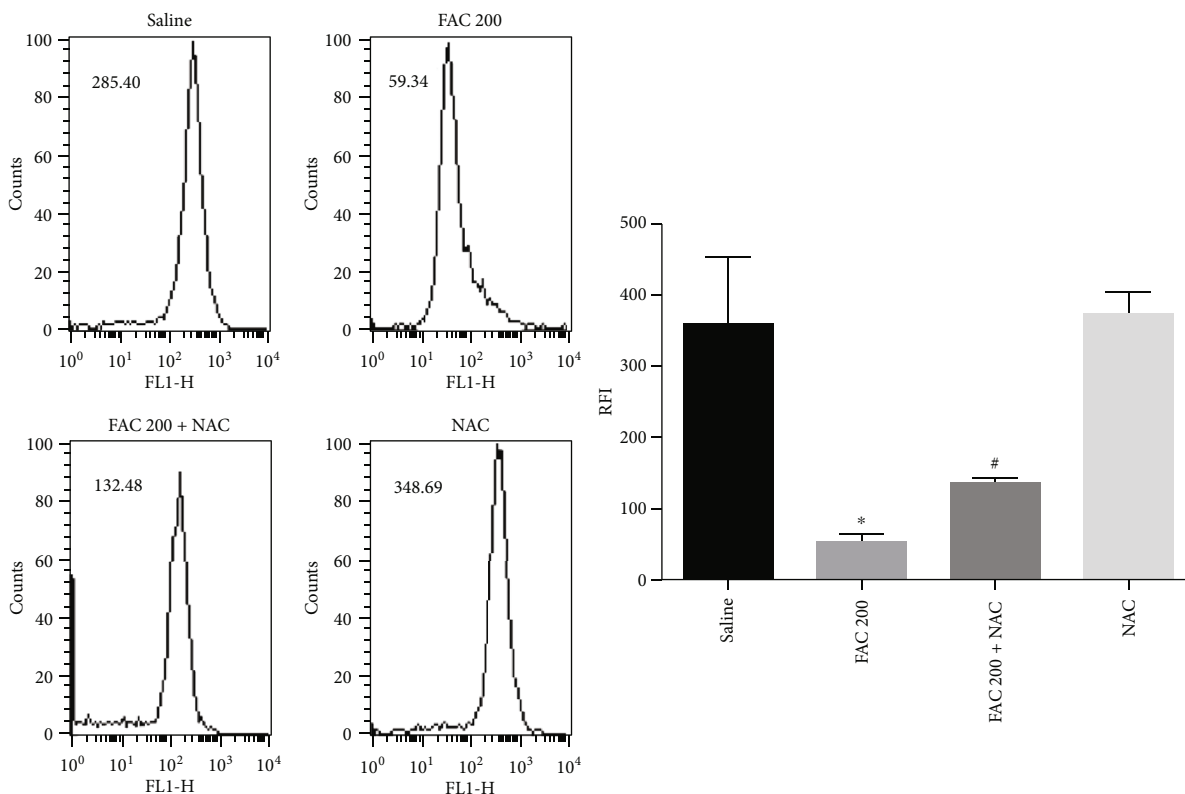
FIGURE 7: ROS are required for iron overload-induced necroptosis in osteoblastic cells. Osteoblasts were treated with 200 μ M FAC with or without NAC (1 mM) for 120 h. (a) Representative graphs were obtained from a flow cytometer after H2DCF-DA staining in osteoblasts. Histogram statistical analysis illustrated the production of ROS in osteoblasts. Data are expressed as the means \pm SD from three independent experiments (* p < 0.05 vs. saline control, # p < 0.05 vs. FAC 200, ANOVA test). (b) Representative data were analyzed using a flow cytometer after Annexin-V/PI double staining in osteoblasts. Histogram analysis demonstrating the ratio of PI positive cells. Values are expressed as the means \pm SD from three independent experiments (* p < 0.05 vs. saline control, # p < 0.05 vs. FAC 200, ANOVA test). (c) Representative western blots of the expression of phosphorylated RIPK1, RIPK3, MLKL, and corresponding total protein. (d) Histogram analysis showing the relative protein levels of phosphorylated RIPK1, RIPK3, MLKL, and corresponding total protein. Data are presented as the means \pm SD from three independent experiments (* p < 0.05 vs. saline control, # p < 0.05 vs. FAC 200, ANOVA test).

poorly understood. The molecular roles of RIPK1 in mediating necroptosis have been controversially discussed. On the one hand, numerous studies indicated that RIPK1 and its kinase activity are necessary for the initiation of necroptosis by various stimulators [43, 44]. On the other hand, RIPK1, through its kinase-independent scaffolding functions, maintains cellular homeostasis by inhibiting necroptosis [15, 45, 46]. In the current study, we showed that selective silencing of RIPK1 in osteoblastic cells sensitizes these cells to necroptosis triggered by iron overload. In contrast to genetic silencing of RIPK1, we indicated that Nec-1 protected against necroptosis induced by iron overload. Although these results seemed to be contradictory, we speculated this phenomenon might be related to kinase-dependent and kinase-independent functions of RIPK1 as discussed above. Furthermore, the exact molecular mechanisms of RIPK1 in mediating osteoblastic necroptosis will be investigated in the future studies. Currently, these results at least revealed that the kinase activity of RIPK1 was essential for iron overload-induced necroptosis in osteoblastic cells. Unlike RIPK1, the ability of RIPK3 in mediating necroptosis has been well established [47]. In our experiment, knockdown of RIPK3 significantly inhibited iron overload-induced necrotic cell death. Similarly, GSK872 also reduced iron overload-

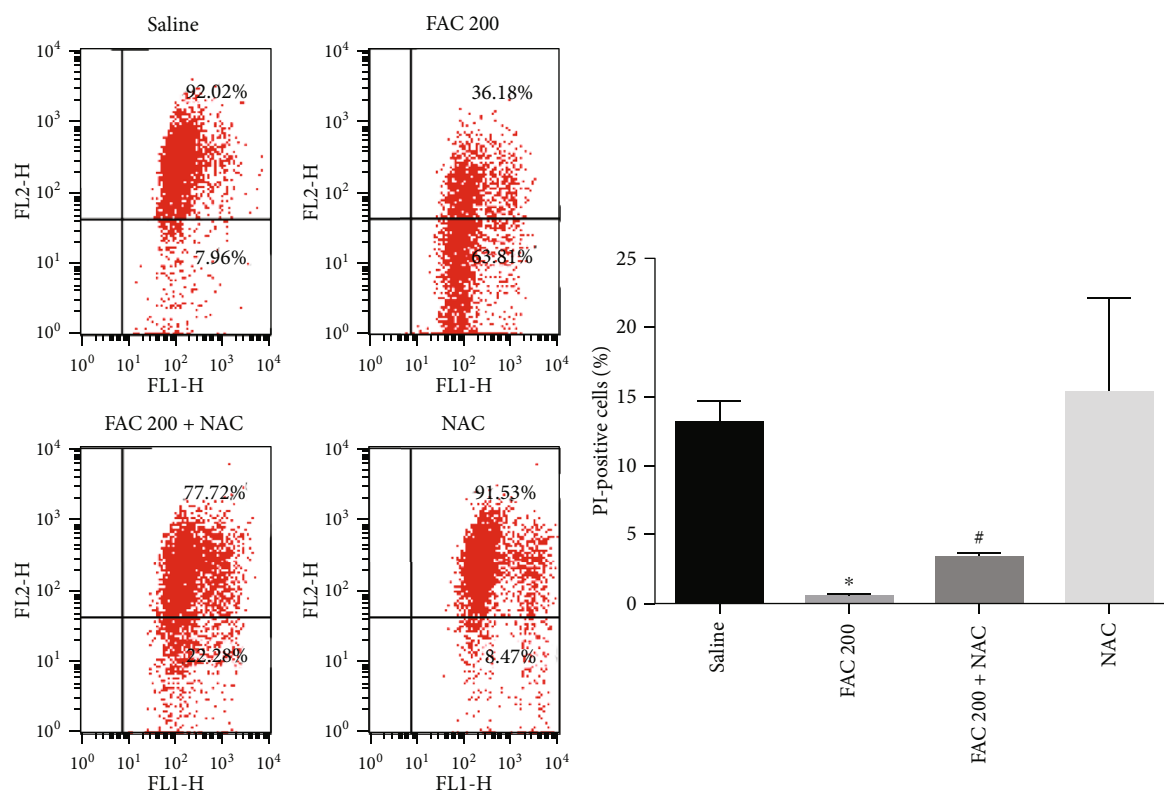
stimulated necrotic cell death in osteoblastic cells, which is consistent with previous studies. Based on these data together, we could possibly conclude that the kinase activity of RIPK1 and RIPK3 is indispensable for iron overload-induced necroptosis in osteoblastic cells.

In addition, mPTP opening has been also identified as an important downstream event for RIPK3-mediated necroptosis [29, 30]. PGAM5, a critical convergence effector of various necroptotic death pathways, could be recruited by phosphorylated RIPK3, then activates DRP1 dephosphorylation, and consequently promotes mPTP opening and necroptotic cell death [48–50]. More interestingly, our results revealed a dose-dependent increase in the levels of RIPK3 phosphorylation, upregulation of PGAM5 and DRP1, and dephosphorylation of DRP1 in mitochondria after treatment with FAC. Furthermore, we observed that the opening of mPTP was markedly increased and the PI-positive ratio of osteoblastic cells also concomitantly elevated. Therefore, we could be possibly concluded that the opening of mPTP is involved in necroptosis of osteoblastic cells in response to iron overload.

A key contribution of this study is the finding that ROS are essential for iron overload-induced necroptosis in osteoblastic cells. ROS have been considered as a critical driving force for necroptosis [19, 51]. Our previous studies have



(a)



(b)

FIGURE 8: Continued.

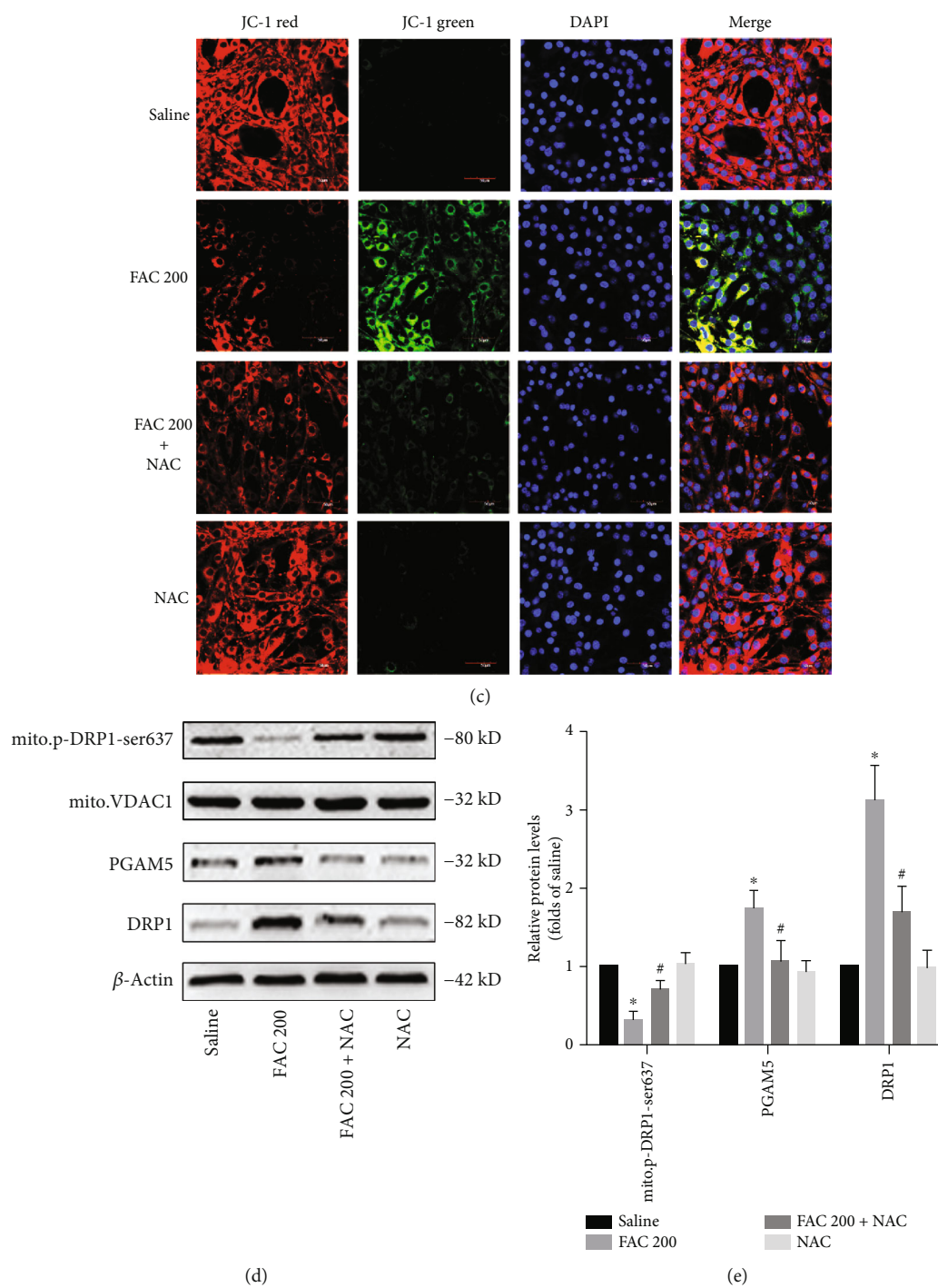


FIGURE 8: ROS are required for iron overload-induced mPTP opening in osteoblastic cells. The opening of mitochondrial permeability transition pore results in the loss of mitochondrial membrane potential. After exposure to FAC (200 μ M) with or without NAC (1 mM) for 120 h, the flow cytometry was used to detect the opening of mPTP and changes of MMP. (a) Representative dot plot of the flow cytometry results illustrated the increase mPTP opening. The quantitative mPTP in osteoblasts is shown by RFI. Data are expressed as the means \pm SD from three independent experiments (* p < 0.05 vs. saline control, # p < 0.05 vs. FAC 200, ANOVA test). (b) Representative dot plot of the flow cytometry results illustrated the decrease MMP. The quantitative MMP in osteoblasts is shown by red/green ratio. Data are expressed as the means \pm SD from three independent experiments (* p < 0.05 vs. saline control, # p < 0.05 vs. FAC 200, ANOVA test). (c) Representative fluorescence images were obtained in situ JC-1 staining by confocal microscopy. Scale bar = 50 μ m. (d) Representative western blots of the total protein expression of PGAM5 and DRP1 and mitochondrial protein expression of phosphorylated DRP1 (Ser637). (e) Histogram analysis showing the relative protein levels of PGAM5 and DRP1 and mitochondrial protein expression of phosphorylated DRP1 (Ser637). Data are presented as the means \pm SD from three independent experiments (* p < 0.05 vs. saline control, # p < 0.05 vs. FAC 200, ANOVA test).

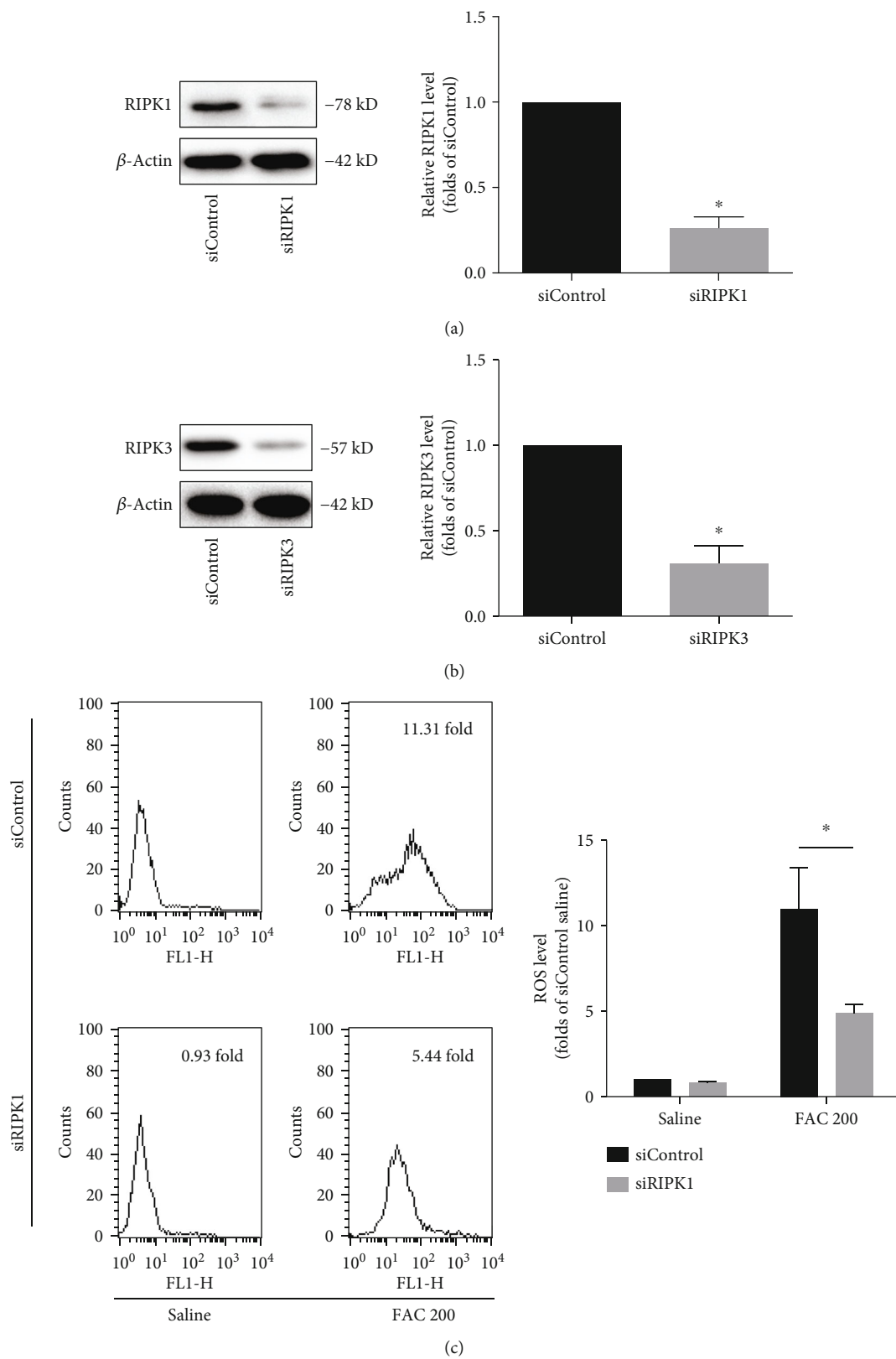


FIGURE 9: Continued.

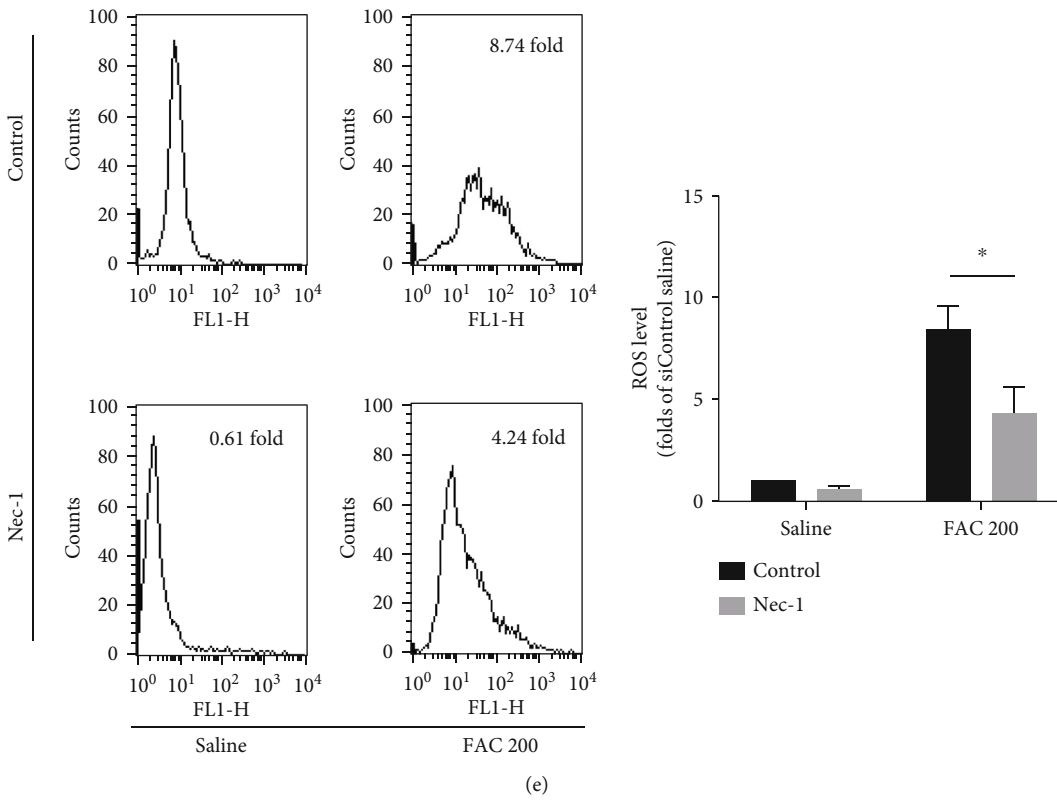
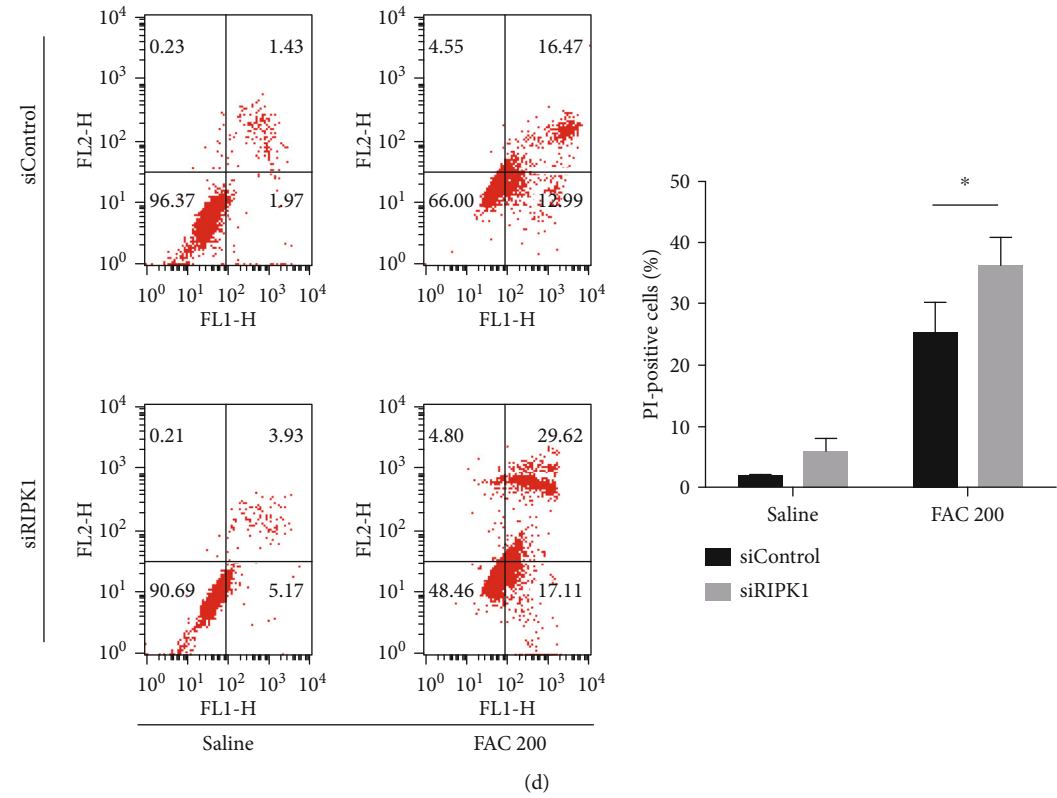


FIGURE 9: Continued.

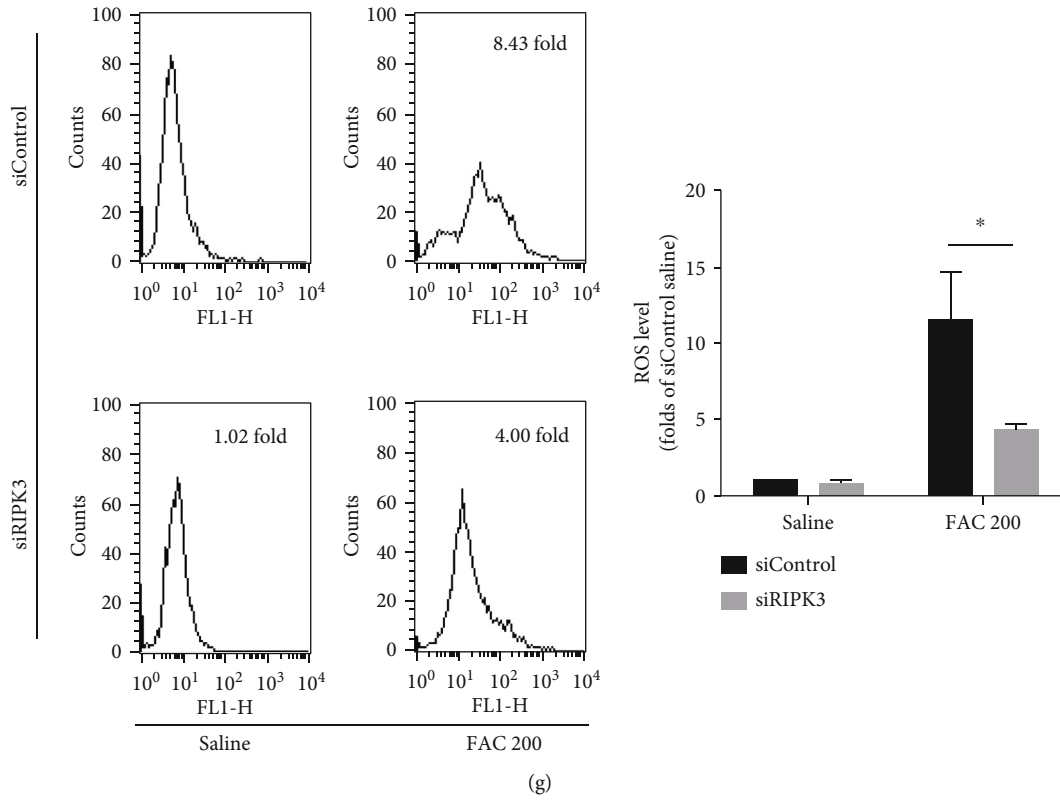
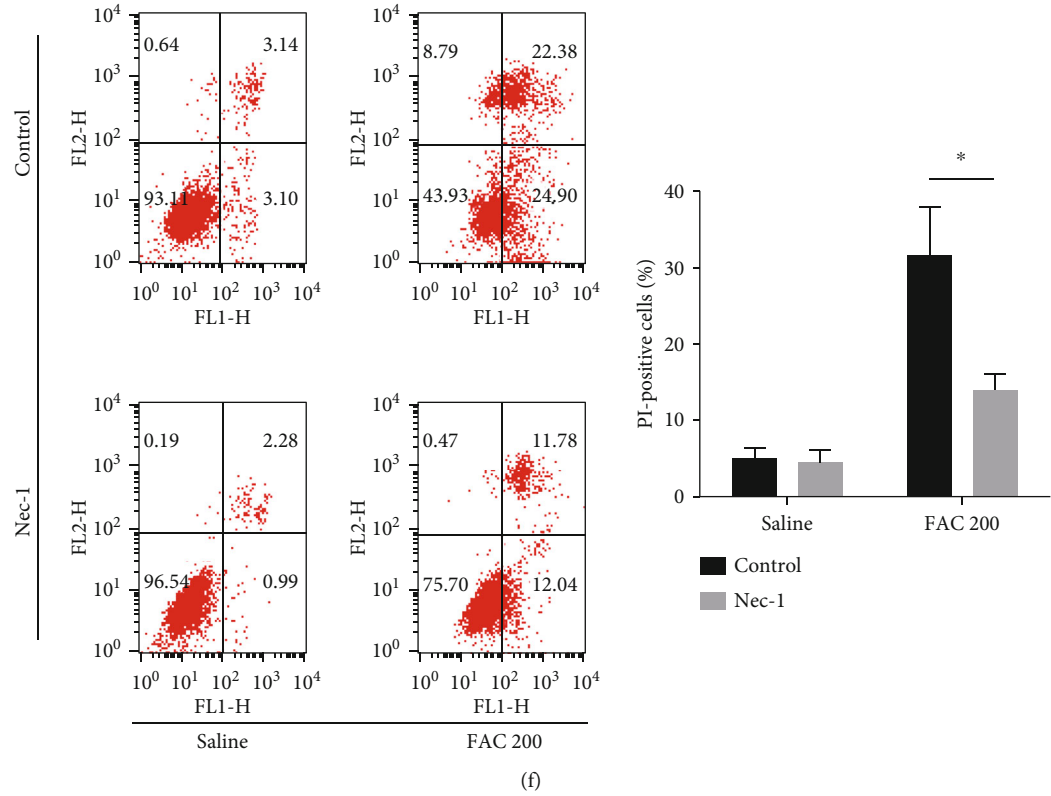


FIGURE 9: Continued.

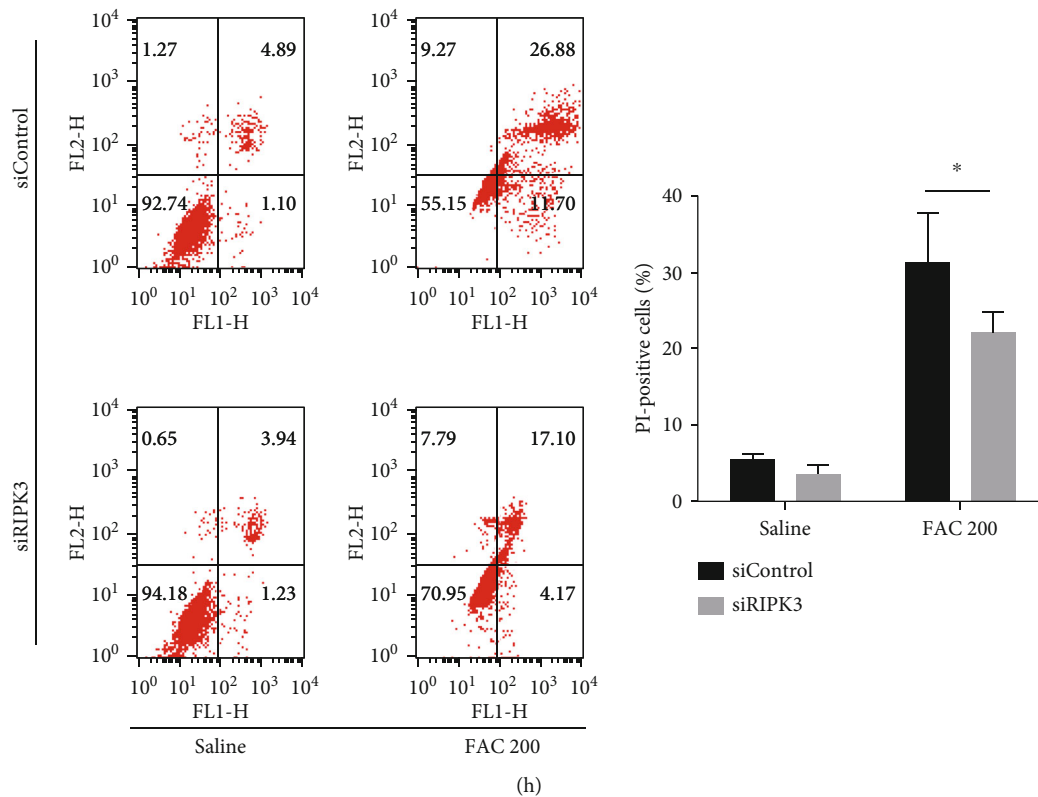


FIGURE 9: RIPK1 and RIPK3 contribute to iron overload-induced ROS. (a, b) The osteoblastic cells were transfected with siControl, siRIPK1, or siRIPK3 for 24 h; then, the expression of RIPK1 and RIPK3 was measured by western blot. Representative western blots of the expression of RIPK1 and RIPK3. Histogram analysis showing the relative protein levels of RIPK1 and RIPK3. Data are presented as the means \pm SD of three independent experiments ($*p < 0.05$ vs. siControl, Student's *t*-tests). (c, d) The osteoblastic cells were treated with FAC (200 μ M) for 120 h with siRIPK1 or siControl. Effect of siRIPK1 on ROS production by H2DCF-DA staining (c). Effect of siRIPK1 on iron overload-induced necrotic cell death by Annexin-V/PI double staining in the osteoblastic cells (d). (e, f) The osteoblastic cells were treated with FAC (200 μ M) for 120 h with or without Nec-1 (20 μ M). Effect of Nec-1 on ROS production by H2DCF-DA staining (e). Effect of Nec-1 on iron overload-induced necrotic cell death by Annexin-V/PI double staining in the osteoblastic cells (f). (g, h) The osteoblastic cells were treated with FAC (200 μ M) for 120 h with siRIPK3 or siControl. Effect of siRIPK3 on ROS production by H2DCF-DA staining (g). Effect of siRIPK3 on iron overload-induced necrotic cell death by Annexin-V/PI double staining in the osteoblastic cells (h). Data are expressed as the means \pm SD from three independent experiments ($*p < 0.05$ vs FAC 200, ANOVA test).

indicated that labile iron stimulated by iron overload contributed to the production of ROS in osteoblastic cells [9]. However, numerous evidence has suggested that the involvement of ROS in necroptosis is cell type-dependent [19]. It is therefore of great interest to explore whether ROS mediate iron overload-induced necroptosis in osteoblastic cells. Accordingly, we demonstrated that exposure with FAC triggered osteoblastic cells to produce ROS in a concentration-related manner. Furthermore, diminishing ROS by NAC strongly reduced iron overload-induced mPTP opening and necrotic cell death. In addition, posttranslational modifications involved by ROS play an essential role during necroptosis execution [19]. Furthermore, we detected the phosphorylation levels of RIPK1, RIPK3, and MLKL, three key upstream molecules of the necroptotic pathway. When NAC was applied, the phosphorylation levels of RIPK1 and RIPK3 dramatically decreased, indicating that ROS promote RIPK1 and RIPK3 phosphorylation in iron overload-induced necroptosis. Meanwhile, by detecting the necessity of key necroptotic molecules for ROS generation, we also found that RIPK1 and RIPK3 are indispensable for iron overload-

induced ROS production, as genetic silencing of these molecules or inhibition of RIPK1 kinase activity by Nec-1 block ROS generation. Collectively, our results strongly suggest that ROS drive the phosphorylation of RIPK1 and RIPK3 and initiate a positive feedback loop involving RIPK1/RIPK3 in the iron overload-induced necroptosis process.

In our experiments, our data were highly reproducible. However, there are also some limitations that need to be considered. First, our study was conducted *in vitro*, and conclusions might not completely reflect the clinical conditions. In the subsequent studies, we will explore the exact mechanisms of iron toxicity *in vivo*. Second, because of technical limits for human osteoblastic cells, MC3T3-E1 cell line was used to investigate the cytotoxicity of iron [9, 52]. Third, our results only elaborate one aspect of iron toxicity pathway in osteoblastic cells. In fact, various pathways may contribute to the activation of iron overload-induced cell death. Therefore, in the subsequent studies, we need to further explore other pathways in iron overload-induced cell death of osteoblastic cells.

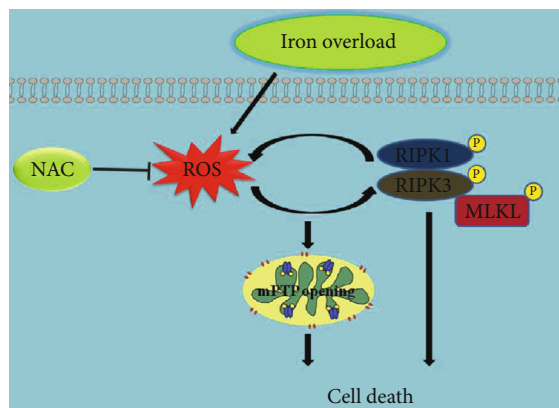


FIGURE 10: Schematic overview demonstrating that ROS-mediated necroptosis is involved in iron overload-caused osteoblastic cell death.

In conclusion, we firstly demonstrated that iron overload induced necroptosis of osteoblastic cells *in vitro*, which is mediated, at least in part, through the RIPK1/RIPK3/MLKL pathway. Moreover, we also revealed that ROS mediated iron overload-induced necroptosis via a positive feedback loop involving RIPK1/RIPK3. The possible mechanisms involved in iron overload-caused osteoblastic cell death are depicted in Figure 10. Importantly, our studies highlight the critical role of ROS in the regulation of iron overload-induced necroptosis in osteoblastic cells and provide a novel strategy to treat iron overload-associated bone disease.

Abbreviations

FAC:	Ferric ammonium citrate
ROS:	Reactive oxygen species
α -MEM:	α -Minimum Essential Medium Eagle
mPTP:	Mitochondrial permeability transition pore
NAC:	N-Acetylcysteine
MMP:	Mitochondrial membrane potential
RIPK1:	Receptor-interacting protein kinase 1
MLKL:	Mixed lineage kinase domain-like
RIPK3:	Receptor-interacting protein kinase 3
FBS:	Fetal bovine serum
Nec-1:	Necrostatin-1
NSA:	Necrosulfonamide
TEM:	Transmission electron microscopy
siRNA:	Small interfering RNA
JC-1:	5',6,6'-Tetrachloro-1,1',3,3'-tetraethyl-benzimidazolcarbocyanine iodide
CCK-8:	Cell counting kit-8.

Data Availability

The data used to support the findings of this study are available from the corresponding author upon request.

Conflicts of Interest

The authors have declared that there are no conflicts of interest.

Authors' Contributions

Qing Tian, Bo Qin, and Yufan Gu have contributed equally to the article.

Acknowledgments

This study was supported by the Joint Funds of Medical Technology R&D Program of Henan Province of China (No. 2018020024) and the Youth fund of then National Natural Science Foundation of China (Grant No. 81902253).

Supplementary Materials

Supplementary 1. Supplementary Figure 1: the protective effects of Nec-1 against iron overload-induced cytotoxicity in osteoblastic cells. After subjecting to FAC (200 μ M) with or without Nec-1 (5-160 μ M) for 120 h, the viability of osteoblastic cells was detected by CCK-8 assays. Values are expressed as the means \pm SD from three independent experiments (* p < 0.05 vs. saline control; # p < 0.05 vs. FAC 200).

Supplementary 2. Supplementary Figure 2: the protective effects of GSK872 against iron overload-induced cytotoxicity in osteoblastic cells. After subjecting to FAC (200 μ M) with or without GSK872 (1-32 μ M) for 120 h, the viability of osteoblastic cells was detected by CCK-8 assays. Values are expressed as the means \pm SD from three independent experiments (* p < 0.05 vs. saline control; # p < 0.05 vs. FAC 200).

Supplementary 3. Supplementary Figure 3: the protective effects of NSA against iron overload-induced cytotoxicity in osteoblastic cells. After subjecting to FAC (200 μ M) with or without NSA (1-32 μ M) for 120 h, the viability of osteoblastic cells was detected by CCK-8 assays. Values are expressed as the means \pm SD from three independent experiments (* p < 0.05 vs. saline control; # p < 0.05 vs. FAC 200) (Supplementary Materials).

References

- [1] T. Nakamura, I. Naguro, and H. Ichijo, "Iron homeostasis and iron-regulated ROS in cell death, senescence and human diseases," *Biochimica et Biophysica Acta - General Subjects*, vol. 1863, no. 9, pp. 1398–1409, 2019.
- [2] S. J. Dixon and B. R. Stockwell, "The role of iron and reactive oxygen species in cell death," *Nature Chemical Biology*, vol. 10, no. 1, pp. 9–17, 2014.
- [3] B.-J. Kim, S. H. Ahn, S. J. Bae et al., "Iron overload accelerates bone loss in healthy postmenopausal women and middle-aged men: a 3-year retrospective longitudinal study," *Journal of Bone and Mineral Research*, vol. 27, no. 11, pp. 2279–2290, 2012.
- [4] K. Steer, M. Stavnychuk, M. Morris, and S. V. Komarova, "Bone health in patients with hematopoietic disorders of bone marrow origin: systematic review and Meta- Analysis," *Journal of Bone and Mineral Research*, vol. 32, no. 4, pp. 731–742, 2017.
- [5] P. Wong, P. J. Fuller, M. T. Gillespie et al., "Thalassemia bone disease: a 19-year longitudinal analysis," *Journal of Bone and Mineral Research*, vol. 29, no. 11, pp. 2468–2473, 2014.

- [6] J. Tsay, Z. Yang, F. P. Ross et al., "Bone loss caused by iron overload in a murine model: importance of oxidative stress," *Blood*, vol. 116, no. 14, pp. 2582–2589, 2010.
- [7] X. Jing, T. Du, K. Chen et al., "Icariin protects against iron overload-induced bone loss via suppressing oxidative stress," *Journal of Cellular Physiology*, vol. 234, no. 7, pp. 10123–10137, 2018.
- [8] H. Isomura, K. Fujie, K. Shibata et al., "Bone metabolism and oxidative stress in postmenopausal rats with iron overload," *Toxicology*, vol. 197, no. 2, pp. 92–99, 2004.
- [9] Q. Tian, S. Wu, Z. Dai et al., "Iron overload induced death of osteoblasts in vitro: involvement of the mitochondrial apoptotic pathway," *Peer J*, vol. 4, p. e2611, 2016.
- [10] A. S.-d. Valle, A. Anel, J. Naval, and I. Marzo, "Immunogenic Cell Death and Immunotherapy of Multiple Myeloma," *Frontiers in Cell and Developmental Biology*, vol. 7, 2019.
- [11] M. Pasparakis and P. Vandenabeele, "Necroptosis and its role in inflammation," *Nature*, vol. 517, no. 7534, pp. 311–320, 2015.
- [12] H. Blaser, C. Dostert, T. W. Mak, and D. Brenner, "TNF and ROS crosstalk in inflammation," *Trends in Cell Biology*, vol. 26, no. 4, pp. 249–261, 2016.
- [13] M. Fritsch, S. D. Günther, R. Schwarzer et al., "Caspase-8 is the molecular switch for apoptosis, necroptosis and pyroptosis," *Nature*, vol. 575, no. 7784, pp. 683–687, 2019.
- [14] K. Newton and G. Manning, "Necroptosis and inflammation," *Annual Review of Biochemistry*, vol. 85, no. 1, pp. 743–763, 2016.
- [15] N. Takahashi, L. Vereecke, M. J. M. Bertrand et al., "RIPK1 ensures intestinal homeostasis by protecting the epithelium against apoptosis," *Nature*, vol. 513, no. 7516, pp. 95–99, 2014.
- [16] L. Sun, H. Wang, Z. Wang et al., "Mixed lineage kinase domain-like protein mediates necrosis signaling downstream of RIP3 kinase," *Cell*, vol. 148, no. 1–2, pp. 213–227, 2012.
- [17] J. A. Rickard, J. A. O'Donnell, J. M. Evans et al., "RIPK1 regulates RIPK3-MLKL-driven systemic inflammation and emergency hematopoiesis," *Cell*, vol. 157, no. 5, pp. 1175–1188, 2014.
- [18] Y. Ito, D. Ofengeim, A. Najafav et al., "RIPK1 mediates axonal degeneration by promoting inflammation and necroptosis in ALS," *Science*, vol. 353, no. 6299, pp. 603–608, 2016.
- [19] Y. Zhang, S. S. Su, S. Zhao et al., "RIP1 autophosphorylation is promoted by mitochondrial ROS and is essential for RIP3 recruitment into necrosome," *Nature Communications*, vol. 8, no. 1, 2017.
- [20] F. Wauquier, A. Daneault, H. Granel et al., "Human enriched serum following hydrolysed collagen absorption modulates bone cell activity: from bedside to bench and vice versa," *Nutrients*, vol. 11, no. 6, p. 1249, 2019.
- [21] R. H. Toor, S. Malik, H. Qamar et al., "Osteogenic potential of hexane and dichloromethane fraction of *Cissus quadrangularis* on murine preosteoblast cell line MC3T3-E1 (subclone 4)," *Journal of Cellular Physiology*, vol. 234, no. 12, pp. 23082–23096, 2019.
- [22] D. Xia, J. Wu, M. Xing et al., "Iron overload threatens the growth of osteoblast cells via inhibiting the PI3K/AKT/FOXO3a/DUSP14 signaling pathway," *Journal of Cellular Physiology*, vol. 234, no. 9, pp. 15668–15677, 2019.
- [23] S. Chen, X. Lv, B. Hu et al., "RIPK1/RIPK3/MLKL-mediated necroptosis contributes to compression-induced rat nucleus pulposus cells death," *Apoptosis*, vol. 22, no. 5, pp. 626–638, 2017.
- [24] S. Chen, X. Lv, B. Hu et al., "Critical contribution of RIPK1 mediated mitochondrial dysfunction and oxidative stress to compression-induced rat nucleus pulposus cells necroptosis and apoptosis," *Apoptosis*, vol. 23, no. 5–6, pp. 299–313, 2018.
- [25] X. Cai, Y. Liu, Y. Hu et al., "ROS-mediated lysosomal membrane permeabilization is involved in bupivacaine-induced death of rabbit intervertebral disc cells," *Redox Biology*, vol. 18, pp. 65–76, 2018.
- [26] L. Zhao, H. Lin, S. Chen et al., "Hydrogen peroxide induces programmed necrosis in rat nucleus pulposus cells through the RIP1/RIP3- PARP-AIF pathway," *Journal of Orthopaedic Research*, vol. 36, no. 4, pp. 1269–1282, 2018.
- [27] Q. Tian, Y. Gu, F. Wang et al., "Upregulation of miRNA-154-5p prevents the tumorigenesis of osteosarcoma," *Biomedicine & Pharmacotherapy*, vol. 124, no. 124, p. 109884, 2020.
- [28] Z. Li, S. Chen, S. Chen, D. Huang, K. Ma, and Z. Shao, "Moderate activation of Wnt/ β -catenin signaling promotes the survival of rat nucleus pulposus cells via regulating apoptosis, autophagy, and senescence," *Journal of Cellular Biochemistry*, vol. 120, no. 8, pp. 12519–12533, 2019.
- [29] Y. Jia, F. Wang, Q. Guo et al., "Curcumol induces RIPK1/RIPK3 complex-dependent necroptosis via JNK1/2-ROS signaling in hepatic stellate cells," *Redox Biology*, vol. 19, pp. 375–387, 2018.
- [30] W. Zhao, H. Feng, W. Sun, K. Liu, J.-J. Lu, and X. Chen, "tert-butyl hydroperoxide (t-BHP) induced apoptosis and necroptosis in endothelial cells: roles of NOX4 and mitochondrion," *Redox Biology*, vol. 11, pp. 524–534, 2017.
- [31] F. Yang, L. Yang, Y. Li et al., "Melatonin protects bone marrow mesenchymal stem cells against iron overload-induced aberrant differentiation and senescence," *Journal of Pineal Research*, vol. 63, no. 3, 2017.
- [32] Z. Wang, H. Jiang, S. Chen, F. Du, and X. Wang, "The mitochondrial phosphatase PGAM5 functions at the convergence point of multiple necrotic death pathways," *Cell*, vol. 148, no. 1–2, pp. 228–243, 2012.
- [33] T. Zhang, Y. Zhang, M. Cui et al., "CaMKII is a RIP3 substrate mediating ischemia- and oxidative stress-induced myocardial necroptosis," *Nature Medicine*, vol. 22, no. 2, pp. 175–182, 2016.
- [34] B. Schenk and S. Fulda, "Reactive oxygen species regulate Smac mimetic/TNF α -induced necroptotic signaling and cell death," *Oncogene*, vol. 34, no. 47, pp. 5796–5806, 2015.
- [35] F. Mitchell, "Bone: high body iron stores lead to bone loss," *Nature Reviews Endocrinology*, vol. 8, no. 9, p. 506, 2012.
- [36] V. De Sanctis, A. T. Soliman, H. Elsefy et al., "Bone disease in β -thalassemia patients: past, present and future perspectives," *Metabolism*, vol. 80, pp. 66–79, 2018.
- [37] F. Rossi, S. Perrotta, G. Bellini et al., "Iron overload causes osteoporosis in thalassemia major patients through interaction with transient receptor potential vanilloid type 1 (TRPV1) channels," *Haematologica*, vol. 99, no. 12, pp. 1876–1884, 2014.
- [38] A. Linkermann and D. R. Green, "Necroptosis," *The New England Journal of Medicine*, vol. 370, no. 5, pp. 455–465, 2014.
- [39] J. Yuan, P. Amin, and D. Ofengeim, "Necroptosis and RIPK1-mediated neuroinflammation in CNS diseases," *Nature Reviews Neuroscience*, vol. 20, no. 1, pp. 19–33, 2019.

- [40] X. Yao, X. Jing, J. Guo et al., "Icariin protects bone marrow mesenchymal stem cells against iron overload induced dysfunction through mitochondrial fusion and fission, PI3K/AKT/mTOR and MAPK pathways," *Frontiers in Pharmacology*, vol. 10, 2019.
- [41] W. Tonnus and A. Linkermann, "The in vivo evidence for regulated necrosis," *Immunological Reviews*, vol. 277, no. 1, pp. 128–149, 2017.
- [42] K. Newton, "RIPK1 and RIPK3: critical regulators of inflammation and cell death," *Trends in Cell Biology*, vol. 25, no. 6, pp. 347–353, 2015.
- [43] W. Zhou and J. Yuan, "SnapShot: necroptosis," *Cell*, vol. 158, no. 2, pp. 464–464.e1, 2014.
- [44] D. Xu, T. Jin, H. Zhu et al., "TBK1 suppresses RIPK1-driven apoptosis and inflammation during development and in aging," *Cell*, vol. 174, no. 6, pp. 1477–1491.e19, 2018.
- [45] M. Dannappel, K. Vlantis, S. Kumari et al., "RIPK1 maintains epithelial homeostasis by inhibiting apoptosis and necroptosis," *Nature*, vol. 513, no. 7516, pp. 90–94, 2014.
- [46] K. Newton, K. E. Wickliffe, D. L. Dugger et al., "Cleavage of RIPK1 by caspase-8 is crucial for limiting apoptosis and necroptosis," *Nature*, vol. 574, no. 7778, pp. 428–431, 2019.
- [47] J. Silke, J. A. Rickard, and M. Gerlic, "The diverse role of RIP kinases in necroptosis and inflammation," *Nature Immunology*, vol. 16, no. 7, pp. 689–697, 2015.
- [48] I. Ganzleben, G.-W. He, C. Günther et al., "PGAM5 is a key driver of mitochondrial dysfunction in experimental lung fibrosis," *Cellular and Molecular Life Sciences*, vol. 76, no. 23, pp. 4783–4794, 2019.
- [49] G.-W. He, C. Günther, A. E. Kremer et al., "PGAM5-mediated programmed necrosis of hepatocytes drives acute liver injury," *Gut*, vol. 66, no. 4, pp. 716–723, 2017.
- [50] S.-L. Zhang, H.-B. Tang, J.-T. Hu et al., "PGAM5-CypD pathway is involved in bromocriptine-induced RIP3/MLKL-dependent necroptosis of prolactinoma cells," *Biomedicine & Pharmacotherapy*, vol. 111, pp. 638–648, 2019.
- [51] Y. Wang, J. Jiao, S. Zhang, C. Zheng, and M. Wu, "RIP3 inhibition protects locomotion function through ameliorating mitochondrial antioxidative capacity after spinal cord injury," *Biomedicine & Pharmacotherapy*, vol. 116, article 109019, 2019.
- [52] W. J. Cen, Y. Feng, S. S. Li et al., "Iron overload induces G1 phase arrest and autophagy in murine preosteoblast cells," *Journal of Cellular Physiology*, vol. 233, no. 9, pp. 6779–6789, 2018.

Research Article

African Vegetables (*Clerodendrum volubile* Leaf and *Irvingia gabonensis* Seed Extracts) Effectively Mitigate Trastuzumab-Induced Cardiotoxicity in Wistar Rats

Olufunke Olorundare,¹ Adejuwon Adeneye ,² Akinyele Akinsola,¹ Sunday Soyemi,³ Alban Mgbahoma,³ Ikechukwu Okoye,⁴ James M. Ntambi,⁵ and Hasan Mukhtar ⁶

¹Department of Pharmacology and Therapeutics, Faculty of Basic Medical Sciences, College of Health Sciences, University of Ilorin, Ilorin, Kwara State, Nigeria

²Department of Pharmacology, Therapeutics and Toxicology, Faculty of Basic Clinical Sciences, Lagos State University College of Medicine, 1-5 Oba Akinjobi Way, G.R.A., Ikeja, Lagos State, Nigeria

³Department of Pathology and Forensic Medicine, Faculty of Basic Clinical Sciences, Lagos State University College of Medicine, 1-5 Oba Akinjobi Way, G.R.A., Ikeja, Lagos State, Nigeria

⁴Department of Oral Pathology and Medicine, Faculty of Dentistry, Lagos State University College of Medicine, 1-5 Oba Akinjobi Way, G.R.A., Ikeja, Lagos State, Nigeria

⁵Department of Nutritional Sciences, College of Agricultural and Life Sciences, University of Wisconsin, Madison, 433 Babcock Drive, Madison, WI 53706-1544, USA

⁶Department of Dermatology, University of Wisconsin, Madison, Medical Science Center, 1300 University Avenue, Madison, WI 53706, USA

Correspondence should be addressed to Adejuwon Adeneye; adeneye2001@yahoo.com

Received 29 May 2020; Revised 14 September 2020; Accepted 22 September 2020; Published 15 October 2020

Academic Editor: Demetrios Kouretas

Copyright © 2020 Olufunke Olorundare et al. This is an open access article distributed under the Creative Commons Attribution License, which permits unrestricted use, distribution, and reproduction in any medium, provided the original work is properly cited.

Trastuzumab (*TZM*) is a humanized monoclonal antibody that has been approved for the clinical management of HER2-positive metastatic breast and gastric cancers but its use is limited by its cumulative dose and off-target cardiotoxicity. Unfortunately, till date, there is no approved antidote to this off-target toxicity. Therefore, an acute study was designed at investigating the protective potential and mechanism(s) of *CVE* and *IGE* in *TZM*-induced cardiotoxicity utilizing cardiac enzyme and oxidative stress markers and histopathological endpoints. 400 mg/kg/day *CVE* and *IGE* dissolved in 5% DMSO in sterile water were investigated in Wistar rats injected with 2.25 mg/kg/day/*i.p.* route of *TZM* for 7 days, using serum *cTnI* and LDH, complete lipid profile, cardiac tissue oxidative stress markers assays, and histopathological examination of *TZM*-intoxicated heart tissue. Results showed that 400 mg/kg/day *CVE* and *IGE* profoundly attenuated increases in the serum *cTnI* and LDH levels but caused no significant alterations in the serum lipids and weight gain pattern in the treated rats. *CVE* and *IGE* profoundly attenuated alterations in the cardiac tissue oxidative stress markers' activities while improving *TZM*-associated cardiac histological lesions. These results suggest that *CVE* and *IGE* could be mediating its cardioprotection via antioxidant, free radical scavenging, and antithrombotic mechanisms, thus, highlighting the therapeutic potentials of *CVE* and *IGE* in the management of *TZM*-mediated cardiotoxicity.

1. Introduction

Trastuzumab, a humanized monoclonal antibody targeted against epidermal growth factor receptor 2 (HER2), was

approved by the United States Food and Drug Administration (FDA) for the clinical management of HER2-positive breast cancers either as an adjuvant or neoadjuvant, and metastatic breast and gastric carcinomas and metastatic

gastric cancer [1]. In mediating its cytotoxic action, trastuzumab is known to bind to the domain IV of the extracellular domain of HER2 and triggers cascade tumor-suppressive actions including the activation of antibody-dependent cell-mediated cytotoxicity, inhibition of HER2 extracellular domain cleavage, disruption of HER2 receptor homo- and heterodimerization extracellular segment of HER2 and consequently resulting in the inhibition of HER2-mediated malignant transformation [1, 2]. Trastuzumab use as a key treatment therapy for advanced HER2-positive breast carcinoma has also been reported to have yielded unequivocal improvements in the clinical treatment outcome of this disease [3]. Clinically, trastuzumab is either used alone or in combination with other cytotoxic agents especially with the anthracycline doxorubicin usually in a pegylated form although it is reported to be most effective in its combination form [4] since DOX enters its target cells by simple diffusion, intercalates into DNA, and inhibits topoisomerase II to hinder and completely stall DNA replication [5]. However, wide-scale clinical use of trastuzumab-based therapies has been significantly limited by its adverse cardiac dysfunctions and dilated cardiomyopathy-related congestive heart failures, which have been reported to occur in up to 27% of HER2-positive metastatic breast cancer patients on its combination therapy with doxorubicin [2]. Trastuzumab has been reported to dysregulate HER2 signaling pathways and suppress autophagy by activating autophagy-inhibitory Erk/mTOR/Ulk 1 signaling cascade in cardiomyocytes and overtly resulting in the massive mitochondrial and toxic reactive oxygen species (ROS) accumulation in human cardiomyocytes [6, 7]. As a clinical strategy of preventing the development of trastuzumab-induced cardiotoxicity, Wu et al. [8] recently investigated and reported the clinical efficacy and attenuation of trastuzumab-induced cardiac dysfunction in HER2-positive breast cancer patients using fixed 440 mg dose monthly administration of trastuzumab. Unfortunately, till date, there are no approved effective therapeutic agent(s) available that could prevent the development of this unwanted/adverse effect of trastuzumab without comprising its efficacy.

Clerodendrum volubile P. Beauv (known as White butterfly in English language) is a climbing and edible West African vegetable, belonging to the *Verbenaceae* family [9] but was recently reclassified to as belonging to the *Labiatae* family [10]. In the Niger-Delta region of Nigeria where the plant is predominantly cultivated for consumption wholly as green leafy vegetable or as food condiment to improve soup taste, it is used for the local management of gouty arthritis, rheumatism, dropsy, swellings/edema, and ulcers [9, 11]. Phytochemically, *Clerodendrum volubile* leaf extracts have been reported to contain secondary metabolites such as alkaloids, flavonoids, saponins, anthraquinone, and cardiac glycoside [12]. The phenolic-rich solvent fractions of the plant extract have been reported to elicit antihyperglycemic activity through α -amylase, α -glucosidase, and improvement in the glucose tolerance while its antihypertensive activity was mediated via angiotensin I converting enzyme inhibition [9, 10]. Similarly, the antioxidative, immunomodulatory,

anti-inflammatory, and cytotoxic activities of the plant have also been reported [12–15]. *Clerodendrum volubile* is reported to be very rich in polyphenols (especially flavonoids) content which is conferred on its potent antioxidant potential [9, 16, 17].

Irvingia gabonensis (Aubry-Lecomte ex O'Rorke) Bail belonging to the family, Irvingiaceae, is known as African Mango (in English). Its common English names include bread tree, African wild mango, wild mango, and bush mango [18, 19], while its local names in Nigeria include "Apon" and "Ogbono" (amongst the Yoruba, Southwest Nigeria and Igbo, Southeast Nigeria, respectively). *Irvingia gabonensis* is widely cultivated in West African countries including southwest and southeast Nigeria, southern Cameroon, Côte d'Ivoire, Ghana, Togo, and Benin, to produce its edible fruit whose seed is used in the preparation of local delicious viscous soup for swallowing yam and cassava puddings [20]. Fat extracted from its seeds is commonly known as dika fat and majorly consists of C12 and C14 fatty acids, alongside with smaller quantities of C10, C16 and C18, glycerides, and proteins [20]. *Irvingia gabonensis* seeds are also a good source of nutrients including a variety of vitamins and minerals such as sodium, calcium, magnesium, phosphorus, and iron. It is also a rich source of flavonoids (quercetin and kaempferol), ellagic acid, mono-, di-, and tri-O-methyl-ellagic acids, and their glycosides which are potent antioxidants [21, 22]. Phytochemical analysis of its seeds showed that it contains tannins, alkaloids, flavonoids, cardiac glycosides, steroids, carbohydrate, volatile oils, and terpenoids [23–25] and its proximate composition of moisture $1.4 \pm 0.11\%$, ash $6.8 \pm 0.12\%$, crude lipid $7.9 \pm 0.01\%$, crude fibre $21.6 \pm 0.45\%$, and crude protein $5.6 \pm 0.20\%$ [25]. Similarly, proximate analysis of its soup shows that it contains 9% protein, 70.42% fat, 4.61% fibre, 1.92% ash, and 11.91% carbohydrate [26]. Specific compounds already isolated from the seed extract of include: methyl 2-[2-formyl-5-(hydroxymethyl)-1 H-pyrrol-1yl]-propanoate, kaempferol-3-O- β -D-6'' (p-coumaroyl) glucopyranoside and lupeol (3 β -lup-20(29)-en-3-ol with lupeol exhibiting the most abundant with the most significant antioxidant activities [27].

In the absence of any clinically approved chemotherapeutic or chemoprophylactic agents for the clinical management of trastuzumab-induced cardiovascular events, the current study was designed at investigating possible ameliorative potential of the ethanol extracts of *Clerodendrum volubile* leaves and *Irvingia gabonensis* seeds in trastuzumab-induced cardiotoxicity in Wistar rats intraperitoneally injected with 2.25 mg/kg/day of trastuzumab for 7 days. The effects of oral pretreatments with 400 mg/kg/day of *Clerodendrum volubile* ethanol leaf extract as well as 400 mg/kg/day of *Irvingia gabonensis* ethanol seed extract were investigated in trastuzumab intoxicated rat hearts using cardiac enzyme biomarkers such as cardiac troponin I (*cTnI*) and cardiac lactate dehydrogenase (LDH), complete lipid profile, cardiovascular disease risk indices (atherogenic index (AI) and coronary artery disease risk index (CRI)), oxidative stress markers, as well as the histopathological studies of the trastuzumab-treated cardiac tissues as measuring endpoints for the study.

2. Materials and Methods

2.1. Plant Materials. Stock of fresh mature whole plants of *Clerodendrum volubile* and fresh seeds of *Irvingia gabonensis* were purchased from Herbal Vendors in Isikan Market in Akure, Ondo State, Nigeria, in the month of February 2020. Samples of the *Clerodendrum volubile* plant obtained were subjected to botanical identification and referencing at the University of Ilorin (UNILORIN) Herbarium with a voucher specimen number: UIL/001/2019/1254 as previously reported by Akinsola (2019) [28]. Fresh leaves, inflorescence, and fruits of *Irvingia gabonensis* were equally processed for botanical identification and authentication and voucher specimen with reference number (UIL/001/2019/1364) was also deposited in UNILORIN Herbarium.

2.2. Extraction Process. Fresh leaves of *Clerodendrum volubile* were destalked from the whole plant, then gently but thoroughly rinsed under running tap water and completely air-dried at the room temperature (28-33°C) until the weight of the dried leaves was constant. The dried leaves were then pulverized using Milling Machine and kept in water- and airtight containers.

1.50 kg of the pulverized leaves was completely macerated in 8 liters of absolute ethanol at room temperature for 5 days but intermittently shaken to ensure complete dissolution. Thereafter, the solution was first filtered with cotton wool and then 110 mm Whatman filter paper. The resultant filtrate was then concentrated *in vacuo* using a rotary evaporator (B'U'CHI Rotavapor® Model R-215, Switzerland) with Vacuum Module V-801 EasyVac®, Switzerland) set at a revolution of 70 rpm and a temperature at 36°C before it was completely dried over a water bath preset at 40°C. The jelly-like, dark-colored residue left behind was weighed, stored in air- and water-proof container which was kept in a refrigerator at 4°C. From this stock, fresh solutions were made whenever required.

%Yield was calculated as $\text{Yield} = \frac{\text{weight of crude extract obtained (g)}}{\text{weight of starting pulverized dry leaf extracted (g)}} \times 100$.

The same procedure was performed with 1.5 kg of the pulverized, dried seeds of *Irvingia gabonensis*.

2.3. Experimental Animals. Young adult male Wistar Albino rats (aged 8-12 weeks old and body weight: 150-190 g) used in this study were obtained from the Animal House of the Lagos State University College of Medicine, Ikeja, Lagos State, Nigeria, after an ethical approval (UERC Approval number: UERC/ASN/2020/2072) was obtained from the University of Ilorin Ethical Review Committee for Postgraduate Research. The rats were handled in accordance with international principles guiding the Use and Handling of Experimental Animals [29]. The rats were maintained on standard rat feed (Ladokun Feeds, Ibadan, Oyo State, Nigeria) and potable water which were made available *ad libitum*. The rats were maintained at an ambient temperature between 28-30°C, humidity of 55 ± 5%, and standard (natural) photoperiod of approximately 12/12 hours of alternating light and dark periodicity.

2.4. Measurement of Body Weight. The body weights of rats were taken on days 1 and 7 of the experiment and determined on a digital rodent weighing scale (®Virgo Electronic Compact Scale, New Delhi, India). The obtained values were expressed in grams (g).

2.5. Induction of Trastuzumab- (TZM-) Induced Cardiotoxicity and Other Drug Treatment of Rats. Prior to commencement of the experiment, rats were randomly allotted into 7 groups of 7 rats per group such that the weight difference between and within groups was not more than ±20% of the average weight of the sample population of rats used for the study. However, the choice of the therapeutic dose range of 400 mg/kg/day of *CVE* and *IGE* was made based on the results of the preliminary studies conducted.

In this experimental repeated-dose model, Group I rats which served as untreated control were orally pretreated with 10 ml/kg/day of sterile water but equally treated with 1 ml/kg/day of sterile water and administered via intraperitoneally for 7 days. Group II and III rats were orally treated with 400 mg/kg/day of *CVE* and *IGE* dissolved in 5% DMSO sterile water (*CVE* and *IGE* being only partly soluble in water and DMSO an organosulfur polar aprotic and inert solvent that readily dissolves both polar and nonpolar compounds) but treated with 1 ml/kg/day of sterile water and administered intraperitoneally for 7 days, respectively. Group IV rats were orally pretreated with 10 ml/kg/day of sterile water 3 hours before intraperitoneal injection of 2.25 mg/kg/day of *TZM* (®CAMMab, Biocon Limited, Km 34 Tumkur Road, T-Bengur, Nelamangala Taluk, Bangalore-56 123, India) dissolved in accompanying sterile water for 7 days. Group V rats which served as the positive control group were equally pretreated with 20 mg/kg/day of Vitamin C 3 hours before treatment with 2.25 mg/kg/day of *TZM* dissolved in sterile water administered intraperitoneally for 7 days. Group VI and VII rats were orally pretreated with 400 mg/kg/day of *CVE* and *IGE* 3 hours before treatment with 2.25 mg/kg of *TZM* dissolved in sterile water and administered intraperitoneally daily for 7 days (Table 1). The choice of vitamin C was made being a standard antioxidant agent, and its effect as positive control was compared with other treatment groups. The dose of *TZM* adopted was as described by Poon et al. [30] and Riccio et al. [31].

2.6. Blood Sample Collection. On the 7th day which was the last day of the experiment, the rats were weighed and later fasted overnight but drinking water was made available *ad libitum*. On the 8th day, fasted rats were sacrificed and whole blood samples were collected directly from the heart under inhaled diethyl ether anesthesia. Blood samples were carefully collected with a fine 21G Needle and 5 ml Syringe (Hangzhou Longde Medical Products Co. Ltd., Hangzhou, China) without causing damage to the heart tissues. The rat heart, liver, and kidneys were identified, harvested *en bloc*, and weighed on a digital weighing scale.

2.7. Biochemical Assays. Blood samples obtained directly from the heart chamber were allowed to clot and then centrifuged at 5000 rpm to separate clear sera from the clotted

TABLE 1: Group treatment of rats.

Groups	Treatments
Group I	10 ml/kg/day of sterile water <i>p.o.</i> for 7 days + 1 ml/kg/day of sterile water given <i>i.p.</i> for 7 days
Group II	400 mg/kg/day of CVE dissolved in 5% DMSO-sterile water <i>p.o.</i> for 7 days + 1 ml/kg/day of sterile water given <i>i.p.</i> for 7 days
Group III	400 mg/kg/day of IGE dissolved in 5% DMSO-sterile water <i>p.o.</i> for 7 days + 1 ml/kg/day of sterile water given <i>i.p.</i> for 7 days
Group IV	10 ml/kg/day of sterile water <i>p.o.</i> for 7 days + 2.25 mg/kg/day of TZM dissolved in sterile water given <i>i.p.</i> for 7 days
Group V	20 mg/kg/day of vitamin C dissolved in sterile water <i>p.o.</i> for 7 days + 2.25 mg/kg/day of TZM dissolved in sterile water given <i>i.p.</i> for 7 days
Group VI	400 mg/kg/day of CVE dissolved in 5% DMSO-sterile water <i>p.o.</i> for 7 days + 2.25 mg/kg/day of TZM dissolved in sterile water given <i>i.p.</i> for 7 days
Group VII	400 mg/kg/day of IGE dissolved in 5% DMSO-sterile water <i>p.o.</i> for 7 days + 2.25 mg/kg/day of TZM dissolved in sterile water given <i>i.p.</i> for 7 days

blood samples. The clear samples were obtained for assays of the following biochemical parameters: serum cardiac troponin I, LDH, TG, TC, and cholesterol fractions (HDL-c, LDL-c, and VLDL-c). Serum lipids were assayed using methods of Tietz [32] while serum *cTnI* and LDH were estimated standard bioassay procedures.

2.8. Calculation of AI and CRI. AI was calculated as $\text{LDL} - \text{c} (\text{mg/dl}) \div \text{HDL} - \text{c} (\text{mg/dl})$ [33] while CRI was calculated as $\text{TC} (\text{mg/dl}) \div \text{HDL} - \text{c} (\text{mg/dl})$ [34].

2.9. Determination of Antioxidant Activities in the Rat Cardiac Tissues. After the rats were sacrificed humanely under inhaled diethyl ether, the heart was harvested *en bloc*. The heart was gently and carefully divided into two halves (each consisting of the atrium and ventricle) using a new surgical blade. The left half of the heart was briskly rinsed in ice-cold 1.15% KCl solution in order to preserve the oxidative enzyme activities of the heart before being placed in a clean sample bottle which itself was in an ice-pack filled cooler. This is to prevent the breakdown of the oxidative stress enzymes in these organs.

2.9.1. Determination of SOD Activities in the Heart Tissues. Superoxide dismutase activity was determined by its ability to inhibit the autooxidation of epinephrine by the increase in absorbance at 480 nm as described by Paoletti et al. [35]. Enzyme activity was calculated by measuring the change in absorbance at 480 nm for 5 minutes.

2.9.2. Determination of CAT Activities in the Heart Tissues. Tissue CAT activities were determined by the method described by Hadwan [36]. The specific activity of CAT was expressed as U/ml.

2.9.3. Determination of GSH, GPx, and GST Activities in the Heart Tissue. The reduced glutathione (GSH) content in the heart tissue was estimated according to the method described by Rahman et al. [37]. To the homogenate, 10% TCA was added and centrifuged. One millilitre of the supernatant was treated with 0.5 ml of Elman's reagent (19.8 mg of 5,5-dithiobisnitro benzoic acid (DTNB) in 100 ml of 0.1% sodium nitrate) and -3.0 ml of phosphate buffer (0.2 M, pH 8.0). The absorbance was read at 412 nm. Similarly, GPx and GST activities were determined using the method of Faraji et al. [38] and Vontas et al. [39].

2.9.4. Determination of MDA Activities in the Heart Tissues. The method of Buege and Aust [40] was adopted in determining MDA activities in the cardiac tissue. One millilitre of supernatant was added to 2 ml of (1:1:1 ratio) TCA-TBA-HCl reagent (thiobarbituric acid 0.37%, 0.24 N HCl, and 15% TCA) tricarboxylic acid, thiobarbituric acid, reagent boiled at 100°C for 15 minutes, and allowed to cool. Flocculent material was removed by centrifuging at 3000 rpm for ten minutes. The supernatant was removed, and the absorbance was read at 532 nm against a blank. MDA was calculated using the molar extinction for MDA-TBA-complex of $1.56 \times 10^5 \text{ m}^{-1} \text{ cm}^{-1}$.

2.9.5. Histopathological Studies of the Heart. Using the remaining equally divided harvested heart, the right halves of the seven randomly selected rats from each treatment and control groups were subjected to histopathological examinations, the right ventricle being the most susceptible to doxorubicin toxicity of the heart chambers. After rinsing in normal saline, the dissected right half of was preserved in 10% formo-saline before it was completely dehydrated in absolute (100%) ethanol. It was then embedded in routine paraffin blocks. From the embedded paraffin blocks, 4-5 μm thick sections of the tissue was prepared and stained with hematoxylin-eosin stain. These were examined under a photomicroscope (Model N-400ME, CEL-TECH Diagnostics, Hamburg, Germany) connected with a host computer. Sections were illuminated with white light from a 12 V halogen lamp (100 W) after filtering with a 520 nm monochromatic filter. The slides were examined for associated histopathological lesions [41].

2.10. Statistical Analysis. Data were presented as mean \pm S.D. and mean \pm S.E.M. of seven observations for the body weight and biochemical parameters, respectively. Statistical analysis was done using a two-way analysis of variance followed by post hoc test, Student-Newman-Keuls test on GraphPad Prism Version 5. Statistical significance was considered at $p < 0.05$, $p < 0.01$, and $p < 0.001$.

3. Results

3.1. %Yield. Complete extraction of the pulverized dry leaves *Clerodendrum volubile* in absolute ethanol was calculated to be 8.39%. The resultant residue was a dark color, sticky and jelly-like, sweet-smelling (bland) residue which was not completely soluble in water but completely soluble in methanol and ethanol. Similarly, complete extraction of *Irvingia*

gabonensis ethanol seed extract in absolute ethanol resulted in a yield of 58%, which was a dark brown oily and aromatic residue that was only soluble in methanol and ethanol.

3.2. Effect of CVE and IGE on the Average Body Weight of TZM-Treated Rats. Table 2 shows the effect of repeated daily intraperitoneal injection with 2.25 mg/kg of TZM and oral pretreatments with 20 mg/kg/day of vit. C and 400 mg/kg/day of CVE and IGE, respectively, on the average body weight on days 1 and 7, percentage weight change (% Δ wt.), and relative heart weight of treated rats. Repeated intraperitoneal TZM injection did not significantly alter ($p > 0.05$) the weight gain pattern and relative heart weight in the TZM only treated (Group IV) rats when compared to untreated control (normal) rats (Group II) as well as CVE- (Group VI) and IGE- (Group VII) pretreated rats (Table 2). Similarly, vit. C pretreatment did not significantly alter the weight gain pattern and relative heart weight in the TZM-treated rats (Table 2).

3.3. Effect of CVE and IGE on Cardiac Marker Enzymes (LDH and *cTnI*) of TZM-Treated Rats. Repeated daily intraperitoneal TZM injection for 7 days resulted in significant increases ($p < 0.0001$) in the serum LDH and *cTnI* levels when compared to that of untreated negative (control) (Group I) values (Table 3). However, 400 mg/kg/day of CVE and IGE oral pretreatments significantly attenuated ($p < 0.0001$) increases in the serum LDH and *cTnI* levels (Table 3). Similarly, 20 mg/kg/day of vit. C pretreatment also significantly ($p < 0.001$ and $p < 0.0001$) attenuated increases in the serum LDH and *cTnI* though at a lower level of statistical significance when compared to either CVE or IGE (Table 3).

3.4. Effect of CVE and IGE on the Serum Lipids (TG, TC, HDL-c, LDL-c, and VLDL-c) Level of TZM-Treated Rats. Repeated TZM intraperitoneal injections did not cause significant ($p > 0.05$) alterations in the serum lipids measured when compared to the untreated control (Group I) values (Table 4). However, repeated daily oral pretreatments with 400 mg/kg/day of CVE and IGE resulted in insignificant reductions in the serum levels of TG, TC, HDL-c, LDL-c, and VLDL-c when compared to TZM only-treated rats (Table 4). Similarly, vit. C did not cause significant ($p > 0.05$) alterations in the serum TG, TC, LDL-c, and VLDL-c levels when compared to TZM only-treated rats (Table 4).

3.5. Effect of CVE and IGE on the Atherogenic Index (AI) and Coronary Artery Disease Index (CRI) of TZM-Treated Rats. Repeated intraperitoneal injections with 2.25 mg/kg/day of TZM to treated rats resulted in an insignificant ($p > 0.05$) increase in the AI and CRI values when compared to the untreated control (Group I), CVE only treated (Group II), and IGE only treated (Group III) values (Table 5). Oral pretreatments with 400 mg/kg/day of CVE and IGE, however, resulted in insignificant ($p > 0.05$) reductions in the AI and CRI values when compared to TZM only-treated rats (Table 5). Similar insignificant reductions ($p > 0.05$) in the AI and CRI values were caused by 20 mg/kg/day of vit. C oral pretreatment (Table 5).

TABLE 2: Effect of repeated oral pretreatments with 400 mg/kg/day of CVE and IGE on the average body weights on days 1 and 7, percentage change in weight (% Δ wt.) and relative heart weight (RHW) of TZM-treated rats.

Group	Day 1 bwt. (g)	Day 7 bwt. (g)	% Δ wt.	RHW
I	175.8 \pm 25.2	183.9 \pm 20.5	05.1 \pm 04.9	0.25 \pm 0.01
II	178.2 \pm 27.9	189.9 \pm 34.4	06.2 \pm 05.1	0.30 \pm 0.02
III	183.4 \pm 37.7	190.0 \pm 39.9	03.5 \pm 02.9	0.36 \pm 0.04
IV	177.1 \pm 20.4	188.5 \pm 23.6	06.4 \pm 02.6	0.37 \pm 0.01
V	176.2 \pm 20.5	185.0 \pm 23.5	06.0 \pm 05.4	0.38 \pm 0.02
VI	171.5 \pm 17.7	178.4 \pm 17.2	04.2 \pm 04.1	0.34 \pm 0.02
VII	171.5 \pm 21.4	180.7 \pm 22.9	04.0 \pm 04.3	0.40 \pm 0.03

TABLE 3: Effect of 400 mg/kg/day of CVE and IGE on serum LDH and *cTn I* in TZM-intoxicated rats.

Treatment groups	LDH (U/L)	<i>cTn I</i> (ng/ml)
I	2826 \pm 637.1	04.46 \pm 01.04
II	3733 \pm 365.0	05.05 \pm 01.38
III	3634 \pm 318.8	05.23 \pm 01.26
IV	7200 \pm 371.7 ^{c+}	83.86 \pm 13.04 ^{c+}
V	2813 \pm 344.4 ^{c-}	11.06 \pm 02.50 ^{b-}
VI	3483 \pm 310.9 ^{c-}	06.35 \pm 02.05 ^{c-}
VII	3104 \pm 405.0 ^{c-}	04.45 \pm 02.73 ^{c-}

^{c+} represents a significant increase at $p < 0.0001$ when compared to Groups I-III values while ^{b-} and ^{c-} represent significant decreases at $p < 0.001$ and $p < 0.0001$, respectively, when compared to untreated positive (TZM only-treated only) control values, respectively.

3.6. Effect of CVE and IGE on the Cardiac Tissue Oxidative Stress Markers (GSH, GST, GPx, SOD, CAT, and MDA) of TZM-Treated Rats. Repeated TZM intraperitoneal injection to treated rats resulted in significant attenuation ($p < 0.05$ and $p < 0.0001$) in SOD, CAT, GST activities, and GSH levels while there were significant increases ($p < 0.0001$) in the GPx and MDA activities (Table 6). However, repeated oral treatments with 400 mg/kg/day of CVE and IGE significantly ($p < 0.001$ and $p < 0.0001$) attenuated the alterations in the activities of these oxidative stress markers in the cardiac tissue restoring their activities to normal as recorded for Groups I-III values. These values were also comparable to those of vit. C-treated group (Table 6).

3.7. Histological Effect of CVE and IGE on TZM-Treated Heart. Repeated intraperitoneal injections of rats with 2.25 mg/kg/day of TZM for 7 days resulted in marked vascular congestion, intraparenchymal hemorrhage, and coronary artery microthrombi formation with the preservation of the cardiac myocyte cytoarchitecture (Figure 1). This is in sharp contrast with normal coronary artery and cardiomyocyte architecture recorded for Groups I-III cardiac muscle that were orally treated with 10 ml/kg/day of sterile water, 400 mg/kg/day of CVE, and 400 mg/kg/day of IGE only, respectively, with no remarkable histological changes in the

TABLE 4: Effect of 400 mg/kg/day of *CVE* and *IGE* on serum lipid profile of *TZM*-treated rats.

Groups	Serum lipids				
	TG (mmol/l)	TC (mmol/l)	HDL-c (mmol/l)	LDL-c (mmol/l)	VLDC-c (mmol/l)
I	1.00 ± 0.11	1.37 ± 0.11	0.40 ± 0.03	0.51 ± 0.10	0.45 ± 0.05
II	0.79 ± 0.06	1.41 ± 0.13	0.41 ± 0.04	0.64 ± 0.08	0.36 ± 0.04
III	0.79 ± 0.09	1.47 ± 0.12	0.44 ± 0.04	0.67 ± 0.09	0.36 ± 0.04
IV	0.96 ± 0.05	1.53 ± 0.09	0.44 ± 0.02	0.66 ± 0.09	0.43 ± 0.02
V	0.94 ± 0.10	1.51 ± 0.10	0.44 ± 0.02	0.64 ± 0.07	0.43 ± 0.04
VI	0.86 ± 0.09	1.40 ± 0.13	0.40 ± 0.03	0.62 ± 0.07	0.39 ± 0.04
VII	0.80 ± 0.06	1.45 ± 0.08	0.42 ± 0.03	0.67 ± 0.04	0.36 ± 0.03

TABLE 5: Effect of 400 mg/kg/day of *CVE* and *IGE* on atherogenic index (AI) and coronary artery disease index (CRI) in *TZM*-intoxicated rats.

Treatment groups	AI	CRI
I	01.19 ± 0.17	03.39 ± 0.08
II	01.53 ± 0.13	03.45 ± 0.11
III	01.34 ± 0.22	03.39 ± 0.04
IV	01.65 ± 0.16	03.52 ± 0.16
V	01.18 ± 0.06	03.42 ± 0.10
VI	01.42 ± 0.10	03.50 ± 0.09
VII	01.59 ± 0.09	03.45 ± 0.07

treated heart muscles (Figures 2–4). However, repeated oral pretreatments with 20 mg/kg/day of vit. C (standard antioxidant drug), 400 mg/kg/day of *CVE*, and 400 mg/kg/day of *IGE* markedly improved *TZM*-induced coronary artery histopathological alterations (Figures 5–7) with coronary artery recanalization recorded in *IGE* pretreated, *TZM*-treated (Group VII) rats (Figure 7).

4. Discussion

Trastuzumab either used alone or in combination with other agents from other classes of cytotoxic agents has remained a cornerstone and key strategy in the clinical management of patients with metastatic breast carcinoma overexpressing the HER2 protein [42, 43]. Despite its wide application in this regard, its clinical use has been limited by its cumulative dose-limiting but reversible cardiotoxicity which manifests as a life-threatening dilated cardiomyopathy and congestive cardiac failure [43, 44]. Unfortunately, till date, there are no approved effective chemotherapeutic/chemoprophylactic options available in its amelioration despite efforts being directed towards developing an effective therapeutic alternative, one of which is the antianginal agent, ranolazine, which has been reported to blunt trastuzumab cardiotoxicity mediated via redox-mediated mechanisms [31]. However, ranolazine's clinical use is known to be limited by its serious side effects such as bradycardia, syncope attacks, hematuria, acute renal failure, and its predilection to liver cirrhosis [45, 46]. Therefore, this study investigated the ameliorative potential

of *CVE* and *IGE* in *TZM*-related cardiotoxicity in experimental rats. In doing this, experimental *TZM* cardiotoxicity was reliably induced in the treated rats following repeated daily intraperitoneal injection of 2.25 mg/kg of *TZM* for 7 days as evidenced by profound elevations in the serum cardiac markers (*cTnI* and LDH), alterations in the serum lipids profile and cardiovascular disease risk indices, and marked alteration in the oxidative stress markers. All of these biochemical changes were corroborated by remarkable histological lesions such as vascular congestion, intraparenchymal hemorrhage, coronary artery endothelial thickening, and thrombi formation. *cTnI* and LDH are considered reliable markers of cardiotoxicity and are as such used in monitoring drug-induced-cardiotoxicities including *TZM* [47–52]. The fact that the serum levels of *cTnI* and LDH were significantly elevated following repeated administration for 7 days is a strong indication that *TZM*-induced cardiac damage was reliably established and in consonance with reports of other studies [49, 51, 53]. However, repeated oral pretreatments with vitamin C, *CVE*, and *IGE* profoundly attenuated elevations in serum levels of these cardiac markers, thus, indicating the potential therapeutic role of these agents in mitigating the deleterious effects of *TZM* on the integrity cardiac myocytes.

Another significant finding of this study is the effect of *TZM* treatment on the circulating lipids levels. Prolonged *TZM* treatment was also being documented to be associated with dyslipidemia which is characterized by significant increases in the serum triglycerides, very low-density lipoprotein cholesterol (VLDL-c), and low-density lipoprotein cholesterol (LDL-c) [54, 55]. The findings of our study are in agreement with this assertion although *TZM* treatment for 7 days in our study was associated with slight improvements in the circulating lipids levels as well as the cardiovascular disease risk indices. The variance between our result of study and other studies could have resulted from the short duration of *TZM* treatment. This remains a hypothesis until validated by similar studies of longer duration. In the same vein, neither *TZM* treatment nor extracts pretreatment treatment causes any significant changes in the weight gain pattern of the treated rats. Again, it is possible that the short duration of the studies could be responsible for this.

TZM like other anticancer agents such as cisplatin has been reported to cause “acute coronary syndrome” which

TABLE 6: Antioxidant activities of 400 mg/kg/day of *CVE* and *IGE* in *TZM*-intoxicated rat cardiac tissue.

Groups	Antioxidant parameters					
	GSH	GST	GPx	SOD	CAT	MDA
I	26.8 ± 3.0	31.7 ± 1.1	28.5 ± 2.8	08.4 ± 0.6	44.5 ± 1.2	0.4 ± 0.1
II	35.0 ± 3.6	29.3 ± 0.9	32.5 ± 3.3	07.7 ± 0.5	42.0 ± 6.8	0.5 ± 0.3
III	33.5 ± 4.5	22.9 ± 1.7	24.8 ± 1.8	06.2 ± 0.9	33.4 ± 7.2	0.5 ± 0.1
IV	16.7 ± 2.1 ^{c-}	19.8 ± 2.2 ^{c-}	46.9 ± 2.0 ^{ft}	03.6 ± 0.2 ^{c-}	17.7 ± 2.4 ^{c-}	0.8 ± 0.1 ^{ft}
V	29.5 ± 3.3 ^{b+}	24.7 ± 0.6 ^{b+}	19.9 ± 1.1 ^{f-}	06.5 ± 0.7 ^{c+}	26.0 ± 2.6 ^{b+}	0.5 ± 0.1 ^{f-}
VI	28.3 ± 1.6 ^{b+}	25.0 ± 0.5 ^{b+}	19.6 ± 1.8 ^{f-}	08.1 ± 0.6 ^{c+}	26.9 ± 1.2 ^{b+}	0.4 ± 0.1 ^{f-}
VII	34.8 ± 2.7 ^{c+}	26.4 ± 0.5 ^{c+}	16.7 ± 2.1 ^{f-}	07.6 ± 0.7 ^{c+}	30.2 ± 2.6 ^{c+}	0.5 ± 0.1 ^{f-}

^{c-} represents a significant decrease at $p < 0.0001$ when compared to Groups I-III (controls) values while ^{ft} represents a significant increases at $p < 0.0001$ when compared to Groups I-III values; ^{b+} and ^{c+} represent significant increases at $p < 0.05$ and $p < 0.0001$, respectively, when compared to Groups IV values while ^{f-} represents a significant decrease at $p < 0.0001$ when compared to untreated positive control (*TZM* treated only, Group IV).

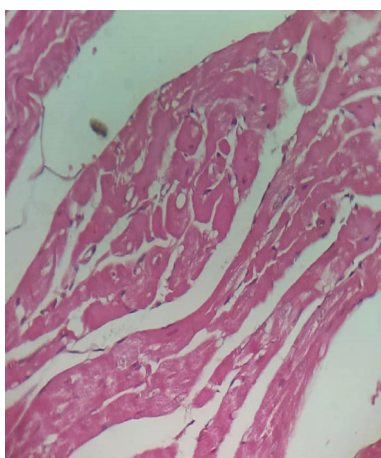


FIGURE 1: A cross-sectional representative of *TZM* intoxicated rat heart pretreated with 10 ml/kg/day of sterile water showing severe vascular congestion and intraparenchymal hemorrhage as well as coronary arterial wall thickening with endothelial microthrombi formation indicative of coronary arteriosclerosis (x400 magnification, hematoxylin-eosin stain).

may manifest as coronary ischemia from coronary artery endothelial thrombi and profound elevation in cardiac enzymes which are often prevented with aspirin and intensive anti-ischemic medication with nitrates and β -blockers [56]. Acute coronary syndrome is believed to equally result from attendant vascular endothelial dysfunction of the coronary artery and peripheral vasculature, and this endothelial dysfunction is considered an early indicator of atherosclerosis [57, 58]. The histological findings of increased coronary artery endothelial thickening and microthrombi in the *TZM*-only treated rat hearts are indicative of the full experimental induction of *TZM*-related arteriosclerosis and *TZM*-induced cardiotoxicity. Vitamin C has previously been reported to improve endothelial function of conduct arteries in patients with chronic cardiac failure [59]. However, the fact that oral pretreatments with *CVE* and *IGE* effectively improved these histological lesions is strongly reflective of the therapeutic potential effects of these extracts against *TZM*-associated endothelial dysfunction.

Oxidative stress (the shift in the balance between oxidants and antioxidants in favor of oxidants) is the net result of an imbalance between ROS production and destruction (the latter being regulated by antioxidant defense system) [60, 61]. ROS (free radicals and non-radicals) are produced from molecular oxygen as a result of normal cellular metabolism and the 3 major ROS that are of physiological significance are superoxide anion ($O_2^{\cdot-}$), hydroxyl radical ($\cdot OH$), and hydrogen peroxide (H_2O_2) [60]. Oxidative stress is a consequence of an increased generation of these free radicals and/or reduced physiological activity of antioxidant defenses against free radicals. In containing the activities of the ROS, the body system has evolved an innate antioxidant system to mitigate the possible deleterious effects of oxidative stress on the body organs/systems [60, 62, 63]. The antioxidant systems are basically of two types, namely, enzymatic antioxidants which include SOD, CAT, GSH Px, GSTs, and heme oxygenase-1 and nonenzymatic antioxidants which include vitamins (vitamins C and E), β -carotene, uric acid, and GSH, a tripeptide (L- γ -glutamyl-L-cysteinyl-L-glycine) that comprise a thiol (sulfhydryl) group (e.g., thioredoxin-1 (Trx-1)) [60, 64]. These antioxidant systems are known to mediate their antioxidant activities via several mechanisms which include the inhibition of free radical formations; protection of cells against apoptosis by interacting with proapoptotic and antiapoptotic signaling pathways; regulation and activation of several transcription factors, such as AP-1, NF- κ B, and Sp-1; superoxide and oxygen-free radical scavenging activities [65–70]. Pleiotropic deleterious effects of oxidative stress are observed in numerous disease states and are also implicated in a variety of drug-induced toxicities. Identifiable drugs are alkylating anthracycline antineoplastic agents (doxorubicin), antiretroviral (azidovudine), anti-inflammatory (diclofenac), platinum-based antineoplastic agent (cisplatin), antipsychotic (chlorpromazine) [71], and most recently, a HER2 directed monoclonal antibody (trastuzumab) [7, 72]. However, the effectiveness of conventional cytotoxic drugs is largely based on the generation of ROS and consequently on the increase of oxidative stress that exceeds the reduction capacity of cancerous tissue, resulting in apoptotic cell death [73], and most of the adverse effects emanating from chemotherapy result from excess ROS

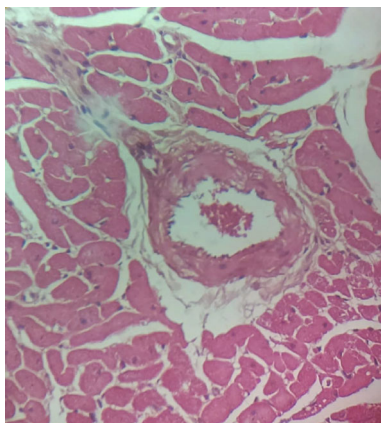


FIGURE 2: A cross-sectional representative of the normal rat heart showing normal cardiac histoarchitecture (x400 magnification, hematoxylin-eosin stain).

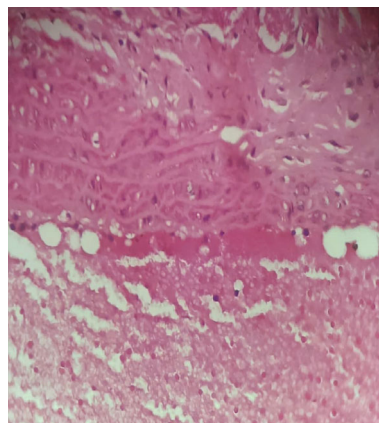


FIGURE 4: A cross-sectional representative of the 400 mg/kg/day of IGE treated-rat heart showing normal cardiac histoarchitecture (x400 magnification, hematoxylin-eosin stain).

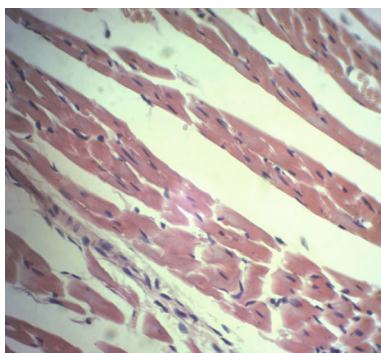


FIGURE 3: A cross-sectional representative of the 400 mg/kg/day of CVE treated-rat heart showing normal cardiac histoarchitecture with mild pericardiac fat deposit (x400 magnification, hematoxylin-eosin stain).

production in healthy tissues, such as anthracycline-mediated cardiotoxicity, and nephrotoxicity triggered by platinum compounds [74, 75] which are mainly based on the interaction of OH^\bullet with target tissue DNA [76, 77]. *TZM* has been reported to potentiate cardiomyocyte toxicity through a “dual-hit” mechanism, which includes alterations in antiapoptotic signalling pathways in cardiomyocytes, inhibition of the neuregulin-1 survival signaling pathway, and angiotensin II-induced activation of NADPH oxidase, with the ability to further increase reactive oxygen species production, ultimately resulting in dilated cardiomyopathy [78, 79].

The present study showed that *TZM* had significant effects on the oxidative stress markers such as SOD, CAT, GST, and GSH whose activities and levels in the treated cardiac tissues were suppressed while the cardiac tissue activities and levels of GPx and MDA were profoundly elevated. These results are similar to others previously reported [31, 80, 81]. *TZM* induces cardiomyocyte toxicity through a mitochondrial pathway depending on ROS production and oxidative stress. *TZM* activates proapoptotic proteins such as *Bax* and induces *mPTP* opening, and these eventually result in

mitochondrial defects and dysfunctions [82]. Classes of conventional drugs such as angiotensin-converting enzyme inhibitor (ACEI), angiotensin receptor blocker (ARB), mineralocorticoid receptor antagonist (MRA), nonsteroidal anti-inflammatory drug (NSAID), and lecithinized human recombinant superoxide dismutase (PC-SOD) have been reported to offer cardioprotection against DOX-mediated cardiotoxicities [83]. Natural antioxidant supplements such as coenzyme Q10 [84] and N-acetylcysteine (administered either alone or with vitamins E and C) [85] have been reported to mitigate anthracycline- (doxorubicin-) mediated left ventricular dysfunction and remodeling while melatonin [86] and levocarnitine [87] have also been tested in the clinical setting with positive results. Similarly, plant-derived small molecules such as arjunolic acid, anthocyanins, apigenin, avicularin, berberine, baicalein, caffeic acid, gingerol, ginsenosides, calceolarioside, cannabidiol, carotenoids, chrysin, catechins, chrysoeriol, curcumin, eugenol, frederine, diosgenin, hesperidin, and kaempferol have all been reported to positively mitigate doxorubicin-mediated cardiotoxicity [88]. However, ours is the first to report the mitigating effect of plant extracts and indeed *Clerodendrum volubile* leaf and *Irvingia gabonensis* seed extracts against *TZM*-induced cardiotoxicity. Plant secondary metabolites especially polyphenols such as flavonoids, epicatechin, catechin, anthocyanidins, epigallocatechin gallate, carotenoids, terpenoids, sesquiterpenoids, and unsaturated fatty acids have been reported to protect against the deleterious effects of oxidative stress, reduce blood pressure, and improve endothelial dysfunction through several mechanisms [89, 90] which include activation of eNOS and reduced endothelial ET-1 secretion which are key in NO/cGMP pathway [91–95], as well as through activation of Akt/eNOS pathway [96]. Proanthocyanidins are also known to possess antithrombotic properties that are associated with endothelial protection and inhibition of inflammatory cells adhesion because it decreases P-selectin expression, thus, inhibiting leucocyte recruitment and thrombosis [96–98]. Proanthocyanidins are also known to have anti-inflammatory and antioxidant effects and improve

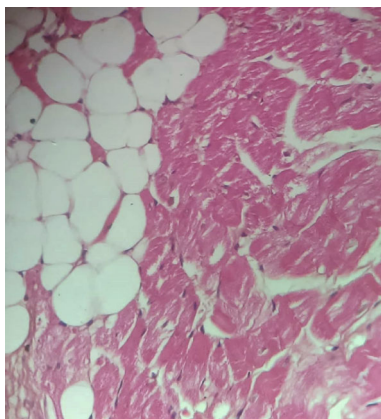


FIGURE 5: A photomicrograph of cross-sectional representative of *TZM* intoxicated rat heart orally pretreated with 20 mg/kg/day of vit. C showing mild vascular congestion, mild intraparenchymal hemorrhage, and increased pericardial fat thickness (x400 magnification, hematoxylin-eosin stain).

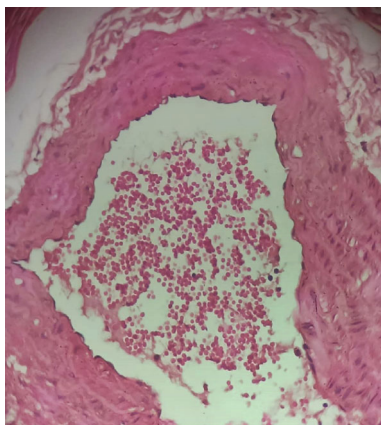


FIGURE 6: A photomicrograph of cross-sectional representative of *TZM* intoxicated rat heart treated with 400 mg/kg/day of *CVE* showing mild intraparenchymal hemorrhage with thickened coronary arterial wall suggestive of coronary arteriosclerosis (x400 magnification, hematoxylin-eosin stain).

circulating HDL-c levels without causing dyslipidemia, thus, exhibiting endothelium-protective, antiatherogenic, and cardioprotective activities [97, 99, 100]. Although coronary artery microthrombi formation was observed histopathologically in the rat hearts intoxicated with *TZM* but this was for profoundly improved with repeated oral *CVE* and *IGE* pretreatments with coronary artery revascularization observed in rat heart pretreated with *IGE*. *CVE* and *IGE* have reported to be abundantly rich in polyphenols and have been attributed to responsible for the high antioxidant activities of the plants [9, 16, 17, 25, 27]. Thus, the presence of polyphenols in high amounts in these extracts could be responsible for the observed cardioprotection offered against *TZM* cardiotoxicity. Similarly, oleanolic acid has been reported to be abundantly present in *CVE* and *IGE* and is known to decrease oxidative stress, apoptosis, and proteasomal activity following ischemia-reperfusion injury [101], antihyperlipidemic, and cardioprotective effects [23, 102]. Thus, the presence of

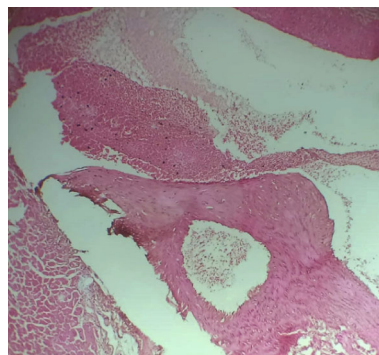


FIGURE 7: A photomicrograph of cross-sectional representative of *TZM* intoxicated rat heart treated with 400 mg/kg/day *IGE* showing mild vascular congestion and coronary artery recanalization (x100 magnification, hematoxylin-eosin stain).

this oil and other secondary metabolites could have also contributed to the cardioprotection offered by these extracts.

The clinical use of antioxidants in recent years has gained considerable interest. Epidemiological studies have suggested that diets (fruits and vegetables) that are richly high in antioxidant contents including vitamins A, C, and E and other phenolic contents might help decrease the risk of cardiovascular diseases (such as atherosclerosis, preeclampsia, or hypertension) and other chronic noncommunicable diseases such as diabetes mellitus, whose etiopathogenesis are thought to be mediated by oxidative stress [103]. Similarly, antioxidants have been documented to have useful clinical application in ameliorating drugs and xenobiotic toxicity. Drug, xenobiotic and environmental pollutant biotransformation results in the overproduction of free radicals in the body leading to lipid peroxidation, oxidative stress, and oxidative damage [104]. The ROS, thus, generated either directly or indirectly through the mediation of oxidative and inflammatory signals, disrupt the cellular equilibrium, and cause mitogenesis, mutagenesis, genotoxicity, and cytotoxicity and form the underlying pathophysiology for diseases such as diabetes, hypertension, atherosclerosis, cancer, Parkinsonism, and Alzheimer's disease [104]. However, studies have shown the benefit of antioxidants in protection against drug- and xenobiotic-induced toxicities. For example, the beneficial role of citrus fruit-derived flavonoid (diosmin) in ameliorating and preventing methotrexate-induced oxidative and inflammatory markers, suggesting the promising protective role of diosmin against methotrexate-induced toxicities in patients with cancer and autoimmune diseases have been reported [105]. Similarly, the protective effects of green tea (*Camellia sinensis*) on nicotine exposure-induced oxidative damage in mice leading to behavioral alterations including physical development, neuromotor maturation, and behavioral performance in newborn male and female mice have been demonstrated [106]. In another study, the cardioprotective role of the flavonoid and phenolic contents of *Murraya koenigii* (L.) Spreng. leaf extract against doxorubicin-induced cardiotoxicity in rat model was reported, indicating the protective potential of *Murraya koenigii* (L.) Spreng. leaf extract as an adjuvant therapy with doxorubicin [107]. Thus, in line with the above, the flavonoid and phenolic contents in

CVE and *IGE* could be useful adjuvant therapy to ameliorate *TZM*-mediated cardiotoxicity.

The chemopreventive role of the standard antioxidant drug, vitamin C, in doxorubicin/trastuzumab-mediated cardiotoxicity which are primarily mediated via reactive oxidative stress, nitrosative stress, and inflammatory pathways is well documented (Fujita et al., 1982; Shimpo et al., 1991; Vincent et al., 2013; Akolkar et al., 2017; Singh et al., 2018; Carrasco et al., 2020) [108–113]. Vitamin C and its derivatives were reported to prevent myocardial lipoperoxidation and subsequent doxorubicin-mediated cardiomyopathy, thus, prolonged the life expectancy of experimental animals treated with doxorubicin [108, 109]. Vitamin C was also reported to mediate its cardioprotection via multimodal mechanisms which include reduced protein carbonyl formation, NOS activity, protein nitrosylation, iNOS expression, expression of apoptotic proteins (*Bax*, *Bnip-3*, *Bak*, and caspase-3), as well as decreased cardiac TNF- α , IL-1 β , and IL-6 levels and increased Vitamin C transporter proteins (SVCT-2 and GLUT-4) [114]. Thus, the results of this study are in complete agreement with those of earlier studies where vitamin C pretreatments either prevented or ameliorated the deleterious effects of *TZM*-induced myocardial cellular oxidative damage.

Another notable finding of this study is the effect of *TZM* and the oral pretreatments with *CVE*, *IGE*, and Vit. C. *TZM*, unlike anthracycline cytotoxic agents, have been reported not to alter the lipid profile of cancer patients on it although pre-existing diabetes mellitus, dyslipidemia, and obesity along with a number of cardiovascular risk factors and comorbidities are known to increase the propensity for cardiotoxicity in cancer patients on anthracycline/*TZM* therapy (Jawa et al., 2016; Kosalka et al., 2019; Abdel-Rasaq et al., 2019; Georgiadis et al., 2020) [115–118]. Going by the fact that repeated *TZM* injections did not significantly alter the complete lipids profile including the cardiovascular disease risk indices including AI and CRI of treated rats strongly indicated our result to be in tandem with earlier studies. AI is known to be a strong, reliable, and independent predictor of ischemic heart diseases including coronary artery disease and acute myocardial infarction (Cai et al., 2017; Kazemi et al., 2018; Gómez-Álvarez et al., 2020) [119–121]. AI is known to be a better predictor of coronary artery disease than traditional lipid parameters and other lipid ratios such as CRI and lipoprotein combined index (Cai et al., 2017) [119]. AI also reflects the lipid-driven inflammatory state in acute coronary syndrome (Zhan et al., 2016) [122]. The mere fact that *TZM* did not alter the value of this predictor is an indication that *TZM* does not mediate its cardiac dysfunction via the atherogenic mechanism. Similarly, this further strengthens the fact that *CVE* and *IGE* possess cardioprotective potentials.

5. Conclusion

Overall, results of our study for the first time showed that *CVE* and *IGE* effectively attenuated *TZM*-induced cardiotoxicity and their cardioprotective activities were mediated via antioxidant, free radical scavenging, antilipoperoxidation mechanisms although their antithrombotic mechanism

remains plausible but more studies are required in this direction.

Abbreviations

Akt/eNOS:	Akt-dependent phosphorylation of endothelial nitric oxide synthase
AI:	Atherogenic index
AST:	Aspartate transaminase
<i>Bak</i> :	B-cell associated k protein
<i>Bax</i> :	B-cell associated x protein
<i>Bnip3</i> :	Bcl-2 adenovirus E1B 19 kDa-interacting protein 3
CAT:	Catalase
CRI:	Coronary artery index
<i>cTn I</i> :	Cardiac troponin I
<i>CVE</i> :	<i>Clerodendrum volubile</i> ethanol leaf extract
DMSO:	Dimethyl sulfoxide
DPPH:	1,1-diphenyl-2-picrylhydrazyl
DTNB:	5,5-dithiobisnitro benzoic acid
eNOS:	Endothelial nitric oxide synthase
ET-1:	Endothelin-1
GLUT-4:	Glucose transporter protein-4
GPx:	Glutathione peroxidase
GSH:	Reduced glutathione
GST:	Glutathione S-transferase
HCl:	Hydrochloric acid
HDL-c:	High-density lipoprotein cholesterol
<i>IGE</i> :	<i>Irvingia gabonensis</i> ethanol seed extract
IL-1 β :	Interleukin-1 beta
IL-6:	Interleukin-6
iNOS:	Induced nitric oxide synthase
<i>i.p.</i> :	Intraperitoneal
KCl:	Potassium chloride
LDH:	Lactate dehydrogenase
LDL-c:	Low-density lipoprotein cholesterol
MDA:	Malondialdehyde
<i>mPTP</i> :	Mitochondrial permeability transition pore
NO/cGMP:	Nitric oxide-cyclic guanosine monophosphate
NOS:	Nitric oxide synthase
<i>p.o.</i> :	<i>Per os</i>
% Δ wt:	Percentage change in weight
RHW:	Relative heart weight
ROS:	Reactive oxygen species
S.D.:	Standard deviation of the mean
S.E.M.:	Standard error of the mean
SOD:	Superoxidase dismutase
SVCT-2:	Sodium-dependent vitamin C cotransporter isoform 2
TBA:	Thiobarbituric acid
TC:	Total cholesterol
TCA:	Tricarboxylic acid
TG:	Triglyceride
TNF- α :	Tumor necrosis factor-alpha
<i>TZM</i> :	Trastuzumab (r-DNA origin)
UNILORIN:	University of Ilorin
UV:	Ultraviolet
Vit. C:	Vitamin C
VLDL-c:	Very low-density lipoprotein cholesterol.

Data Availability

Answer: Yes. Comment.

Conflicts of Interest

The authors have none to declare.

Authors' Contributions

Olufunke Olorundare designed the experimental protocol for this study and was involved in the manuscript writing; Adejuwon Adeneye supervised the research, analyzed data, and wrote the manuscript; Akinyele Akinsola is an M.Sc. student in Olufunke Olorundare's laboratory who performed the laboratory research; Sunday Soyemi and Alban Mgbehoma independently read and interpreted the histopathological slides of the cardiac tissues prepared; James Ntambi and Hasan Mukhtar are our collaborator in the U.S.A. who read through the manuscript.

Acknowledgments

The authors deeply appreciate the technical assistance provided by the Laboratory Manager, Dr. Sarah John-Olabode and other staff of the Laboratory Services, AFRIGLOBAL MEDICARE, Mobolaji Bank Anthony Branch Office, Ikeja, Lagos, Nigeria, in assaying for the serum cardiac biomarkers and lipid profile. Similarly, the technical support of staff of LASUCOM Animal House for the care of the Experimental Animals used for this study and Mr. Sunday O. Adenekan of BIOLIFE CONSULTS in the area of oxidative stress markers analysis are much appreciated. This research was funded by Tertiary Education Trust Fund (TETFUND) Nigeria, through its National Research Fund (TETFUND/NRF/UII/LORIN/STI/VOL.1/B2.20.12) as a collaborative research award to both Professors Olufunke Olorundare and Hasan Mukhtar.

References

- [1] N. Mohan, J. Jiang, M. Dokmanovic, and W. J. Wu, "Trastuzumab-mediated cardiotoxicity: current understanding, challenges, and frontiers," *Antibody Therapeutics*, vol. 1, no. 1, pp. 13–17, 2018.
- [2] J. J. Gemmete and S. K. Mukherji, "Trastuzumab (Herceptin)," *American Journal of Neuroradiology*, vol. 32, no. 8, pp. 1373–1374, 2011.
- [3] A. A. Onitilo, J. M. Engel, and R. V. Stankowski, "Cardiovascular toxicity associated with adjuvant trastuzumab therapy: prevalence, patient characteristics, and risk factors," *Therapeutic Advances in Drug Safety*, vol. 5, no. 4, pp. 154–166, 2014.
- [4] M. F. Rimawi, R. Schiff, and C. K. Osborne, "Targeting HER2 for the treatment of breast cancer," *Annual Review of Medicine*, vol. 66, no. 1, pp. 111–128, 2015.
- [5] Y. You, Z. Xu, and Y. Chen, "Doxorubicin conjugated with a trastuzumab epitope and an MMP-2 sensitive peptide linker for the treatment of HER2-positive breast cancer," *Drug Delivery*, vol. 25, no. 1, pp. 448–460, 2018.
- [6] N. Mohan, Y. Shen, Y. Endo, M. K. ElZarrad, and W. J. Wu, "Trastuzumab, but not pertuzumab, dysregulates HER2 signaling to mediate inhibition of autophagy and increase in reactive oxygen species production in human cardiomyocytes," *Molecular Cancer Therapeutics*, vol. 15, no. 6, pp. 1321–1331, 2016.
- [7] N. Mohan, J. Jiang, and W. J. Wu, "Implications of autophagy and oxidative stress in trastuzumab-mediated cardiac toxicities," *Austin Pharmacology & Pharmaceutics*, vol. 2, no. 1, p. 1005, 2017.
- [8] Y.-Y. Wu, T.-C. Huang, T.-N. Tsai et al., "The clinical efficacy and cardiotoxicity of fixed-dose monthly trastuzumab in HER2-positive breast cancer: A single institutional analysis," *PLoS One*, vol. 11, no. 3, article e0151112, 2016.
- [9] S. A. Adefegha and G. Oboh, "Antioxidant and inhibitory properties of Clerodendrum volubile leaf extracts on key enzymes relevant to non-insulin dependent diabetes mellitus and hypertension," *Journal of Taibah University for Science*, vol. 10, no. 4, pp. 521–533, 2018.
- [10] O. L. Erukainure, R. M. Hafizur, N. Kabir et al., "Suppressive effects of Clerodendrum volubile P. Beauv. [Labiatae] methanolic extract and its fractions on type 2 diabetes and its complications," *Frontiers in Pharmacology*, vol. 9, p. 8, 2018.
- [11] O. L. Erukainure, O. A. T. Ebuehi, I. M. Choudhary et al., "Iridoid glycoside from the leaves of Clerodendrum volubile Beauv. shows potent antioxidant activity against oxidative stress in rat brain and hepatic tissues," *Journal of Dietary Supplements*, vol. 11, no. 1, pp. 19–29, 2014.
- [12] A. Fred-Jaiyesimi and A. Adekoya, "Pharmacognostic studies and anti-inflammatory activities of Clerodendrum volubile P Beauv leaf," *International Journal of Phytomedicine*, vol. 4, no. 3, pp. 414–418, 2012.
- [13] O. L. Erukainure, M. Z. Zaruwa, M. I. Choudhary et al., "Dietary fatty acids from leaves of Clerodendrum Volubile Induce cell cycle arrest, downregulate matrix metalloproteinase-9 expression, and modulate redox status in human breast cancer," *Nutrition and Cancer*, vol. 68, no. 4, pp. 634–645, 2016.
- [14] O. L. Erukainure, M. A. Mesaik, O. Atolani, A. Muhammad, C. I. Chukwuma, and M. S. Islam, "Pectolinarigenin from the leaves of Clerodendrum volubile shows potent immunomodulatory activity by inhibiting T- cell proliferation and modulating respiratory oxidative burst in phagocytes," *Bio-medicine & Pharmacotherapy*, vol. 93, pp. 529–535, 2017.
- [15] S. Afolabi, O. Olorundare, G. Gyebi et al., "Cytotoxic potentials of Clerodendrum volubile against prostate cell lines and its possible proteomic targets," *Journal of Clinical Nutrition and Food Sciences*, vol. 2, no. 2, pp. 46–53, 2019.
- [16] C. T. Senjobi, T. R. Fasola, and P. I. Aziba, "Phytochemical and analgesic evaluation of methanol leaf extract of Clerodendrum volubile Linn," *IFE Journal of Science*, vol. 19, no. 1, pp. 141–145, 2017.
- [17] A. A. Ajao, O. M. Oseni, O. T. Oladipo, Y. A. Adams, Y. O. Mukaila, and A. A. Ajao, "Clerodendrum volubile P. Beauv (Lamiaceae), an underutilized indigenous vegetable of utmost nutritive and pharmacological importance," *Beni-Suef University Journal of Basic and Applied Sciences*, vol. 7, no. 4, pp. 606–611, 2018.
- [18] H. M. Burkill, *The Useful Plants of West Tropical Africa*, vol. 2, Royal Botanic Gardens, Kew, London, 1985.
- [19] L. Karalliedde and I. Gawarammana, *Traditional Herbal Medicines - a Guide to the Safer Use of Herbal Medicines*, Hammersmith Press, London, 2008.

- [20] J. I. Okogun, *Drug discovery through ethnobotany in Nigeria: some results. In: advances in Phytomedicine - Ethnomedicine and drug discovery*, M. M. Iwu and J. C. Wootton, Eds., vol. 1, Elsevier, London, 2002.
- [21] J. Sun and P. Chen, "Ultra high-performance liquid chromatography with high-resolution mass spectrometry analysis of African mango (*Irvingia gabonensis*) seeds, extract, and related dietary supplements," *Journal of Agricultural and Food Chemistry*, vol. 60, no. 35, pp. 8703–8709, 2012.
- [22] U. F. Ezeruike and J. M. Prieto, "The use of plants in the traditional management of diabetes in Nigeria: pharmacological and toxicological considerations," *Journal of Ethnopharmacology*, vol. 155, no. 2, pp. 857–924, 2014.
- [23] F. M. Awah, P. N. Uzoegwu, P. Ifeonu et al., "Free radical scavenging activity, phenolic contents and cytotoxicity of selected Nigerian medicinal plants," *Food Chemistry*, vol. 131, no. 4, pp. 1279–1286, 2012.
- [24] D. C. Don Lawson, "Proximate analysis and phytochemical screening of *Irvingia gabonensis* (Ogbono cotyledon)," *Bio-medical Journal of Scientific and Technical Research*, vol. 5, no. 4, pp. 4643–4646, 2018.
- [25] G. K. Mahunu, L. Quansa, H. E. Tahir, and A. A. Mariod, "*Irvingia gabonensis*: phytochemical constituents, bioactive compounds, traditional and medicinal uses," in *Wild Fruits: Composition, Nutritional Value and Products*, A. Mariod, Ed., Springer, Cham, 2019.
- [26] O. Oladimeji and T. O. Fasuan, "Characterization of *Irvingia gabonensis* (Ogbono) soup and optimization of process variables," *International Journal of Food Engineering and Technology*, vol. 2, no. 2, pp. 41–50, 2019.
- [27] O. O. Ekpe, C. O. Nwaehujor, C. E. Ejiofor, W. Arikpo Peace, E. Woruji Eliezer, and T. Amor Emmanuel, "*Irvingia gabonensis* seeds extract fractionation, its antioxidant analyses and effects on red blood cell membrane stability," *Pharmacology*, vol. 1, pp. 337–353, 2019.
- [28] A. O. Akinsola, *Vasorelaxant and Cardioprotective Properties of Clerodendrum Volubile Leaf Extract on Doxorubicin-Induced Toxicities in Wistar Rats A M.Sc. Pharmacology Dissertation submitted to the Postgraduate School, University of Ilorin, Ilorin, Nigeria, 2019.*
- [29] National Research Council (US) Committee for the Update of the Guide for the Care and Use of Laboratory Animals, *Guide for the Care and Use of Laboratory Animals*, The National Academies Press, Washington D.C., U.S.A, 2011.
- [30] K. A. Poon, K. Flagella, J. Beyer et al., "Preclinical safety profile of trastuzumab emtansine (T-DM1): mechanism of action of its cytotoxic component retained with improved tolerability," *Toxicology and Applied Pharmacology*, vol. 273, no. 2, pp. 298–313, 2013.
- [31] G. Riccio, S. Antonucci, C. Coppola et al., "Ranolazine attenuates trastuzumab-induced heart dysfunction by modulating ROS production," *Frontiers in Physiology*, vol. 9, no. 38, 2018.
- [32] N. W. Tietz, *Textbook of Clinical Chemistry*, C. A. Burtis and E. R. Ashwood, Eds., W. B. Saunders, Philadelphia, U.S.A, 1999.
- [33] R. D. Abbott, P. W. Wilson, W. B. Kannel, and W. P. Castelli, "High density lipoprotein cholesterol, total cholesterol screening, and myocardial infarction. The Framingham Study," *Arteriosclerosis*, vol. 8, no. 3, pp. 207–211, 1988.
- [34] S. Alladi and K. R. Shanmugasundaram, "Induction of hypercholesterolemia by supplementing soy protein with acetate generating amino acids," *Nutrition Reports International*, vol. 40, pp. 893–899, 1989.
- [35] F. Paoletti, D. Aldinucci, A. Mocali, and A. Caparrini, "A sensitive spectrophotometric method for the determination of superoxide dismutase activity in tissue extracts," *Analytical Biochemistry*, vol. 154, no. 2, pp. 536–541, 1986.
- [36] M. H. Hadwan, "Simple spectrophotometric assay for measuring catalase activity in biological tissues," *BMC Biochemistry*, vol. 19, no. 1, p. 7, 2018.
- [37] I. Rahman, A. Kode, and S. K. Biswas, "Assay for quantitative determination of glutathione and glutathione disulfide levels using enzymatic recycling method," *Nature Protocols*, vol. 1, no. 6, pp. 3159–3165, 2006.
- [38] B. Faraji, H. K. Kang, and J. L. Valentine, "Methods compared for determining glutathione peroxidase activity in blood," *Clinical Chemistry*, vol. 33, no. 4, pp. 539–543, 1987.
- [39] J. G. Vontas, A. A. Enayati, G. J. Small, and J. Hemingway, "A simple biochemical assay for glutathione S-transferase activity and its possible field application for screening glutathione S-transferase-based insecticide resistance," *Pesticide Biochemistry and Physiology*, vol. 68, no. 3, pp. 184–192, 2000.
- [40] J. A. Buege and S. D. Aust, "Microsomal lipid peroxidation," *Methods in Enzymology*, vol. 52, pp. 302–310, 1978.
- [41] M. Slaoui and L. Fiette, "Histopathology procedures: from tissue sampling to histopathological evaluation," *Methods in Molecular Biology*, vol. 691, pp. 69–82, 2011.
- [42] D. L. Keefe, "Trastuzumab-associated cardiotoxicity," *Cancer*, vol. 95, no. 7, pp. 1592–1600, 2002.
- [43] S. Karmakar, R. Dixit, A. Nath, S. Kumar, and S. Karmakar, "Dilated cardiomyopathy following trastuzumab chemotherapy," *Indian Journal of Pharmacology*, vol. 44, no. 1, pp. 131–133, 2012.
- [44] A. Sandoo, G. D. Kitas, and A. R. Carmichael, "Endothelial dysfunction as a determinant of trastuzumab-mediated cardiotoxicity in patients with breast cancer," *Anticancer Research*, vol. 34, no. 3, pp. 1147–1151, 2014.
- [45] B. M. Reddy, H. S. Weintraub, and A. Z. Schwartzbard, "Ranolazine: a new approach to treating an old problem," *Texas Heart Institute Journal*, vol. 37, no. 6, pp. 641–647, 2010.
- [46] M. Reed and D. Nicolas, "*Ranolazine*" in: *StatPearls [Internet]*, StatPearls Publishing, Treasure Island (FL), 2019, <https://www.ncbi.nlm.nih.gov/books/NBK507828/>.
- [47] K. B. Wallace, E. Hausner, E. Herman et al., "Serum troponins as biomarkers of drug-induced cardiac toxicity," *Toxicologic pathology*, vol. 32, pp. 106–121, 2016.
- [48] D. Singh, A. Thakur, and W. H. W. Tang, "Utilizing cardiac biomarkers to detect and prevent chemotherapy-induced cardiomyopathy," *Current Heart Failure Reports*, vol. 12, no. 3, pp. 255–262, 2015.
- [49] A. Sugaya, S. Ishiguro, S. Mitsuhashi et al., "Interstitial lung disease associated with trastuzumab monotherapy: a report of 3 cases," *Molecular and Clinical Oncology*, vol. 6, no. 2, pp. 229–232, 2017.
- [50] R. Simões, L. M. Silva, A. L. V. M. Cruz, V. G. Fraga, A. de Paula Sabino, and K. B. Gomes, "Troponin as a cardiotoxicity marker in breast cancer patients receiving anthracycline-based chemotherapy: a narrative review," *Biomedicine & Pharmacotherapy*, vol. 107, pp. 989–996, 2018.
- [51] W. Zhu, L. Ma, J. Qian et al., "The molecular mechanism and clinical significance of LDHA in HER2-mediated progression

- of gastric cancer,” *American Journal of Translational Research*, vol. 10, no. 7, pp. 2055–2067, 2018.
- [52] M. Sternberg, E. Pasini, C. Chen-Scarabelli et al., “Elevated cardiac troponin in clinical scenarios beyond obstructive coronary artery disease,” *Medical Science Monitor*, vol. 25, pp. 7115–7125, 2019.
- [53] K. Altundag, “More predictive markers were identified for trastuzumab-induced cardiotoxicity,” *Medical Oncology*, vol. 35, no. 1, 2018.
- [54] E. Jobard, O. Trédan, T. Bachelot et al., “Longitudinal serum metabolomics evaluation of trastuzumab and everolimus combination as pre-operative treatment for HER-2 positive breast cancer patients,” *Oncotarget*, vol. 8, no. 48, pp. 83570–83584, 2017.
- [55] W. Tian, Y. Yao, G. Fan et al., “Changes in lipid profiles during and after (neo)adjuvant chemotherapy in women with early-stage breast cancer: A retrospective study,” *PLoS ONE*, vol. 14, no. 8, article e0221866, 2019.
- [56] A. K. Dimos, P. N. Stougianoss, and A. G. Trikas, “First, do no harm chemotherapy or healthy heart?,” *Hellenic Journal of Cardiology*, vol. 53, no. 2, pp. 127–136, 2012.
- [57] A. Lerman and A. M. Zeiher, “Endothelial function: cardiac events,” *Circulation*, vol. 111, no. 3, pp. 363–368, 2005.
- [58] L. Morbidelli, S. Donnini, and M. Ziche, “Targeting endothelial cell metabolism for cardio-protection from the toxicity of antitumor agents,” *Cardio-Oncology*, vol. 2, no. 1, 2016.
- [59] B. Hornig, N. Arakawa, C. Kohler, and H. Drexler, “Vitamin C improves endothelial function of conduit arteries in patients with chronic heart failure,” *Circulation*, vol. 97, no. 4, pp. 363–368, 1998.
- [60] E. Birben, U. M. Sahiner, C. Sackesen, S. Erzurum, and O. Kalayci, “Oxidative stress and antioxidant defense,” *World Allergy Organization Journal*, vol. 5, no. 1, pp. 9–19, 2012.
- [61] B. Poljsak, D. Šuput, and I. Milisav, “Achieving the balance between ROS and antioxidants: when to use the synthetic antioxidants,” *Oxidative Medicine and Cellular Longevity*, vol. 2013, Article ID 956792, 11 pages, 2013.
- [62] L. He, T. He, S. Farrar, L. Ji, T. Liu, and X. Ma, “Redox homeostasis by elimination of reactive oxygen species,” *Cellular Physiology and Biochemistry*, vol. 2012, article 645460, 2012.
- [63] I. S. Harris and G. M. DeNicola, “The complex interplay between antioxidants and ROS in cancer,” *Trends in Cell Biology*, vol. 30, no. 6, pp. 440–451, 2020.
- [64] R. Masella, R. di Benedetto, R. Vari, C. Filesi, and C. Giovannini, “Novel mechanisms of natural antioxidant compounds in biological systems: involvement of glutathione and glutathione-related enzymes,” *The Journal of Nutritional Biochemistry*, vol. 16, no. 10, pp. 577–586, 2005.
- [65] V. W. Bunker, “Free radicals, antioxidants and ageing,” *Medical Laboratory Sciences*, vol. 49, no. 4, pp. 299–312, 1992.
- [66] J. D. Hayes and D. J. Pulford, “The glutathione S-transferase supergene family: regulation of GST and the contribution of the isoenzymes to cancer chemoprotection and drug resistance,” *Critical Reviews in Biochemistry and Molecular Biology*, vol. 30, pp. 445–600, 2008.
- [67] J. D. Hayes and L. I. McLellan, “Glutathione and glutathione-dependent enzymes represent a co-ordinately regulated defence against oxidative stress,” *Free Radical Research*, vol. 31, pp. 273–300, 2009.
- [68] D. A. Dickinson and H. J. Forman, “Glutathione in defense and signaling: lessons from a small thiol,” *Annals of the New York Academy of Sciences*, vol. 973, no. 1, pp. 488–504, 2002.
- [69] S.-G. Cho, Y. H. Lee, H.-S. Park et al., “Glutathione S-transferase mu modulates the stress activated signals by suppressing apoptosis signal-regulating kinase 1,” *The Journal of Biological Chemistry*, vol. 276, no. 16, pp. 12749–12755, 2001.
- [70] A. El-Agamey, G. M. Lowe, D. J. McGarvey et al., “Carotenoid radical chemistry and antioxidant/pro-oxidant properties,” *Archives of Biochemistry and Biophysics*, vol. 430, no. 1, pp. 37–48, 2004.
- [71] D. G. Deavall, E. A. Martin, J. M. Horner, and R. Roberts, “Drug-induced oxidative stress and toxicity,” *Journal of toxicology*, vol. 2012, Article ID 645460, 13 pages, 2012.
- [72] H. R. Teppo, Y. Soini, and P. Karihtala, “Reactive oxygen species-mediated mechanisms of action of targeted cancer therapy,” *Oxidative Medicine and Cellular Longevity*, vol. 2017, 11 pages, 2017.
- [73] S. A. Castaldo, J. R. Freitas, N. V. Conchinha, and P. A. Madureira, “The tumorigenic roles of the cellular REDOX regulatory systems,” *Oxidative Medicine and Cellular Longevity*, vol. 2016, Article ID 8413032, 17 pages, 2016.
- [74] P. Angsutararux, S. Luanpitpong, and S. Issaragrisil, “Chemotherapy-induced cardiotoxicity: overview of the roles of oxidative stress,” *Oxidative Medicine and Cellular Longevity*, vol. 2015, Article ID 795602, 13 pages, 2015.
- [75] T. Karasawa and P. S. Steyger, “An integrated view of cisplatin-induced nephrotoxicity and ototoxicity,” *Toxicology Letters*, vol. 237, no. 3, pp. 219–227, 2015.
- [76] A. C. Begg, F. A. Stewart, and C. Vens, “Strategies to improve radiotherapy with targeted drugs,” *Nature Reviews. Cancer*, vol. 11, no. 4, pp. 239–253, 2011.
- [77] E. C. Halperin, L. W. Brady, C. A. Perez, and D. E. Wazer, *Perez & Brady’s Principles and Practice of Radiation Oncology*, LWW, Wolters Kluwer Health/Lippincott Williams & Wilkins, 6th edition, 2013.
- [78] M. Zeglinski, A. Ludke, D. S. Jassal, and P. K. Singal, “Trastuzumab-induced cardiac dysfunction: a ‘dual-hit’,” *Experimental and Clinical Cardiology*, vol. 16, no. 3, pp. 70–74, 2011.
- [79] W. Abdel-Razaq, M. Alzahrani, M. Al Yami, F. Almugibl, M. Almotham, and R. Alregaibah, “Risk factors associated with trastuzumab-induced cardiotoxicity in patients with human epidermal growth factor receptor 2-positive breast cancer,” *Journal of Pharmacy & Bioallied Sciences*, vol. 11, no. 4, pp. 348–354, 2019.
- [80] L. G. T. Lemos, V. J. Victorino, A. C. S. A. Herrera et al., “Trastuzumab-based chemotherapy modulates systemic redox homeostasis in women with HER2-positive breast cancer,” *International Immunopharmacology*, vol. 27, no. 1, pp. 8–14, 2015.
- [81] S. Gorini, A. de Angelis, L. Berrino, N. Malara, G. Rosano, and E. Ferraro, “Chemotherapeutic drugs and mitochondrial dysfunction: focus on doxorubicin, trastuzumab and sunitinib,” *Oxidative Medicine and Cellular Longevity*, vol. 2018, Article ID 7582730, 15 pages, 2018.
- [82] L. I. Gordon, M. A. Burke, A. T. Singh et al., “Blockade of the erbB2 receptor induces cardiomyocyte death through mitochondrial and reactive oxygen species-dependent pathways,”

- The Journal of Biological Chemistry*, vol. 284, no. 4, pp. 2080–2087, 2009.
- [83] J. E. Finet and W. H. W. Tang, “Protecting the heart in cancer therapy,” *F1000 Research*, vol. 7, article 1566, 2018.
- [84] D. Iarussi, U. Auricchio, A. Agretto et al., “Protective effect of coenzyme Q₁₀ on anthracyclines cardiotoxicity: control study in children with acute lymphoblastic leukemia and non-Hodgkin lymphoma,” *Molecular Aspects of Medicine*, vol. 15, pp. S207–S212, 1994.
- [85] C. Myers, R. Bonow, S. Palmeri et al., “A randomized controlled trial assessing the prevention of doxorubicin cardiomyopathy by N-acetylcysteine,” *Seminars in oncology*, vol. 10, 1 (Suppl 1), pp. 53–55, 1983.
- [86] P. Lissoni, S. Barni, M. Mandalà et al., “Decreased toxicity and increased efficacy of cancer chemotherapy using the pineal hormone melatonin in metastatic solid tumour patients with poor clinical status,” *European Journal of Cancer*, vol. 35, no. 12, pp. 1688–1692, 1999.
- [87] R. Waldner, C. Laschan, A. Lohninger et al., “Effects of doxorubicin-containing chemotherapy and a combination with L-carnitine on oxidative metabolism in patients with non-Hodgkin lymphoma,” *Journal of Cancer Research and Clinical Oncology*, vol. 132, no. 2, pp. 121–128, 2006.
- [88] S. Ojha, H. Al Taei, S. Goyal et al., “Cardioprotective potentials of plant-derived small molecules against doxorubicin associated cardiotoxicity,” *Oxidative Medicine and Cellular Longevity*, vol. 2016, Article ID 5724973, 19 pages, 2016.
- [89] C. P. Bondonno, X. Yang, K. D. Croft et al., “Flavonoid-rich apples and nitrate-rich spinach augment nitric oxide status and improve endothelial function in healthy men and women: a randomized controlled trial,” *Free Radical Biology and Medicine*, vol. 52, no. 1, pp. 95–102, 2012.
- [90] N. D. Fisher, S. Hurwitz, and N. K. Hollenberg, “Habitual flavonoid intake and endothelial function in healthy humans,” *Journal of the American College of Nutrition*, vol. 31, no. 4, pp. 275–279, 2012.
- [91] K. Kawakami, S. Aketa, H. Sakai, Y. Watanabe, H. Nishida, and M. Hirayama, “Antihypertensive and vasorelaxant effect of water-soluble proanthocyanidins from persimmon leaf tea in spontaneously hypertensive rats,” *Bioscience Biotechnology and Biochemistry*, vol. 75, pp. 1435–1439, 2014.
- [92] M. Gómez-Guzmán, R. Jiménez, M. Sánchez et al., “Epicatechin lowers blood pressure, restores endothelial function, and decreases oxidative stress and endothelin-1 and NADPH oxidase activity in DOCA-salt hypertension,” *Free Radical Biology and Medicine*, vol. 52, no. 1, pp. 70–79, 2012.
- [93] M. E. Woodcock, W. J. Hollands, A. Konic-Ristic et al., “Bioactive-rich extracts of persimmon, but not nettle, Sideritis, dill or kale, increase eNOS activation and NO bioavailability and decrease endothelin-1 secretion by human vascular endothelial cells,” *Journal of the Science of Food and Agriculture*, vol. 93, no. 14, pp. 3574–3580, 2013.
- [94] N. Papageorgiou, D. Tousoulis, A. Katsargyris et al., “Antioxidant treatment and endothelial dysfunction: is it time for flavonoids?,” *Recent Patents on Cardiovascular Drug Discovery*, vol. 8, no. 2, pp. 81–92, 2013.
- [95] S. Upadhyay and M. Dixit, “Role of polyphenols and other phytochemicals on molecular signaling,” *Oxidative Medicine and Cellular Longevity*, vol. 2015, Article ID 504253, 15 pages, 2015.
- [96] G. Vilahur, T. Padró, L. Casaní et al., “Polyphenol-enriched diet prevents coronary endothelial dysfunction by activating the Akt/eNOS pathway,” *Revista Española de Cardiología*, vol. 68, no. 3, pp. 216–225, 2015.
- [97] Y. Zhang, H. Shi, W. Wang et al., “Antithrombotic effect of grape seed proanthocyanidins extract in a rat model of deep vein thrombosis,” *Journal of Vascular Surgery*, vol. 53, no. 3, pp. 743–753, 2011.
- [98] J. Minatti, E. Wazlawik, M. A. Hort et al., “Green tea extract reverses endothelial dysfunction and reduces atherosclerosis progression in homozygous knockout low-density lipoprotein receptor mice,” *Nutrition Research*, vol. 32, no. 9, pp. 684–693, 2012.
- [99] Y. Shen, N. C. Ward, J. M. Hodgson et al., “Dietary quercetin attenuates oxidant-induced endothelial dysfunction and atherosclerosis in apolipoprotein E knockout mice fed a high-fat diet: a critical role for heme oxygenase-1,” *Free Radical Biology and Medicine*, vol. 65, pp. 908–915, 2013.
- [100] W. R. Leifert and M. Y. Abeywardena, “Cardioprotective actions of grape polyphenols,” *Nutrition Research*, vol. 28, no. 11, pp. 729–737, 2008.
- [101] S. S. Hassellund, A. Flaa, S. E. Kjeldsen et al., “Effects of anthocyanins on cardiovascular risk factors and inflammation in pre-hypertensive men: a double-blind randomized placebo-controlled crossover study,” *Journal of Human Hypertension*, vol. 27, no. 2, pp. 100–106, 2013.
- [102] A. T. Mbaveng, R. Hamm, and V. Kuete, “Harmful and protective effects of terpenoids from African medicinal plants,” in *Toxicological Survey of African Medicinal Plants*, V. Kuete, Ed., pp. 557–576, Elsevier, London, 2014.
- [103] R. Rodrigo, C. Guichard, and R. Charles, “Clinical pharmacology and therapeutic use of antioxidant vitamins,” *Fundamental & Clinical Pharmacology*, vol. 21, no. 2, pp. 111–127, 2007.
- [104] M. M. Abdel-Daim, Y. M. Moustafa, M. Umezawa, K. V. Ramana, and E. Azzini, “Applications of antioxidants in ameliorating drugs and xenobiotics toxicity: mechanistic approach,” *Oxidative Medicine and Cellular Longevity*, vol. 2017, Article ID 4565127, 2 pages, 2017.
- [105] M. M. Abdel-Daim, H. A. Khalifa, A. I. Abushouk, M. A. Dkhil, and S. A. al-Quraishy, “Diosmin attenuates methotrexate-induced hepatic, renal, and cardiac injury: a biochemical and histopathological study in mice,” *Oxidative Medicine and Cellular Longevity*, vol. 2017, Article ID 3281670, 10 pages, 2017.
- [106] J. S. Ajarem, G. Al-Basher, A. A. Allam, and A. M. Mahmoud, “Camellia sinensis Prevents perinatal nicotine-induced neurobehavioral alterations, tissue injury, and oxidative stress in male and female mice newborns,” *Oxidative Medicine and Cellular Longevity*, vol. 2017, Article ID 5985219, 16 pages, 2017.
- [107] J. A. N. Sandamali, R. P. Hewawasam, K. A. P. W. Jayatilaka, and L. K. B. Mudduwa, “Cardioprotective potential of Murraya koenigii(L.) Spreng. leaf extract against doxorubicin-induced cardiotoxicity in rats,” *eCAM*, vol. 2020, article 6023737, pp. 1–16, 2020.
- [108] K. Fujita, K. Shinpo, K. Yamada et al., “Reduction of adriamycin toxicity by ascorbate in mice and Guinea pigs,” *Cancer Research*, vol. 42, no. 1, pp. 309–316, 1982.
- [109] K. Shimpō, T. Nagatsu, K. Yamada et al., “Ascorbic acid and adriamycin toxicity,” *The American Journal of Clinical Nutrition*, vol. 54, no. 6, pp. 1298S–1301S, 1991.

- [110] D. T. Vincent, Y. F. Ibrahim, M. G. Espey, and Y. J. Suzuki, "The role of antioxidants in the era of cardio-oncology," *Cancer Chemotherapy and Pharmacology*, vol. 72, no. 6, pp. 1157–1168, 2013.
- [111] G. Akolkar, D. da Silva Dias, P. Ayyappan et al., "Vitamin C mitigates oxidative/nitrosative stress and inflammation in doxorubicin-induced cardiomyopathy," *AJP Heart and Circulatory Physiology*, vol. 313, no. 4, pp. H795–H809, 2017.
- [112] K. Singh, M. Bhorl, Y. A. Kasu, G. Bhat, and T. Marar, "Antioxidants as precision weapons in war against cancer chemotherapy induced toxicity – exploring the armoury of obscurity," *Saudi Pharmaceutical Journal*, vol. 26, no. 2, pp. 177–190, 2018.
- [113] R. Carrasco, M. C. Ramirez, K. Nes et al., "Prevention of doxorubicin-induced cardiotoxicity by pharmacological non-hypoxic myocardial preconditioning based on docosahexaenoic acid (DHA) and carvedilol direct antioxidant effects: study protocol for a pilot, randomized, double-blind, controlled trial (CarDHA trial)," *Trials*, vol. 21, no. 1, article 137, 2020.
- [114] G. Akolkar, *Cardioprotective role of Vitamin C in the mitigation of oxidative/nitrosative stress in doxorubicin-induced cardiotoxicity*, A Ph.D. Thesis submitted to the Faculty of Graduate Studies, University of Manitoba, Winnipeg, Manitoba, Canada, 2017.
- [115] Z. Jawa, R. M. Perez, L. Garlie et al., "Risk factors of trastuzumab-induced cardiotoxicity in breast cancer," *Medicine*, vol. 95, no. 44, article e5195, 2016.
- [116] P. Kosalka, C. Johnson, M. Turek et al., "Effect of obesity, dyslipidemia, and diabetes on trastuzumab-related cardiotoxicity in breast cancer," *Current Oncology*, vol. 26, no. 3, pp. e314–e321, 2019.
- [117] O. Aseyev, C. Johnson, M. Turek, A. Law, J. A. Sulpher, and S. F. Dent, "Trastuzumab-related cardiotoxicity in patients with breast cancer with comorbidities of obesity, dyslipidemia, and diabetes," *Journal of Clinical Oncology*, vol. 34, no. 15, p. e12503, 2016.
- [118] N. Georgiadis, K. Tsarouhas, R. Rezaee et al., "What is considered cardiotoxicity of anthracyclines in animal studies Corrigendum in/10.3892/or.2020.7717," *Oncology Reports*, vol. 44, no. 3, pp. 798–818, 2020.
- [119] G. Cai, G. Shi, S. Xue, and W. Lu, "The atherogenic index of plasma is a strong and independent predictor for coronary artery disease in the Chinese Han population," *Medicine*, vol. 96, no. 37, article e8058, 2017.
- [120] T. Kazemi, M. Hajhosseini, M. Moossavi, M. Hemmati, and M. Ziaee, "Cardiovascular risk factors and atherogenic indices in an Iranian population: Birjand East of Iran," *Clinical Medicine Insights: Cardiology*, vol. 12, article 1179546818759286, 2018.
- [121] E. Gómez-Álvarez, J. Verdejo, S. Ocampo, C. I. Ponte-Negretti, E. Ruíz, and M. M. Ríos, "The CNIC-polypill improves atherogenic dyslipidemia markers in patients at high risk or with cardiovascular disease: results from a real-world setting in Mexico," *IJC Heart & Vasculature*, vol. 29, article 100545, 2020.
- [122] Y. Zhan, T. Xu, and X. Tan, "Two parameters reflect lipid-driven inflammatory state in acute coronary syndrome: atherogenic index of plasma, neutrophil-lymphocyte ratio," *BMC cardiovascular disorders*, vol. 16, no. 1, p. 96, 2016.

Review Article

Roles of Reactive Oxygen Species in Cardiac Differentiation, Reprogramming, and Regenerative Therapies

Jialiang Liang , Min Wu, Chen Chen, Mingjie Mai, Jinsong Huang , and Ping Zhu 

Guangdong Cardiovascular Institute, Guangdong Provincial People's Hospital, Guangdong Academy of Medical Sciences, Guangzhou, Guangdong 510100, China

Correspondence should be addressed to Jinsong Huang; jasonwong32@hotmail.com and Ping Zhu; tanganqier@163.com

Received 29 May 2020; Accepted 22 July 2020; Published 29 August 2020

Guest Editor: Giulio Agnetti

Copyright © 2020 Jialiang Liang et al. This is an open access article distributed under the Creative Commons Attribution License, which permits unrestricted use, distribution, and reproduction in any medium, provided the original work is properly cited.

Reactive oxygen species (ROS) have been implicated in mechanisms of heart development and regenerative therapies such as the use of pluripotent stem cells. The roles of ROS mediating cell fate are dependent on the intensity of stimuli, cellular context, and metabolic status. ROS mainly act through several targets (such as kinases and transcription factors) and have diverse roles in different stages of cardiac differentiation, proliferation, and maturation. Therefore, further detailed investigation and characterization of redox signaling will help the understanding of the molecular mechanisms of ROS during different cellular processes and enable the design of targeted strategies to foster cardiac regeneration and functional recovery. In this review, we focus on the roles of ROS in cardiac differentiation as well as transdifferentiation (direct reprogramming). The potential mechanisms are discussed in regard to ROS generation pathways and regulation of downstream targets. Further methodological optimization is required for translational research in order to robustly enhance the generation efficiency of cardiac myocytes through metabolic modulations. Additionally, we highlight the deleterious effect of the host's ROS on graft (donor) cells in a paracrine manner during stem cell-based implantation. This knowledge is important for the development of antioxidant strategies to enhance cell survival and engraftment of tissue engineering-based technologies. Thus, proper timing and level of ROS generation after a myocardial injury need to be tailored to ensure the maximal efficacy of regenerative therapies and avoid undesired damage.

1. Introduction

Myocardial infarction (MI) is an anemic infarct disease associated with cell death of myocardium and frequently causes heart failure or cardiac arrest [1]. Recently, the promising therapeutic strategies have emerged for regeneration of cardiomyocytes (CMs) or remuscularization of the myocardium in MI [2], including induction of endogenous CM proliferation, direct reprogramming of nonmyocytes to CMs, and transplantation of pluripotent stem cell- (PSC-) derived CMs. Although these studies have demonstrated substantial potentials of *in vitro* and *in vivo* CM regeneration, several notable challenges remain to be addressed before translation to a clinical setting. For instance, insufficient long-term engraftment and integration with host tissue after transplantation remains a critical hurdle for using PSC-CMs in regen-

erative therapy [3]. Other issues including low regeneration efficiency, immaturity, and tumorigenic risk would compromise the therapeutic effects of new regenerative approaches [2, 4]. Therefore, it is important to converge various biochemical strategies with methods developed for regeneration of functional CM to overcome these challenges [5].

Current protocols of CM regeneration have been developed based on activating the embryonic cardiomyogenesis-induced signaling pathways and gene regulatory networks [6]. Most studies of CM regeneration are focusing on the contributions of transcriptional mechanisms including gene programming, epigenetic chromatin modifications, and biochemical differentiation cues [7]. Energy metabolism is central to mammalian heart development and function, and metabolic processes can be modulated to support the contractile apparatus of regenerated CMs [8]. The change in

energy metabolism impacts the ability of stem cell self-renewal, differentiation, and cell fate decision [9]. Although the coordination of genetic networks with developmental bioenergetics is critical to CM phenotype specification, the underlying metabolic mechanisms that drive cardiac differentiation are not fully known.

The metabolic processes in heart development and disease are regulated by redox signaling through the direct effects of O_2 levels and the byproduct-reactive oxygen species (ROS) [10]. Emerging evidence shows that the production and signaling of ROS plays an important role in heart development and pathogenesis of cardiovascular disease [11, 12]. ROS serve as an important driver of cell cycle arrest in post-natal CMs, and the mechanisms of CM proliferation have been summarized comprehensively [13, 14]. In this review, we discuss the current state of the art in effect of redox signaling on the strategies of myocardial regeneration including PSC-CM differentiation and cardiac reprogramming. In addition, we focus on the effect of ROS on PSC-CM engraftment in the host environment and highlight the importance of antioxidant approaches for enhancing efficacy of cell therapy.

2. Generation and Function of ROS

Here, we briefly outline the sources, forms, and functions of ROS related to cardiac biology.

2.1. Main Sources of Cellular ROS. Oxidation and reduction (redox signaling) induce changes in structural and functional characteristics of molecules or proteins by loss or gain of an electron, thus mediating transmission and amplification of metabolic signals. The major molecules that participate in redox signaling are ROS that are byproducts of the metabolism of oxygen such as superoxide, hydrogen peroxide, and hydroxyl radical [15]. Cellular ROS mostly originate from superoxide $O_2^{\cdot-}$ produced by nicotinamide adenine dinucleotide phosphate (NADPH) oxidases (NOXs), the electron transport chain (ETC) in the mitochondria, or the nitric oxide synthases (NOSs).

The NOX family includes seven NOX isoforms with distinct catalytic subunits and they are crucial regulators of redox signaling in multiple body systems and organisms [16]. NOX enzymes can transfer electrons from NADPH to oxygen across biological membranes to produce ROS in both phagocytic and nonphagocytic cells [16, 17]. Mitochondrial ETC transfers electrons from NADH (nicotinamide adenine dinucleotide hydrogen) and succinate along a controlled redox path during respiratory ATP synthesis. However, the electron flow in ETC is an imperfect process, and occasionally oxygen molecules may undergo one- or two-electron reduction reactions to form ROS [18]. Depending on mitochondrial states of respiration, complexes I and III of the ETC may contribute to ROS production through leakage of electrons [18, 19]. NOSs catalyze the conversion of L-arginine to L-citrulline and NO, but can become uncoupled under pathological conditions and switch to ROS production [20].

2.2. ROS Exert Different Physiological and Pathological Functions. ROS can be classified depending on their chemical properties into two groups: one-electron oxidants (e.g., free radical $O_2^{\cdot-}$ and HO^{\cdot}) and two-electron oxidants (e.g., nonradical H_2O_2) [21]. Superoxide $O_2^{\cdot-}$ can diffuse within a cell with a relatively longer half-life as compared with other radicals but is neither a strong oxidant nor a powerful reductant [22]. Hydrogen peroxide H_2O_2 is stable, diffuses within and between cells, and can function as a signaling molecule or second messenger in the regulation of a variety of biological processes [23]. Hydroxyl radical HO^{\cdot} is formed from H_2O_2 via Fenton chemistry in the presence of Fe^{2+} . HO^{\cdot} , the most reactive ROS, is responsible for DNA damage, oxidative stress, and lipid oxidation, but its short half-life (10^{-9} s) restricts its damaging effects [24, 25]. Therefore, H_2O_2 appears to be a critical ROS molecule in redox-dependent signal transduction.

It is known that a physiological H_2O_2 flux activates signaling pathways by reversible oxidation of effector proteins. H_2O_2 oxidizes the thiol side chain of cysteine residues of the targeted functional motifs [26]. The cysteine residues are modified with highly susceptible thiolate anions under physiological condition, while oxidation of these anions into sulfenic forms can change the activity and function of proteins such as protein tyrosine kinases and transcription factors (TFs) [27, 28], thereby modulating the downstream gene expression and cell behaviors.

The borderline between “oxidative eustress” (beneficial responses) and “oxidative distress” (deleterious responses) in different pathophysiological settings is highly context dependent and remains to be clearly characterized in health and disease [29]. When ROS concentrations remain at physiological levels, they are indispensable in maintaining cell signaling and redox homeostasis. However, excessive production of ROS or oxidative stress has been associated with disease pathogenesis including cardiovascular disease and cancer [30]. ROS regulate diverse processes such as cell death, calcium handling, and cardiac hypertrophy involved in the pathophysiology of heart failure [31].

ROS levels are influenced not only by their generation rate but also by ROS-scavenging systems or antioxidants. Endogenous antioxidant defense system exists to detoxify ROS, repair oxidative damage, and maintain redox homeostasis [32]. Specific endogenous antioxidants such as catalase, peroxiredoxins, thioredoxin, and glutathione peroxidases can prevent potential damage of overoxidation by H_2O_2 [33, 34]. Our previous study also demonstrated that H_2O_2 -induced CM hypertrophy was improved by activation of antioxidant heme oxygenase-1 (HO-1) [35].

In addition, the compartmentalization and temporal profiles of ROS need to be considered to interpret the consequences of downstream signaling cascades. For instance, elevated mitochondrial ROS is a principal source of oxidative stress leading to arrhythmias and contractile dysfunction in heart failure, and reduction of mitochondrial ROS (rather than cytoplasmic ROS) can prevent and reverse electrical instability and sudden cardiac death [36]. Thus, the physiological roles of ROS and their toxic effects are complicated, which are influenced by a multitude of factors including

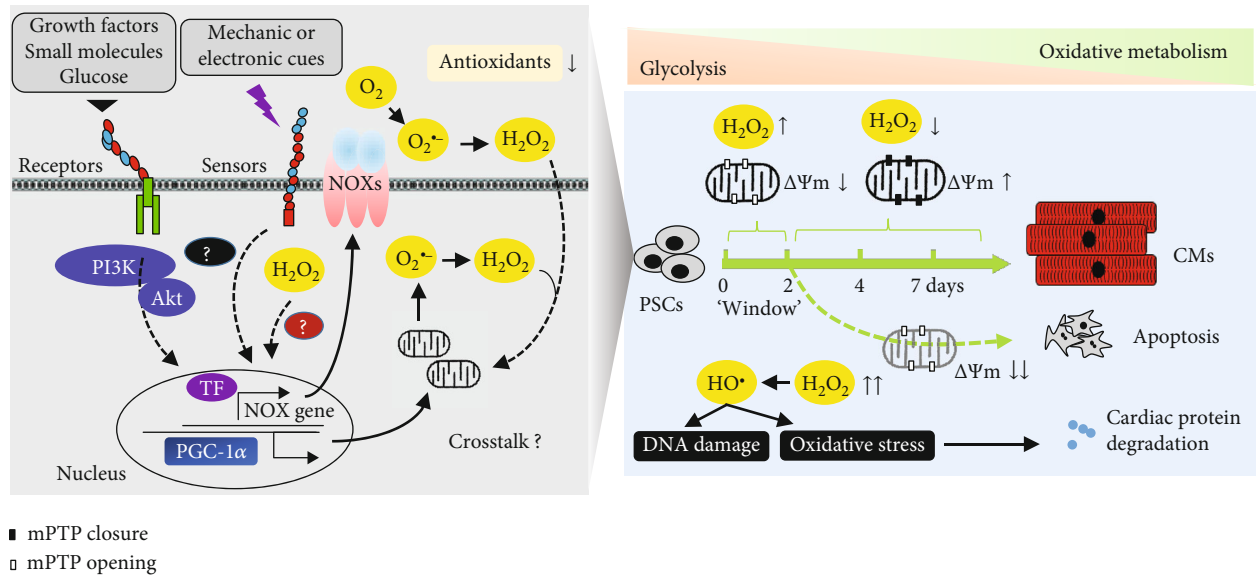


FIGURE 1: ROS are important for initial stage of differentiation but dispensable for the late stage. ROS are generated by multiple pathways and involved in differentiation of PSCs in response to developmental cues. After closure of mPTP, ROS are decreased and redox signaling is set for further differentiation and functional maturation, while excessive ROS levels would inhibit this process through increased oxidative stress and degradation of structural proteins, eventually leading to apoptotic cell death. NOXs: NADPH oxidases; TF: transcription factor; PGC-1 α : peroxisome proliferator-activated receptor γ coactivator 1 α ; mPTP: mitochondrial permeability transition pore; PSCs: pluripotent stem cells; CMs: cardiomyocytes.

concentration, source, distribution, and type of ROS. We discuss the complex roles of ROS, H₂O₂ in particular, in CM differentiation and heart regenerative therapy below.

3. ROS Mediate Cardiac Differentiation of PSCs

PSCs including iPSCs (induced pluripotent stem cells) and ESCs (embryonic stem cells) have emerged as one of the promising cell resources used to differentiate into functional CMs for heart regeneration [37]. Activation of embryonic signaling pathways including Activin, TGF- β , Wnt, and BMP is essential for development of CM lineage [38]. Multiple complex interactions between these conserved signaling pathways control the initial differentiation, proliferation, and maturation of myocardium to establish the cardiovascular system [38]. The delineation of specific redox-sensitive pathways and mechanisms that contribute to different components of CM regeneration processes may facilitate to fine-tune existing protocols or devise novel strategies in heart disease modeling and therapy.

New CMs can be generated from mesodermal progenitors during spontaneous differentiation (embryoid body (EB) formation or a monolayer induction) of PSCs by using growth factors and small molecules mimicking developmental signals [39, 40]. For stem cell culture and maintenance, ROS scavengers or antioxidant supplements are extensively used to prevent cellular oxidative stress [41]. However, β -mercaptoethanol and other thiol-based antioxidant supplements may cause changes to cellular redox state and then reduce the cardiogenic potential of stem cells [42]. The molecular mechanisms involved in metabolism and ROS regulation of PSC differentiation are still poorly understood

and merit further investigation to optimize stem cell culture methods.

3.1. Generation of ROS in Early Differentiation Stage.

Accumulating evidence shows that intracellular ROS are a critical signal to trigger CM differentiation of stem cells (Figure 1). The intracellular ROS level was increasing in early stage of mouse ESC differentiation [43]. The differentiation cues (e.g., growth factors, small molecules, mechanical stimulus, and electrical fields) were found to increase ROS level in ESCs, while cardiac lineage formation would be impaired by inhibition of ROS-generating pathways or ROS activity [44–46].

Compared to differentiated cells, PSCs have few immature mitochondria (that are globular in shape with poor cristae structure) and mostly rely on glycolysis to meet their energy demands [47, 48]. Therefore, cardiac specification and excitation-contraction coupling require a switch of glycolytic metabolism towards more efficient mitochondrial oxidative metabolism in PSCs. The energetic switch during differentiation of ESCs was programmed by rearrangement of the metabolic transcriptome (encoding enzymes of glycolysis, fatty acid oxidation, the Krebs cycle, and the ETC) and development of a mature mitochondrial network [49]. ROS are subsequently generated during oxidative metabolism in redox regulation of mitochondrial biogenesis and promote cardiac differentiation and maturation [50]. Thus, ROS generation is potential crosstalk between genetic and metabolic signaling in directing cell fate.

The mechanisms underlying ROS generation remain poorly known in current studies of initiating cardiac differentiation of PSCs. A cytokine-PI3-kinase-NOXs cascade was reported as an initial signal of ROS upregulation in cardiac

differentiation of mouse ESCs [43, 45], suggesting the role of ROS as intracellular second messengers. Additionally, stimulation of fatty acid metabolism by activation of peroxisome proliferator-activated receptor- α may be an upstream signal of NOX4-induced ROS generation in mouse ESCs, while mitochondrial electron transport was not involved in this process [51]. Mechanical strain-NOXs, metabotropic glutamate receptor 5, and the PI3K/AKT pathway may also contribute to ROS generation in cardiomyogenesis of ESCs [52–54]. Other studies showed a high expression level of NOX4 in mouse ESCs and demonstrated it as an important source of ROS signals involved in cardiomyogenesis by using siRNA approach [55]. NOX4-induced ROS was also an important signal of differentiating cardiac progenitors under stimulation of magnetic fields [56].

While most of the above studies involve activation of NOX4, ROS derived from mitochondria also play an important signaling role in differentiation and maturation. Specific antagonists had been used to demonstrate an essential role of complex III activity of the mitochondrial ETC in cardiac differentiation and calcium oscillations [57]. In mitochondria of cardiac myocytes, complex III is the principal site for ROS production during the oxidation of complex I substrates [58]. Importantly, a high glucose concentration had been shown to promote cardiac differentiation of ESCs *via* mitochondrial ROS generation [59]. Temporally reduced antioxidant activity of peroxiredoxin-2 *via* nitrosylation can cause transient endogenous ROS accumulation and promote ESC-derived cardiomyogenesis [60]. During cardiac differentiation of human ESCs, PGC-1 α -dependent mitochondrial biogenesis was associated with increased ROS levels in the CM population [61]. Therefore, cellular ROS are tightly regulated by a variety of proteins involved in the redox regulation of PSCs undergoing a metabolic switch when they differentiate.

ROS may be differently generated in multiple subcellular compartments in targeted cells. Communications between these distinct sites of ROS generation are also functionally relevant to cardiac differentiation. NOX4 can be activated by mitochondrial ROS in differentiated ESCs under the high glucose condition, suggesting an integrated signal between NOXs and mitochondrial ETC [59]. Moreover, a feed-forward regulation of ROS generation was shown by H₂O₂-induced NOX4 gene expression in cardiac differentiation [62]. Intriguingly, an increasing level of ROS can lead to further release of mitochondrial ROS, termed ROS-induced ROS release, which propagates and amplifies ROS production and effects in cardiac myocytes [63], although this remains undetermined in cardiac differentiation.

The location of ROS generation should be considered when interpreting their effects. Although instructive, the antioxidant compounds do not readily identify the source of ROS due to low specificity. The dynamics of H₂O₂ metabolism can be assessed by the use of fluorescent probes and other redox-sensitive tools [64]. H₂O₂ release and cell distribution can be visualized by new ratiometric reporters that have been targeted to subcellular compartments [65]. These molecular tools will be a more specific system for *in vivo* monitoring of cardiac redox signaling and heterogeneity of individual cell responses to oxidants.

3.2. Continuous Exposure to ROS Inhibits Cardiomyogenesis. The physiological range of H₂O₂ concentrations was estimated to be between 1 and 10 nM, but it depends on several parameters including cell type and developmental stage [66]. Exogenous H₂O₂ is a useful tool to determine the direct contribution of ROS in CM differentiation. Stimulation of cardiomyogenesis by exogenous H₂O₂ (10 nM) was showed to increase the number of beating EB containing CMs and the expression of cardiac genes at 2–3 induction days [43, 55, 62]. Several cardiogenic TFs and cytokines were upregulated by addition of H₂O₂ in ESCs [67].

In addition to ROS sources, the role of ROS in cardiac differentiation is dependent on metabolism phases and redox balance. Continuous exposure to ROS at a high concentration may overwhelm the antioxidative capacity of cells, thereby exerting a detrimental effect on cell differentiation. Indeed, exogenous H₂O₂ (100 nM) was showed to inhibit the beating activity of EBs from day 5 to 12 [68]. Excessive H₂O₂ levels (1 μ M) can reduce and degrade Gata4 protein in P19 stem cells [69]. Moreover, increase of intracellular ROS level was responsible for inhibitory effect of valproic acid on cardiomyogenesis [70]. The enforced expression of the pyruvate dehydrogenase phosphatase catalytic subunit 1 gene increased mitochondrial ROS levels in ESCs and inhibited cardiac differentiation [71].

These data suggest that a particular window of “cardiopoietic programming” [72] may exist where a proper level of ROS is important for cardiac differentiation during early stages. During the early period of cardiac differentiation, a high ROS level and low ATP production from immature mitochondria of PSCs may help themselves (or regenerative cells) to adapt to the stress of metabolic switch. After metabolic demand is fulfilled, activation of endogenous antioxidant defense will decrease ROS level to avoid excessive oxidative stress on genetic programming of further CM differentiation and maturation (Figure 1).

Accumulating evidence points out that the redox signaling is associated with mitochondrial permeability transition (MPT) regulating myocyte differentiation and maturation. MPT is caused by the opening of mitochondrial permeability transition pores (mPTP) in the inner mitochondrial membrane. mPTP opening can couple to mitochondrial ETC-dependent ROS production in unstressed cells [73], while mechanisms by which mPTP regulates ROS remain to be determined. Importantly, a study of heart development showed that mPTP opening was nonpathologic in embryonic cardiac myocytes (E9.5) with immature mitochondrial structure and function, low ATP production, and high ROS levels [74]. Differentiation of embryonic CMs was accelerated after closure of mPTP accompanied with decreased ROS levels, whereas concurrent treatment with oxidant and mPTP blocker inhibited differentiation [74]. Therefore, the beneficial effect of ROS in the window of “cardiopoietic programming” would be offset after closure of mPTP.

Recently, some mPTP inhibitors have been assessed for inducing cardiac differentiation. mPTP inhibition by cyclosporine-A increased ROS generation, but addition of antioxidants rather than prooxidant can enhance cardiomyogenesis [75]. Prolonged closure of mPTP with cyclosporine-

A in human iPSC-derived endothelial cells resulted in more mature mitochondria, prevention of ROS leakage, and functional improvements [76]. These studies suggested that the redox signaling is a cardiogenic regulatory factor lying the downstream of mPTP inhibition. The approaches relying on manipulation of redox status should be dependent on monitoring the mode of mPTP.

There are several common features (e.g., cytochrome c release and caspase activation) that govern cell differentiation and apoptosis [77, 78]. MPT and ROS are known to involve in the etiology of several pathological conditions related to necrosis and apoptosis [79], while they can trigger cell differentiation as discussed above. Basic ROS activity contributes to cell differentiation but can induce caspase-dependent apoptosis once the oxidative stress exceeds a certain threshold [80]. Lower levels of ROS, loss of one p53 isoform, and reversible loss of the mitochondrial membrane potential were observed in the differentiating cells as compared to the apoptotic cells that were induced by doxorubicin treatment (an antitumor agent or useful tool with cardiotoxicity), although these features were absent in undifferentiated ESCs [81]. This study indicated that the timing, intensity, and reversibility of activation of mitochondrion-dependent apoptotic pathway may determine whether a cell dies or differentiates.

3.3. ROS Regulate Cardiac Gene Transcription and Expression. ROS have been considered as critical small-molecule messengers in cell signaling transduction. Several signal transducers are redox-sensitive and can be reversibly or irreversibly modified by ROS, providing a link with the control of gene expression [82]. Principal modifications are selective oxidation or nitrosylation of key redox-sensitive cysteine residues in kinases with low ionization pKa (4-5 vs. 8.5 in nonreactive cysteines of most other proteins) [83]. Cysteine oxidation results in either inhibition or activation of targeted molecules depending on the tertiary structure [83]. Furthermore, ROS have been implicated in modulating epigenetic pathways including histone modifications, DNA modifications, expression of noncoding RNAs, and ATP-dependent chromatin remodeling in cardiovascular diseases [84]. Herein, we discuss the direct targets of ROS involved in the mechanisms of cardiac differentiation and heart regeneration (Figure 2).

In response to differentiation cues such as growth factors, the downstream cell signaling pathways will be activated before the gene transcription determining cardiac lineage [85]. Tightly controlling phosphorylation of mitogen-activated protein kinase (MAPK) is important for early mesoderm and subsequent CM formation [86]. ROS were shown to enhance differentiation of human ESCs into bipotent mesendoderm *via* the activation of MAPK family [87]. The phosphorylation of p38 MAPK was inhibited by knockdown of NOX4 and nuclear translocation of Mef2c was prevented, thereby reducing cardiac differentiation [55]. Activation of p38 MAPK was eliminated by an antioxidant in ESCs, and p38 phosphorylation may provide a checkpoint during mesodermal differentiation to the cardiac lineage [59]. These studies suggested that activation of p38 MAPK was closely related to high ROS levels.

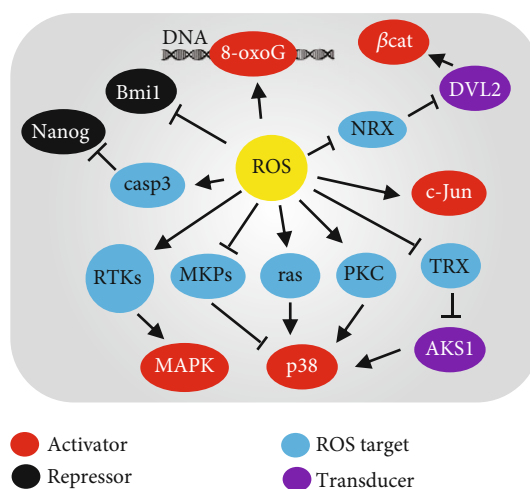


FIGURE 2: A possible network of molecular events targeted by ROS related to cardiac differentiation pathways. The activators or repressors of cardiac gene expression can be directly or indirectly regulated through ROS modifying the redox-sensitive molecules. 8-oxoG: 8-oxoguanine; β cat: β -catenin; casp3: caspase3; DVL2: dishevelled segment polarity protein 2; NRX: nucleoredoxin; TRX: thioredoxin; ASK1: apoptosis signal-regulating kinase 1; PKC: protein kinase C; RTKs: receptor tyrosine kinases; MAPKs: mitogen-activated protein kinases; MKPs: MAPK phosphatases.

In contrast, activation of p38 MAPK mediated by ROS was involved in inhibiting cardiac differentiation of murine ESCs [88], suggesting that the effects of p38 MAPK may be different in distinct timing of differentiation. It remains unknown how ROS can interact with p38 MAPK signaling during cardiogenesis. Oxidative modifications of upstream signaling proteins or receptor kinases by ROS may be a plausible mechanism for activation of the MAPK pathways [89]. Apoptosis signal-regulating kinase 1 (ASK1) was an upstream protein of p38 MAPK and bound to reduced thioredoxin in unstressed HEK293A cells, while thioredoxin can be oxidized upon oxidative stress and disassociate from ASK1, thereby leading to p38 phosphorylation *via* oligomerization of ASK1 [90]. Alternatively, degradation or inactivation of MAPK phosphatase by ROS-related ubiquitin-proteasome system may contribute to activation of the MAPK pathways in ESCs and other cells [91, 92]. Therefore, MAPKs might not be directly redox-sensitive but instead rely on ROS-mediated upstream proteins such as ras and PKC [93]. These potential mechanisms of ROS-related pathways need to be further determined in the setting of cardiac differentiation.

Cardiac commitment of PSCs is controlled by the regulatory network of TFs such as Nkx2.5, Gata4, and Tbx5 [6, 85]. Although these TFs might not be directly targeted by ROS, their transcription can be regulated by other epigenetic modulators or constitutively active TFs (e.g., AP1 and HIF1 α) that are ROS-sensing in vascular cells [94]. Expression of earliest cardiogenic TFs such as Gata4 and Mef2c was dependent upon Nox4-generated ROS that activate redox-sensitive TFs including c-Jun in P19 stem cells [95]. Moreover, extrinsic ROS can enhance the redox-sensitive

caspase-mediated degradation of Oct4 and Nanog (pluripotent factors), thereby activating Gata4 and Nkx2.5 promoters that were repressed by Nanog/Hdac4 complex in P19 stem cells [69]. Interestingly, an increase of ROS due to removal of antioxidant in medium can induce epigenetic DNA modifications (such as 8-oxoG) on Tbx5 promoter, leading to Tbx5 activation that enhanced cardiac differentiation of ESCs [96]. Bmi1 is an epigenetic repressor silencing cardiac genes in steady state of cardiac progenitors, while ROS and oxidative damage induced Bmi1 delocalization from canonical DNA targets, therefore triggering an imbalance toward upregulation of differentiation-related genes and downregulation of stemness-related genes in cardiac progenitors [97]. In neural progenitor cell lines, ROS may induce dissociation of redox-sensitive targets such as nucleoredoxin from dishevelled complex that was responsible for activation of the Wnt/ β -catenin cascade in transcription of differentiation-related genes [98]. Although different cell models including ESCs have been tested, ROS may regulate downstream gene expression through a common mechanism targeting the transcription-related factors.

The above mechanism studies suggest that identification of redox-sensitive targets helps to delineate how ROS or oxidative stress contributes to cell fate decision. New methods are therefore needed to screen ROS targets and verify their redox functions in various models of cardiomyogenesis and heart regeneration on a global scale. For instance, cysteine reactivity in response to oxidative modifications can be labeled using chemical probes and further assessed by quantitative mass spectrometry in targeted proteins or in a whole proteome scale [99, 100]. In addition to protein assays, several methods have been developed using next-generation sequencing to assess the genome wide distribution of oxidative DNA modifications [101]. Importantly, several computational tools and databases have been developed for analysis of redox-sensitive cysteines and annotation of ROS-related proteins and peroxidase families [102, 103]. Thus, these chemical-genetic methods enable detailed characterization of protein or DNA modifications that are targeted by ROS in the redox environment related to CM regeneration.

4. Unexploited Role of ROS in Direct Cardiac Reprogramming

Transdifferentiation is a new paradigm that has been devised to generate cardiac lineage-specific cells directly from somatic cells, by combining transient overexpression of the cardiac specific TFs. The retroviral transfections of Gata4, Mef2c, and Tbx5 (or with Hand2) reprogrammed mouse postnatal cardiac or skin fibroblasts directly into CM-like cells (termed induced CMs (iCMs)), but with low efficiency [104–106]. The TF overexpression was an inefficient method to induce cardiac reprogramming, and the infected cells lacked some molecular and electrophysiological phenotypes of mature CMs [107]. Therefore, researchers are exhibiting tremendous enthusiasm and interest in the quest to elucidate the mechanisms of iCM generation and further enhance

reprogramming efficiency. The current progress in this field has been summarized in other reviews [108, 109].

Yet, it remains unknown whether ROS are involved in the process of direct cardiac reprogramming. A preliminary study showed that the treatment of vitamin E nicotinate (an antioxidant) facilitated application of direct cardiac reprogramming approach to repair heart damage *in vivo* [110]. Further investigation should determine whether the observed effects were related to the elimination of ROS or redox imbalance in iCMs or injured host CMs. Exogenous ROS incubation, use of redox-sensitive probes, treatment of antioxidants in different induction timing, and loss-of-function studies of ROS-associated genes would be helpful strategies to address the unexplored role of ROS in both *in vitro* and *in vivo* direct cardiac reprogramming.

The studies of ROS in induced pluripotency reprogramming may bring new insights into genetic resetting during direct cardiac lineage conversion. NOX expression and ROS generation were increased in the early stage of iPSC reprogramming, whereas antagonism of ROS using antioxidants or knockdown of NOXs decreased reprogramming efficiency [111]. Excessive ROS generation impaired iPSC generation, and antioxidant enzymes such as Gpx2 and Nrf2 were upregulated in the late phase of reprogramming [111, 112]. Therefore, these data indicate that the kinetics and intensity of redox signaling is critical for efficient cell reprogramming. Importantly, short-term opening of mPTP has been found during the early stage of somatic cell reprogramming into iPSCs, as accompanied with activation of mitochondrial ROS [113]. Furthermore, ROS generation triggered by activation of innate immune signaling is required for pluripotent reprogramming and lineage transdifferentiation [114].

The precise mechanisms of direct cardiac reprogramming are not well understood. Recently, next-generation sequencing techniques have been employed not only to decipher the transcriptional mechanisms of cardiac TFs but also to uncover the dynamic process of cell fate reprogramming in a genome-wide scale or at a single-cell level [115–117]. These data suggest that innate immune signaling is critical for cardiac fate acquisition at early stage and cell cycle exit is essential for successful reprogramming. It is conceivable that immune response genes can be activated due to the common use of viral vectors for reprogramming gene delivery [118, 119]. For instance, expression of Toll-like receptor 3 (an immune regulatory gene) contributed to human cardiac reprogramming through impacting DNA methylation status of cardiac loci [115]. Given that ROS can interact with innate immune receptors including Toll-like receptors and NOD-like receptors [120], it is likely that ROS are an important signal during the early stage of cardiac reprogramming and redox balance ensures the further functional maturation of iCMs, which is similar to cardiac differentiation as discussed above. However, it is unknown whether the innate immune pathways are still reactivated in alternative, nonviral reprogramming approaches such as chemically induced CM-like cells [121]. Despite the complexity, the ultimate goal of cardiac TFs or reprogramming factors is to convert the fibroblasts to contracting muscle cells with a high metabolic demand. Based on gene expression of metabolic enzymes,

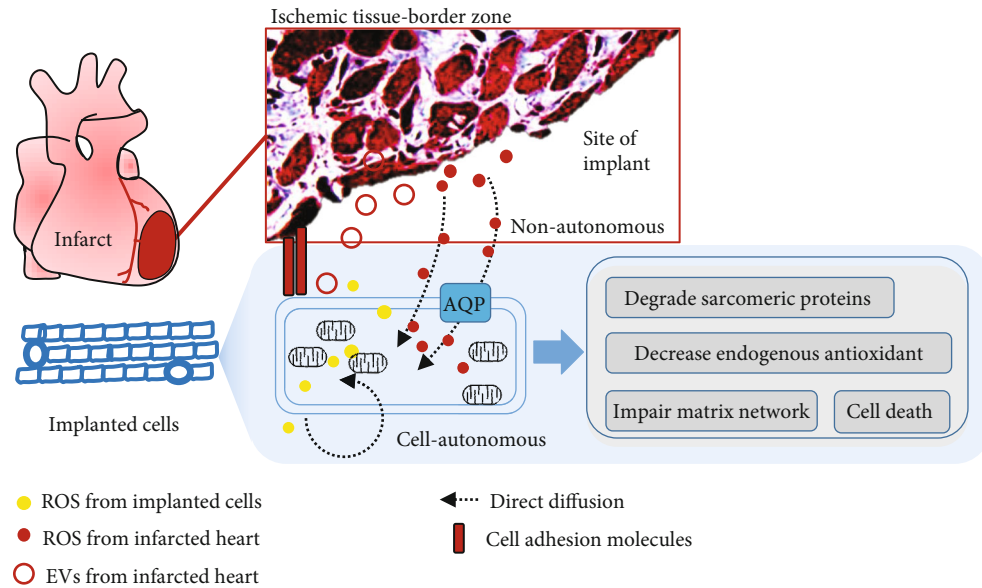


FIGURE 3: Potential interactions between the ischemic heart and implanted cells contribute to low engraftment efficiency. When stem cells or PSC-CMs are implanted, intracellular ROS would be increased and induce cell death in a cell-autonomous manner in response to the hypoxic microenvironment. Paracrine effects of host's ROS are involved in regulation of the graft cell fate and may lead to engrafted cell death in a nonautonomous manner. EVs: extracellular vesicles; AQP: aquaporin.

iCMs utilized fatty acid oxidation as the main pathway, which was distinguishable from iPSC-CMs primarily using glycolysis [122]. All above findings encourage further investigation of ROS in the mechanisms of cardiac reprogramming with respect to chromatin accessibility changes, innate immune response, cell cycle regulation, and metabolic switch.

5. ROS Affect Regenerative Therapy in the Infarcted Heart

Currently, PSCs are the main cell sources that can definitively generate cardiovascular cells (seed cells) in high quantities for MI therapy using cardiac tissue engineering [123]. However, insufficient integration of transplanted cells with ischemic tissue remains a major hurdle for clinical translation of using engineered heart tissues (EHTs) in regenerative therapy. Understanding of the healing process of MI, including inflammatory, proliferative, and maturation phases, is important for design and timing selection of cell transplantation in patients. There exists a potential feedback loop (cell-cell interaction) between the host infarcted myocardium and the engraftment of implanted cells, as discussed by us [124]. In this section, we integrate the current evidence to speculate how ROS affect the cell survival and functional engraftment of implanted or regenerated CMs in the infarcted heart (Figure 3).

5.1. A High Level of Intracellular or Extracellular ROS Harms Graft Cell Survival. Clinical application of stem cell therapies requires large-scale cell culture technologies such as bioreactors that allow for conditional manipulations of the survival, differentiation, and maturation of PSC-CMs [125]. Maintenance of low cellular H_2O_2 concentration may facilitate

in vitro maturation of PSC-CMs [126]. However, PSC-CMs appear to be particularly sensitive to hypoxia and nutrient deprivation-induced cell death associated with increased ROS formation and modulation of key nutrient sensors [127]. A gradual cessation of contractility with increased intracellular ROS and loss of calcium transients was found in mouse PSC-CMs after short-term exposure to monochromatic light [128]. It is likely that ROS-induced protein glutathionylation contributes to a loss of myofibril integrity and degradation of sarcomeric proteins in CMs [129]. Cellular ROS are substantially elevated in cardiovascular cells during ischemia and reperfusion procedure and also involved in the post-MI remodeling of heart failure [36, 130]. Excessive ROS generation depletes endogenous antioxidant defenses in the ischemic heart and primes the cell for oxidative damage at reperfusion [130]. ROS also can persistently impair myocardial matrix network by nonenzymatic protein degradation and modification or activating specific proteolytic enzymes [130]. Therefore, maintenance of redox homeostasis through reduced intrinsic ROS generation and increased antioxidant defense mechanism may promote therapeutic efficacy of cardiac cell replacement approaches (see later).

Extracellular ROS and oxidative stress are critical components of harsh conditions in the infarcted myocardium. Despite the short half-lives, extracellular ROS likely participate in cell-cell communications at the site of ischemia. NOX isoforms are responsible for generation of superoxide ($O_2^{\cdot -}$) toward intracellular or extracellular space and its autocrine or paracrine-like action [131]. Unlike superoxide free radicals ($O_2^{\cdot -}$) with a negative charge, H_2O_2 is known as a membrane permeable molecule which can diffuse through the mitochondrial and cell membranes. Therefore, ROS can serve as a paracrine-diffusible signal to mediate nearby cells. For instance, H_2O_2 increased in the infarct core can diffuse

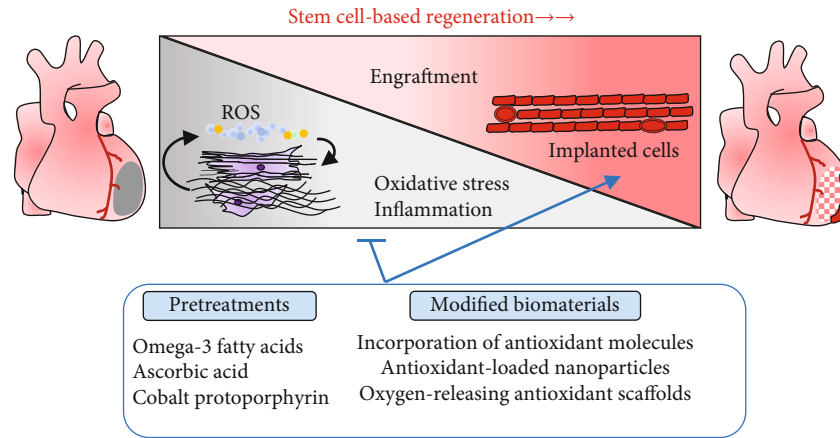


FIGURE 4: Overview of antioxidant approaches to enhance stem cell-based regeneration. Antioxidant strategies including pretreatments and modified biomaterials targeting the ROS signaling can be applied to enhance the engraftment of implanted stem cells or PSC-CMs.

into circulating cells and produce 3-nitrotyrosine that was cytotoxic and contributed to decreased recruitment of endogenous progenitor cells to the site of injury [132]. ROS generated in the infarcted heart can hinder the adhesiveness of injected cells *via* interference of focal adhesion molecules [133]. Interestingly, several aquaporins (water channels) have been identified to facilitate movement of H_2O_2 across cell membranes at a much higher rate than passive diffusion [134], but their roles remain largely unknown in cardiac cells or regenerated CMs.

5.2. New Insights of ROS in Intercellular Communications. New lines of evidence show that ROS signaling can be transferred in a diffusion-independent fashion from donor cells to nearby cells [135]. For instance, pericardial ROS were shown to directly modulate the expression of cell adhesion and cytoskeleton molecules that facilitate interaction between the pericardial cells and cardiac myocytes [136]. In addition, extracellular vesicles such as exosomes that derived from CMs in response to H_2O_2 were shown to exacerbate apoptosis of transplanted stem cells [137]. ROS were contained in microvesicles isolated from endothelial cells after hypoxia-reoxygenation, leading to apoptosis and oxidative stress in myoblasts [138]. A study of spinal injury brought a novel sight from finding of exosomal delivery of ROS-producing NOX2 to the injury site and triggering inflammation [139]. The potential mechanisms of ROS and their producers transferring through exosomes or microvesicles require further research in the setting of MI and cell therapies. Knowledge obtained from these studies helps to interpret a possibility that ischemic myocardium-derived ROS target engrafted stem cells or PSC-CMs in a paracrine manner *via* extracellular vesicles or free diffusion.

6. Convergences of Antioxidants and Cell-Based Therapy

When the oxidative insult overwhelms the endogenous antioxidant defense system during MI, a prolonged elevation in ROS levels leads to chronic inflammation with scarring and

tissue dysfunction [140]. Therefore, proper timing and level of ROS generation after MI injury need to be tailored to ensure maximal efficacy in order to avoid undesired damage. Nevertheless, pharmacological interventions using nonselective antioxidants (e.g., vitamin C, vitamin E, and β -carotene) failed to show a significant impact on prevention or treatment of cardiovascular disease in trials [140]. Noneffective or harmful outcome of these antioxidants is likely owing to low drug specificity or disturbed the redox balance signaling. Moreover, systemic delivery of antioxidants might be limited by low bioavailability or low effective levels in the site of injury. To this end, stable materials are being developed for localized antioxidant activity. We could also take advantage of novel biomaterials using in cardiac tissue engineering to scavenge ROS, enhance graft survival, and achieve replenishment of the lost myocardium (Figure 4).

To obtain functional EHT for cell therapy, natural biomaterials or synthetic nanomaterials have been used to provide mechanical, electroactive support and generate 2D or 3D cardiac sheets [141, 142]. Nonetheless, oxidative stress would be generated due to a detrimental immune response to biomaterials at the site of implantation [143]. It remains challenging to identify biocompatible, biodegradable scaffolds that allow cell migration into infarct zone and protect cells against the oxidative stress. Antioxidants function in different mechanisms, such as free radical scavengers, singlet oxygen quenchers, inactivators of peroxides, chelators of redox metal ion, and quenchers of secondary oxidation products and inhibitors of prooxidative enzymes [144]. We focus on the antioxidative biomaterials that are cardiac-compatible and also show application potential to enhance graft cell survival in preclinical studies.

Recently, incorporation of small antioxidant molecules into polymeric scaffold is a straightforward means to retain the antioxidant activity. For instance, a degradable polyurethane backbone conjugating with ascorbic acid was shown to provide sustainable antioxidant properties and robust mechanical support for CM growth, which rescued CM death under oxidative stress [145]. Interestingly, incorporation of calcium peroxide into an antioxidant hydrophobic polymer

can yield a 3D scaffold with a sustained oxygen release as well as attenuation of free radicals [146]. The development of scaffolds with oxygen-releasing and antioxidant properties will offer a unique solution to protect graft from hypoxia-induced cell death by providing sufficient oxygen and attenuating the oxidative stress during oxygen generation, leading to better survival of the critically perfused tissues [146]. Additionally, the antioxidant property of injectable hydrogel can be enhanced by structural introduction of antioxidants such as citric acid and glutathione, and their protective potential effects on graft cells have been determined in MI or oxidative stress models [147, 148]. Antioxidant-loaded nanoparticles can be embedded in hydrogel that possesses a highly porous structure, and this system might have an excellent biocompatibility to support the adhesion and survival of CMs for injectable cardiac tissue engineering [149, 150].

The development of scaffold-based cell delivery techniques is in the early stages for cardiac tissue engineering, and there are still opportunities to incorporate additional treatments to modulate the antioxidative and anti-inflammatory process. Pharmacological pretreatments (such as omega-3 fatty acids and cobalt protoporphyrin) have beneficent effects on survival of ESC-CMs as evidenced by upregulation of HO-1 and decreased ROS levels under oxidative or hypoxic conditions [151, 152]. Future study will reveal new targets and pharmacological compounds to enhance cell engraftment of EHTs after delineating the mechanisms by which the fate of transplanted cells is mediated by increased ROS or downregulated endogenous antioxidant system.

7. Perspectives and Conclusion

In light of the extensive impact of ROS on different aspects of cell differentiation and metabolic homeostasis, there has been continued interest in targeting ROS for therapeutic benefit in the development of heart regenerative medicine. The potential of redox signaling to promote or inhibit CM differentiation may depend upon the ROS source, cell context, and probably the magnitude of ROS generation. It should be noted that the beneficial or detrimental roles of ROS in this scenario do not necessarily need to be mutually exclusive. Cellular ROS may act through several targets and have diverse roles in different stages of cardiac differentiation, proliferation, and maturation. Stem cells are thought to maintain a low basal level of ROS for preserving their functions in quiescence, while increased ROS after differentiation can be countered by the antioxidant defense system to avoid sustained oxidative stress. Although mouse or human ESCs provide a unique experimental model to study the role of ROS and ROS-generating enzymes in the regulation of CM differentiation *in vitro*, it remains further investigation in human iPSCs to refine the methodologies regulating cellular redox states *via* metabolic modulations for translational research. Improvement in omic technologies, including genetic screening, single-cell approach, and large-scale profiling of redox-sensitive targets, will undoubtedly advance the understanding of the complexities of ROS and antioxidant pathways during cardiac differentiation and heart development. Addi-

tionally, the detailed role of ROS has not been determined in direct cardiac transdifferentiation (reprogramming). Further investigation of epigenetic mechanisms, innate immune response, and mitochondrial regulation will bring new insights into the field of metabolic reprogramming in order to enhance the CM conversion efficiency.

ROS also play a role in applications of cardiac regenerative therapies for MI treatment. Intracellular ROS are increased and induce cell death of implanted stem cells or PSC-CMs in a cell-autonomous manner in the ischemic microenvironment. Paracrine effects of host's cells on the site of implant also likely cause graft cell death in a nonautonomous manner due to uptake of transferred ROS. Yet, this remains to be elucidated to what extent potential paracrine mechanisms contribute to the low engraftment and survival rate of stem cell-based therapies. It will help to address this question by the gain- and loss-of-function studies of the relevant genes in ROS generation pathways in host and donor cells, respectively. This knowledge is important for the design and selection of antioxidant strategies for development of tissue engineering-based technologies. Natural or synthetic biomaterials with antioxidant activity have been used in tissue engineering scaffolds. Further optimization of cardiac tissue engineering needs in-depth evaluation of new biomaterials in regard to donor-host cell coupling, immunogenicity, antioxidant and anti-inflammatory activity, and mechanical and electronic properties. These antioxidant intervention approaches should ensure protecting against infarct expansion, ventricular rupture, and other potentially devastating post-MI complications and avoid disruption of other important signaling of self-healing processes when combining with stem cell-based technology.

Conflicts of Interest

The authors indicated no potential conflicts of interest.

Authors' Contributions

J.L., C.C., M.W., M.M., J.H., and P.Z. did the manuscript writing and the final approval of the manuscript. Jialiang Liang, Min Wu, and Chen Chen contributed equally to this work.

Acknowledgments

This work was supported by the National Key Research and Development Program of China (2018YFA0108700 and 2017YFA0105602), the NSFC Projects of International Cooperation and Exchanges (81720108004), the National Natural Science Foundation of China (81974019), the Research Team Project of Natural Science Foundation of Guangdong Province of China (2017A030312007), the Key Program of Guangzhou Science Research Plan (201904020047), and the Special Project of Dengfeng Program of Guangdong Provincial People's Hospital (DFJH201812, KJ012019119, and KJ012019423) to P.Z.

References

- [1] K. Thygesen, J. S. Alpert, A. S. Jaffe et al., "Third universal definition of myocardial infarction," *Journal of the American College of Cardiology*, vol. 60, no. 16, pp. 1581–1598, 2012.
- [2] H. Sadek and E. N. Olson, "Toward the goal of human heart regeneration," *Cell Stem Cell*, vol. 26, no. 1, pp. 7–16, 2020.
- [3] J. Riegler, M. Tiburcy, A. Ebert et al., "Human engineered heart muscles engraft and survive long term in a rodent myocardial infarction model," *Circulation Research*, vol. 117, no. 8, pp. 720–730, 2015.
- [4] A. Oikonomopoulos, T. Kitani, and J. C. Wu, "Pluripotent stem cell-derived cardiomyocytes as a platform for cell therapy applications: progress and hurdles for clinical translation," *Molecular Therapy*, vol. 26, no. 7, pp. 1624–1634, 2018.
- [5] T. J. Kolanowski, C. L. Antos, and K. Guan, "Making human cardiomyocytes up to date: derivation, maturation state and perspectives," *International Journal of Cardiology*, vol. 241, pp. 379–386, 2017.
- [6] E. N. Olson, "Gene regulatory networks in the evolution and development of the heart," *Science*, vol. 313, no. 5795, pp. 1922–1927, 2006.
- [7] F. X. Galdos, Y. Guo, S. L. Paige, N. J. VanDusen, S. M. Wu, and W. T. Pu, "Cardiac Regeneration," *Circulation Research*, vol. 120, no. 6, pp. 941–959, 2017.
- [8] G. D. Lopaschuk and J. S. Jaswal, "Energy metabolic phenotype of the cardiomyocyte during development, differentiation, and postnatal maturation," *Journal of Cardiovascular Pharmacology*, vol. 56, no. 2, pp. 130–140, 2010.
- [9] S. Tatapudy, F. Aloisio, D. Barber, and T. Nystul, "Cell fate decisions: emerging roles for metabolic signals and cell morphology," *EMBO Reports*, vol. 18, no. 12, pp. 2105–2118, 2017.
- [10] T. V. A. Murray, A. Ahmad, and A. C. Brewer, "Reactive oxygen at the heart of metabolism," *Trends in Cardiovascular Medicine*, vol. 24, no. 3, pp. 113–120, 2014.
- [11] C. X. C. Santos, N. Anilkumar, M. Zhang, A. C. Brewer, and A. M. Shah, "Redox signaling in cardiac myocytes," *Free Radical Biology and Medicine*, vol. 50, no. 7, pp. 777–793, 2011.
- [12] N. Panth, K. R. Paudel, and K. Parajuli, "Reactive oxygen species: a key hallmark of cardiovascular disease," *Advances in Medicine*, vol. 2016, Article ID 9152732, 12 pages, 2016.
- [13] A. C. Cardoso, A. H. M. Pereira, and H. A. Sadek, "Mechanisms of neonatal heart regeneration," *Current Cardiology Reports*, vol. 22, no. 5, p. 33, 2020.
- [14] B. N. Puente, W. Kimura, S. A. Muralidhar et al., "The oxygen-rich postnatal environment induces cardiomyocyte cell-cycle arrest through DNA damage response," *Cell*, vol. 157, no. 3, pp. 565–579, 2014.
- [15] H. J. Forman, F. Ursini, and M. Maiorino, "An overview of mechanisms of redox signaling," *J Mol Cell Cardiol*, vol. 73, no. 2–9, pp. 2–9, 2014.
- [16] K. Bedard and K. H. Krause, "The NOX family of ROS-generating NADPH oxidases: physiology and pathophysiology," *Physiological Reviews*, vol. 87, no. 1, pp. 245–313, 2007.
- [17] J. D. Lambeth, "NOX enzymes and the biology of reactive oxygen," *Nature Reviews. Immunology*, vol. 4, no. 3, pp. 181–189, 2004.
- [18] M. P. Murphy, "How mitochondria produce reactive oxygen species," *The Biochemical Journal*, vol. 417, no. 1, pp. 1–13, 2009.
- [19] H. Sies, "Role of metabolic H₂O₂ generation: redox signaling and oxidative stress," *The Journal of Biological Chemistry*, vol. 289, no. 13, pp. 8735–8741, 2014.
- [20] D. A. Kass and A. M. Shah, "Redox and nitrosative regulation of cardiac remodeling," *Antioxidants & Redox Signaling*, vol. 18, no. 9, pp. 1021–1023, 2013.
- [21] A. Bachi, I. Dalle-Donne, and A. Scaloni, "Redox proteomics: chemical principles, methodological approaches and biological/biomedical promises," *Chemical Reviews*, vol. 113, no. 1, pp. 596–698, 2012.
- [22] X. Xu and E. A. Arriaga, "Qualitative determination of superoxide release at both sides of the mitochondrial inner membrane by capillary electrophoretic analysis of the oxidation products of triphenylphosphonium hydroethidine," *Free Radical Biology & Medicine*, vol. 46, no. 7, pp. 905–913, 2009.
- [23] E. A. Veal, A. M. Day, and B. A. Morgan, "Hydrogen peroxide sensing and signaling," *Molecular Cell*, vol. 26, no. 1, pp. 1–14, 2007.
- [24] Q. Wang, F. Ding, N. Zhu, H. Li, P. He, and Y. Fang, "Determination of hydroxyl radical by capillary zone electrophoresis with amperometric detection," *Journal of Chromatography A*, vol. 1016, no. 1, pp. 123–128, 2003.
- [25] M. Dizdaroglu and P. Jaruga, "Mechanisms of free radical-induced damage to DNA," *Free Radical Research*, vol. 46, no. 4, pp. 382–419, 2012.
- [26] S. G. Rhee, "Cell signaling: H₂O₂, a necessary evil for cell signaling," *Science*, vol. 312, no. 5782, pp. 1882–1883, 2006.
- [27] B. C. Dickinson and C. J. Chang, "Chemistry and biology of reactive oxygen species in signaling or stress responses," *Nature Chemical Biology*, vol. 7, no. 8, pp. 504–511, 2011.
- [28] E. Le Moal, V. Pialoux, G. Juban et al., "Redox control of skeletal muscle regeneration," *Antioxidants & Redox Signaling*, vol. 27, no. 5, pp. 276–310, 2017.
- [29] H. Sies and D. P. Jones, "Reactive oxygen species (ROS) as pleiotropic physiological signalling agents," *Nat Rev Mol Cell Biol*, vol. 21, no. 7, pp. 363–383, 2020.
- [30] R. J. Koene, A. E. Prizment, A. Blaes, and S. H. Konety, "Shared risk factors in cardiovascular disease and cancer," *Circulation*, vol. 133, no. 11, pp. 1104–1114, 2016.
- [31] A. D. Hafstad, A. A. Nabeebaccus, and A. M. Shah, "Novel aspects of ROS signalling in heart failure," *Basic Research in Cardiology*, vol. 108, no. 4, p. 359, 2013.
- [32] E. Birben, U. M. Sahiner, C. Sackesen, S. Erzurum, and O. Kalayci, "Oxidative stress and antioxidant defense," *World Allergy Organization Journal*, vol. 5, no. 1, pp. 9–19, 2012.
- [33] S. G. Rhee, K. S. Yang, S. W. Kang, H. A. Woo, and T. S. Chang, "Controlled elimination of intracellular H₂O₂: regulation of peroxiredoxin, catalase, and glutathione peroxidase via post-translational modification," *Antioxidants & Redox Signaling*, vol. 7, no. 5–6, pp. 619–626, 2005.
- [34] H. Yamawaki and B. C. Berk, "Thioredoxin: a multifunctional antioxidant enzyme in kidney, heart and vessels," *Current Opinion in Nephrology and Hypertension*, vol. 14, no. 2, pp. 149–153, 2005.
- [35] M. Zhao, H. Guo, J. Chen et al., "5-Aminolevulinic acid combined with sodium ferrous citrate ameliorates H₂O₂-induced cardiomyocyte hypertrophy via activation of the MAPK/Nrf2/HO-1 pathway," *American Journal of Physiology. Cell Physiology*, vol. 308, no. 8, pp. C665–C672, 2015.
- [36] S. Dey, D. DeMazumder, A. Sidor, D. B. Foster, and B. O'Rourke, "Mitochondrial ROS drive sudden cardiac death

- and chronic proteome remodeling in heart failure,” *Circulation Research*, vol. 123, no. 3, pp. 356–371, 2018.
- [37] C. Tu and J. Zoldan, “Moving iPSC-derived cardiomyocytes forward to treat myocardial infarction,” *Cell Stem Cell*, vol. 23, no. 3, pp. 322–323, 2018.
- [38] S. M. Evans, D. Yelon, F. L. Conlon, and M. L. Kirby, “Myocardial lineage development,” *Circulation Research*, vol. 107, no. 12, pp. 1428–1444, 2010.
- [39] C. L. Mummery, J. Zhang, E. S. Ng, D. A. Elliott, A. G. Elefanty, and T. J. Kamp, “Differentiation of human embryonic stem cells and induced pluripotent stem cells to cardiomyocytes: a methods overview,” *Circulation Research*, vol. 111, no. 3, pp. 344–358, 2012.
- [40] I. Karakikes, M. Ameen, V. Termglinchan, and J. C. Wu, “Human induced pluripotent stem cell-derived cardiomyocytes: insights into molecular, cellular, and functional phenotypes,” *Circulation Research*, vol. 117, no. 1, pp. 80–88, 2015.
- [41] J. Ji, V. Sharma, S. Qi et al., “Antioxidant supplementation reduces genomic aberrations in human induced pluripotent stem cells,” *Stem Cell Reports*, vol. 2, no. 1, pp. 44–51, 2014.
- [42] C. Tu, A. Allen, W. Deng, O. Conroy, M. Nambiar, and J. Zoldan, “Commonly used thiol-containing antioxidants reduce cardiac differentiation and alter gene expression ratios of sarcomeric isoforms,” *Experimental Cell Research*, vol. 370, no. 1, pp. 150–159, 2018.
- [43] H. Sauer, G. Rahimi, J. Hescheler, and M. Wartenberg, “Role of reactive oxygen species and phosphatidylinositol 3-kinase in cardiomyocyte differentiation of embryonic stem cells,” *FEBS Letters*, vol. 476, no. 3, pp. 218–223, 2000.
- [44] E. Serena, E. Figallo, N. Tandon et al., “Electrical stimulation of human embryonic stem cells: cardiac differentiation and the generation of reactive oxygen species,” *Experimental Cell Research*, vol. 315, no. 20, pp. 3611–3619, 2009.
- [45] H. Sauer, W. Neukirchen, G. Rahimi, F. Grünheck, J. Hescheler, and M. Wartenberg, “Involvement of reactive oxygen species in cardiotrophin-1-induced proliferation of cardiomyocytes differentiated from murine embryonic stem cells,” *Experimental Cell Research*, vol. 294, no. 2, pp. 313–324, 2004.
- [46] Y. B. Wo, D. Y. Zhu, Y. Hu, Z. Q. Wang, J. Liu, and Y. J. Lou, “Reactive oxygen species involved in prenylflavonoids, icariin and icaritin, initiating cardiac differentiation of mouse embryonic stem cells,” *Journal of Cellular Biochemistry*, vol. 103, no. 5, pp. 1536–1550, 2008.
- [47] S. Varum, A. S. Rodrigues, M. B. Moura et al., “Energy metabolism in human pluripotent stem cells and their differentiated counterparts,” *PLoS One*, vol. 6, no. 6, article e20914, 2011.
- [48] X. Xu, S. Duan, F. Yi, A. Ocampo, G. H. Liu, and J. C. Izpisua Belmonte, “Mitochondrial regulation in pluripotent stem cells,” *Cell Metabolism*, vol. 18, no. 3, pp. 325–332, 2013.
- [49] S. Chung, P. P. Dzeja, R. S. Faustino, C. Perez-Terzic, A. Behfar, and A. Terzic, “Mitochondrial oxidative metabolism is required for the cardiac differentiation of stem cells,” *Nature Clinical Practice Cardiovascular Medicine*, vol. 4, no. S1, pp. S60–S67, 2007.
- [50] H. B. Suliman, F. Zobi, and C. A. Piantadosi, “Heme oxygenase-1/carbon monoxide system and embryonic stem cell differentiation and maturation into cardiomyocytes,” *Antioxidants & Redox Signaling*, vol. 24, no. 7, pp. 345–360, 2016.
- [51] F. Sharifpanah, M. Wartenberg, M. Hannig, H. M. Piper, and H. Sauer, “Peroxisome proliferator-activated receptor α agonists enhance cardiomyogenesis of mouse ES cells by utilization of a reactive oxygen species-dependent mechanism,” *Stem Cells*, vol. 26, no. 1, pp. 64–71, 2008.
- [52] M. Schmelter, B. Ateghang, S. Helmig et al., “Embryonic stem cells utilize reactive oxygen species as transducers of mechanical strain-induced cardiovascular differentiation,” *The FASEB Journal*, vol. 20, no. 8, pp. 1182–1184, 2006.
- [53] J. S. Heo and J. C. Lee, “ β -catenin mediates cyclic strain-stimulated cardiomyogenesis in mouse embryonic stem cells through ROS-dependent and integrin-mediated PI3K/Akt pathways,” *Journal of Cellular Biochemistry*, vol. 112, no. 7, pp. 1880–1889, 2011.
- [54] L. Zhou, Y. Huang, Y. Zhang et al., “mGluR5 stimulating Homer-PIKE formation initiates icariin induced cardiomyogenesis of mouse embryonic stem cells by activating reactive oxygen species,” *Experimental Cell Research*, vol. 319, no. 10, pp. 1505–1514, 2013.
- [55] J. Li, M. Stouffs, L. Serrander et al., “The NADPH oxidase NOX4 drives cardiac differentiation: role in regulating cardiac transcription factors and MAP kinase activation,” *Molecular Biology of the Cell*, vol. 17, no. 9, pp. 3978–3988, 2006.
- [56] M. M. Bekhite, H. R. Figulla, H. Sauer, and M. Wartenberg, “Static magnetic fields increase cardiomyocyte differentiation of FLK-1⁺ cells derived from mouse embryonic stem cells via Ca²⁺ influx and ROS production,” *International Journal of Cardiology*, vol. 167, no. 3, pp. 798–808, 2013.
- [57] D. Spitkovsky, P. Sasse, E. Kolossov et al., “Activity of complex III of the mitochondrial electron transport chain is essential for early heart muscle cell differentiation,” *The FASEB Journal*, vol. 18, no. 11, pp. 1300–1302, 2004.
- [58] Q. Chen, E. J. Vazquez, S. Moghaddas, C. L. Hoppel, and E. J. Lesnefsky, “Production of reactive oxygen species by mitochondria: central role of complex III,” *The Journal of Biological Chemistry*, vol. 278, no. 38, pp. 36027–36031, 2003.
- [59] F. L. Crespo, V. R. Sobrado, L. Gomez, A. M. Cervera, and K. McCreath, “Mitochondrial reactive oxygen species mediate cardiomyocyte formation from embryonic stem cells in high glucose,” *Stem Cells*, vol. 28, no. 7, pp. 1132–1142, 2010.
- [60] B. Wu, H. Yu, Y. Wang et al., “Peroxiredoxin-2 nitrosylation facilitates cardiomyogenesis of mouse embryonic stem cells via XBP-1s/PI3K pathway,” *Free Radical Biology and Medicine*, vol. 97, pp. 179–191, 2016.
- [61] M. J. Birket, S. Casini, G. Kosmidis et al., “PGC-1 α and Reactive Oxygen Species Regulate Human Embryonic Stem Cell-Derived Cardiomyocyte Function,” *Stem Cell Reports*, vol. 1, no. 6, pp. 560–574, 2013.
- [62] M. Buggisch, B. Ateghang, C. Ruhe et al., “Stimulation of ES-cell-derived cardiomyogenesis and neonatal cardiac cell proliferation by reactive oxygen species and NADPH oxidase,” *Journal of Cell Science*, vol. 120, no. 5, pp. 885–894, 2007.
- [63] D. B. Zorov, C. R. Filburn, L. O. Klotz, J. L. Zweier, and S. J. Sollott, “Reactive oxygen species (ROS-induced) ROS release: a new phenomenon accompanying induction of the mitochondrial permeability transition in cardiac myocytes,” *The Journal of Experimental Medicine*, vol. 192, no. 7, pp. 1001–1014, 2000.
- [64] D. S. Bilan and V. V. Belousov, “In vivo imaging of hydrogen peroxide with hyper probes,” *Antioxidants & Redox Signaling*, vol. 29, no. 6, pp. 569–584, 2018.

- [65] N. M. Mishina, Y. A. Bogdanova, Y. G. Ermakova et al., "Which antioxidant system shapes intracellular H₂O₂ Gradients?," *Antioxidants & Redox Signaling*, vol. 31, no. 9, pp. 664–670, 2019.
- [66] O. Lyublinskaya and F. Antunes, "Measuring intracellular concentration of hydrogen peroxide with the use of genetically encoded H₂O₂ biosensor hyper," *Redox Biology*, vol. 24, no. 24, p. 101200, 2019.
- [67] S. K. Law, C. S.-L. Leung, K. L. Yau et al., "Regulation of multiple transcription factors by reactive oxygen species and effects of pro-inflammatory cytokines released during myocardial infarction on cardiac differentiation of embryonic stem cells," *International Journal of Cardiology*, vol. 168, no. 4, pp. 3458–3472, 2013.
- [68] M. Puc at, P. Travo, M. T. Quinn, and P. Fort, "A dual role of the GTPase Rac in cardiac differentiation of stem cells," *Molecular Biology of the Cell*, vol. 14, no. 7, pp. 2781–2792, 2003.
- [69] T. Li, X. Zhang, K. Jiang, J. Liu, and Z. Liu, "Dural effects of oxidative stress on cardiomyogenesis via Gata4 transcription and protein ubiquitination," *Cell Death & Disease*, vol. 9, no. 2, p. 246, 2018.
- [70] L. Na, M. Wartenberg, H. Nau, J. Hescheler, and H. Sauer, "Anticonvulsant valproic acid inhibits cardiomyocyte differentiation of embryonic stem cells by increasing intracellular levels of reactive oxygen species," *Birth defects research Part A, Clinical and molecular teratology*, vol. 67, no. 3, pp. 174–180, 2003.
- [71] H. J. Heo, H. K. Kim, J. B. Youm et al., "Mitochondrial pyruvate dehydrogenase phosphatase 1 regulates the early differentiation of cardiomyocytes from mouse embryonic stem cells," *Experimental & Molecular Medicine*, vol. 48, no. 8, article e254, 2016.
- [72] A. Behfar, C. Perez-Terzic, R. S. Faustino et al., "Cardiopoietic programming of embryonic stem cells for tumor-free heart repair," *The Journal of Experimental Medicine*, vol. 204, no. 2, pp. 405–420, 2007.
- [73] W. Wang, H. Fang, L. Groom et al., "Superoxide flashes in single mitochondria," *Cell*, vol. 134, no. 2, pp. 279–290, 2008.
- [74] J. R. Hom, R. A. Quintanilla, D. L. Hoffman et al., "The permeability transition pore controls cardiac mitochondrial maturation and myocyte differentiation," *Developmental Cell*, vol. 21, no. 3, pp. 469–478, 2011.
- [75] S. W. Cho, J. S. Park, H. J. Heo et al., "Dual modulation of the mitochondrial permeability transition pore and redox signaling synergistically promotes cardiomyocyte differentiation from pluripotent stem cells," *Journal of the American Heart Association*, vol. 3, no. 2, article e000693, 2014.
- [76] G. L. Tiemeier, G. Wang, S. J. Dumas et al., "Closing the mitochondrial permeability transition pore in hiPSC-derived endothelial cells induces glycocalyx formation and functional maturation," *Stem Cell Reports*, vol. 13, no. 5, pp. 803–816, 2019.
- [77] S. Akbari-Birgani, S. Hosseinkhani, S. Mollamohamadi, and H. Baharvand, "Delay in apoptosome formation attenuates apoptosis in mouse embryonic stem cell differentiation," *The Journal of Biological Chemistry*, vol. 289, no. 24, pp. 16905–16913, 2014.
- [78] P. Fernando, J. F. Kelly, K. Balazsi, R. S. Slack, and L. A. Megeney, "Caspase 3 activity is required for skeletal muscle differentiation," *Proceedings of the National Academy of Sciences of the United States of America*, vol. 99, no. 17, pp. 11025–11030, 2002.
- [79] D. J. Hausenloy and D. M. Yellon, "The mitochondrial permeability transition pore: its fundamental role in mediating cell death during ischaemia and reperfusion," *Journal of Molecular and Cellular Cardiology*, vol. 35, no. 4, pp. 339–341, 2003.
- [80] A. Nugud, D. Sandeep, and A. T. El-Serafi, "Two faces of the coin: minireview for dissecting the role of reactive oxygen species in stem cell potency and lineage commitment," *Journal of Advanced Research*, vol. 14, pp. 73–79, 2018.
- [81] P. Ghiasi, S. Hosseinkhani, H. Ansari et al., "Reversible permeabilization of the mitochondrial membrane promotes human cardiomyocyte differentiation from embryonic stem cells," *Journal of Cellular Physiology*, vol. 234, no. 1, pp. 521–536, 2018.
- [82] M. Schieber and N. S. Chandel, "ROS function in redox signaling and oxidative stress," *Current biology : CB*, vol. 24, no. 10, pp. R453–R462, 2014.
- [83] Y. M. W. Janssen-Heininger, B. T. Mossman, N. H. Heintz et al., "Redox-based regulation of signal transduction: principles, pitfalls, and promises," *Free Radical Biology & Medicine*, vol. 45, no. 1, pp. 1–17, 2008.
- [84] T. Kietzmann, A. Petry, A. Shvetsova, J. M. Gerhold, and A. G rlach, "The epigenetic landscape related to reactive oxygen species formation in the cardiovascular system," *British Journal of Pharmacology*, vol. 174, no. 12, pp. 1533–1554, 2017.
- [85] J. Lewandowski, T. J. Kolanowski, and M. Kurpisz, "Techniques for the induction of human pluripotent stem cell differentiation towards cardiomyocytes," *Journal of Tissue Engineering and Regenerative Medicine*, vol. 11, no. 5, pp. 1658–1674, 2017.
- [86] H. Kempf, M. Lecina, S. Ting, R. Zweigerdt, and S. Oh, "Distinct regulation of mitogen-activated protein kinase activities is coupled with enhanced cardiac differentiation of human embryonic stem cells," *Stem Cell Research*, vol. 7, no. 3, pp. 198–209, 2011.
- [87] A.-R. Ji, S.-Y. Ku, M. S. Cho et al., "Reactive oxygen species enhance differentiation of human embryonic stem cells into mesendodermal lineage," *Experimental & Molecular Medicine*, vol. 42, no. 3, pp. 175–186, 2010.
- [88] H. Fang, L. Cong, Y. Zhi, H. Xu, X. Jia, and S. Peng, "T-2 toxin inhibits murine ES cells cardiac differentiation and mitochondrial biogenesis by ROS and p-38 MAPK-mediated pathway," *Toxicology Letters*, vol. 258, pp. 259–266, 2016.
- [89] Y. Son, Y. K. Cheong, N. H. Kim, H. T. Chung, D. G. Kang, and H. O. Pae, "Mitogen-activated protein kinases and reactive oxygen species: how can ROS activate MAPK pathways?," *J Signal Transduct*, vol. 2011, article 792639, pp. 1–6, 2011.
- [90] G. Fujino, T. Noguchi, A. Matsuzawa et al., "Thioredoxin and TRAF family proteins regulate reactive oxygen species-dependent activation of ASK1 through reciprocal modulation of the N-terminal homophilic interaction of ASK1," *Molecular and Cellular Biology*, vol. 27, no. 23, pp. 8152–8163, 2007.
- [91] R. Smiley, P. Naik, R. McCallum, and M. Showkat Ali, "Reactive oxygen species overproduction and MAP kinase phosphatase-1 degradation are associated with gastroparesis in a streptozotocin-induced male diabetic rat model," *Neurogastroenterology & Motility*, vol. 30, no. 3, article e13218, 2018.

- [92] M. Demasi, V. Simoes, and D. Bonatto, "Cross-talk between redox regulation and the ubiquitin-proteasome system in mammalian cell differentiation," *Biochimica et Biophysica Acta*, vol. 1850, no. 8, pp. 1594–1606, 2015.
- [93] G. A. Knock and J. P. T. Ward, "Redox regulation of protein kinases as a modulator of vascular function," *Antioxidants & Redox Signaling*, vol. 15, no. 6, pp. 1531–1547, 2011.
- [94] S. Kohlgrüber, A. Upadhye, N. Dyballa-Rukes, C. A. McNamara, and J. Altschmied, "Regulation of transcription factors by reactive oxygen species and nitric oxide in vascular physiology and pathology," *Antioxidants & Redox Signaling*, vol. 26, no. 13, pp. 679–699, 2017.
- [95] T. V. A. Murray, I. Smyrniak, A. M. Shah, and A. C. Brewer, "NADPH oxidase 4 regulates cardiomyocyte differentiation via redox activation of c-Jun protein and the cis-regulation of GATA-4 gene transcription," *The Journal of Biological Chemistry*, vol. 288, no. 22, pp. 15745–15759, 2013.
- [96] J. Park, J. W. Park, H. Oh, F. S. Maria, J. Kang, and X. Tian, "Gene-specific assessment of guanine oxidation as an epigenetic modulator for cardiac specification of mouse embryonic stem cells," *PLoS One*, vol. 11, no. 6, article e0155792, 2016.
- [97] D. Herrero, M. Tomé, S. Cañón et al., "Redox-dependent BMI1 activity drives in vivo adult cardiac progenitor cell differentiation," *Cell Death and Differentiation*, vol. 25, no. 4, pp. 809–822, 2018.
- [98] T. Rharass, H. Lemcke, M. Lantow, S. A. Kuznetsov, D. G. Weiss, and D. Panáková, "Ca²⁺-mediated mitochondrial reactive oxygen species metabolism augments Wnt/ β -catenin pathway activation to facilitate cell differentiation," *The Journal of Biological Chemistry*, vol. 289, no. 40, pp. 27937–27951, 2014.
- [99] J. van der Reest, S. Lilla, L. Zheng, S. Zanivan, and E. Gottlieb, "Proteome-wide analysis of cysteine oxidation reveals metabolic sensitivity to redox stress," *Nature Communications*, vol. 9, no. 1, p. 1581, 2018.
- [100] E. Weerapana, C. Wang, G. M. Simon et al., "Quantitative reactivity profiling predicts functional cysteines in proteomes," *Nature*, vol. 468, no. 7325, pp. 790–795, 2010.
- [101] A. R. Poetsch, "The genomics of oxidative DNA damage, repair, and resulting mutagenesis," *Computational and Structural Biotechnology Journal*, vol. 18, pp. 207–219, 2020.
- [102] B. Savelli, Q. Li, M. Webber et al., "RedoxiBase: a database for ROS homeostasis regulated proteins," *Redox Biol*, vol. 26, p. 101247, 2019.
- [103] M. A. Sun, Q. Zhang, Y. Wang, W. Ge, and D. Guo, "Prediction of redox-sensitive cysteines using sequential distance and other sequence-based features," *BMC Bioinformatics*, vol. 17, no. 1, p. 316, 2016.
- [104] M. Ieda, J. D. Fu, P. Delgado-Olguin et al., "Direct reprogramming of fibroblasts into functional cardiomyocytes by defined factors," *Cell*, vol. 142, no. 3, pp. 375–386, 2010.
- [105] J. A. Efe, S. Hilcove, J. Kim et al., "Conversion of mouse fibroblasts into cardiomyocytes using a direct reprogramming strategy," *Nature Cell Biology*, vol. 13, no. 3, pp. 215–222, 2011.
- [106] K. Song, Y. J. Nam, X. Luo et al., "Heart repair by reprogramming non-myocytes with cardiac transcription factors," *Nature*, vol. 485, no. 7400, pp. 599–604, 2012.
- [107] J. X. Chen, M. Krane, M. A. Deutsch et al., "Inefficient reprogramming of fibroblasts into cardiomyocytes using Gata4, Mef2c, and Tbx5," *Circulation Research*, vol. 111, no. 1, pp. 50–55, 2012.
- [108] T. Sadahiro and M. Ieda, "Direct cardiac reprogramming for cardiovascular regeneration and differentiation," *The Keio Journal of Medicine*, 2019.
- [109] B. Keepers, J. Liu, and L. Qian, "What's in a cardiomyocyte - And how do we make one through reprogramming?," *Biochimica et Biophysica Acta (BBA) - Molecular Cell Research*, vol. 1867, no. 3, p. 118464, 2020.
- [110] Y. J. Suzuki and N. V. Shultz, "Antioxidant regulation of cell reprogramming," *Antioxidants*, vol. 8, no. 8, p. 323, 2019.
- [111] G. Zhou, S. Meng, Y. Li, Y. T. Ghebre, and J. P. Cooke, "Optimal ROS signaling is critical for nuclear reprogramming," *Cell Reports*, vol. 15, no. 5, pp. 919–925, 2016.
- [112] K. E. Hawkins, S. Joy, J. M. K. M. Delhove et al., "Nrf2 orchestrates the metabolic shift during induced pluripotent stem cell reprogramming," *Cell Reports*, vol. 14, no. 8, pp. 1883–1891, 2016.
- [113] Z. Ying, G. Xiang, L. Zheng et al., "Short-term mitochondrial permeability transition pore opening modulates histone lysine methylation at the early phase of somatic cell reprogramming," *Cell Metabolism*, vol. 28, no. 6, pp. 935–945.e5, 2018.
- [114] S. Meng, P. Chanda, R. A. Thandavarayan, and J. P. Cooke, "Transflammation: how innate immune activation and free radicals drive nuclear reprogramming," *Antioxidants & Redox Signaling*, vol. 29, no. 2, pp. 205–218, 2018.
- [115] Y. Zhou, Z. Liu, J. D. Welch et al., "Single-cell transcriptomic analyses of cell fate transitions during human cardiac reprogramming," *Cell Stem Cell*, vol. 25, no. 1, pp. 149–164.e9, 2019, e149.
- [116] N. R. Stone, C. A. Gifford, R. Thomas et al., "Context-specific transcription factor functions regulate epigenomic and transcriptional dynamics during cardiac reprogramming," *Cell Stem Cell*, vol. 25, no. 1, pp. 87–102.e9, 2019, e109.
- [117] H. Hashimoto, Z. Wang, G. A. Garry et al., "Cardiac reprogramming factors synergistically activate genome-wide cardiogenic stage-specific enhancers," *Cell Stem Cell*, vol. 25, no. 1, pp. 69–86.e5, 2019, e65.
- [118] J. Lee, N. Sayed, A. Hunter et al., "Activation of innate immunity is required for efficient nuclear reprogramming," *Cell*, vol. 151, no. 3, pp. 547–558, 2012.
- [119] N. Sayed, W. T. Wong, F. Ospino et al., "Transdifferentiation of human fibroblasts to endothelial cells: role of innate immunity," *Circulation*, vol. 131, no. 3, pp. 300–309, 2015.
- [120] Y. Chen, Z. Zhou, and W. Min, "Mitochondria, oxidative stress and innate immunity," *Frontiers in Physiology*, vol. 9, 2018.
- [121] N. Cao, Y. Huang, J. Zheng et al., "Conversion of human fibroblasts into functional cardiomyocytes by small molecules," *Science*, vol. 352, no. 6290, pp. 1216–1220, 2016.
- [122] Y. Zhou, L. Wang, Z. Liu et al., "Comparative gene expression analyses reveal distinct molecular signatures between differentially reprogrammed cardiomyocytes," *Cell Reports*, vol. 20, no. 13, pp. 3014–3024, 2017.
- [123] Y. Yoshida and S. Yamanaka, "Induced pluripotent stem cells 10 years later: for cardiac applications," *Circulation Research*, vol. 120, no. 12, pp. 1958–1968, 2017.
- [124] J. Liang, W. Huang, L. Jiang, C. Paul, X. Li, and Y. Wang, "Concise review: reduction of adverse cardiac scarring

- facilitates pluripotent stem cell-based therapy for myocardial infarction,” *Stem Cells*, vol. 37, no. 7, pp. 844–854, 2019.
- [125] K. Ronaldson-Bouchard, K. Yeager, D. Teles et al., “Engineering of human cardiac muscle electromechanically matured to an adult-like phenotype,” *Nature Protocols*, vol. 14, no. 10, pp. 2781–2817, 2019.
- [126] N. Momtahan, C. O. Crosby, and J. Zoldan, “The Role of Reactive Oxygen Species in *In Vitro* Cardiac Maturation,” *Trends in Molecular Medicine*, vol. 25, no. 6, pp. 482–493, 2019.
- [127] A. Brodarac, T. Šarić, B. Oberwallner et al., “Susceptibility of murine induced pluripotent stem cell-derived cardiomyocytes to hypoxia and nutrient deprivation,” *Stem Cell Res Ther*, vol. 6, no. 1, 2015.
- [128] G. Singh, D. Sridharan, M. Khan, and P. B. Seshagiri, “Mouse embryonic stem cell-derived cardiomyocytes cease to beat following exposure to monochromatic light: association with increased ROS and loss of calcium transients,” *American Journal of Physiology. Cell Physiology*, vol. 317, no. 4, pp. C725–C736, 2019.
- [129] D. N. P. Munkanatta Godage, G. C. VanHecke, K. T. G. Samarasinghe et al., “SMYD2 glutathionylation contributes to degradation of sarcomeric proteins,” *Nature Communications*, vol. 9, no. 1, p. 4341, 2018.
- [130] K. Raedschelders, D. M. Ansley, and D. D. Y. Chen, “The cellular and molecular origin of reactive oxygen species generation during myocardial ischemia and reperfusion,” *Pharmacology & Therapeutics*, vol. 133, no. 2, pp. 230–255, 2012.
- [131] G. Zhang, F. Zhang, R. Muh et al., “Autocrine/paracrine pattern of superoxide production through NAD(P)H oxidase in coronary arterial myocytes,” *American Journal of Physiology. Heart and Circulatory Physiology*, vol. 292, no. 1, pp. H483–H495, 2007.
- [132] N. I. Moldovan, M. Anghelina, S. Varadharaj et al., “Reoxygenation-derived toxic reactive oxygen/nitrogen species modulate the contribution of bone marrow progenitor cells to remodeling after myocardial infarction,” *Journal of the American Heart Association*, vol. 3, no. 1, article e000471, 2014.
- [133] H. Song, M. J. Cha, B. W. Song et al., “Reactive oxygen species inhibit adhesion of mesenchymal stem cells implanted into ischemic myocardium via interference of focal adhesion complex,” *Stem Cells*, vol. 28, no. 3, pp. 555–563, 2010.
- [134] G. Tamma, G. Valenti, E. Grossini et al., “Aquaporin membrane channels in oxidative stress, cell signaling, and aging: recent advances and research trends,” *Oxidative medicine and cellular longevity*, vol. 2018, Article ID 1501847, 14 pages, 2018.
- [135] A. Hervera, C. X. Santos, F. De Virgiliis, A. M. Shah, and S. Di Giovanni, “Paracrine mechanisms of redox signalling for postmitotic cell and tissue regeneration,” *Trends in Cell Biology*, vol. 29, no. 6, pp. 514–530, 2019.
- [136] H. Y. Lim, H. Bao, Y. Liu, and W. Wang, “Select Septate Junction Proteins Direct ROS-Mediated Paracrine Regulation of *Drosophila* Cardiac Function,” *Cell Reports*, vol. 28, no. 6, pp. 1455–1470.e4, 2019, e1454.
- [137] M. Hu, G. Guo, Q. Huang et al., “The harsh microenvironment in infarcted heart accelerates transplanted bone marrow mesenchymal stem cells injury: the role of injured cardiomyocytes-derived exosomes,” *Cell Death & Disease*, vol. 9, no. 3, p. 357, 2018.
- [138] Q. Zhang, M. Shang, M. Zhang et al., “Microvesicles derived from hypoxia/reoxygenation-treated human umbilical vein endothelial cells promote apoptosis and oxidative stress in H9c2 cardiomyocytes,” *BMC Cell Biology*, vol. 17, no. 1, p. 25, 2016.
- [139] A. Hervera, F. De Virgiliis, I. Palmisano et al., “Reactive oxygen species regulate axonal regeneration through the release of exosomal NADPH oxidase 2 complexes into injured axons,” *Nature Cell Biology*, vol. 20, no. 3, pp. 307–319, 2018.
- [140] K. Sugamura and J. F. Keaney, “Reactive oxygen species in cardiovascular disease,” *Free Radical Biology and Medicine*, vol. 51, no. 5, pp. 978–992, 2011.
- [141] J. Liang and Y. Wang, “Stem/progenitor cell based therapies for repair of myocardial infarction: current developments in methods of cell delivery,” *Surgery: Current Research*, vol. 3, no. 2, p. 131, 2013.
- [142] N. Baheiraei, H. Yeganeh, J. Ai, R. Gharibi, M. Azami, and F. Faghihi, “Synthesis, characterization and antioxidant activity of a novel electroactive and biodegradable polyurethane for cardiac tissue engineering application,” *Materials Science and Engineering: C*, vol. 44, pp. 24–37, 2014.
- [143] S. Franz, S. Rammelt, D. Scharnweber, and J. C. Simon, “Immune responses to implants - a review of the implications for the design of immunomodulatory biomaterials,” *Biomaterials*, vol. 32, no. 28, pp. 6692–6709, 2011.
- [144] A. M. Pisoschi and A. Pop, “The role of antioxidants in the chemistry of oxidative stress: a review,” *European Journal of Medicinal Chemistry*, vol. 97, pp. 55–74, 2015.
- [145] P. A. Shiekh, A. Singh, and A. Kumar, “Engineering bioinspired antioxidant materials promoting cardiomyocyte functionality and maturation for tissue engineering application,” *ACS Applied Materials & Interfaces*, vol. 10, no. 4, pp. 3260–3273, 2018.
- [146] P. A. Shiekh, A. Singh, and A. Kumar, “Oxygen-releasing antioxidant cryogel scaffolds with sustained oxygen delivery for tissue engineering applications,” *ACS Applied Materials & Interfaces*, vol. 10, no. 22, pp. 18458–18469, 2018.
- [147] J. Li, Y. Shu, T. Hao et al., “A chitosan-glutathione based injectable hydrogel for suppression of oxidative stress damage in cardiomyocytes,” *Biomaterials*, vol. 34, no. 36, pp. 9071–9081, 2013.
- [148] J. Yang, R. van Lith, K. Baler, R. A. Hoshi, and G. A. Ameer, “A thermoresponsive biodegradable polymer with intrinsic antioxidant properties,” *Biomacromolecules*, vol. 15, no. 11, pp. 3942–3952, 2014.
- [149] T. Hao, J. Li, F. Yao et al., “Injectable fullerene/alginate hydrogel for suppression of oxidative stress damage in brown adipose-derived stem cells and cardiac repair,” *ACS Nano*, vol. 11, no. 6, pp. 5474–5488, 2017.
- [150] Y. Qu, J. Tang, L. Liu, L. L. Song, S. Chen, and Y. Gao, “ α -Tocopherol liposome loaded chitosan hydrogel to suppress oxidative stress injury in cardiomyocytes,” *International Journal of Biological Macromolecules*, vol. 125, pp. 1192–1202, 2019.
- [151] P. Shabani, Z. Ghazizadeh, S. Gorgani-Firuzjaee et al., “Cardioprotective effects of omega-3 fatty acids and ascorbic acid improve regenerative capacity of embryonic stem cell-derived cardiac lineage cells,” *BioFactors*, vol. 45, no. 3, pp. 427–438, 2019.
- [152] J. Luo, M. S. Weaver, B. Cao et al., “Cobalt protoporphyrin pretreatment protects human embryonic stem cell-derived cardiomyocytes from hypoxia/reoxygenation injury in vitro and increases graft size and vascularization in vivo,” *Stem Cells Translational Medicine*, vol. 3, no. 6, pp. 734–744, 2014.

Research Article

The Impact of Lipoprotein Apheresis on Oxidative Stress Biomarkers and High-Density Lipoprotein Subfractions

Agnieszka Mickiewicz ¹, Ewelina Kreft,² Agnieszka Kuchta ², Ewa Wieczorek,² Joanna Marłęga,¹ Agnieszka Ćwiklińska,² Milena Paprzycka,² Marcin Gruchała,¹ Marcin Fijałkowski,¹ and Maciej Jankowski²

¹1st Department of Cardiology, Medical University of Gdansk, Gdansk, Poland

²Department of Clinical Chemistry, Medical University of Gdansk, Gdansk, Poland

Correspondence should be addressed to Agnieszka Kuchta; agakuchta@gumed.edu.pl

Received 29 April 2020; Accepted 27 July 2020; Published 6 August 2020

Guest Editor: Laura Sartiani

Copyright © 2020 Agnieszka Mickiewicz et al. This is an open access article distributed under the Creative Commons Attribution License, which permits unrestricted use, distribution, and reproduction in any medium, provided the original work is properly cited.

Lipoprotein apheresis (LA) treatment results in a substantial reduction of low-density lipoprotein- (LDL-) cholesterol and lipoprotein(a) concentrations, which consequently decreases the rate of cardiovascular events. The additional benefit of LA may be associated with its impact on the composition and quality of high-density lipoprotein (HDL) particles, inflammation, and oxidative stress condition. To verify the effects of LA procedure, the current study is aimed at analyzing the effect of a single apheresis procedure with direct hemadsorption (DALI) and cascade filtration (MONET) on oxidative stress markers and HDL-related parameters. The study included eleven patients with familial hypercholesterolemia and hyperlipoproteinemia(a) treated with regular LA (DALI or MONET). We investigated the pre- and postapheresis concentration of the lipid-related oxidative stress markers 8-isoPGF₂, oxLDL, TBARS, and PON-1. We also tracked potential changes in the main HDL apolipoproteins (ApoA-I, ApoA-II) and cholesterol contained in HDL subfractions. A single session of LA with DALI or MONET techniques resulted in a similar reduction of lipid-related oxidative stress markers. Concentrations of 8-isoPGF₂ and TBARS were reduced by ~60% and ~30%, respectively. LA resulted in a 67% decrease in oxLDL levels along with a ~19% reduction in the oxLDL/ApoB ratio. Concentrations of HDL cholesterol, ApoA-I, ApoA-II, and PON-1 activity were also reduced by LA sessions, with more noticeable effects seen in the MONET technique. The quantitative proportions between HDL₂ and HDL₃ cholesterol did not change significantly by both methods. In conclusion, LA treatment with MONET or DALI system has a small nonselective effect on lowering HDL particles without any changes in the protein composition of these particles. Significant reduction in the level of oxidative stress parameters and less oxidation of LDL particles may provide an additional benefit of LA therapy.

1. Introduction

Atherosclerosis and related cardiovascular disease represent a major health problem in Western countries and constitute a leading cause of morbidity and mortality [1]. The relationship among elevated low-density lipoprotein (LDL) particles, their oxidation, and the progression of atherosclerosis is well recognized [2]. More recently, an increased lipoprotein(a) (lp(a)) level was identified as a major cardiovascular lipid-related risk factor [3, 4].

Lipid-lowering medications, diet, and lifestyle modification do not always achieve the intended and restrictive therapeutic goals and proper reduction of cardiovascular event rate [5]. Individuals with severe familial hypercholesterolemia (FH) and those with high levels of lp(a) may require extracorporeal treatment with lipoprotein apheresis (LA). Specific columns not only remove LDL particles and lp(a) but also affect the concentration of chylomicrons, very-low-density lipoproteins (VLDL), and high-density lipoproteins (HDL) [6]. Several techniques of LA are available. The

elimination mechanism can either be based on precipitation (heparin-mediated extracorporeal LDL precipitation—H.E.L.P.), membrane filtration (Membrane Filtration Optimized Novel Extracorporeal Treatment—MONET), adsorption from whole blood (direct adsorption by polyacrylate/polyacrylamide—DALI), or immunoabsorption (IA).

Selective LA therapies, regardless of the technique used, have been shown to be safe and reduce the rate of adverse cardiac or vascular events [7–9]. Recent studies have suggested that the clinical benefits of LA may be associated with the impact of LA on inflammation and oxidative stress condition [10–12]. Published data have proved that increased oxidative stress in patients with FH enhanced the proatherogenic properties of LDL particles and participated in the acceleration of atherosclerosis [13]. However, investigations on the effect of single apheresis procedures on oxidative stress parameters are rare and remain inconclusive. While some have shown that LA treatment can decrease oxidative stress biomarkers [11, 14], others have demonstrated the enhancement of oxidative processes [15, 16].

Another interesting phenomenon is the effect of LA on HDL particles. The low HDL cholesterol phenotype observed in FH patients may also contribute to premature atherosclerosis. HDL particles possess multiple antiatherogenic functions related to their participation in reverse cholesterol transport, as well as antioxidant and anti-inflammatory capacity [17]. In this context, the depletion of HDL particles may be understood as a counterproductive result of LA. However, HDL particles are a very heterogeneous group of particles that differ in composition and functionality. Therefore, the assessment of the impact of LA only on the amount of HDL cholesterol does not reflect the potential changes in the composition and quality of these particles.

In the current study, we aimed to more fully explain the effect of apheresis by analyzing the effect of a single apheresis procedure using the MONET and DALI techniques on lp(a), lipid-related oxidative stress markers, including isoprostanes (8-iso-prostaglandin F_{2a}), thiobarbituric acid reactive substances (TBARS), and oxidized LDL particles (oxLDL). In addition, we evaluated the level of major apolipoproteins contained in HDL particles (ApoA-I, ApoA-II), assessed the activity of the HDL-related antioxidant enzyme paraoxonase-1 (PON-1), and tracked potential changes in cholesterol in HDL₂ and HDL₃ subfractions.

2. Methods

2.1. Subjects. The study cohort consisted of eleven patients on regular LA therapy. The indication for LA in eight patients was FH with the inability to achieve LDL-C treatment goals using maximally tolerated lipid-lowering therapy. Three patients had isolated hyperlipoproteinemia(a) with an lp(a) level above 100 mg/dl and LDL-C levels on target. Regular LA treatment was performed at biweekly intervals using two methods, according to the patients' characteristics and indications, as previously described [18, 19]. Seven individuals were treated with the cascade filtration method (MONET) and four with the direct hemadsorption (DALI) technique. The anticoagulation was based on heparin and cit-

TABLE 1: Demographic and clinical data.

Parameters	MONET ($n = 7$)	DALI ($n = 4$)	P
Gender (M/F)	4/3	2/2	0.472
Age (years)	59 ± 13	54 ± 6	0.953
Height (cm)	170 ± 10	169 ± 9	0.979
Weight (kg)	86 ± 24	86 ± 10	0.788
BMI (kg/m ²)	29 ± 6	30 ± 6	0.486
HR (bpm)	61 ± 9	64 ± 5	0.271
SBP (mmHg)	124 ± 6	118 ± 11	0.978
DBP (mmHg)	72 ± 7	72 ± 4	0.472

Continuous values are presented as means ± standard deviation. Potential differences between MONET and DALI techniques were analyzed using ANOVA for unrelated variables or Pearson's chi-squared test for nominal data. BMI: body mass index; DBP: baseline diastolic blood pressure; HR: baseline resting heart rate; SBP: baseline systolic blood pressure.

rate infusion. Each procedure was designed and conducted to achieve LDL-C and lp(a) reduction of at least 60% and processed at least 45 ml of plasma volume per kg of body weight in MONET procedures or 1.5l of blood volume in DALI sessions.

FH was diagnosed based on the Dutch Lipid Clinic Network Score, validated in the Polish population [20]. Before the initiation of LA, all subjects were treated with maximally tolerated lipid-lowering therapy to achieve recommended LDL-C treatment goals [5, 21]. The study was performed in accordance with the ethical guidelines of the 1975 Declaration of Helsinki and was approved by the Medical Ethics Committee of the Medical University of Gdańsk (Project code: 428/2018-2019). All of the participants provided written informed consent.

2.2. Laboratory Measurements. Blood samples were obtained from peripheral blood, in a fasting state directly before apheresis sessions and immediately after the apheresis procedure, as previously described [18]. The serum was separated after centrifugation at 1000 g for 15 min and was stored at -80°C until analysis.

The total cholesterol (TC) and triacylglycerols (TAG) were measured using commercially available enzymatic kits obtained from Pointe Scientific (Warsaw, Poland). The LDL-cholesterol (LDL-C) levels were measured using commercially available Direct LDL Kits from Abbott Laboratories (Chicago, United States). The HDL was isolated by the precipitation of apolipoprotein B-containing lipoproteins with heparin and manganese chloride, and the HDL-cholesterol (HDL-C) was measured in the supernatant using a kit obtained from Pointe Scientific. HDL₂ and HDL₃ subfractions were isolated by density gradient (HDL₂:1.06-1.125, HDL₃:1.125-1.25) ultracentrifugation in a Beckman Coulter TLA 120 2 [22]. lp(a) concentrations were measured using a commercially available lp(a) kit from Abbott Laboratories (Chicago, United States). The ApoB, ApoA-I, and ApoA-II concentrations were determined using the nephelometric method with antibodies obtained from Siemens Healthcare Diagnostics (Eschborn, Germany) with a Behring laser nephelometer. The paraoxonase-1 activity was measured in serum

TABLE 2: Impact of lipoprotein apheresis on plasma lipids and apolipoproteins.

Parameters	MONET			DALI		
	Preapheresis	Postapheresis	<i>P</i>	Preapheresis	Postapheresis	<i>P</i>
TC (mg/dl)	178 ± 63	92 ± 28	0.002*	169 ± 63	94 ± 29	0.019*
LDL-C (mg/dl)	136 ± 62	50 ± 26	<0.001*	137 ± 68	50 ± 34	0.012*
ApoB (g/l)	1.19 ± 0.35	0.53 ± 0.19	0.002*	1.28 ± 1.62	0.53 ± 0.36	0.002*
Non-HDL-C (mg/dl)	142 ± 61	61 ± 33	0.002*	134 ± 73	63 ± 34	0.043*
TAG (mg/dl)	188 (98-255)	78 (55-111)	0.017**	182 (158-340)	85 (61-182)	0.067**
lp(a) (mg/dl)	79 (12-116)	17 (5-60)	0.017**	119 (32-274)	30 (8-71)	0.068**
HDL-C (mg/dl)	36 ± 6	30 ± 6	<0.001*	34 ± 8	31 ± 12	0.012*
HDL ₂ -C (mg/dl)	22 ± 3	19 ± 3	0.018*	22 ± 7	20 ± 6	0.003*
HDL ₃ -C (mg/dl)	14 ± 3	11 ± 3	<0.001*	12 ± 5	11 ± 5	0.015*
HDL ₂ -C/HDL ₃ -C ratio	1.65 ± 0.15	1.7 ± 0.22	0.404*	1.9 ± 0.45	1.9 ± 0.5	0.996*
ApoA-I (g/l)	1.41 ± 0.28	1.15 ± 0.13	0.003*	1.45 ± 0.27	1.26 ± 0.02	0.046*
ApoA-II (g/l)	0.32 ± 0.06	0.25 ± 0.06	0.003	0.31 ± 0.08	0.30 ± 0.08	0.009
ApoB/ApoA-I	0.85 ± 0.29	0.48 ± 0.20	<0.001	1.00 ± 0.63	0.47 ± 0.36	0.02*

Continuous values are presented as means ± standard deviation or as medians (25th-75th percentile). Potential differences between pre- and postapheresis results were analyzed using *ANOVA for related variables or **a nonparametric Friedman test.

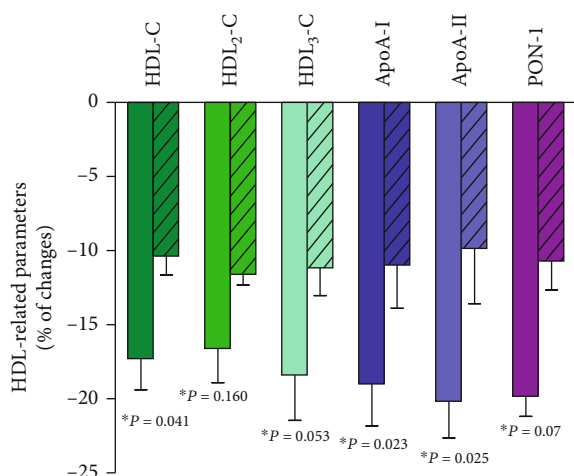


FIGURE 1: Percentage changes in HDL-related parameters due to the apheresis sessions. Bar graphs showing percentage changes in HDL-related parameters due to the MONET (open bar) and DALI (dashed bar) sessions. Values are presented as mean ± standard deviation. *The multivariate ANOVA for related variables was used to assess the impact of the method on the changes in individual parameters.

with paraoxon ethyl as the substrate, according to the procedure described earlier [23]. The concentration of TBARS was analyzed by fluorescence spectroscopy using a modified thio-barbituric acid-reactive substance [24]. oxLDL was analyzed using an enzyme immunoassay kit (EIAab, China), and 8-Iso-PGF₂α was analyzed in plasma using an enzyme immunoassay kit (Cayman Chemical, USA).

2.3. Statistical Analysis. Statistical analyses were performed using STATISTICA software, version 13 (StatSoft, Kraków, Poland). The Shapiro–Wilk test was used to test the deter-

mined normality of the distribution of variables. The variables were expressed as mean ± SD (standard deviation) or as medians with 25th and 75th percentiles. The one-way analysis of variance (ANOVA) for related variables or the *Friedman test* was used to assess the changes in individual parameters due to apheresis sessions, and the multivariate ANOVA was used to assess the impact of the apheresis technique on these changes. Pearson's chi-squared test was used to compare categorical variables. *P* values below 0.05 were considered to be statistically significant.

3. Results

The demographic and clinical data are presented in Table 1. The detailed characteristics of all investigated patients (*n* = 11) are shown in Supplemental Table S1. Of the eleven patients undergoing lipoprotein apheresis treatment, 7 were diagnosed with hypertension, 2 were diagnosed with diabetes, and 5 were past smokers. Ten patients had coronary artery disease (CAD). Of the eleven, ten patients were administered a potent statin in combination with ezetimibe and one patient was stain naïve due to mitochondrial myopathy.

The two investigated apheresis techniques, MONET and DALI, were similarly effective in lowering LDL-C (by 62% and 67%, respectively) and lp(a) (by 60% and 74%, respectively) and resulted in a comparable reduction of TC (by 45% and 43%, respectively), non-HDL-C concentration (by 51% and 53%, respectively), and TG concentration (by 53% and 52%, respectively) (Table 2).

The HDL-C, ApoA-I, and ApoA-II concentrations and PON-1 activity were reduced with the MONET technique on an average by 17%, 19%, 20%, and 20%, respectively. The decrease in the above parameters with the DALI technique was approximately halved (Figure 1). The reduction of cholesterol concentration was similar for both HDL₂ and

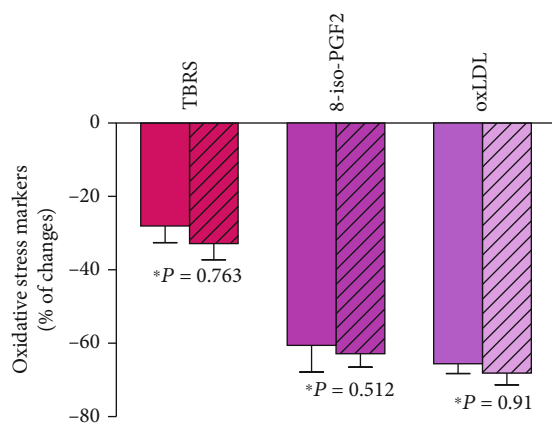


FIGURE 2: Percentage changes due to the apheresis sessions. Bar graphs showing percentage changes in oxidative stress markers due to the MONET (open bar) and DALI (dashed bar) session. Values are presented as mean \pm standard deviation. *The multivariate ANOVA for related variables was used to assess the impact of the method on the changes in individual parameters.

HDL₃ (~17% using the MONET technique and ~11% using the DALI technique). The quantitative proportions of HDL₂ and HDL₃ cholesterol did not change significantly due to the LA sessions, irrespective of the method used (Table 2).

A single session of LA using both the investigated techniques resulted in a significant reduction of oxidative stress marker levels, in addition to lowered lipid parameters. The 8-isoPGF2 concentration was reduced by 60% and 62%, TBARS concentration by 28% and 32%, and oxLDL concentration by 66% and 68% for the MONET and DALI techniques, respectively (Figure 2). In parallel, we noticed 21% and 17% reductions, respectively, in the oxLDL/ApoB ratio (Table 3).

4. Discussion

We have shown that the MONET and DALI techniques are similar in terms of the reduction of stress marker levels and proatherogenic lipoproteins. The obtained results are in line with previously published data [16] and confirmed the selectivity of atherogenic lipid removal, showing only a slight reduction in HDL cholesterol levels, which was more noticeable with the MONET technique. A decrease in HDL cholesterol of 12-20%, depending on the type of LA, is well-known and can be considered an unwanted effect of the treatment [25]. The participation of HDL particles in reverse cholesterol transport as well as their antioxidant and anti-inflammatory properties is thought to be protective in atherosclerosis. Nevertheless, HDL particles are a heterogeneous fraction. Accumulating evidence indicates that in the presence of systemic inflammation, HDL particles become dysfunctional, mainly as a result of the oxidation of their lipid and protein components, becoming cytotoxic and contributing to accelerated atherosclerosis [26]. Thus, the depletion of this subtype of particles would be beneficial even for patients

at high cardiovascular risk. However, data on the impact of apheresis on individual HDL subfractions and their properties are scarce. Opole et al. analyzed 10 subjects treated with the H.E.L.P. system and 3 patients treated with the lipoprotein adsorption technique and showed selective removal of proinflammatory HDL particles. This was explained by a change in lipoprotein composition and surface charge resulting in a less negative cation, which may have enhanced its removal by LA [27]. Using the DALI technique, Orsoni et al. demonstrated that the highest reduction in HDL particles by LA was the result of a reduction in the HDL₂ subfraction, which contained ~70% of total HDL ApoE [28]. Nevertheless, other studies conducted by these researchers showed no effect of apheresis on the ability of HDL particles to promote reverse cholesterol transport [29]. In our study, the decrease in serum ApoA-I, ApoA-II concentration, and activity of the HDL-linked antioxidant enzyme PON-1 was parallel to the decrease in HDL-C concentration. Moreover, we did not observe a change in the quantitative proportions of HDL₂ and HDL₃ cholesterol due to the apheresis sessions. Thus, it can be assumed that LA caused an unselective depletion of HDL subfractions and that this was more pronounced in the MONET technique. The smaller degree of HDL cholesterol reduction when using the DALI technique indicates that the adsorption techniques have a lower influence on HDL-related parameters.

Since oxidative stress is believed to play a major pathogenic role in vascular disease, the impact of apheresis on oxidative stress parameters appears to be clinically important, especially considering patients with FH and hyperlipoproteinemia(a) are characterized by the intensification of prooxidative processes [30]. Our study showed a clear decrease in oxidative stress parameters after a single apheresis session, which is in line with previous studies showing a significant reduction in free oxygen radicals and an increase in free oxygen radical defense [11, 14]. Nevertheless, not all studies have shown a positive impact of apheresis on systemic oxidative burden. Kopprasch et al., analyzing oxidant generation by phagocytes in whole blood and isolated leukocytes, demonstrated a transiently increased production of reactive oxygen species (ROS) following H.E.L.P. apheresis, while also suggesting a biochemical benefit of a single DALI treatment, namely, lower systemic oxidative burden in comparison to HELP and IA procedures [13].

In our work, we did not observe differences between the impact of the MONET and DALI techniques on lipid-related oxidative stress parameters, including a ~60% reduction in 8-isoPGF2 levels, which are the most valid in vivo lipid peroxidation biomarkers and exert proatherogenic function via their vasoconstrictive platelet-activating and mitogenic properties [31, 32]. We also noticed a decrease in oxLDL concentration. An increase in the oxidation of LDL due to prolonged intravascular residence time has been established as one of the key pathogenic mechanisms for the development of premature coronary lesions in hypercholesterolemia. In our work, along with the decrease in the oxLDL level, we noted reductions in the oxLDL/ApoB ratio, which may reflect the ratio of oxidatively modified LDL to total LDL

TABLE 3: Impact of lipoprotein apheresis on plasma oxidative stress marker level.

Parameters	MONET			DALI		
	Preapheresis	Postapheresis	<i>P</i>	Preapheresis	Postapheresis	<i>P</i>
8-Isoprostane (pg/ml)	29 (19-93)	11 (8-18)	0.01**	33 (27-40)	12 (9-26)	0.001**
TBARS ($\mu\text{mol/l}$)	3.1 \pm 0.4	2.1 \pm 0.1	0.001	2.8 \pm 0.8	1.8 \pm 0.4	0.027*
oxLDL (ng/ml)	62 \pm 21	20 \pm 5	<0.001	63 \pm 14	20 \pm 5	0.005*
oxLDL/ApoB (ng/mg)	57 \pm 11	43 \pm 16	0.008	60 \pm 34	52 \pm 34	0.008*
PON-1 (U/l)	186 \pm 94	146 \pm 71	0.002	225 \pm 65	191 \pm 52	0.057*

The values are presented as means \pm standard deviation or as medians (25th and 75th percentile). Potential differences between pre- and postapheresis results were analyzed using *ANOVA for related variables or **a nonparametric Friedman test.

particles. A decrease in LDL susceptibility to oxidation after lipid apheresis has been noted earlier [33]. Some researchers have speculated that exogenous removal of LDL induces changes in the chemical composition, such as an increase in the content of vitamin E, oleic acid, and arachidonic acid in LDL particles, which may lead to increased resistance against oxidation [34].

A computer simulation study by Donner et al., investigating the effect of dextran sulfate apheresis and HELP techniques on LDL oxidizability and performing, reported a decrease in the susceptibility of LDL to oxidation after apheresis session as the result of an altered ratio between freshly produced (less susceptible to oxidation) and older (more susceptible to oxidation) LDL particles. This speculation seems to be independent of the apheresis method and can also explain the lower ratio of oxidatively modified LDL to total LDL particles after MONET and DALI techniques observed in our study [35].

Our study has some limitations. The most important is the relatively small sample size. This is primarily because although LA treatment is fully reimbursed in Poland, only 4 centers offer such last-line therapy. To our knowledge, only 20 patients are currently undergoing regular LA in Poland. In conclusion, LA sessions, in addition to lowering the concentration of proatherogenic lipoproteins, have an acute, minor, nonselective effect on lowering HDL particles but do not change the protein composition of these particles and do not appear to affect their antioxidant properties associated with PON-1 activity. We observed a significant reduction in the level of oxidative stress parameters and demonstrated a reduction in the oxidation of LDL particles, which may provide additional benefit to LA therapy.

Data Availability

The data (database in Excel) used to support the findings of this study are available from the corresponding author upon request (agnieszka.kuchta@gumed.edu.pl).

Conflicts of Interest

The authors declare that there is no conflict of interest regarding the publication of this paper.

Authors' Contributions

Agnieszka Mickiewicz and Ewelina Kreft equally contributed to this work.

Acknowledgments

This work was supported by the Medical University of Gdańsk, under grant nos. ST 02-0125/07/524 and ST 02-0085/07/182.

Supplementary Materials

Table S1: detailed characteristics of investigated patients. (*Supplementary Materials*)

References

- [1] F. Mach, C. Baigent, A. L. Catapano et al., "2019 ESC/EAS guidelines for the management of dyslipidaemias: *lipid modification to reduce cardiovascular risk*: The Task Force for the management of dyslipidaemias of the European Society of Cardiology (ESC) and European Atherosclerosis Society (EAS)," *European Heart Journal*, vol. 41, no. 1, pp. 111–188, 2020.
- [2] M. Rafeian-Kopaei, M. Setorki, M. Doudi, A. Baradaran, and H. Nasri, "Atherosclerosis: process, indicators, risk factors and new hopes," *International Journal of Preventive Medicine*, vol. 5, no. 8, pp. 927–946, 2014.
- [3] A. Laschkolnig, B. Kollerits, C. Lamina et al., "Lipoprotein (a) concentrations, apolipoprotein (a) phenotypes, and peripheral arterial disease in three independent cohorts," *Cardiovascular Research*, vol. 103, no. 1, pp. 28–36, 2014.
- [4] B. G. Nordestgaard, M. J. Chapman, K. Ray et al., "Lipoprotein (a) as a cardiovascular risk factor: current status," *European Heart Journal*, vol. 31, no. 23, pp. 2844–2853, 2010.
- [5] F. M. Szymański, M. Barylski, B. Cybulska et al., "Recommendation for the management of dyslipidemia in Poland — third declaration of Sopot. Interdisciplinary expert position statement endorsed by the Polish Cardiac Society working group on cardiovascular pharmacotherapy," *Cardiology Journal*, vol. 25, no. 6, pp. 655–665, 2018.
- [6] G. R. Thompson, "Lipoprotein apheresis," *Current Opinion in Lipidology*, vol. 21, no. 6, pp. 487–491, 2010.
- [7] V. J. J. Schettler, C. L. Neumann, C. Peter et al., "Current insights into the German Lipoprotein Apheresis Registry

- (GLAR) – almost 5 years on,” *Atherosclerosis Supplements*, vol. 30, pp. 50–55, 2017.
- [8] G. R. Thompson, “The evidence-base for the efficacy of lipoprotein apheresis in combating cardiovascular disease,” *Atherosclerosis. Supplements*, vol. 14, no. 1, pp. 67–70, 2013.
 - [9] G. Thompson and K. G. Parhofer, “Current role of lipoprotein apheresis,” *Current Atherosclerosis Reports*, vol. 21, no. 7, pp. 26–26, 2019.
 - [10] A. Hovland, K. T. Lappégard, and T. E. Mollnes, “LDL apheresis and inflammation—implications for atherosclerosis,” *Scandinavian Journal of Immunology*, vol. 76, no. 3, pp. 229–236, 2012.
 - [11] J. Wen, Q. Dong, G. Liu et al., “Improvement of oxidative stress status by lipoprotein apheresis in Chinese patients with familial hypercholesterolemia,” *Journal of Clinical Laboratory Analysis*, vol. 34, no. 5, article e23161, 2020.
 - [12] H. Liu, C. G. Zhu, C. J. Cui et al., “P650Lipopolysaccharide-nuclear factor-kappa B pathway and lipoprotein apheresis effects in patients with familial hypercholesterolemia and coronary artery disease,” *European Heart Journal*, vol. 40, Supplement_1, 2019.
 - [13] S. Kopprasch, S. R. Bornstein, S. Bergmann, J. Graessler, B. Hohenstein, and U. Julius, “Long-term follow-up of circulating oxidative stress markers in patients undergoing lipoprotein apheresis by direct adsorption of lipids (DALI),” *Atherosclerosis Supplements*, vol. 30, pp. 115–121, 2017.
 - [14] V. Blaha, M. Blaha, D. Solichova et al., “Antioxidant defense system in familial hypercholesterolemia and the effects of lipoprotein apheresis,” *Atherosclerosis Supplements*, vol. 30, pp. 159–165, 2017.
 - [15] C. Otto, J. Berster, B. Otto, and K. G. Parhofer, “Effects of two whole blood systems (DALI and Liposorber D) for LDL apheresis on lipids and cardiovascular risk markers in severe hypercholesterolemia,” *Journal of Clinical Apheresis*, vol. 22, no. 6, pp. 301–305, 2007.
 - [16] K. P. Mellwig, E. Pulawski, D. Horstkotte, and F. van Buuren, “Lipid apheresis: oxidative stress, rheology, and vasodilatation,” *Clinical Research in Cardiology Supplements*, vol. 7, no. S1, pp. 45–49, 2012.
 - [17] A. Kontush and M. J. Chapman, “Antiatherogenic function of HDL particle subpopulations: focus on antioxidative activities,” *Current Opinion in Lipidology*, vol. 21, no. 4, pp. 312–318, 2010.
 - [18] A. Mickiewicz, J. Borowiec-Wolna, W. Bachorski et al., “Long-term lipoprotein apheresis in the treatment of severe familial hypercholesterolemia refractory to high intensity statin therapy: three year experience at a lipoprotein apheresis centre,” *Cardiology Journal*, vol. 26, no. 6, pp. 669–679, 2019.
 - [19] D. Kanikowska, K. Korybalska, A. Mickiewicz et al., “Flaxseed (*Linum Usitatissimum* L.) supplementation in patients undergoing lipoprotein apheresis for severe hyperlipidemia—a pilot study,” *Nutrients*, vol. 12, no. 4, p. 1137, 2020.
 - [20] A. Mickiewicz, M. Chmara, M. Futema et al., “Efficacy of clinical diagnostic criteria for familial hypercholesterolemia genetic testing in Poland,” *Atherosclerosis*, vol. 249, pp. 52–58, 2016.
 - [21] A. L. Catapano, I. Graham, G. de Backer et al., “2016 ESC/EAS guidelines for the management of dyslipidaemias,” *European Heart Journal*, vol. 37, no. 39, pp. 2999–3058, 2016.
 - [22] P. A. McPherson, I. S. Young, B. McKibben, and J. McEneny, “High density lipoprotein subfractions: isolation, composition, and their duplicitous role in oxidation,” *Journal of Lipid Research*, vol. 48, pp. 86–95, 2007.
 - [23] S. Maeda, S. Nakanishi, M. Yoneda et al., “Associations between small dense LDL, HDL subfractions (HDL2, HDL3) and risk of atherosclerosis in Japanese-Americans,” *Journal of Atherosclerosis and Thrombosis*, vol. 19, no. 5, pp. 444–452, 2012.
 - [24] M. Yokode, T. Kita, Y. Kikawa, T. Ogorochi, S. Narumiya, and C. Kawai, “Stimulated arachidonate metabolism during foam cell transformation of mouse peritoneal macrophages with oxidized low density lipoprotein,” *The Journal of Clinical Investigation*, vol. 81, no. 3, pp. 720–729, 1988.
 - [25] G. R. Thompson, “LDL apheresis,” *Atherosclerosis*, vol. 167, no. 1, pp. 1–13, 2003.
 - [26] N. Bellanger, A. Orsoni, Z. Julia et al., “Atheroprotective reverse cholesterol transport pathway is defective in familial hypercholesterolemia,” *Arteriosclerosis, Thrombosis, and Vascular Biology*, vol. 31, no. 7, pp. 1675–1681, 2011.
 - [27] I. O. Opole, J. M. Belmont, A. Kumar, and P. M. Moriarty, “Effect of low-density lipoprotein apheresis on inflammatory and noninflammatory high-density lipoprotein cholesterol,” *The American Journal of Cardiology*, vol. 100, no. 9, pp. 1416–1418, 2007.
 - [28] A. Orsoni, S. Saheb, J. H. Levels et al., “LDL-apheresis depletes apoE-HDL and pre- β 1-HDL in familial hypercholesterolemia: relevance to atheroprotection,” *Journal of Lipid Research*, vol. 52, no. 12, pp. 2304–2313, 2011.
 - [29] A. Orsoni, E. F. Villard, E. Bruckert et al., “Impact of LDL apheresis on atheroprotective reverse cholesterol transport pathway in familial hypercholesterolemia,” *Journal of Lipid Research*, vol. 53, no. 4, pp. 767–775, 2012.
 - [30] K. Arai, A. Orsoni, Z. Mallat et al., “Acute impact of apheresis on oxidized phospholipids in patients with familial hypercholesterolemia,” *Journal of Lipid Research*, vol. 53, no. 8, pp. 1670–1678, 2012.
 - [31] S. H. Wilson, P. J. Best, L. O. Lerman, D. R. Holmes, D. M. Richardson, and A. Lerman, “Enhanced coronary vasoconstriction to oxidative stress product, 8-epi-prostaglandinF_{2 α} , in experimental hypercholesterolemia,” *Cardiovascular Research*, vol. 44, no. 3, pp. 601–607, 1999.
 - [32] P. Minuz, C. Fava, and A. Lechi, “Lipid peroxidation, isoprostanes and vascular damage,” *Pharmacological Reports*, vol. 58, pp. 57–68, 2006.
 - [33] Y. Tsurumi-Ikeya, K. Tamura, K. Azuma et al., “Sustained inhibition of oxidized low-density lipoprotein is involved in the long-term therapeutic effects of apheresis in dialysis patients,” *Arteriosclerosis, Thrombosis, and Vascular Biology*, vol. 30, no. 5, pp. 1058–1065, 2010.
 - [34] C. Napoli, G. Ambrosio, N. Scarpato et al., “Decreased low-density lipoprotein oxidation after repeated selective apheresis in homozygous familial hypercholesterolemia,” *American Heart Journal*, vol. 133, no. 5, pp. 585–595, 1997.
 - [35] M. G. Donner, K. G. Parhofer, W. O. Richter, and P. Schwandt, “Low-density lipoprotein (LDL) oxidizability before and after LDL apheresis,” *Metabolism*, vol. 48, no. 7, pp. 881–886, 1999.

Research Article

Ticagrelor Conditioning Effects Are Not Additive to Cardioprotection Induced by Direct NLRP3 Inflammasome Inhibition: Role of RISK, NLRP3, and Redox Cascades

Claudia Penna ¹, **Manuela Aragno** ¹, **Alessia Sofia Cento** ¹, **Saveria Femminò** ¹,
Isabella Russo ¹, **Federica Dal Bello** ², **Fausto Chiazza** ³, **Debora Collotta** ³,
Gustavo Ferreira Alves ³, **Massimo Bertinaria** ³, **Elisa Zicola** ¹, **Valentina Mercurio** ⁴,
Claudio Medana ², **Massimo Collino** ³, and **Pasquale Pagliaro** ¹

¹Department of Clinical and Biological Sciences, University of Turin, Turin, Italy

²Department of Molecular Biotechnology and Health Sciences, University of Turin, Turin, Italy

³Department of Drug Science and Technology, University of Turin, Turin, Italy

⁴Department of Translational Medical Sciences, Federico II University, Naples, Italy

Correspondence should be addressed to Massimo Collino; massimo.collino@unito.it
and Pasquale Pagliaro; pasquale.pagliaro@unito.it

Received 6 April 2020; Revised 7 June 2020; Accepted 26 June 2020; Published 4 August 2020

Academic Editor: José P. Andrade

Copyright © 2020 Claudia Penna et al. This is an open access article distributed under the Creative Commons Attribution License, which permits unrestricted use, distribution, and reproduction in any medium, provided the original work is properly cited.

Inhibition of either P2Y₁₂ receptor or the nucleotide-binding oligomerization domain- (NOD-) like receptor pyrin domain containing 3 (NLRP3) inflammasome provides cardioprotective effects. Here, we investigate whether direct NLRP3 inflammasome inhibition exerts additive effects on myocardial protection induced by the P2Y₁₂ receptor antagonist Ticagrelor. Ticagrelor (150 mg/kg) was orally administered to rats for three consecutive days. Then, isolated hearts underwent an ischemia/reperfusion (30 min ischemia/60 min reperfusion; IR) protocol. The selective NLRP3 inflammasome inhibitor INF (50 μM) was infused before the IR protocol to the hearts from untreated animals or pretreated with Ticagrelor. In parallel experiments, the hearts isolated from untreated animals were perfused with Ticagrelor (3.70 μM) before ischemia and subjected to IR. The hearts of animals pretreated with Ticagrelor showed a significantly reduced infarct size (IS, 49 ± 3% of area at risk, AAR) when compared to control IR group (69 ± 2% of AAR). Similarly, *ex vivo* administration of INF before the IR injury resulted in significant IS reduction (38 ± 3% of AAR). Myocardial IR induced the NLRP3 inflammasome complex formation, which was attenuated by either INF pretreatment *ex vivo*, or by repeated oral treatment with Ticagrelor. The beneficial effects induced by either treatment were associated with the protective Reperfusion Injury Salvage Kinase (RISK) pathway activation and redox defence upregulation. In contrast, no protective effects nor NLRP3/RISK modulation were recorded when Ticagrelor was administered before ischemia in isolated heart, indicating that Ticagrelor direct target is not in the myocardium. Our results confirm that Ticagrelor conditioning effects are likely mediated through platelets, but are not additives to the ones achieved by directly inhibiting NLRP3.

1. Introduction

Ischemic heart disease remains the leading cause of morbidity in the Western world, and the number of deaths from acute myocardial infarction (AMI) is also rapidly rising in the developing world. Although restoration of early blood

flow to the ischemic myocardium with thrombolysis is presently the most effective therapy to limit infarct size, reperfusion alone is inadequate to salvage the damaged myocardium and may result in myocardial ischemia/reperfusion (IR) injury, which is characterized by excessive oxidative stress and inflammatory response [1–3]. In fact, as shown by both

preclinical and clinical studies, the excess myocardial cell death resulting from the restoration of blood and oxygen supply can contribute up to 50% of the final infarct size [1–3].

In clinical practice, P2Y₁₂ adenosine diphosphate (ADP) receptor antagonists are standard of care in AMI patients undergoing primary percutaneous intervention. Several preclinical studies have convincingly shown that these drugs significantly protect against IR injury, suggesting that these pleiotropic effects could be even more important than their antiaggregant properties in this specific clinical setting [4–8]. Clinical trials have shown that the nonthienopyridine P2Y₁₂ antagonists such as Ticagrelor and Cangrelor were associated to lower incidence of cardiovascular mortality, AMI, or stroke compared with the thienopyridine P2Y₁₂ antagonists, Clopidogrel and Prasugrel [9]. These differences have been ascribed, at least in part, to better and more consistent pharmacokinetic profile of the nonthienopyridine P2Y₁₂ antagonists (Ticagrelor and Cangrelor) that do not require hepatic P450-mediated metabolic conversion of the prodrug (e.g., Clopidogrel and Prasugrel) into active forms to ensure P2Y₁₂ receptor inhibition. Moreover, Ticagrelor is the only P2Y₁₂ antagonist that increases tissue adenosine levels *via* inhibition of the equilibrative nucleoside transporter 1 (ENT1) by protecting the extracellular adenosine from intracellular metabolism [10–12]. This effect has been suggested to further contribute to the drug-induced cardioprotection [13–15], despite a recently published paper clouding this hypothesis [8].

Although different cell types (including endothelial cells [16]) express P2Y₁₂ receptors, the conditioning effect of P2Y₁₂ receptor-inhibitors has been attributed to the modulation of platelet sphingosine kinase activity and perhaps to sphingosine 1-phosphate (S1P) release [5, 17]. Since P2Y₁₂ antagonists reduce infarct size but do not eliminate it, some other processes must be responsible of residual IR injury. Indeed, additive cardioprotective effects have been demonstrated by the combination of Ticagrelor and Rosuvastatin [13]. More recently, Audia et al. [4] demonstrated that a highly selective caspase-1 inhibitor provides additional and sustained infarct size reduction when added to Ticagrelor in preclinical models of IR injury. Caspase-1 activation is a critical choke point for eliciting activation of the inflammatory cascade NLRP3 (NOD-like receptor family, pyrin domain-containing3) inflammasome. The NLRP3 inflammasome is a large multimeric protein complex which interacts with an apoptosis-associated speck-like protein including a caspase recruitment domain (ASC), thus recruiting and activating caspase-1, which in turn mediates the cleavage of inactive prointerleukin- (IL-) 1 β and IL-18 into their active forms [18]. We and others have previously demonstrated the pivotal role of the NLRP3 inflammasome in cardiometabolic disorders, including myocardial ischemia reperfusion injury, [19–23] and several NLRP3 inhibitors, including the small molecule INF we recently developed, have been tested in animal model of IR injury, showing salvage of part of the myocardium at risk [24, 25]. The cardioprotective role of NLRP3 inhibitors is attributable, at least in part, to their ability to modify protective pathways and redox environment of cells [24, 26].

In the present study, we evaluate (1) the ability of Ticagrelor and INF, alone and in combination, to reduce infarct size following IR injury, (2) the potential mechanisms of cross-talk between the two drug treatments underlying their myocardial protection, and (3) the relevance of the presence of blood in mediating cardioprotective effects and the platelet mediators released after Ticagrelor exposure.

2. Materials and Methods

2.1. Ex Vivo Rat Model of Heart IR Injury. Male Wistar rats (Harlan Laboratories, Udine, Italy) 5–6 months old, reaching a body weight of 450–550 g, were anesthetized with sodium pentothal (50 mg/kg) by intraperitoneal injections and heparinized (800 U/100 g b.w., i.m.) before being culled by cervical dislocation. The hearts were then rapidly excised, placed in an ice-cold buffer solution, and weighed. The excised hearts were rapidly perfused by the Langendorff technique with Krebs-Henseleit bicarbonate buffer containing (mM) NaCl 118, NaHCO₃ 25, KCl 4.7, KH₂PO₄ 1.2, MgSO₄ 1.2, CaCl₂ 1.25, and Glucose 11. The buffer was gassed with 95% O₂:5% CO₂. The hearts were perfused in constant flow mode to achieve a perfusion pressure of about 80 mmHg. To assess the conditions of experimental preparation, coronary perfusion pressure was monitored during all experiments [27], and flow rate was checked in a specific time period. The temperature of the perfusion system was maintained at 37°C. After a 30 min stabilization period, the hearts were subjected to a protocol of IR, which consisted in 30 min of global no-flow, normothermic ischemia followed by a period of 60 min of reperfusion. At the end of perfusion period, the hearts were rapidly removed from the perfusion apparatus and divided in two parts by a coronal section (perpendicular to the long axis). The apical part of the left ventricle (LV, less than 1/3 of ventricular mass) was frozen rapidly in liquid nitrogen and stored at -80°C and subsequently used for Western blot analysis; the basal part of the LV was used for infarct size assessment.

The protocol was approved by the Institutional Animal Care and Use Committee of the University of Turin and conformed to the European Directive 2010/63/EU on the protection of animals used for scientific purposes.

2.2. Drug Treatments. Rats ($n = 6 - 8$ per group) received water or Ticagrelor (TIC, 150 mg/kg/d) by oral gavage for 3 days (oTIC). Then, the isolated hearts were submitted to ischemia/reperfusion as described above (IR and oTIC groups). A subgroup of isolated hearts from oTIC rats were exposed to the selective NLRP3 inflammasome inhibitor INF (50 μ M) in the perfusate for 20 min before ischemia (oTIC+exINF). In a subsequent series of experiments, the isolated hearts from control rats were pretreated with 3.70 μ M Ticagrelor or 50 μ M exINF or both in the perfusate for 20 min before ischemia (exTIC, exINF, and exTIC+exINF groups, respectively). After stabilization, sham hearts underwent 90 min perfusion only and served as control group (Figure 1).

A stock solution of 200 mM INF in DMSO was prepared and was then diluted at a final concentration of 50 μ M in the

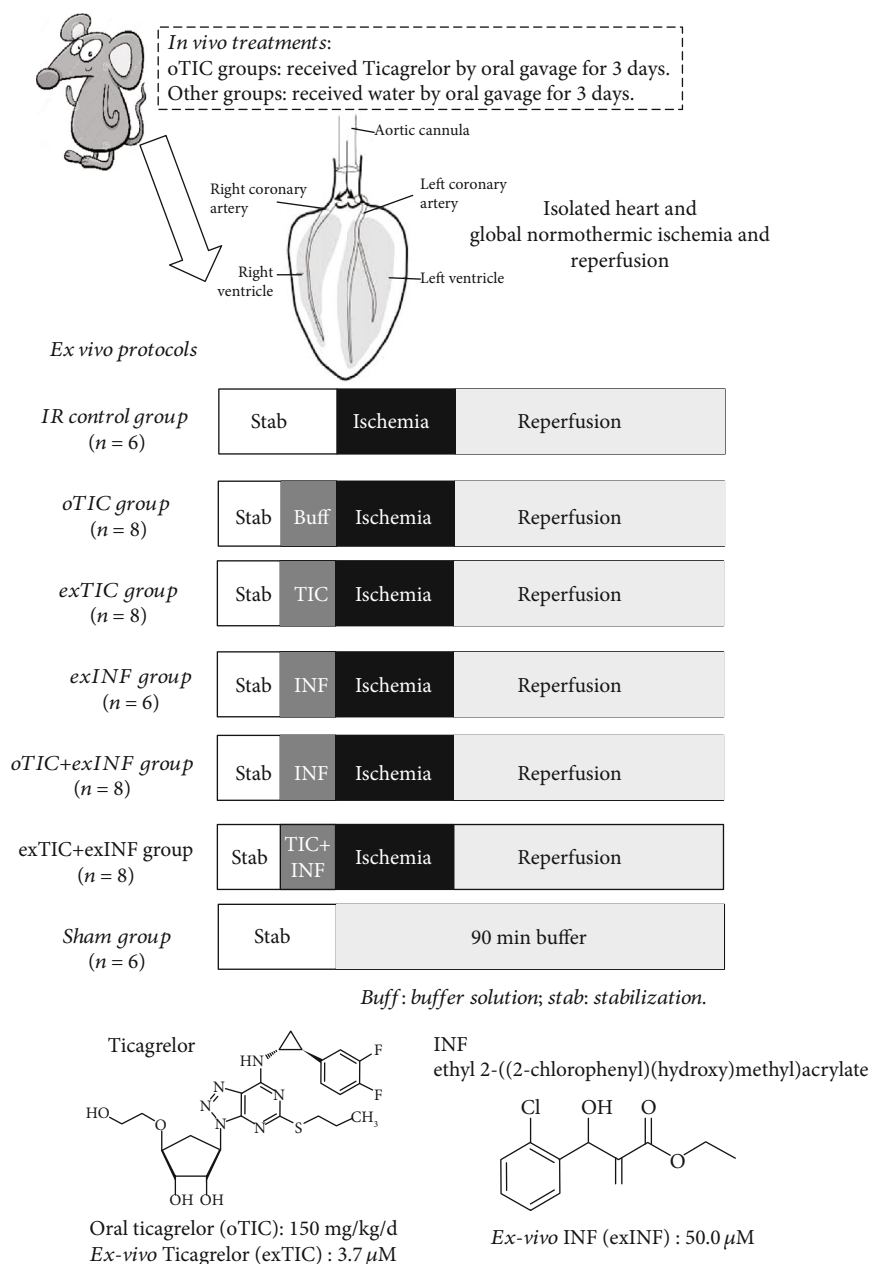


FIGURE 1: Schematic representation of rat treatments *in vivo* and various protocols *ex vivo*. Rats received water or Ticagrelor (TIC) by oral gavage for 3 days; then, hearts were isolated and perfused. After stabilization, isolated hearts were submitted to specific treatment and then to global ischemia/reperfusion protocol.

perfusion buffer. The description of the synthesis of the inhibitor as well as the *in vitro* biological effects has been already published. INF is an acrylate derivative originally synthesized by Cocco et al. [28] and selected, among the tested compounds, as the most effective inhibitor of NLRP3 activation (IC_{50} of 1.26×10^{-7} M and 1.58×10^{-7} M in LPS/ATP-triggered and LPS/nigericin-triggered pyroptosis, respectively). As previously documented [29, 30], INF inhibits the NLRP3 ATPase activity of isolated human-recombinant NLRP3 protein as well as caspase-1 activation, and it acts as covalent NLRP3 inhibitor through irreversible binding to nucleophilic residues present in NLRP3, with a reactivity of $0.824 \pm 0.017 \text{ M}^{-1} \text{ s}^{-1}$, measured as second-

order rate constant (k_2) for the reaction with cysteamine. Ticagrelor was dissolved at $3.70 \mu\text{M}$ concentration in Krebs solution. The *in vivo* dose of Ticagrelor and the *in vitro* concentrations of both Ticagrelor and INF were chosen according to previous studies demonstrating their efficacy against myocardial IR injury [13, 24, 28, 31].

2.3. Infarct Size Assessment. Infarct areas were assessed at the end of the 60 min reperfusion with the nitro-blue-tetrazolium (NBT) technique. The basal part of the left ventricle was dissected by transverse sections into two/three slices. Following 20 min of incubation at 37°C in 0.1% solution NBT (Sigma-Aldrich, St. Louis, MO, USA) in phosphate

buffer, unstained necrotic tissue was carefully separated from stained viable tissue by an independent observer, who was unaware of the protocols. Since the ischemia was global and we analyzed only the basal part of the ventricle, the necrotic mass was expressed as a percentage of the analyzed ischemic tissue [32].

2.4. Preparation of Tissue Extracts. As previously described [33], the heart apex was homogenized at 10% (*w/v*) in a Potter-Elvehjem homogenizer (Wheaton, NJ, USA) using a homogenization buffer (containing 20 mM HEPES, pH 7.9, 1 mM MgCl₂, 0.5 mM EDTA, 1 mM EGTA, 1 mM dithiothreitol (DTT), 0.5 mM phenylmethyl sulphonyl fluoride (PMSF), 0.5% Nonidet P-40, phosphatase, and protease inhibitors) and centrifuged at 1300 × g for 5 min at 4°C. To obtain the cytosolic fraction, supernatants were removed and centrifuged at 16000 × g at 4°C for 40 minutes. The pelleted nuclei were resuspended in extraction buffer containing 20 mM HEPES (pH 7.9), 1.5 mM MgCl₂, 420 mM NaCl, 0.2 mM EDTA, 20% glycerol, 1 mM EGTA, phosphatase, and protease inhibitors and incubated in ice for 30 minutes followed by centrifugation at 16000 × g for 20 min at 4°C. The resulting supernatants containing nuclear proteins were carefully removed, and protein content was determined on both nuclear and cytosolic extracts using the bicinchoninic acid (BCA) protein assay following the manufacturer's directions (Thermo Fisher Scientific, Rockford, IL). Protein extracts were stored at -80°C until use.

2.5. Determination of IL-1β in Heart Homogenates. Commercially available ELISA kit (R&D Systems, Abingdon, UK) was used to measure concentrations of IL-1β in tissue homogenates, according to the manufacturer's instructions.

2.6. Western Blot Analysis. Equal amounts of total protein extracts were separated by SDS-PAGE and electrotransferred to nitrocellulose membrane (GE-Healthcare Europe, Milan, Italy). Membranes were probed with rabbit anti-NLRP3 (Abcam, Cambridge, UK), rabbit anti-caspase-1 (Santa Cruz Biotechnology, Dallas, TX, USA), mouse anti-Ser⁴⁷³ Akt (Cell Signaling Technology, Danver, MA, USA), rabbit anti-total Akt (Cell Signaling Technology, Danver, MA, USA), rabbit anti-Ser⁹ GSK-3β (Abcam, Cambridge, UK), anti-total GSK-3β (Cell Signaling Technology, Danver, MA, USA), anti-Ser⁶⁶⁰ PKC and total PKC (Santa Cruz Biotechnology, Dallas, TX, USA), SOD2 (Novus Biologicals, Centennial, CO, USA), and NRF2 (Thermo Fisher Scientific, Waltham, MA, USA) followed by incubation with appropriate HRP-conjugated secondary antibodies (BioRad). Proteins were detected with Clarity Western ECL substrate (BioRad, California, USA) and quantified by densitometry using analytic software (Quantity-One, BIO-RAD Image Lab Software.6.0.1.). Results were normalized with respect to densitometric value of mouse anti-tubulin (Abcam, Cambridge, UK), and autoradiograms showing statistically significant differences in terms of gel-loading homogeneity were excluded from the following biomarkers analyses.

2.7. Platelet Release of S1P and Adenosine. Fasting venous blood sample from four male healthy volunteers (mean age:

38 ± 2 years) was withdrawn without stasis and anticoagulated with citrate-dextrose solution (ACD, with the final ACD/blood ratio 1:6 vol/vol). The human platelet study was authorized by "Comitato Etico Interaziendale San Luigi Gonzaga," authorization n. 155/2017, and informed consent was obtained in accordance with the 1964 Declaration of Helsinki and its later amendments. The platelet-rich plasma, obtained by centrifugation at 100 × g for 20 min, underwent further centrifugation at 2000 × g for 10 min, and pellet was washed 2 times at 37°C in HEPES-Na buffer (mmol/L): 10 HEPES Na, 140 NaCl, 2.1 MgSO₄, 10 D-glucose, and pH 7.4. Platelets were counted by automatic blood cells counter (Mythic 18, Orphèe, Switzerland) and resuspended to a final concentration of 2 × 10¹¹ cells/L in phosphate-buffered saline containing 1% BSA. The contamination of white blood cells was less than 1/10⁴ platelets. Platelet samples were subjected to stirring (1200 rpm speed at 37°C) in both the absence and presence of Ticagrelor (5000 ng/mL, 30 min) or thrombin receptor-activating peptide (TRAP-6) (Mascia Brunelli, Monza, Milan, Italy) (10 μmol/L, 8 min), then centrifuged at 4000 rpm for 10 min. Supernatants were stored at -20°C until sphingosine, S1P, and adenosine measurements.

2.8. Sample Preparation for UHPLC-Tandem Mass Analysis. 100 μL of platelet samples and heart homogenates were added with 2 mL of 0.1% trifluoroacetic acid in chloroform/methanol 1/1 and with internal standards (adenosine and S1P d7) at 300 μg/L as final concentration. After vortex in g for 30 seconds, 0.5 mL of chloroform and 0.5 mL of water were added. After centrifugation, organic phase was recovered and extracted twice with 1 mL of chloroform. The solution was dried overnight under vacuum (Centrivap, Labconco, Kansas City, MO, USA) and reconstituted with 100 μL of eluents A/B 7/3.

2.9. UHPLC-Tandem Mass Analytical Method. The analyses of sphingolipids and adenosine were performed using a Nexera (Shimadzu, Milan, Italy) UHPLC coupled through an ESI source to a Qtrap5500 triple quadrupole analyzer (Sciex, Milan, Italy).

The chromatographic separation was achieved with a Kinetex column (1.7 μm, 100 × 2.1 mm, 100 Å, Phenomenex, Bologna, Italy) with 0.1% formic acid in water/acetonitrile 8/2 (eluent A) and 0.1% formic acid in isopropanol/acetonitrile 8/2 (eluent B). The separation gradient was from 5 to 100% of B in 7 minutes, followed by column reconditioning. Flow rate was set at 400 μL min⁻¹, and injection volume was 3 μL. The LC column effluent was delivered to the ESI ion source, using air as both 1 and 2 gasses (40 and 50 arbitrary units, respectively), and the ion voltage was 5.0 kV. Curtain gas (nitrogen) was 30 arbitrary units.

The multiple reaction monitoring (MRM) transitions and parameters were C18-Sph (*m/z*) 300@282 CE 13 V; C18-S1P (*m/z*) 380@264 CE 21 V; and adenosine (*m/z*) 268@136 CE 21 V. For the internal standard, the MRM transition was C18-S1P d7 (*m/z*) 387@271 CE 19 V. The lower limit of detection (LLOQ) was 0.50 μg/L for all analytes.

2.10. Materials. Unless otherwise stated, all compounds were purchased from the Sigma-Aldrich Company Ltd. (St. Louis, Missouri, USA).

2.11. Statistical Analysis. All values are expressed as means \pm SEM and were analyzed by ANOVA test followed by Bonferroni's posttest and Student's *t*-test. A *P* value < 0.05 was considered statistically significant.

3. Results

3.1. Infarct Size Was Reduced by Ticagrelor In Vivo but Not Ex Vivo. Rat hearts exposed to a 30 min global ischemia and 60 min reperfusion developed infarction which was $69.5 \pm 2.3\%$ of ischemic area at risk (AAR). Infarct size was significantly reduced by rat pretreatment for 3 days with Ticagrelor (oTIC, infarct size $49.6 \pm 3.9\%$ of AAR, $P < 0.01$ vs. IR group). No protective effects were recorded when Ticagrelor was added *ex vivo* to the perfusate of excised hearts from untreated animals (exTIC, infarct size $68.6 \pm 3.0\%$ of AAR), thus suggesting that Ticagrelor protection was only triggered in the intact organism (Figure 2). Coronary flow and perfusion pressure measured during stabilization in the IR group (10 ± 1 mL/min/g and 80 ± 2 mmHg, respectively) were not statistically different from those recorded in the treated groups, thus suggesting similar oxygen demands among groups.

3.2. Ticagrelor and INF Do Not Exert Additive Effects on Infarct Size Limitation. When INF was added *ex vivo* to the perfusate before ischemia (exINF), we observed a significant reduction in infarct size (exINF, infarct size $38.3 \pm 3.0\%$ of AAR, $P < 0.05$ vs. IR group), comparable to the one achieved by oTIC alone (Figure 2).

Interestingly, exINF did not exert additive effects on protection against infarct size evoked by oral Ticagrelor pretreatment, as the reduction in infarct size evoked by the combination was almost identical to that obtained herein with either Ticagrelor or exINF alone (oTIC+exINF, infarct size $44.1 \pm 1.9\%$ of AAR, $P < 0.05$ vs. IR group). Similarly, no priming effects on exINF protection were recorded when Ticagrelor was coadministered *ex vivo* in the perfusate only (exTIC+exINF, infarct size $52.2 \pm 2.7\%$ of AAR).

3.3. Ticagrelor Pretreatment Prevented NLRP3 Inflammasome Activation and Downstream Signaling. Expression level and activation of the downstream signaling of NLRP3 inflammasome were assessed by Western blotting analysis in protein extracts obtained from the apical portion of hearts pretreated or not with either Ticagrelor or INF and exposed to IR.

As expected, the INF pretreatment effectively reduced the IR-induced NLRP3 upregulation and activation, resulting in significant reduction of the cleaved active p10 subunit of caspase-1 (Figures 3(a) and 3(b)). As a consequence of reduced caspase-1 activation, the levels of IL-1 β , that reached the highest concentrations after 60 min of reperfusion, showed a mild but still significant decrease in the exINF group (Figure 3(c)). Notably, both Western blotting analysis and ELISA assay demonstrated that similar inhibition of NLRP3 expression and activation could be reached when rats

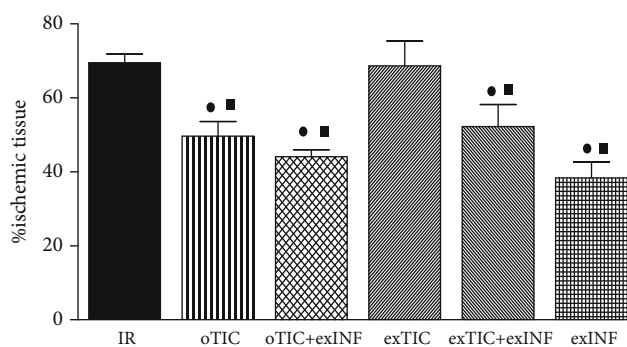


FIGURE 2: Infarct size. Data analyzed by one-way ANOVA followed by a Bonferroni post hoc test and expressed as mean \pm SEM. $n = 6 - 8$ per group. Statistical significance: $\bullet P < 0.05$ vs. IR and $\blacksquare P < 0.05$ vs. exTIC.

were pretreated with Ticagrelor (oTIC), but not when Ticagrelor was added in the perfusate only (exTIC). Besides, no further NLRP3 inflammasome inhibition was recorded when INF was added in the perfusate of heart from rats previously exposed to Ticagrelor pretreatment (oTIC+exINF).

3.4. Risk Pathway Protective Activity Was Enhanced by Either Oral Ticagrelor Pretreatment Or INF Heart Exposure. Since RISK pathway is activated by both pre- and postconditioning treatments [34], we quantified expression and activity (in terms of phosphorylation) of its key members. After 60 min of reperfusion, slight but not significant increase in phosphorylation rate of Akt, GSK-3 β , and PKC (Figures 4(a)–4(c), respectively) was recorded in untreated hearts exposed to IR protocol, when compared to the sham group. The phosphorylation rates of Akt, GSK-3 β , and PKC induced by the 60 min reperfusion were all increased massively in oTIC and exINF (both $P < 0.05$ vs. sham; $P = \text{NS}$ among groups). No additive effects were recorded when the two treatments were combined. Interestingly, *ex vivo* Ticagrelor exposure 20 min prior to ischemia only did not significantly modify the activation of the RISK pathway evoked by IR and/or INF.

3.5. Ticagrelor and INF Improved IR-Induced Antioxidant Response. SOD2 is an important endogenous antioxidant and provides protection against myocardial IR. Consistently with other studies [24], we found that IR led to increased expression of SOD2 ($P < 0.05$ vs. sham). All treatments blunted IR-induced SOD upregulation. However, in oTIC, oTIC+exINF, and exTIC+exINF groups, the levels of SOD2 were significantly lower than that of IR group ($P < 0.05$ vs. IR, Figure 5(a)). A reduction in SOD2 levels was also recorded in the heart of mice treated with INF only when compared to IR group, without reaching statistical significance (Figure 5(a)).

The Western blot analysis on the expression levels of the antioxidant transcription factor Nrf2 showed that its nuclear translocation was reduced by IR when compared to sham (Figure 5(b)). All treatments blunted IR-induced reduction of Nrf2 nuclear translocation. However, only in oTIC the

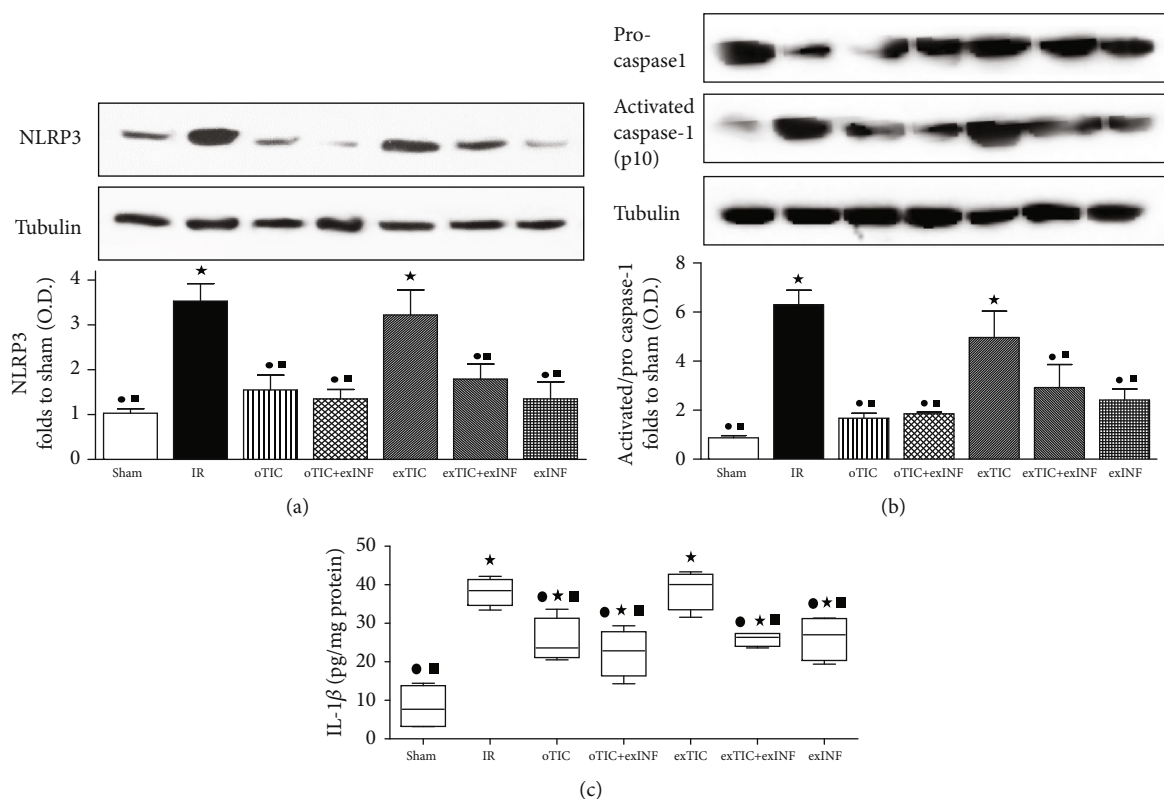


FIGURE 3: Western blotting analysis on (a) NLRP3, (b) pro- and activated caspase, and (c) quantification of IL1 β by ELISA kit assay. Data analyzed by one-way ANOVA followed by a Bonferroni post hoc test and expressed as mean \pm SEM. $n = 6 - 8$ per group. Statistical significance: ● $P < 0.05$ vs. IR; ★ $P < 0.05$ vs. sham, ■ $P < 0.05$ vs. exTIC. Representative blots are shown of at least three different experiments.

levels of Nrf2 nuclear translocation were significantly higher than in IR and similar to sham (Figure 5(b)).

3.6. Oral Ticagrelor Pretreatment Resulted in S1P and Adenosine Overaccumulation in the Heart. As shown in Figure 6, a marked increase in the myocardial concentration of either S1P or adenosine was recorded in the postischemic heart from rats exposed to the oral Ticagrelor pretreatment (oTIC) when compared to IR only, whereas *ex vivo* administration of Ticagrelor or exINF did not significantly affect their levels. Combining Ticagrelor and INF (oTIC+exINF) did not further increase S1P or adenosine accumulation in the heart in comparison to oTIC alone.

3.7. Ticagrelor Enhanced S1P and Adenosine Release from Platelets. Sphingosine, S1P, and adenosine were evaluated in the supernatant of human platelet samples subjected to stirring (1200 rpm speed at 37°C) with or without Ticagrelor (5000 ng/mL, 30 min) (Table 1). Ticagrelor-treated samples show high level of S1P in the supernatant and low level of sphingosine if compared to control ($P < 0.05$). Adenosine concentration increased significantly compared to control in the supernatant of Ticagrelor-treated platelets. The positive control was obtained by incubating human platelet with TRAP-6 (10 μ mol/L, 8 min). The values of the release of S1P and adenosine in the supernatant in TRAP-6 group were significantly higher than control and Ticagrelor-treated platelets (data not shown).

4. Discussion

The present study further extends previous findings on Ticagrelor cardioprotective effects, confirming that the protection was dependent upon its administration *in vivo*, as adding the P2Y12 antagonist *ex vivo* to the perfusate in excised hearts does not counteract the IR injury. Here, we confirm our previous data [24] that the specific and direct inhibition of NLRP3 by exINF results in a significant reduction in infarct size. Most notably, adding INF just before ischemia does not further improve cardioprotection induced by Ticagrelor pretreatment (3 days), with no significant effect of the combination over each drug alone. We then aimed to assess whether Ticagrelor primes the isolated hearts exposed to the inflammasome inhibitor. Administration of Ticagrelor to the perfusate *ex vivo* does not enhance the heart response to exINF, showing no interactions between the two treatments.

Indeed, Ticagrelor has been shown to modulate the expression on blood cells of toll-like receptors, key receptors involved in NLRP3 regulation [35]. Here, we show that the reduction in infarct size achieved by oral Ticagrelor is, at least in part, attributable to a cardioprotective effect mediated by the inhibition of the NLRP3 inflammasome pathway, as similar inhibitory effects on the activation of pivotal markers of the inflammasome cascade were recorded when either pharmacological tools (oral Ticagrelor or exINF) were used. With these two treatments, there is also an upregulation of the RISK pathway and a limitation of IR-induced oxidative stress.

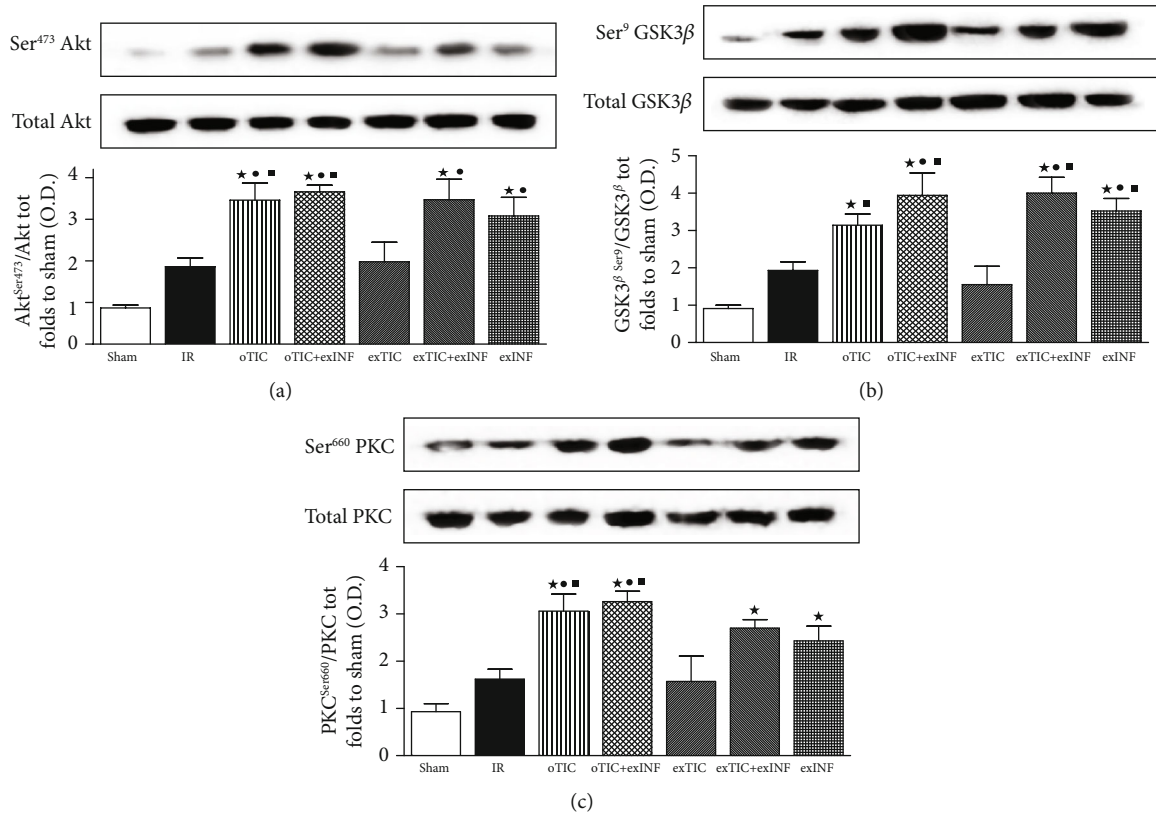


FIGURE 4: Western blotting analysis on (a) Akt, (b) GSK3 β , and (c) PKC. Data analyzed by one-way ANOVA followed by a Bonferroni post hoc test and expressed as mean \pm SEM. $n = 6 - 8$ per group. Statistical significance: $\bullet P < 0.05$ vs. IR; $\ast P < 0.05$ vs. sham, $\blacksquare P < 0.05$ vs. exTIC. Representative blots are shown of at least three different experiments.

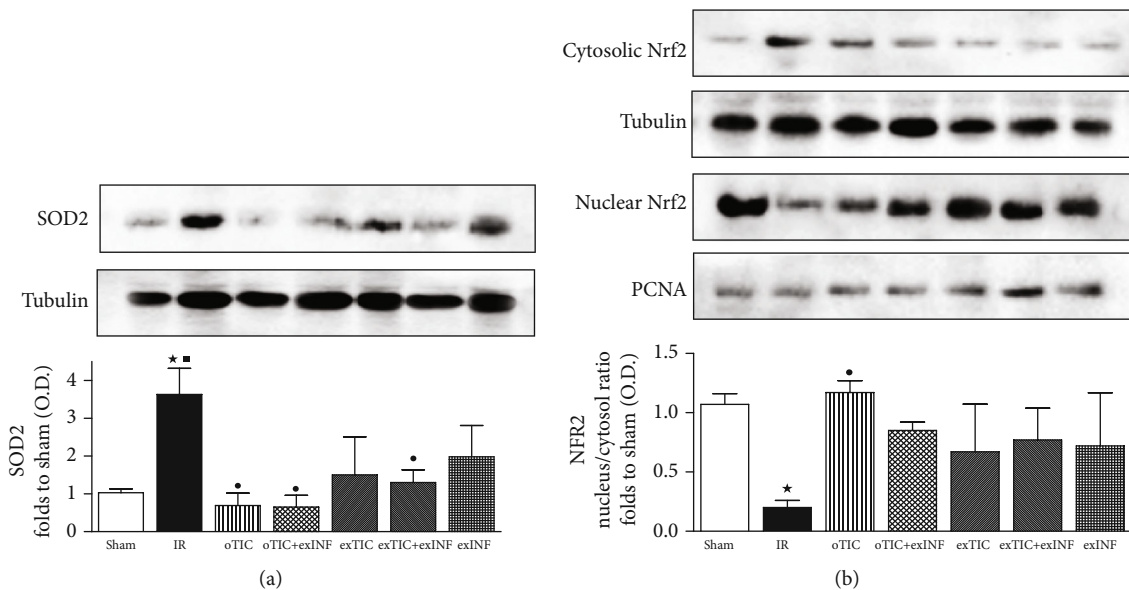


FIGURE 5: Western blotting analysis on (a) SOD2 and (b) nuclear and cytosolic Nrf2. Data analyzed by one-way ANOVA followed by a Bonferroni post hoc test and expressed as mean \pm SEM. $n = 6 - 8$ per group. Statistical significance: $\bullet P < 0.05$ vs. IR; $\ast P < 0.05$ vs. sham, $\blacksquare P < 0.05$ vs. exTIC. Representative blots are shown of at least three different experiments.

To the best of our knowledge, so far, only another study has suggested that cardioprotection of Ticagrelor tested in models of acute myocardial injury can be partially attrib-

able to inhibition of mRNA levels of NLRP3 and IL-1 β in the heart of diabetic rats [13]. Here, we extended these observations to nondiabetic conditions and we documented

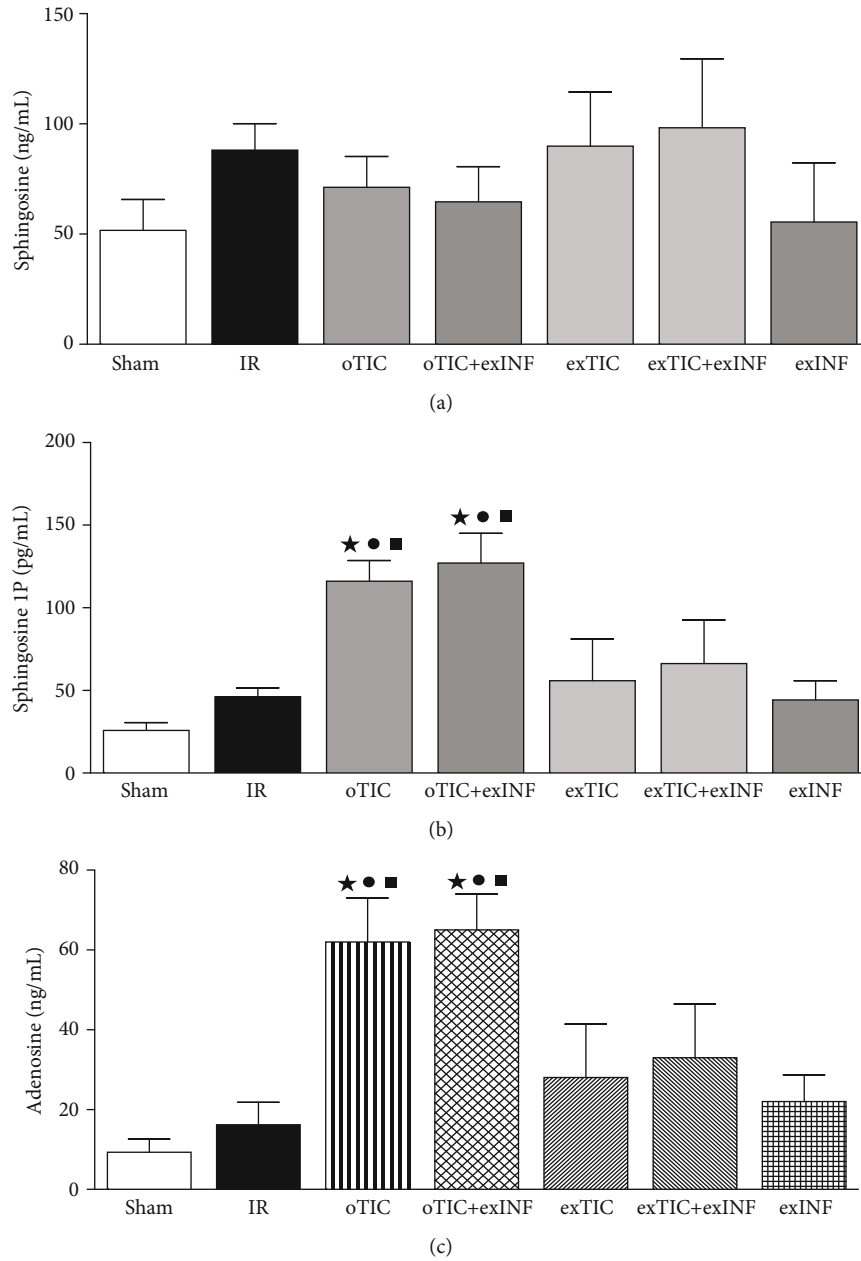


FIGURE 6: Myocardial levels of sphingosine, sphingosine 1P (S-1P), and adenosine. Data analyzed by one-way ANOVA followed by a Bonferroni post hoc test and expressed as mean \pm SEM. $n = 6 - 8$ per group. Statistical significance: ● $P < 0.05$ vs. IR; ★ $P < 0.05$ vs. sham, ■ $P < 0.05$ vs. exTIC.

TABLE 1: Level of sphingosine, sphingosine 1P (S-1P), and adenosine released by platelets exposed to Ticagrelor.

	Sphingosine (ng/mL)	S-1P (ng/mL)	Adenosine (ng/mL)
Control	356.9 \pm 44.3	94.3 \pm 29.0	18.8 \pm 5.8
Ticagrelor	68.4 \pm 2.4*	300.7 \pm 38.5*	48.8 \pm 5.4*

Level of sphingosine, S-1P, and adenosine, measured with UHPLC-tandem mass analysis, in the supernatant of human platelet subjected to stirring (1200 rpm speed at 37°C) incubated in absence and presence of Ticagrelor (5000 ng/mL, 30 min). Data analyzed by Student's t test and expressed as mean \pm SEM; $n = 6 - 8$ per group in duplicate. Statistical significance: * $P < 0.05$ vs. control.

that Ticagrelor, when administered to rats *in vivo*, evokes significant decrease of protein levels of NLRP3, resulting in lower activation of caspase-1, thus counteracting the IR-induced accumulation of active IL-1 β proteins in the heart.

A pharmacological approach with cardioprotective inhibitors has suggested that cardioprotection induced by P2Y12 antagonists is due to a conditioning phenomenon rather than to their antiplatelet effect [6]. In the presence of

sphingosine kinase inhibitor, Cangrelor's antiplatelet effect seems intact; nevertheless, *in vivo* studies did not definitively rule out a contribution from the antiplatelet effect in limiting IR injury. Our study, in which the P2Y₁₂ antagonist was administered *in vivo* and myocardial infarct subsequently induced *ex vivo*, in the absence of platelets, definitively confirms that the protective effect is mainly due to a preconditioning effect *in vivo* that lasts throughout the IR procedure *ex vivo*. The lack of cardioprotection by Ticagrelor when administered in the *ex vivo* model further support the idea of a blood cell-mediated preconditioning effect [5, 8, 31]. Given the apparent dependence upon the presence of blood in mediating Ticagrelor effects [5, 17], it would seem logical to propose that the cardioprotective effect of Ticagrelor is dependent on platelets and likely the P2Y₁₂ receptor. This is supported by previous observations showing that chemically distinct P2Y₁₂ antagonists have similar cardioprotective properties [6, 16, 17]. We thus investigated the ability of Ticagrelor to affect platelet ability to release S1P, an essential, bioactive lysophospholipid mediator that regulates various physiological functions such as lymphocyte trafficking, inflammation, and behavioural characteristics of the vascular system [36]. Platelets are among the major source of S1P in the circulation [17, 37], and platelet-derived S1P has been demonstrated to exert a critical role in the repair of pivotal microvascular structures during injury [38, 39]. Ticagrelor is unique in being an inhibitor of equilibrative nucleotide transporter 1 (ENT1) [6, 13, 14, 16]. Here, we confirm these effects in isolated human platelets, as revealed by an increase in S1P and adenosine release after exposure to Ticagrelor. Ticagrelor was previously demonstrated to raise tissue levels of adenosine, which is a known endogenous cardioprotective substance in pathophysiological conditions of the heart, including myocardial ischemia and heart failure [40, 41]. This effect has been suggested to involve inhibition of ENT1 in heart tissue [13–15]. However, so far, no experimental evidence of direct effects of Ticagrelor on ENT1 has been reported. Besides, our findings on the lack of cardioprotection by Ticagrelor on the isolated heart cloud this hypothesis of cardioprotection through interference with cardiac ENT1 [8]. Thereby, its effects on increasing adenosine levels in heart tissue could derive from an effect of Ticagrelor on a subgroup of blood cells. Both erythrocytes and platelets are known to release different substances in blood stream, including adenosine and S1P [17, 42, 43]. Here, we demonstrated for the first time that Ticagrelor increased the levels of adenosine released from platelets, thus suggesting that this effect might contribute, together with S1P, to the cardioprotection recorded when Ticagrelor was administered *in vivo* only.

The contribution of blood-derived S1P and adenosine in mediating the myocardial protective effects of Ticagrelor was confirmed by showing that both S1P and adenosine reached the highest concentrations in the heart of rats orally exposed to Ticagrelor. While the increase in myocardial adenosine levels has been already documented in the IR heart of rats orally pretreated with Ticagrelor [13], so far, no direct myocardial detection of S1P or comparison of adenosine/S1P myocardial levels between *in vivo* vs. *ex vivo* treatments has been reported in the literature. Thus, our study adds a further

interesting piece of evidence on the ability of Ticagrelor to cause blood cells to release substances, which may contribute to cardioprotection. In fact, either S1P or adenosine has been already demonstrated to evoke protective effects throughout activation of the protective survival RISK pathway in the heart [44, 45]. As Ticagrelor protection seems to depend at least in part on the same signaling cascade modulate S1P and adenosine, it seemed likely that these endogenous components would be involved in Ticagrelor's protective mechanism. Interestingly, both the treatment (Ticagrelor and exINF) in aerobic conditions do not affect myocardial perfusion, thus suggesting an unchanged oxygen demand in comparison to untreated hearts. Moreover, the levels of components of either NLRP3 or RISK pathways in sham animals were lower than those detected in all IR groups (protected and nonprotected), thus suggesting that in aerobic conditions, the pharmacological treatments do not influence the myocardial metabolism, but may trigger mechanisms that will make the hearts more resistant to IR challenge boosting RISK activation in postischemic phase. Indeed, the RISK pathway is an intrinsic prosurvival signaling cascade evoked by IR itself which confers protection against the reperfusion insult by avoiding the opening of the mitochondrial permeability transition pore at the onset of reperfusion [34, 46]. Potentiation of RISK activation in the early minutes of reperfusion contributes to cardioprotection induced by preconditioning protocols. Actually, in protected hearts, the phosphorylation of RISK enzymes peaks at 10–15 minutes of reperfusion and progressively wanes thereafter [34, 47–49]. A two-threefold higher phosphorylation level after 60 min of reperfusion is a strong indication of kinase involvement in protection, especially if we consider that the reduction in infarct size in protected hearts resulted in a ~20% increase in vital tissue when compared to control IR hearts. As previously documented [6], pharmacological inhibition of the RISK pathway blunted the protective effects of P2Y₁₂ antagonists against IR, thus further supporting the hypothesis that their mechanisms of cardioprotection utilize specific signal transduction of myocardial protection rather than inhibition of intravascular coagulation. Our study extends these findings confirming cross-talk mechanisms linking NLRP3 inflammasome to RISK pathway in cardioprotection, which have been so far faintly suggested [50–52], but not convincingly demonstrated. Besides, it shows that Ticagrelor uses similar mechanisms of protection evoked by a NLRP3 inflammasome inhibitor, leading to activation of the RISK pathway. The lack of additive effects of the drug combination may be explained considering that additional protection cannot be induced by strategies that share common prosurvival signaling pathways such as the P2Y₁₂ antagonist and the NLRP3 inflammasome inhibitor. However, previous studies demonstrated that treatment with a caspase-1 inhibitor prior to ischemia or reperfusion adds its protection to the one elicited by the P2Y₁₂ antagonist, Cangrelor [4, 7]. Differently from INF that directly targets NLRP3 complex formation, direct caspase-1 inhibitors may influence not only inflammatory response but also glycolytic, mitochondrial, and pyroptotic cell death [4]; thus, the additional beneficial effects recorded by these authors could be due to interference with

any of these pathways beyond the inhibition of the NLRP3 inflammasome-caspase axis. Another substantial difference between our study and that of Audia et al. [4] is that these authors had higher coronary flow when the caspase-1 inhibitor was used, while we perfused the hearts at constant flow, to avoid flow effects on IR injury.

The role of oxidative stress in contributing to IR injury is not clear [53, 54]. Overall, it seems that IR-dependent oxidative stress is reduced by all protective treatments. However, only Ticagrelor pretreatment displays a consistent effect in limiting the oxidative component as suggested by the significant increase in nuclear levels of Nrf2 and by the downregulation of SOD2. Nevertheless, also for this mechanism, there are not apparent differences between Ticagrelor and INF. Moreover, the antioxidant effect of Ticagrelor given orally seems stronger than that observed when it is given *ex vivo*.

5. Limitation of the Study

Our results confirm Ticagrelor conditioning effects, which are not additives to the cardioprotection achieved by directly inhibiting NLRP3. It is likely that this lack of additive effect is due to the activation of RISK pathway by both treatments. Other studies demonstrated additive effect when P2Y₁₂ and a downstream NLRP3 factor, namely, caspase-1, were inhibited [4, 7], thus confirming that the cross-talk between NLRP3 and RISK cardioprotective pathways is quite complex [36]. Besides, here, we did not test the impact of the proposed pharmacological treatments on the tested signaling cascades at basal condition. Therefore, further studies are needed to fully elucidate the cross-talk among mechanisms linking NLRP3 complex, redox state, and RISK pathway. Finally, we must consider that all experimental paradigms have disadvantages and advantages. For instance, we used gavage to administer Ticagrelor instead of a spontaneous intake which is more physiological, as gavage guarantees a more constant dosage, which is recommendable in cardioprotection studies [55]. Determining which blood-derived factors mediate Ticagrelor-induced cardioprotection was beyond the scope of this study. Nevertheless, the fact that Ticagrelor increases platelet release of both adenosine and S1P suggests these factors as important players that deserve further investigations.

6. Conclusions

In conclusion, we confirm that Ticagrelor requires the presence of blood to act as conditioning agent. Importantly, we demonstrate that the cardioprotective effects of Ticagrelor are not due to a direct action on the myocardial tissue nor to its antiaggregating effect, whereas the NLRP3 inhibitor, INF, is able to act directly on the heart. Nevertheless, these two drugs given before ischemia activate a similar protective pathway, involving RISK pathway and redox modulation, without additive cardioprotective effects.

Abbreviations

RISK: Reperfusion Injury Salvage Kinase
IR: Ischemia/reperfusion

AMI: Acute myocardial infarction
NLRP3: Nucleotide-binding oligomerization domain- (NOD-) like receptor pyrin domain containing 3
IS: Infarct size
AAR: Area at risk
INF: NLRP3 inflammasome inhibitor.

Data Availability

The data used to support the findings of this study are available from the corresponding author (MC and PP) upon request.

Conflicts of Interest

The authors declare that they have no conflicts of interest.

Authors' Contributions

Claudia Penna and Manuela Aragno are shared first authors of this study. PP and MC drafted the first version of the manuscript and supervised the writing. CP and MA made the revision and statistical management of paper and figures. EZ and SF made the isolated hearts. ASC, MA, MC, and FC made the WB analysis. IR isolated human platelets. CM and FDB made the HPLC analysis. MB and GFA made INF. All authors evaluated retrieved papers and their reference lists to identify additional relevant articles. All authors actively contributed to the study, revised the manuscript, and approved the final version of the manuscript. Claudia Penna, Manuela Aragno, Massimo Collino, and Pasquale Pagliaro contributed equally to this work. Pasquale PAGLIARO and Massimo COLLINO are shared senior authors of this study.

Acknowledgments

This study was funded by the University of Turin, Ricerca Locale Ex-60% (Grants: PAGP_RILO_16_01; PENC_RILO, ARAM_RILO, COLM_RILO) and by MIUR (PAGP_FFABR_17_01 and PENC_FFABR_17_01, COLM_FFABR_17_01).

References

- [1] D. J. Hausenloy, S. B. Ong, and D. M. Yellon, "The mitochondrial permeability transition pore as a target for preconditioning and postconditioning," *Basic Research in Cardiology*, vol. 104, no. 2, pp. 189–202, 2009.
- [2] P. Pagliaro, F. Moro, F. Tullio, M. G. Perrelli, and C. Penna, "Cardioprotective pathways during reperfusion: focus on redox signaling and other modalities of cell signaling," *Antioxidants & Redox Signaling*, vol. 14, no. 5, pp. 833–850, 2011.
- [3] C. Penna, M. G. Perrelli, and P. Pagliaro, "Mitochondrial pathways, permeability transition pore, and redox signaling in cardioprotection: therapeutic implications," *Antioxidants & Redox Signaling*, vol. 18, no. 5, pp. 556–599, 2013.
- [4] J. P. Audia, X. M. Yang, E. S. Crockett et al., "Caspase-1 inhibition by VX-765 administered at reperfusion in P2Y₁₂ receptor antagonist-treated rats provides long-term reduction in

- myocardial infarct size and preservation of ventricular function,” *Basic Research in Cardiology*, vol. 113, no. 5, 2018.
- [5] M. V. Cohen, X. M. Yang, J. White, D. M. Yellon, R. M. Bell, and J. M. Downey, “Cangrelor-mediated cardioprotection requires platelets and sphingosine phosphorylation,” *Cardiovascular Drugs and Therapy*, vol. 30, no. 2, pp. 229–232, 2016.
- [6] X. M. Yang, Y. Liu, L. Cui et al., “Platelet P2Y₁₂ blockers confer direct postconditioning-like protection in reperfused rabbit hearts,” *Journal of Cardiovascular Pharmacology and Therapeutics*, vol. 18, no. 3, pp. 251–262, 2013.
- [7] X. M. Yang, J. M. Downey, M. V. Cohen, N. A. Housley, D. F. Alvarez, and J. P. Audia, “The highly selective caspase-1 inhibitor VX-765 provides additive protection against myocardial infarction in rat hearts when combined with a platelet inhibitor,” *Journal of Cardiovascular Pharmacology and Therapeutics*, vol. 22, no. 6, pp. 574–578, 2017.
- [8] X. M. Yang, S. Gadde, J. P. Audia, D. F. Alvarez, J. M. Downey, and M. V. Cohen, “Ticagrelor does not protect isolated rat hearts, thus clouding its proposed cardioprotective role through ENT 1 in heart tissue,” *Journal of Cardiovascular Pharmacology and Therapeutics*, vol. 24, no. 4, pp. 371–376, 2019.
- [9] R. Koski and B. Kennedy, “Comparative review of oral P2Y₁₂ inhibitors,” *P & T: a peer-reviewed journal for formulary management*, vol. 43, no. 6, pp. 352–357, 2018.
- [10] D. Armstrong, C. Summers, L. Ewart, S. Nylander, J. E. Sidaway, and J. J. van Giezen, “Characterization of the adenosine pharmacology of ticagrelor reveals therapeutically relevant inhibition of equilibrative nucleoside transporter 1,” *Journal of Cardiovascular Pharmacology and Therapeutics*, vol. 19, no. 2, pp. 209–219, 2014.
- [11] L. Bonello, M. Laine, N. Kipson et al., “Ticagrelor increases adenosine plasma concentration in patients with an acute coronary syndrome,” *Journal of the American College of Cardiology*, vol. 63, no. 9, pp. 872–877, 2014.
- [12] M. Cattaneo, R. Schulz, and S. Nylander, “Adenosine-mediated effects of ticagrelor: evidence and potential clinical relevance,” *Journal of the American College of Cardiology*, vol. 63, no. 23, pp. 2503–2509, 2014.
- [13] Y. Birnbaum, G. D. Birnbaum, I. Birnbaum, S. Nylander, and Y. Ye, “Ticagrelor and rosuvastatin have additive cardioprotective effects via adenosine,” *Cardiovascular Drugs and Therapy*, vol. 30, no. 6, pp. 539–550, 2016.
- [14] G. Vilahur, M. Gutiérrez, L. Casani et al., “Protective effects of ticagrelor on myocardial injury after infarction,” *Circulation*, vol. 134, no. 22, pp. 1708–1719, 2016.
- [15] Y. Ye, G. D. Birnbaum, J. R. Perez-Polo, M. K. Nanhwan, S. Nylander, and Y. Birnbaum, “Ticagrelor protects the heart against reperfusion injury and improves remodeling after myocardial infarction,” *Arteriosclerosis, Thrombosis, and Vascular Biology*, vol. 35, no. 8, pp. 1805–1814, 2015.
- [16] S. Nylander and R. Schulz, “Effects of P2Y₁₂ receptor antagonists beyond platelet inhibition-comparison of ticagrelor with thienopyridines,” *British Journal of Pharmacology*, vol. 173, no. 7, pp. 1163–1178, 2016.
- [17] S. M. Davidson, I. Andreadou, L. Barile et al., “Circulating blood cells and extracellular vesicles in acute cardioprotection,” *Cardiovascular Research*, vol. 115, no. 7, pp. 1156–1166, 2019.
- [18] R. Mastrocola, M. Aragno, G. Alloatti, M. Collino, C. Penna, and P. Pagliaro, “Metaflammation: tissue-specific alterations of the NLRP3 inflammasome platform in metabolic syndrome,” *Current Medicinal Chemistry*, vol. 25, no. 11, pp. 1294–1310, 2018.
- [19] F. Chiazza, A. Couturier-Maillard, E. Benetti et al., “Targeting the NLRP3 inflammasome to reduce diet-induced metabolic abnormalities in mice,” *Molecular Medicine*, vol. 21, no. 1, pp. 1025–1037, 2015.
- [20] M. Collino, E. Benetti, M. Rogazzo et al., “Reversal of the deleterious effects of chronic dietary HFCS-55 intake by PPAR- δ agonism correlates with impaired NLRP3 inflammasome activation,” *Biochemical Pharmacology*, vol. 85, no. 2, pp. 257–264, 2013.
- [21] S. Cannito, E. Morello, C. Bocca et al., “Microvesicles released from fat-laden cells promote activation of hepatocellular NLRP3 inflammasome: a pro-inflammatory link between lipotoxicity and non-alcoholic steatohepatitis,” *PLoS One*, P. Strnad, Ed., vol. 12, no. 3, article e0172575, 2017.
- [22] E. Benetti, R. Mastrocola, G. Vitarelli et al., “Empagliflozin protects against diet-induced NLRP-3 inflammasome activation and lipid accumulation,” *The Journal of Pharmacology and Experimental Therapeutics*, vol. 359, no. 1, pp. 45–53, 2016.
- [23] D. Nigro, F. Menotti, A. S. Cento et al., “Chronic administration of saturated fats and fructose differently affect SREBP activity resulting in different modulation of Nrf2 and Nlrp3 inflammasome pathways in mice liver,” *The Journal of Nutritional Biochemistry*, vol. 42, pp. 160–171, 2017.
- [24] R. Mastrocola, C. Penna, F. Tullio et al., “Pharmacological inhibition of NLRP3 inflammasome attenuates myocardial ischemia/reperfusion injury by activation of RISK and mitochondrial pathways,” *Oxidative Medicine and Cellular Longevity*, vol. 2016, Article ID 5271251, 11 pages, 2016.
- [25] S. Toldo, A. G. Mauro, Z. Cutter et al., “The NLRP3 inflammasome inhibitor, OLT1177 (dapansutrile), reduces infarct size and preserves contractile function after ischemia reperfusion injury in the mouse,” *Journal of Cardiovascular Pharmacology*, vol. 73, no. 4, pp. 215–222, 2019.
- [26] R. Mastrocola, M. Collino, C. Penna et al., “Maladaptive modulations of NLRP3 inflammasome and cardioprotective pathways are involved in diet-induced exacerbation of myocardial ischemia/reperfusion injury in mice,” *Oxidative Medicine and Cellular Longevity*, vol. 2016, Article ID 3480637, 12 pages, 2016.
- [27] H. E. Bøtker, D. Hausenloy, I. Andreadou et al., “Practical guidelines for rigor and reproducibility in preclinical and clinical studies on cardioprotection,” *Basic Research in Cardiology*, vol. 113, no. 5, pp. 39–39, 2018.
- [28] M. Cocco, D. Garella, A. StiloDi et al., “Electrophilic warhead-based design of compounds preventing NLRP3 inflammasome-dependent pyroptosis,” *Journal of Medicinal Chemistry*, vol. 57, no. 24, pp. 10366–10382, 2014.
- [29] M. Cocco, G. Miglio, M. Giorgis et al., “Design, synthesis, and evaluation of acrylamide derivatives as direct NLRP3 inflammasome inhibitors,” *ChemMedChem*, vol. 11, no. 16, pp. 1790–1803, 2016.
- [30] M. Cocco, C. Pellegrini, H. Martínez-Banaclocha et al., “Development of an acrylate derivative targeting the NLRP3 inflammasome for the treatment of inflammatory bowel disease,” *Journal of Medicinal Chemistry*, vol. 60, no. 9, pp. 3656–3671, 2017.
- [31] A. Moulias, I. Xanthopoulou, and D. Alexopoulos, “Does ticagrelor improve endothelial function?,” *Journal of Cardiovascular Pharmacology and Therapeutics*, vol. 24, no. 1, pp. 11–17, 2019.

- [32] C. Penna, F. Tullio, A. Merlino et al., "Postconditioning cardioprotection against infarct size and post-ischemic systolic dysfunction is influenced by gender," *Basic Research in Cardiology*, vol. 104, no. 4, pp. 390–402, 2009.
- [33] S. M. Coldewey, E. Benetti, M. Collino et al., "Elevation of serum sphingosine-1-phosphate attenuates impaired cardiac function in experimental sepsis," *Scientific Reports*, vol. 6, no. 1, 2016.
- [34] X. Rossello and D. M. Yellon, "The RISK pathway and beyond," *Basic Research in Cardiology*, vol. 113, no. 1, 2018.
- [35] A. J. van der Ven, N. Riksen, G. Rongen et al., "Differential effects of platelets and platelet inhibition by ticagrelor on TLR2- and TLR4-mediated inflammatory responses," *Thrombosis and Haemostasis*, vol. 113, no. 5, pp. 1035–1045, 2015.
- [36] F. Tukijan, M. Chandrakanthan, and L. N. Nguyen, "The signalling roles of sphingosine-1-phosphate derived from red blood cells and platelets," *British Journal of Pharmacology*, vol. 175, no. 19, pp. 3741–3746, 2018.
- [37] N. Urtz, F. Gaertner, M.-L. von Bruehl et al., "Sphingosine 1-phosphate produced by sphingosine kinase 2 intrinsically controls platelet aggregation in vitro and in vivo," *Circulation Research*, vol. 117, no. 4, pp. 376–387, 2015.
- [38] R. L. Proia and T. Hla, "Emerging biology of sphingosine-1-phosphate: its role in pathogenesis and therapy," *The Journal of Clinical Investigation*, vol. 125, no. 4, pp. 1379–1387, 2015.
- [39] Z. Wang, K. Chen, Y. Han et al., "Irisin protects heart against ischemia-reperfusion injury through a SOD2-dependent mitochondria mechanism," *Journal of Cardiovascular Pharmacology*, vol. 72, no. 6, pp. 259–269, 2018.
- [40] M. V. Cohen, C. P. Baines, and J. M. Downey, "Ischemic preconditioning: from adenosine receptor to K_{ATP} channel," *Annual Review of Physiology*, vol. 62, pp. 79–109, 2000.
- [41] M. Kitakaze and M. Hori, "Adenosine therapy: a new approach to chronic heart failure," *Expert Opinion on Investigational Drugs*, vol. 9, no. 11, pp. 2519–2535, 2000.
- [42] E. M. Golebiewska and A. W. Poole, "Platelet secretion: from haemostasis to wound healing and beyond," *Blood Reviews*, vol. 29, no. 3, pp. 153–162, 2015.
- [43] J. Öhman, R. Kudira, S. Albinsson, B. Olde, and D. Erlinge, "Ticagrelor induces adenosine triphosphate release from human red blood cells," *Biochemical and Biophysical Research Communications*, vol. 418, no. 4, pp. 754–758, 2012.
- [44] S. J. Somers, M. Frias, L. Lacerda, L. H. Opie, and S. Lecour, "Interplay between SAFE and RISK pathways in sphingosine-1-phosphate-induced cardioprotection," *Cardiovascular Drugs and Therapy*, vol. 26, no. 3, pp. 227–237, 2012.
- [45] W. J. Zang, L. Sun, and X. J. Yu, "Cardioprotection of ischemic postconditioning and pharmacological post-treatment with adenosine or acetylcholine," *Acta physiologica Sinica*, vol. 59, no. 5, pp. 593–600, 2007.
- [46] D. J. Hausenloy and D. M. Yellon, "New directions for protecting the heart against ischaemia-reperfusion injury: targeting the Reperfusion Injury Salvage Kinase (RISK)-pathway," *Cardiovascular Research*, vol. 61, no. 3, pp. 448–460, 2004.
- [47] P. Ferdinandy, D. J. Hausenloy, G. Heusch, G. F. Baxter, and R. Schulz, "Interaction of risk factors, comorbidities, and comedication with ischemia/reperfusion injury and cardioprotection by preconditioning, postconditioning, and remote conditioning," *Pharmacological Reviews*, vol. 66, no. 4, pp. 1142–1174, 2014.
- [48] C. Penna, C. Angotti, and P. Pagliaro, "Protein S-nitrosylation in preconditioning and postconditioning," *Experimental Biology and Medicine*, vol. 239, no. 6, pp. 647–662, 2014.
- [49] M. V. Cohen and J. M. Downey, "Signalling pathways and mechanisms of protection in pre- and postconditioning: historical perspective and lessons for the future," *British Journal of Pharmacology*, vol. 172, no. 8, pp. 1913–1932, 2015.
- [50] S. Femminò, P. Pagliaro, and C. Penna, "Obesity and cardioprotection," *Current Medicinal Chemistry*, vol. 27, no. 2, pp. 230–239, 2020.
- [51] Ø. Sandanger, E. Gao, T. Ranheim et al., "NLRP3 inflammasome activation during myocardial ischemia reperfusion is cardioprotective," *Biochemical and Biophysical Research Communications*, vol. 469, no. 4, pp. 1012–1020, 2016.
- [52] C. J. Zuurbier, "NLRP3 inflammasome in cardioprotective signaling," *Journal of Cardiovascular Pharmacology*, vol. 74, no. 4, pp. 271–275, 2019.
- [53] H. Y. Sun, N. P. Wang, F. Kerendi et al., "Hypoxic postconditioning reduces cardiomyocyte loss by inhibiting ROS generation and intracellular Ca^{2+} overload," *American Journal of Physiology. Heart and Circulatory Physiology*, vol. 288, no. 4, pp. H1900–H1908, 2005.
- [54] Z. Xu, M. V. Cohen, J. M. Downey, T. L. vanden Hoek, and Z. Yao, "Attenuation of oxidant stress during reoxygenation by AMP 579 in cardiomyocytes," *American Journal of Physiology. Heart and Circulatory Physiology*, vol. 281, no. 6, pp. H2585–H2589, 2001.
- [55] X. M. Yang, L. Cui, A. Alhammouri, J. M. Downey, and M. V. Cohen, "Triple therapy greatly increases myocardial salvage during ischemia/reperfusion in the in situ rat heart," *Cardiovascular Drugs and Therapy*, vol. 27, no. 5, pp. 403–412, 2013.